



University of HUDDERSFIELD

University of Huddersfield Repository

Tutuianu, Anca

Investigating how oncogenic miRNA alters the genetics of Breast Cancer

Original Citation

Tutuianu, Anca (2021) Investigating how oncogenic miRNA alters the genetics of Breast Cancer. Doctoral thesis, University of Huddersfield.

This version is available at <https://eprints.hud.ac.uk/id/eprint/35624/>

The University Repository is a digital collection of the research output of the University, available on Open Access. Copyright and Moral Rights for the items on this site are retained by the individual author and/or other copyright owners. Users may access full items free of charge; copies of full text items generally can be reproduced, displayed or performed and given to third parties in any format or medium for personal research or study, educational or not-for-profit purposes without prior permission or charge, provided:

- The authors, title and full bibliographic details is credited in any copy;
- A hyperlink and/or URL is included for the original metadata page; and
- The content is not changed in any way.

For more information, including our policy and submission procedure, please contact the Repository Team at: E.mailbox@hud.ac.uk.

<http://eprints.hud.ac.uk/>



PHD THESIS

**Investigating how oncogenic miRNA alters
the genetics of Breast Cancer**

Anca Tutuianu

1951156

Supervised by

Dr. James BOYNE

Prof. Roger PHILLIPS

Dr. Wayne ROBERTS

Dr. Kirsten RICHES-SUMAN

Prof. Valerie SPEIRS

September 14, 2021

I, **Anca Tutuianu**, declare that this thesis titled *Investigating how oncogenic miRNA alters the genetics of Breast Cancer* and the work presented in it are my own. I confirm that:

- Where any part of this thesis has previously been submitted for a degree or any other qualification at this University or any other institution, this has been clearly stated.
- Where I have consulted the published work of others, this is always clearly attributed.
- Where I have quoted from the work of others, the source is always given. With the exception of such quotations, this thesis is entirely my own work.
- I have acknowledged all main sources of help.
- Where the thesis is based on work done by myself jointly with others, I have made clear exactly what was done by others and what I have contributed myself.

Abstract

The underlying causes of breast cancer (BC) are diverse, however, there is a striking association between type 2 diabetes (T2DM) and both the likelihood of a woman developing breast cancer and her risk of dying. While the mechanisms behind this association remain to be fully understood, this project focused on the emerging link between platelet derived microparticles (PMPs) and BC tumourigenesis in the context of a T2DM diagnosis. Other studies have shown that PMPs have the potential to alter target cell function via delivery of RISC-associated miRNAs. Recently, a role for platelet-derived microparticles (PMPs) as drivers of metastasis has emerged for several cancers. This raises the intriguing possibility that an elevated risk of BC development and metastasis in T2DM patients might be explained by increased levels of circulating PMPs. This project has investigated the impact of purified PMPs on a range of BC cell lines and demonstrated that both diabetic platelet derived microparticles (DPMP) and non-diabetic platelet derived microparticles (NDPMP) had different effects, depending on the BC cell type. This project has found, through phenotypic and molecular analysis, including RNA seq, that DPMPs favour influencing triple negative BC, with miR-21 playing an important role in this interaction. NDPMPs, however, still present an influence over other types of BC that should not be ignored, giving them the potential of being used as therapeutic targets as well.

Acknowledgements

Firstly, I would like to thank my original supervisors, Dr. Boyne and Dr. Roberts, for the chance to be part of this project and for the opportunities it brought with it. I would also like to thank my other supervisors, Prof. Phillips, Dr. Riches-Suman and Prof. Valerie Speirs for their continuous support and important lessons during my time working with them.

Secondly I would like to thank my parents, my sister and my grandparents, as well as the rest of the family, for their moral support and constant encouraging throughout this project. I would especially like to add Matt, Kasia, Charlie and Geanina, as well as my archery family for being there for me when I needed it.

Contents

Abstract	1
Acknowledgements	1
Abbreviations	12
1 Introduction	16
1.1 Platelets	16
1.2 Platelet microparticles	24
1.3 Breast Cancer	33
1.4 Type 2 Diabetes Mellitus	47
1.5 Project Aims	50
2 Materials and Methods	53
2.1 Cell lines	53
2.2 Mycoplasma detection and elimination	54
2.3 Platelet microparticle collection	56
2.4 Platelet microparticle characterisation	58
2.5 Cell viability measurement of BC cells incubated in the presence of PMPs	64

2.6	Cell Phenotype Characterisation in the presence and absence of PMPs	65
2.7	RNA extraction	69
2.8	Quantification of RNA	74
2.9	RT-qPCR analysis using the miRCURY LNA miRNA Qiagen Kit	78
2.10	Next Generation RNA Sequencing	82
2.11	Protein Expression Analysis	84
2.12	Seahorse Metabolic Analysis	85
2.13	Inhibition of miRNA-21 activity in BC cells	87
2.14	Statistical Analysis	88
3	Platelet Microparticle Isolation and Characterisation	90
3.1	PMP Isolation	90
3.2	PMP characterisation	93
3.3	PMPs as transport vectors	98
3.4	PMPs alter cellular morphology	103
3.5	PMPs increase BC cell motility	110
3.6	Chapter discussion	119
4	miRNA-seq analysis of non-diabetic and type 2 diabetic-derived PMPs	126
4.1	Quality control analysis	127
4.2	Next Generation RNA Sequencing	131
4.3	Chapter discussion	144

5	The effects of DPMPs versus NDPMPs on breast cancer cell lines	147
5.1	Cell Viability	148
5.2	The influence of PMPs on cellular migration	151
5.3	The influence of PMPs on cellular invasion	159
5.4	The effect of DPMPs on BC cell morphology	160
5.5	The influence of PMPs on EMT.	168
5.6	Influence of PMPs on cellular metabolism	171
5.7	miRNA target confirmation	173
5.8	The effect of miR-21 inhibition in MDA-MB-231 cells	179
5.9	Chapter discussion	188
6	Discussion	196
	Presentation and Posters	204
	Appendices	205
	Appendix 1	206
	Appendix 2	207
	Bibliography	215

List of Figures

1.1	Brief visualisation of thrombopoiesis	18
1.2	Visual representation of the diversity of platelet receptors and their agonists within different cellular processes.	21
1.3	Incidence of female breast cancer by age group.	35
1.4	Anatomical structures present in the breast.	43
2.1	Graphical representation of the wound formation used for the scratch wound assay for 6 well plates.	67
3.1	PMP sample visualisation under the NanoSight NS300	96
3.2	Results of PMP sample analysis via the Nanosight NS300 . . .	99
3.3	Platelet microparticle characterisation using the BD Biosciences Accuri flow cytometer: forward scatter vs. side scatter. . . .	100
3.4	Platelet microparticle characterisation using the BD Biosciences Accuri flow cytometer: analysis via colour filters.	101
3.5	Platelet microparticle characterisation using the BD Biosciences Accuri flow cytometer: fluorescently tagged PMPs with anti-CD41a and anti-Annexin V antibodies.	102

3.6	Platelet microparticle characterisation using the BD Biosciences Accuri flow cytometer: fluorescently tagged PMPs with anti-CD41a antibodies.	102
3.7	Platelet microparticle characterisation using the BD Biosciences Accuri flow cytometer: fluorescently tagged PMPs with anti-Annexin V antibodies.	103
3.8	Representative fluorescent microscopy images of MDA-MB-231 cell line incubated with PMPs	104
3.9	Representative confocal microscopy images of MCF-7 cell line incubated with PMPs	105
3.10	Representative confocal microscopy images of MDA-MB-231 cell line incubated with PMPs	106
3.11	Representative confocal microscopy images of MDA-MB-231 cell line incubated with PMPs	107
3.12	Representative confocal microscopy images of MDA-MB-231 cell line incubated with PMPs	108
3.13	Representation of the effect of PMPs on the circularity of the MDA-MB-231 cells they were co-incubated with.	111
3.14	Representative images of MDA-MB-231 under x60 magnification.	112
3.15	Silhouettes of random MDA-MB-231 cells obtained from images captured at 0 hours.	113
3.16	Silhouettes of random MDA-MB-231 cells obtained from images captured at 2 hours.	114

3.17	Representation of the effect of PMPs on the surface and spread of the MDA-MB-231 cells they were co-incubated with.	115
3.18	Scratch wound analysis of MDA-MB-231 and MCF-7 cells.	117
3.19	Scratch wound analysis of MDA-MB-453 and HB2 cells.	118
4.1	miRNA expression comparison between ND and D PMP RNA. (I)	133
4.2	miRNA expression comparison between ND and D PMP RNA.(II)	134
4.3	miRNA expression comparison between ND and D PMP RNA.(III)	135
4.4	Gene Ontology, sub-ontology molecular function.	136
4.5	Gene Ontology, sub-ontology biological process.	137
4.6	List of DPMP miRNAs, ranked by logFC.	139
4.7	Visual representation of top abundance of miRNAs in both NDPMPs and DPMPs.	140
5.1	MCF-7 cell viability analysis.	149
5.2	MDA-MB-231 cell viability analysis	150
5.3	MDA-MB-231 migration measured using transwell chambers.	155
5.4	MCF-7 migration measured using transwell chambers.	156
5.5	MDA-MB-453 migration measured using transwell chambers.	157
5.6	T47D migration measured using transwell chambers.	158
5.7	MDA-MB-231 invasion levels measured using transwell chambers.	161
5.8	MCF-7 invasion levels measured using transwell chambers.	162
5.9	MDA-MB-453 invasion levels measured using transwell chambers.	163

5.10	T47D invasion levels measured using transwell chambers. . . .	164
5.11	Graphical representation of the effect of DPMPs on the circularity of the MDA-MB-231 cells they were co-incubated with.	166
5.12	Graphical representation of the effect of DPMPs on the area of the MDA-MB-231 cells they were co-incubated with. . . .	167
5.13	mRNA expression levels of EMT markers measured from total RNA of MDA-MB-231 cells.	169
5.14	mRNA expression levels of EMT markers measured from total RNA of MCF-7 cells.	170
5.15	Energy phenotype test analysis of the effects of PMPs on MDA-MB-231 cell line.	174
5.16	Energy phenotype test analysis of the effects of PMPs on MCF-7 cell line.	175
5.17	Energy phenotype test analysis of the effects of PMPs on MDA-MB-453 cell line.	176
5.18	Energy phenotype test analysis of the effects of PMPs on T47D cell line.	177
5.19	Stem-loop qPCR analysis of gene expression levels of miR-21 and let-7 in cells incubated in the presence of 100 $\mu\text{g}/\text{ml}$ of either NDPMPs or DPMPs for 48 hours.	180
5.20	miRNA expression levels of targets identified via RNA Seq in MDA-MB-231 cells, untreated with Actinomycin D, treated with 100 $\mu\text{g}/\text{ml}$ NDPMPs or DPMPs.	181

5.21	miRNA expression levels of targets identified via RNA Seq in incubated MDA-MB-231 cells, treated with 1 $\mu\text{g}/\text{ml}$ Actinomycin D, in the presence of 100 $\mu\text{g}/\text{ml}$ NDPMPs or DPMPs. .	182
5.22	RT-qPCR analysis of selected miRNA targets in ACTMD treated MDA-MB-231 cells.	183
5.23	miR-21 expression in MDA-MB-231 cells following inhibition treatment using both normal and fast forward transfection protocols.	185
5.24	Migration levels of MDA-MB-231 cells with inhibited miR-21.	186
5.25	The effect of NDPMPs and DPMPs on migration levels of transfected MDA-MB-231 cells.	187

List of Tables

2.1	List of breast cancer cell lines used	55
2.2	PCR amplification for the VenorGeM Classic detection kit . .	55
2.3	NanoSight NS300 machine protocol for PMP analysis	61
2.4	List of total RNA extraction kits used in this project.	69
2.5	List of primers and oligonucleotides for RT-qPCR using PCR BioSystems reagents.	75
2.6	Incubation settings for the CFX 96 (BioRad) for RT-qPCR using the PCR Biosystems kit	76
2.7	Incubation settings for the CFX 96 (BioRad) for Stem-Loop qPCR	78
2.9	List of miRNA primers	81
2.8	Incubation settings for the CFX 96 (BioRad) for the miR- CURY LNA RT-qPCR kit	81
2.10	List of antibodies and proteins used in this project.	84
2.11	p value format used in GraphPad Prism 6.2.	89
3.1	Examples of PMP sample concentrations used.	94

4.1	Quality control examples of PMP sample concentrations measured via the Nanosight NS300.	128
4.2	Quality control examples of NDPMP sample via stem-loop RT-qPCR.	129
4.3	Quality control examples of PMP sample concentrations measured via Agilent Bioanalyser.	130
4.4	List of miRNAs present in DPMPs that are typically down-regulated in breast cancer.	141
4.5	List of miRNAs present in DPMPs that are typically upregulated or have presented as both upregulated and downregulated in breast cancer.	142
4.6	List of miRNAs present in DPMPs that are typically upregulated but present no specific association with breast cancer.	143

Abbreviations

ACD	Acid Citrate D extrose
AGES	Advanged G lycation E nd P roducts
Ago2	Argonaute 2
AR	Androgen R eceptor
ATCC	American T ype C ulture C ollection
BC	Breast C ancer
BMI	Body M ass I ndex
CD147	Cluster (of) D ifferentiation 147
cDNA	complementary D eoxyribo N ucleic A cid
C/S	Ty rode's b uffer
CSC	Cancer S tem C ells
DAPI	4',6 d iamidino-2- p henylindole
DMEM	Dulbecco's M odified E agle M edium
DPMP	Diabetic P latelet-derived M icro P articles
ddH₂O	Double D istilled W ater
DNA	D eoxyribo n ucleic A cid
EDTA	E thylene d iamine t etra a cetic A cid
EGFR	E pidermal G rowth F actor R eceptor
EMT	E pithelial (to) M esenchymal T ransition
EMP	E ndothelial M icroparticles
EPB41L3	Erythrocyte (membrane) P rotein B and 4.1 L ike 3
ER	E strogen R eceptor
FCS	F oetal C alf S erum
FDR	F alse D iscovery R ate

GP	G lycoprotein
GAPDH	G lyceraldehyde 3- phosphate d ehydrogenase
HB2	H uman B reast 2
HDL	H igh D ensity L ipoprotein
HEPES	4-(2- H ydroxy ethyl)-1- p iperazineethanesulfonic (acid)
HER2	H uman E pithelial (Growth Factor) R eceptor 2
HUVEC	H uman U mbillical V ein E ndothelial C ells
H & E	H ematoxylin (and) E osin
KCl	K alium (Potassium) C hloride
logFC	log F old C hange
MCF-7	M ichigan C ancer F oundation - 7
MDA-MB-231	M.D. Anderson - M etastasis B reast (Cancer) - 231
MDA-MB-453	M.D. Anderson - M etastasis B reast (Cancer) - 453
Mef2c	M yocyte enhancer factor 2 c
MEM	M inimum E ssential M edium
MgCl₂	M agnesium C hloride
mRNA	m essenger R ibonucleic A cid
miRNA	m icro R ibonucleic A cid
MMP	M atrix M etalloproteinases
MP	M icroparticles
MRP1	M ultidrug R esistence-associated P rotein 1
NaHCO₃	S odium B icarbonate
NaH₂PO₄	M onosodium P hosphate
NDPMP	N on-diabetic P latelet-derived M icro P articles
NRT	N o R everse T ranscriptase
oncomiRNA	o ncogenic m icro R ibonucleic A cid

PBS	Phosphate-Buffered Saline
PCR	Polymerase Chain Reaction
PenStrep	Penicillin & Streptomycin
PET	PolyEthylene Terephthalate
PGE1	Prostaglandin E1
P-gp	P-glycoprotein
PMP	Platelet-derived Microparticle
PR	Progesterone Receptor
PRP	Platelet Rich Plasma
pre-miRNA	precursor-micro Ribonucleic Acid
PS	Phosphatidylserine
PTEN	Phosphatase (and) Tensin (homologue)
qRT-PCR	quantitative Real Time-Polymerase Chain Reaction
RIPA	Radioimmunoprecipitation Assay
RCF/g	Relative Centrifugal Force
SEM	Scanning Electron Microscopy
SNAIL	Zinc finger protein SNAI1
TAE	Tris-base, Acetic (Acid), EDTA
TBST	Tris-Buffered Saline (and) Tween-20
TEM	Transmission Electron Microscopy
TF	Tissue Factor
TMP	Tumour-derived Microparticles
TWIST	TWIST1 gene
T2DM	Type 2 Diabetes Mellitus
U	Unit
UTR	Untranslated Region

VEGF Vascular **E**ndothelial **G**rowth **F**actor

Chapter 1

Introduction

1.1 Platelets

Within the human organism, particularly in the circulatory system, govern a series of processes which maintain a vital balance in order to allow the organism to function correctly. Of these processes there is haemostasis, the process through which a vascular injury is healed by the intervention of platelets, subsequently forming a clot, or thrombus, to prevent a haemorrhage ([Rasche, 2001](#)). As with any organism, disregulations are always a possibility and as such is the case of haemostasis. When an over-activation of the coagulation cascade occurs in the absence of a wound, the process known as thrombosis occurs ([Rasche, 2001](#)).

Platelets represent one of the highest population types of cells within the circulatory system, second to erythrocytes ([Willeit et al.](#),

2013). They have a vital role within the normal functional processes of the human organism. Due to the focus of this study on platelet-derived microparticles (PMPs), this section will present the biology and functions of platelets and the origin of these PMPs.

Platelets, also known as thrombocytes, are discoid, anucleate cytoplasmic fragments between 1 and 4 μm in diameter and 0.5 μm width, with a half-life of up to 5 days (George et al., 1986). Following the differentiation of haematopoietic stem cells in polyploid megakaryocytes, thrombopoietin stimulates these low-motility megakaryocytes to produce preplatelets, via the modification of the megakaryocyte microtubule skeleton and subsequent vesiculation (Bender et al., 2015). The process following this is called thrombopoiesis, see figure 1.1, or platelet formation (Lefrançois et al., 2017; Stegner et al., 2017). Although the general process that leads to the formation of new platelets was believed to be linear and identical in the same manner for all megakaryocytes, den Dekker et al. (2003) has demonstrated that megakaryocyte differentiation occurs via multiple routes depending on the stimulus, thrombin, thromboxane A2 or others, resulting in platelets with different glycoprotein expression. The previous theory that megakaryocytes also produced platelets via apoptosis has been disproved by Josefsson et al. (2014), where platelet production was unaffected following the inhibition of two apoptotic pathways, BAK-BAX-mediated intrinsic apoptosis and Fas ligand-inducible extrinsic apoptosis.

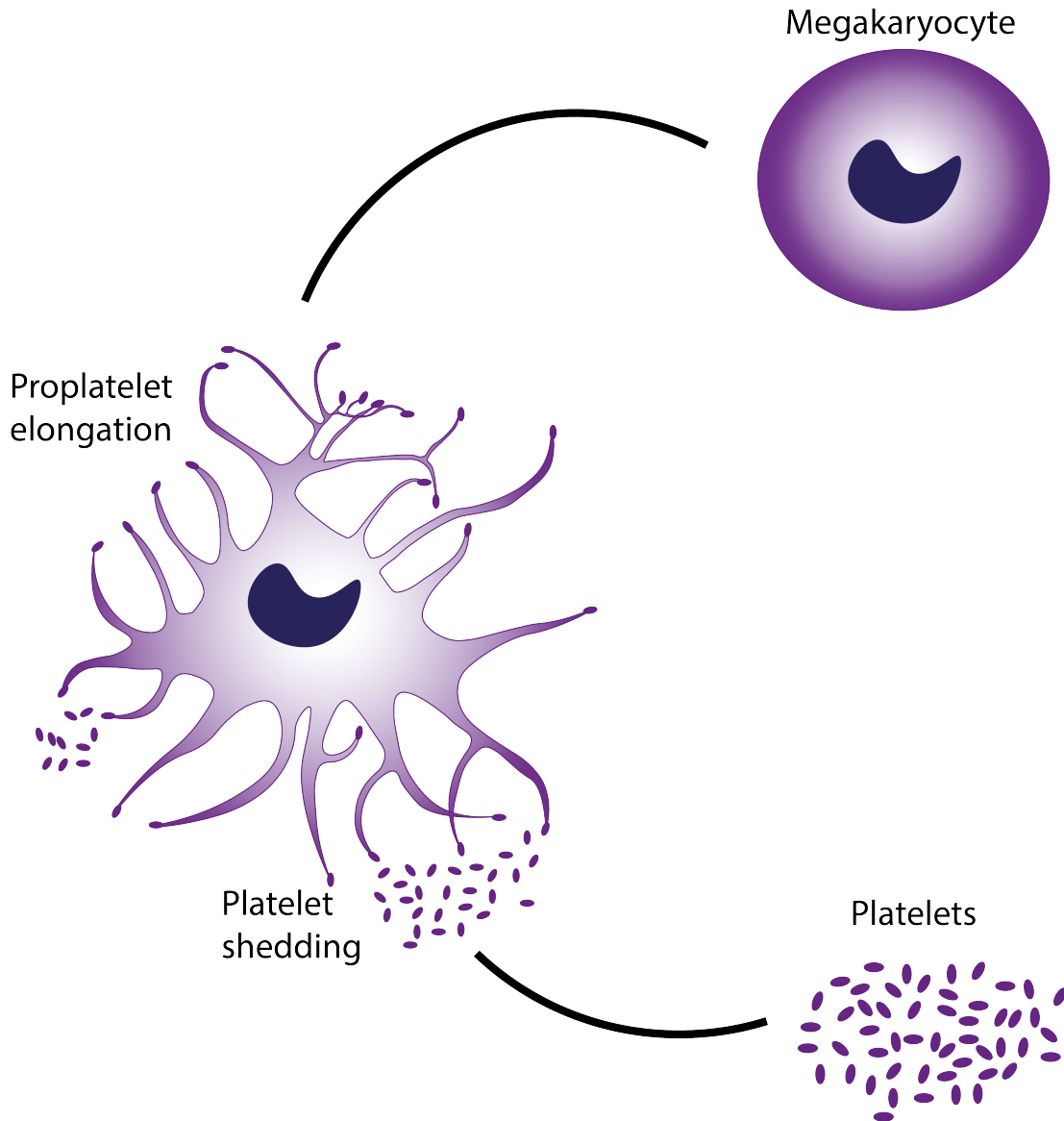


Figure 1.1: **Brief visualisation of thrombopoiesis.** The figure shows the formation of platelets from megakaryocytes in the bone marrow. Following stimulation with thrombopoietin, the actin skeleton of the megakaryocyte begins to alter its shape, leading to the formation of proplatelets and platelet shedding. Personal artistic interpretation of thrombopoiesis.

Thrombopoietin is a protein produced in the liver, as part of a negative feedback loop within the blood. The production of this protein results in low levels of platelets being detected in circulation, either in the case of general regulation or during inflammatory processes ([Grozovsky et al., 2015](#)).

Although their status as "cells" has been argued in the literature due to their lack of nucleus, they are attributed roles and characteristics of cells. Another characteristic of platelets is their heterogeneity, in particular their differences in size, density, protein content and age, as reviewed by [Baaten et al. \(2017\)](#). [Baaten et al. \(2017\)](#) also states that, although lacking in scientific evidence, it is suspected that this heterogeneity can be attributed to the uneven distribution of cellular components during the formation of proplatelets.

Platelets are important elements within haemostasis, as they help regulate the process of healing vascular injuries. The main role of these platelets during primary haemostasis is to prevent blood loss at the site of tissue damage ([Versteeg et al., 2013](#)). This activation is a process comprised of four sequential steps: adhesion, activation, secretion and aggregation. Both breast cancer (BC) and Type 2 Diabetes Mellitus (T2DM) involve high platelet activity, thus resulting in several changes in the haemostatic processes ([Laffont et al., 2013](#)). Although their main role is to help regulate haemostasis, platelets are also known to contain genetic informa-

tion, such as an abundance of microRNAs, with a role beyond that of just haemostasis (Diehl et al., 2012).

Platelets contain a variety of receptors on their surface, depending on the packing of the proplatelets as shown in figure 1.2. Their small size allows them to reach the edges of capillaries, enabling them to identify the site of injury (Krueger et al., 2002). Following disruption within the endothelial vessel wall lining and exposure to the extracellular matrix, platelets bind to the injury site via the Gp Ib/V/IX present on their surface. This allows collagen, normally found in the extracellular space, to bind via mediation to von Willebrand factor (Andrews and Berndt, 2004; Di Lullo et al., 2002). Once platelets become activated, their actin cytoskeletal and microtubules structures alter, creating prolonged projections that spread and secrete signalling molecules to promote adhesion and aggregation (Andrews and Berndt, 2004).

On the surface of these activated platelets, the integrin $\alpha_{IIb}\beta_3$ becomes hyperactivated and releases "inside out" signalling molecules, such as Thromboxane A2 and adenosine diphosphate. With the additional presence of thrombin, a coagulation protease (Sambrano et al., 2001), these secondary mediators activate other proximal platelets, leading to thrombus formation. This process is also called secondary adhesion (Nieswandt et al., 2011).

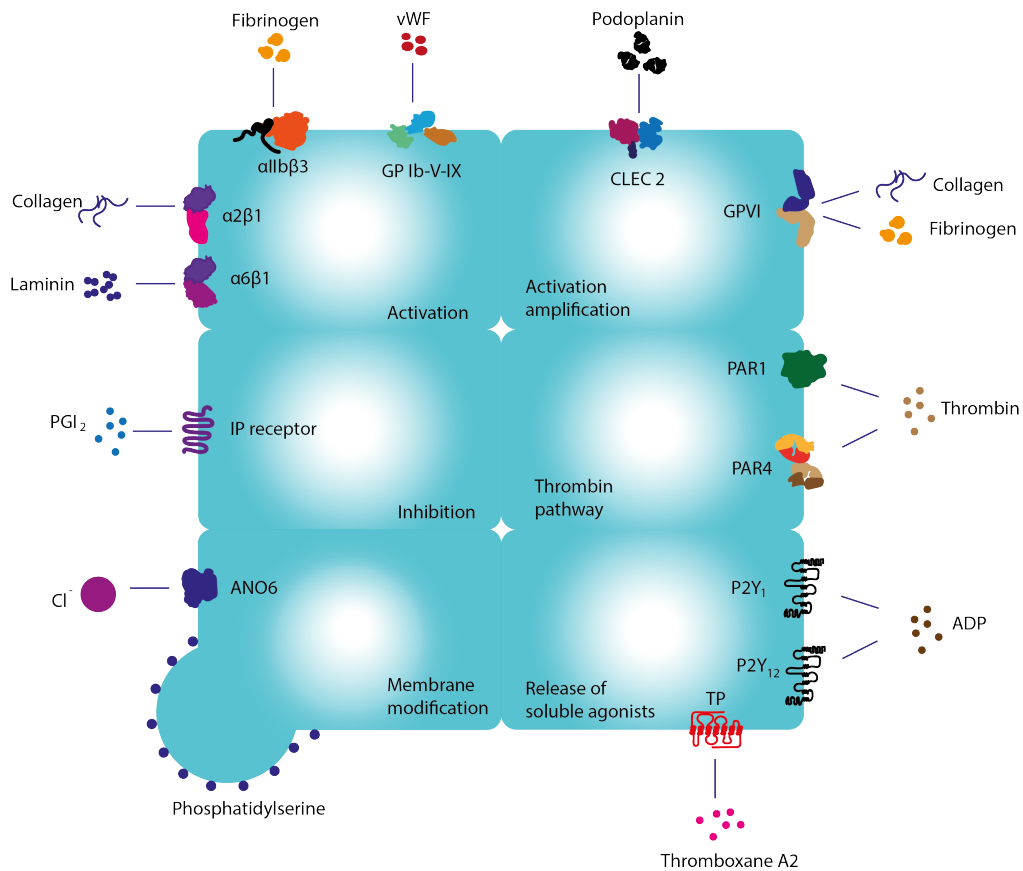


Figure 1.2: **Visual representation of the diversity of platelet receptors and their agonists within different cellular processes.** Visual representation was based on the www.uniprot.org database. Examples of receptors and their corresponding agonists were used from [van der Meijden and Heemskerk \(2019\)](#).

Despite platelets not containing a nucleus, they are still capable of influencing protein synthesis and therefore the composition of PMPs. MicroRNAs are short noncoding RNAs involved in sequence specific post transcriptional regulation of gene expression. Up to 92% of human genes are believed to be regulated by miRNAs, proving they are key players in gene regulation of genetic diseases. miRNAs block gene expression by attaching to messenger RNAs (mRNA), via imperfect complementarity between the miRNA seed region, the 3' UTR region, and generally preventing the translation process from continuing (Landry et al., 2009). Platelets themselves contain miRNA processing machinery, such as Dicer, RNA-binding protein2 and Argonaute 2 protein (Ago2) (Liang et al., 2015). Primary miRNA is converted to miRNA precursors by nuclear ribonuclease III Drosha 1 together with the DiGeorge syndrome critical region 8 protein in the microprocessor complex 2-4c (Landry et al., 2009). Micro-RNA precursors are processed into miRNA in the ribonuclease III Dicer with the help of the TAR RNA-binding protein 2 8, where it becomes coupled with the Argonaute 2 protein and forms miRNA effector complexes. miRNAs recognise the mRNA sequence on the 3' untranslated regions where it binds, rendering the mRNA unable to continue the protein synthesis process (Laffont et al., 2013). The majority of miRNAs are found intracellularly, however, when found freely in various body fluids they can become a stable class of biomarkers in disease (Chen et al., 2008). miRNAs in circulation can normally

be found in exosomes, shedding vesicles, such as platelet derived microparticles, apoptotic bodies or in vesicle-free ribonucleoprotein complexes in association with either Ago2 or HDL (Laffont et al., 2013). Landry et al. (2009) also suggests that pre-miRNA is converted prior to platelet formation, as platelets do not contain all the necessary elements required for this process, but due to the presence of Dicer and Ago2 in platelets, mature miRNA synthesis can be completed directly in platelets.

An example of one of the most abundant miRNAs in platelets is miR-223, which is found normally complexed with Ago2. Under normal conditions, miR-223 is responsible for down-regulating the expression of the P2Y12 gene. The P2Y12 receptor is also used as a target in anti-platelet therapy (Dangwal and Thum, 2013). Some of the most abundant families of miRNAs found in circulation are let-7, miR-199, miR-103, miR-25 and miR-140. The families of let-7 and miR-103 are found in their highest levels in platelets, which could suggest that they play a very important biological role (Dahiya et al., 2015). The same author has previously observed an increase of miR-16 and miR-326 in platelets stored *ex vivo*. Both of these miRNAs play a role in apoptosis. Interestingly, let-7a levels decrease in breast cancer patients post-operatively (Zhu et al., 2009).

1.2 Platelet microparticles

Platelet microparticle formation

Discovered in 1967, platelet microparticles (PMPs) were initially believed to be just "platelet dust", serving no physiological role within circulation ([Mezouar et al., 2014](#)). They are small lipid vesicles, between 0.1 to 1 μm , but typically 200 nm, released through exocytosis. They interact with surrounding cells by promoting the healing process in vascular injuries, via delivery of proteins, non-coding RNA, matrix metalloproteinases (MMPs) and tissue factors ([Semple, 2013](#)). It has also been suggested that PMPs have more stable structures than their origin cells, platelets, however the reasoning was still unknown ([Gilbert et al., 1991](#)).

Microparticles can also be released by other cell types such as megakaryocytes, leukocytes, erythrocytes, endothelial cells and adipocytes ([Flaumenhaft et al., 2009](#)), however this study will focus on the platelet derived microparticles, the most common type of microparticles found in circulation, representing approximately 70% of all circulating microparticles ([Boilard et al., 2010](#)).

Within the haemostatic system, platelets become activated by surrounding cells. When activated, intracellular calcium levels rise and they bind to calpain, a protein responsible for the denaturation of the platelet cytoskeleton through proteolysis ([Fox et al.,](#)

1991). The platelet membrane alters its structure and promotes the release of microvesicles, also called platelet derived microparticles (PMPs). Under normal resting conditions, the outer layer of the platelet plasma membrane is rich in phosphatidylcholine and sphingomyelin and the inner layer is composed of anionic phosphatidylserine (PS) and phosphatidylethanolamine, both sides creating the membrane asymmetry together with the phospholipid transporters scramblase, flippase and floppase. When the parental cells become activated or enter apoptosis, PS becomes rapidly externalised to the outer layer, leading to the formation and release of microparticles into circulation, figure 1.2. Due to this process, PMPs are likely to contain or express typical platelet membrane receptors. In order to allow exposure of PS, the levels of intracellular calcium ions need to increase. This can also affect mitochondrial permeability. PMP release is not only linked to the presence of PS on the membrane, as PS negative cells have been found to release microparticles as well (Varon et al., 2012). One factor that can influence a fast rise in intracellular calcium levels within platelets is complement protein C5b-9, which leads to PMP formation (Sims et al., 1988).

Formation of PMPs can also occur by bypassing the calcium-calpain binding and involves calmodulin, a protein kinase promoter (Sims et al., 1988). When platelets are stimulated with either a combination of thrombin and collagen, calcium ionophore A23187 or

complement protein C5b-9, the surface of the PMPs released from them contains large amounts of factor VIII, fitting the profile that PMPs are important coagulation cascade elements, also at the same time depleting the factor VIII from the surface of the activated platelets (Gilbert et al., 1991).

Other mechanisms by which PMPs are released are shear stress, malignant transformation, hypoxia, oxidative injury and apoptosis, or via contact with cytokines, thrombin or endotoxins (Mezouar et al., 2014). Outside influence also promotes the release of PMPs, through platelets activated by *Staphylococcus aureus* α -toxin (Barry et al., 1997). In the case of rheumatoid arthritis, the higher numbers of microparticles were of platelet origin, and not of megakaryocytes, the difference being that the majority of PMPs did not present surface receptor GPVI, typical of megakaryocytes (Gitz et al., 2014). Interestingly, Gilbert et al. (1991) has measured PMP generation time to be 90 seconds from platelet stimulation.

Another example that can influence PMP release, however, in a negative way, appears to be a rise in 2°C in healthy young men. Heat treatment appears to significantly reduce the levels of circulating microparticles as opposed to control (Bain et al., 2017).

PMP function

PMPs are the most predominant type of microparticles in circulation, occupying a proportion of roughly 70 -85% of total microparticles. Other granulocytes release less than 10% of the total number of microparticles and less than 5% are derived from endothelial cells, red blood cells and monocytes ([Varon et al., 2012](#)).

PMPs regulate inflammation, stimulate coagulation and affect vascular functions ([Semple, 2013](#)). They contain active lipids, proteins, nucleic acids and occasionally surface receptors. PMPs differ in composition depending on the composition and method of shedding of their parental cells ([Bernimoulin et al., 2009](#)). Initially believed to not have any roles in physiology and pathophysiology, PMPs were later proven to contain and transfer a large variety of non-coding RNAs, over 170 species ([Gidlof et al., 2013](#)), playing an important role in the regulation of target cell gene expression ([Varon et al., 2012](#)). PMPs activate intracellular signalling pathways and interact directly with the vascular architecture where they control vascular reactivity and promote angiogenesis ([Mezouar et al., 2014](#)). PMPs share components with their origin cells, such as GPs Ib, IIb, IIIa, P-selectin and thrombospondin, associated with a pro-coagulant behaviour ([Merten et al., 1999](#)). They have the ability to reprogram macrophages, specifically in the spleen and lymph nodes, presenting atheroprotective effects in atherosclerotic mouse models ([Mezouar et al., 2014](#)). As the

components of circulating microparticles differ depending on their cellular and subcellular origin, some circulating microparticles may express active tissue factor (TF), which is a primary initiator of coagulation. Even though it is a rare occurrence, TF-positive MPs will have a significant impact on local cells, as it initiates the coagulation cascade ([Falanga et al., 2012](#)).

Another main function of PMPs is intercellular information transfer through substrate exchange ([Wu et al., 2013](#)). PMPs act as transport bodies between platelets and other cell types or other platelets, within the vascular system ([Semple, 2013](#)). Four types of interactions of PMPs are described in literature. In the first instance, PMPs can produce outside-in signalling, through either ligand-receptor interaction, or by the release of different factors. PMPs bind to thrombin-activated endothelial cells, via the integrin Gp IIb/IIIa receptor ligand, permissive only in activated platelets. Given the origin of PMPs, they can easily bind to the endothelial and sub-endothelial matrix and be absorbed through endocytosis ([Merten et al., 1999](#)). The second type of interactions is the delivery of mRNAs or miRNAs via fusion of PMPs with the target cells. In the third type, PMPs may release several components, such as lipids, proteins or receptors. For the fourth type, PMPs can be internalised into their target cells, such as endothelial cells ([Mezouar et al., 2014](#)).

The PMP membrane and structure offer a sheltered environment for non-coding RNA, as they protect them from RNase, normally abundant in the blood, and offer structural stability to these RNAs during transport (Collino et al., 2010). Larger PMPs also transport mitochondria, influencing the cellular processes and bioenergetics occurring in the receiving cells and have been associated with higher pro-inflammatory responses in cells (Boudreau et al., 2014). Barry et al. (1997) states that PMPs induce platelet activation through concentrated transcellular arachidonic acid, which is metabolised into thromboxane A₂.

PMPs in disease

Considering platelets are devoid of a nucleus, they can only carry on the process of translation, having less quality control mechanisms for the miRNAs synthesised. This aspect can affect PMP secretion, quality of the components and platelet activation rate. Not only this, but altered PMP structure, activity and quantity can affect the development of several diseases. One example that has been studied, in a rather small sample size, Bal et al. (2010) examined the potential difference between PMPs in the context of acute pulmonary embolism. They have confirmed that, *in vivo*, PMPs were the most predominant type of procoagulant microparticle present, as well as being present in higher amounts in acute pulmonary embolism patients compared to matched controls. Taking this difference into consideration, Bal et al. (2010) has not found

a significant difference in procoagulant activity in their patients. Another study, by [Azzam and Zagloul \(2009\)](#), has looked at PMP activity in patients with both rheumatic mitral stenosis and atrial fibrillation. They found that higher platelet activation lead to a significant increase in TF positive PMP release. The presence of the TF suggests high procoagulant activity in these patients, leading to a high inflammatory state, endothelial dysfunction, as well as increased platelet activation. [Azzam and Zagloul \(2009\)](#) mentions that they have identified a direct correlation between the severity of rheumatic mitral stenosis and PMP production. Other disorders associated with a high production of PMPs are also peripheral artery disease ([Tan et al., 2005a](#)), myocardial infarction ([van der Zee et al., 2006](#)), cyanotic congenital heart disease ([Horigome et al., 2002](#)), coronary artery disease ([Tan et al., 2005b](#)), or even natural processes such as ageing ([van der Zee et al., 2006](#)). It is worth mentioning that all of the studies aforementioned have measured the levels of PMPs, particularly PMPs expressing P-selectin, whose presence is strongly associated with coagulation abnormalities.

The high platelet activation rate and subsequent release of high amounts of PMPs into circulation are also associated with Type 2 Diabetes Mellitus. [Koga et al. \(2006\)](#) have looked at the link between the levels of PMPs *in vivo* and the levels of remnant-like lipoprotein particles-cholesterol. This study found that increased levels of remnant-like lipoprotein particles-cholesterol were directly

correlated with the increased rate of platelet activation, therefore leading to an increase in PMP formation and thrombogenic complications. In view of this finding, the authors suggest that treating the high remnant-like lipoprotein particles-cholesterol would directly impact PMP formation and the continuous platelet activation.

[Knijff-Dutmer et al. \(2002\)](#) also remarks that high levels of PMPs are associated with rheumatoid arthritis and possibly directly linked with the evolution of the condition, including the inflammatory processes that occur.

In the case of BC patients, there is an increase in the presence of platelet activation biomarkers P-selectin and B-thromboglobulin, suggesting continuous platelet activation, therefore ongoing PMP release ([Caine et al., 2004](#)). Experiments using BC cell lines MDA-MB-231 and MCF-7 suggest that these cancerous cells influence the release of PMPs containing specific bioactive molecules directed at increasing the metastatic potential of these cancers ([Zarà et al., 2017](#)). Hyper-activation of platelets is associated with high risk of thrombosis in several diseases, including diabetes, whereas hypo-reactivity of platelets leads to the formation of bleeding disorders ([Dangwal and Thum, 2013](#)).

As PMP levels are highly elevated in both BC and T2DM patients, they could be considered valuable biomarkers, as their levels can

be used to estimate the biological state of a subject ([Mezouar et al., 2014](#)). As certain types of cancer express high angiogenic activity, a rise in PMP levels would follow. Although high levels of PMPs have been associated with aggressive tumours and poor clinical outcome, they are not yet considered a sufficient marker for survival rates. Because of their association with aggressive tumours however, PMPs might be considered a possible therapeutic target via anticoagulant treatment ([Singh et al., 2014](#)).

Altered miRNA signatures were identified in T2DM patients, where some had further myocardial infarction. Circulating levels of cancer associated miRNAs have been correlated with circulating PMP levels. High expression levels of miR-21 have been linked with cellular proliferation and tumour development ([Iorio et al., 2005](#)). Some of these platelet-derived microRNAs have been responsive to antiplatelet therapy ([Willeit et al., 2013](#)).

A new family of miRNAs called oncomiRNAs has emerged more recently. One of their main characteristics is promoting tumour invasiveness in breast cancer by suppression of Mef2c (Myocyte enhancer factor 2c) ([Liang et al., 2015](#)). The miRNA, in the case of [Liang et al. \(2015\)](#)'s study, miR-223, targets the 3' UTR of erythrocyte membrane protein band 4.1 like 3 (EPB41L3), it being the most upregulated miRNA in recurrent tumours. In HUVECs, miR-223 targets IGF-1R and induces advanced glycation end products (AGES), and promotes cell invasion in lung cancer ([Liang et al.,](#)

2015).

1.3 Breast Cancer

History and Epidemiology

Since ancient times, the female breast has been seen as a symbol of beauty, femininity and fertility. Written records of breast cancer exist since antiquity, most likely due to the location and easier identification of the disease. The oldest recorded case was found in the Edwin Smith Surgical Papyrus. In the translation by James Henry Breasted, an unknown physician from ancient Egypt was the first to introduce the term "tumour" in his description of the disease, in cases 39 and 45. Case 45, however, represents a closer description of breast cancer as not a result of a direct injury to the patient and the "bulging tumours" are described as cold, hard and not filled with fluid. The physician himself notes there is no treatment for case 45 (Breasted, 1930). The nomenclature of the disease was not established until Galen, who further described the tumour and the associated veins as closely resembling a crab, which is the greek translation for cancer (Lewison, 1953).

The history of BC identification and treatments continue to ancient Greece, where the disease was believed to be healed by making offerings to Asclepius, the god of Medicine (Lyons and Petrucelli, 1988). Hippocrates suggested the theory that breast cancer was

attributed to an imbalance of the four humours, a first look into the cause of breast cancer, described in Homer's Illiad. In the 1st century AD, Leonidas of Alexandria described what could be interpreted as early surgery techniques involving incision and cautery of the tumour site, followed by Albucasis who developed a primitive surgery of mastectomy with the use of caustic pastes and extraction of tissue. This can also be considered an early form of chemotherapy ([Cooper, 1941](#)). From Renaissance until the 21st century, the cause and formation of breast cancer has been investigated and since the invention of the microscope, the humoral imbalance theory was dismissed. The microscope allowed for the observation of the structural differences between normal and cancerous cells, identifying metastatic progresses ([De Moulin, 2012](#)). The 20th century has seen a faster development in treatment and surgery of breast cancer, such as the development of radiation therapy, identification of the hormonal dependency to breast cancer as well as less invasive mastectomies.

Closer to recent years further treatments have been developed that led to the beginning of anti-neoplastic drug clinical trials, achieving promising results, first for Hodgkin's lymphoma, followed by osteosarcomas and colon cancer ([A.S.o.C.O., 2011](#)). In 1971 total mastectomy was introduced, which consisted of removal of only the breast tissue in early stages of breast cancer. This led to better prognostics and a faster recovery, and a few years later, in

1975, adjuvant chemotherapy was prolonging the lives of breast cancer patients over the five year mark. The lumpectomy in the late 1970s has improved the quality of life of cancer patients even further (A.S.o.C.O., 2011).

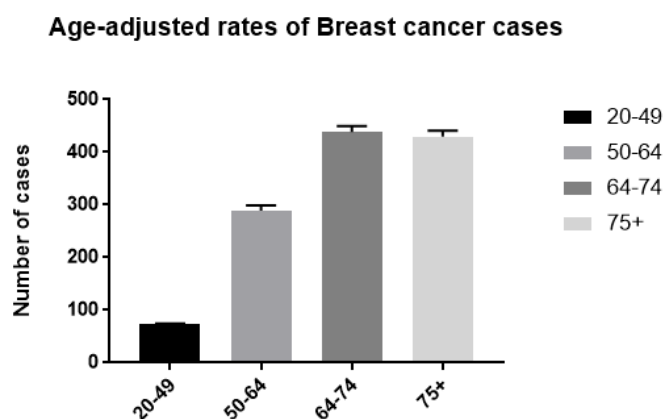


Figure 1.3: **Incidence of female breast cancer by age group.** Data obtained from the National Cancer Institute, Surveillance, Epidemiology and End Results Program, freely available on <https://seer.cancer.gov/>. Results were represented as a graph for better visualisation.

In recent years, the incidence of breast cancer in female patients has increased significantly (Liao et al., 2011). BC is now the most commonly occurring cancer in female patients and roughly one third of all cancers in women (Harris et al., 1992) with a median survival time between 18 to 24 months, depending on the molecular profile of the tumour (Toss et al., 2017). As seen in Figure 1.3, the incidence of breast cancer also increases with age and hormonal

status. Breast cancers of women within the group of 20 to 49 years of age represent less than 6% of the total cases. The highest increase can be observed within the 64-74 years group, representing just over 35% of total breast cancer cases. This follows the trend, as with other cancers, that risk increases with age, with the median age at diagnosis being 62 years ([Ferlay et al., 2015](#); [Liao et al., 2011](#)).

Statistical data used in this text is of US origin, as the National Cancer Institute has compiled detailed data with regards to BC diagnosis and treatment. As reported by the National Cancer Institute, the most prevalent cases of breast cancer diagnosis are white women, 128.6 cases per 100 000 people in the US, followed by black women, 126.9 cases per 100 000 people. Although most cancers are diagnosed in postmenopausal women, there are 4% of the total cases which are diagnosed in women under 40. This is a small number to justify introducing regular screening programs, leaving young people with increased risks. Cancers in young adults are the most aggressive, making it more difficult in this particular group to decrease mortality rates ([Ferlay et al., 2015](#)).

Breast cancer has an incidence of 2% of the overall female population ([McPherson et al., 2000](#)), but it has been reported that mortality rates are increased in black women under the age of 57, after receiving a BC diagnosis ([Jatoi et al., 2005](#)). Data has also been made available from European countries and in 1990 it was observed that 20% more of patients diagnosed with breast can-

cer have passed the 5 year survival mark in the US compared to European countries (Coleman et al., 2008). Although women are predominantly affected by breast cancer, male breast cancer represents 1% of all BC cases. The number of male breast cancer patients has remained generally stable over the last 30 years, with a risk of 1 in 1000 of developing the disease (Howlader et al., 2013).

Development of breast cancer is more predominant in developed countries, rather than developing ones (Ferlay et al., 2010). This suggests that while genetic factors may play a role in the development of the disease, environmental influence is an important risk factor to be taken into consideration. Putting lifestyle and environment aside, the difference between the demographic regions could also be attributed to lower availability of screenings, misdiagnosis or limited availability of treatment (Ferlay et al., 2015). This, as well as an increase of 22% of survival rates since the introduction of BC population-wide screenings, observed between 1973 and 1992, increased the gap between developed and developing countries (Iqbal et al., 2015). Coleman et al. (2008) does raise a few important points regarding data collection, analysis and focus on the different methods of detection, diagnosis and survival rate criteria from a range of different countries. The study has concluded that cancer survival rates depend on the availability of a diagnostic and treatment service, as well as the difference between the investment or under-investment of countries in their health services. The

differences in data collection between high-income and low income countries make it difficult, in current circumstances, to create a useful comparison of cancer survival rates.

Of the risk factors to be considered, women with early menarche have an increased chance of developing breast cancer, with the risk increasing by approximately 50% if the age of menarche is below 12 years of age. If the age of menarche is 15 years or older, then the risk of developing premenopausal breast cancer decreases by 9% for every late year ([Clavel-Chapelon and Gerber, 2002](#)). [Peto \(2001\)](#) agrees that late menarche, early childbirth and early menopause decrease the risk of breast cancer, while combined contraceptives and post-menopausal smoking increase the risk. Breast cancer is the most predominant cancer in pregnant women, with a frequency of 1 in 3000 pregnant women every year ([NationalCancerInstitute, 2018](#)). Medical risk factors are a high BMI, low physical activity, diet, alcohol, smoking, or exposure to secondhand smoke and radiation. [Peto \(2001\)](#) confirms that a high BMI represents a high risk for developing breast cancer, especially in post menopausal women. The Western diet is also viewed as a cofactor, as it is strongly associated with obesity and early menarche ([McPherson et al., 2000](#)). However, [Li et al. \(2013\)](#) argues that on its own, menarche does not represent a statistically significant difference to be categorised as a risk factor, but the interval between menarche and age at first birth represents a more important risk factor.

A study was carried out on the incidence of breast cancer in migrants compared to the local population in Japan and Hawaii, and it found that within two generations, there was no significant difference between the migrants and the native inhabitants. Thus this study suggests that environmental factors are very important in the development of breast cancer ([McPherson et al., 2000](#)).

Some biological factors, identified by the same group are benign breast disease, breast density, lobular carcinoma *in situ*. Apart from these risk factors, there are also genetic factors such as gene mutations, with an example being the *BRCA1* and *2* genes situated on chromosomes 17 and 13 ([McPherson et al., 2000](#)), Li-Fraumeni syndrome, Cowden syndrome and other moderate-risk genes, such as *ATM*, *BRIP1*, *CHEK2*, *NBN*, *PALB2* and *RAD50* ([Rojas and Stuckey, 2016](#))

[McPherson et al. \(2000\)](#) has analysed the incidence of breast cancer within families and suggests that roughly 10% of breast cancer cases can be attributed to genetic factors. This study presents the criteria for identifying people with potential high risk as the following: "One first degree relative with bilateral breast cancer or breast and ovarian cancer or one first degree relative with breast cancer diagnosed under the age of 40 years or one first degree male relative with breast cancer diagnosed at any age or two first or second degree relatives with breast cancer diagnosed under the age of 60 years or ovarian cancer at any age on the same side of

the family or three first or second relatives with breast and ovarian cancer on the same side of the family” (McPherson et al., 2000), and very high risk as ”Families with four or more relatives affected with either breast or ovarian cancer in three generations and one alive affected relative” (McPherson et al., 2000).

Biology of the Breast

The breast tissue begins to form in the 6 week old embryo, by formation of the ”milk line”, also known as the ducts. Originally they extend from the axilla to the inguinal region, but as the embryo develops, the ”milk line” begins to atrophy in all but the pectoral region, where they become hollow, and the nipple begins to form by 8 months (Seltzer, 1994). With age, the breast tissue begins to develop, from a ”breast bud”, the areola begins to grow larger in size and the nipple begins to grow outwards. Oestrogen is the first hormone involved in the development and growth of the breast tissue, with progesterone continuing the formation of the lobes (Seltzer, 1994).

The breast is located on top of the pectoralis major muscle, surrounded by the superficial fascia (Seltzer, 1994), being supported in the back by fibrous stroma and Cooper’s ligaments connecting the fascia to the muscle. The outer region is bordered by the midaxillary line and medially by the sternum and the serratus anterior muscle on the lower border. The upper lateral margin, also named

the tail of Spence, connects to the axillary region (Seltzer, 1994). The breast itself comprises of glandular tissue and adipose tissue, in various levels, depending on a woman's age and weight (Kumar et al., 2005). Each breast is formed of 12-20 lobes, each of those organised in lobules containing 10-100 acini. These acini are connected to ductules leading gradually to the segmental ducts. These ducts drain in the lactiferous sinus which further secretes to the collecting duct leading to the outer surface of the nipple (Seltzer, 1994), see figure 1.4. The blood supply is supported by the internal mammary artery, the axillary artery, the thoracoacromial arteries and the main vein is the internal mammary vein. In terms of lymphatic drainage, the breast is surrounded on the lateral margin by the ipsilateral axillary nodes and medial by the internal mammary nodes (Seltzer, 1994).

Biology of Breast Cancer

Breast cancers have been classified several different ways, mainly by location of initial tumour site and the presence or absence of receptors. In the case of receptor based classification, there can be one or a combination of hormonal receptors for oestrogen (ER), progesterone (PR) and human epidermal growth factor 2 (HER2). Breast cancers devoid of all receptors are classed as triple negative breast cancers and represent some of the rare and most aggressive cases of breast cancer, commonly among young women (Mohamed et al., 2013). Another common type of classification are Lumi-

nal, Basal A and Basal B. These types of cells have different morphologies and invasive potential. Luminal cells are characterised by growth in clusters, showing tight cell-cell junctions, basal B cells present a morphology closer to mesenchymal cells, whereas basal A cells can share characteristics with either of the two other categories ([Neve et al., 2006](#)).

The hallmarks of cancer are sustained proliferation, evasion of growth suppressors and from immune-mediated destruction, apoptosis prevention, tumour promoting inflammation, angiogenesis, tumour invasion and metastasis, genome instability, mutations and deregulations of cellular energetics ([Hanahan and Weinberg, 2011](#)). The presence of metastasis is directly correlated with survival rates. Cells acquire alterations of their phenotype, where endothelial cells lose their phenotypic characteristics and gain mesenchymal characteristics ([Potenta et al., 2008](#)). This process is characterised as epithelial to mesenchymal transition (EMT), followed by intravasation of the cancer cells and their further transport through the circulatory and lymphatic systems. This continues with extravasation, mesenchymal to epithelial transition and, finally, the development of metastatic foci ([Singh et al., 2014](#)). In circulation, platelets and components of the coagulation system support tumour cell survival by protecting them from cytotoxic immune cell recognition. Platelets escort tumour cells in the circulation to the site of extravasation ([Saito et al., 2021](#)). Patients with breast cancer

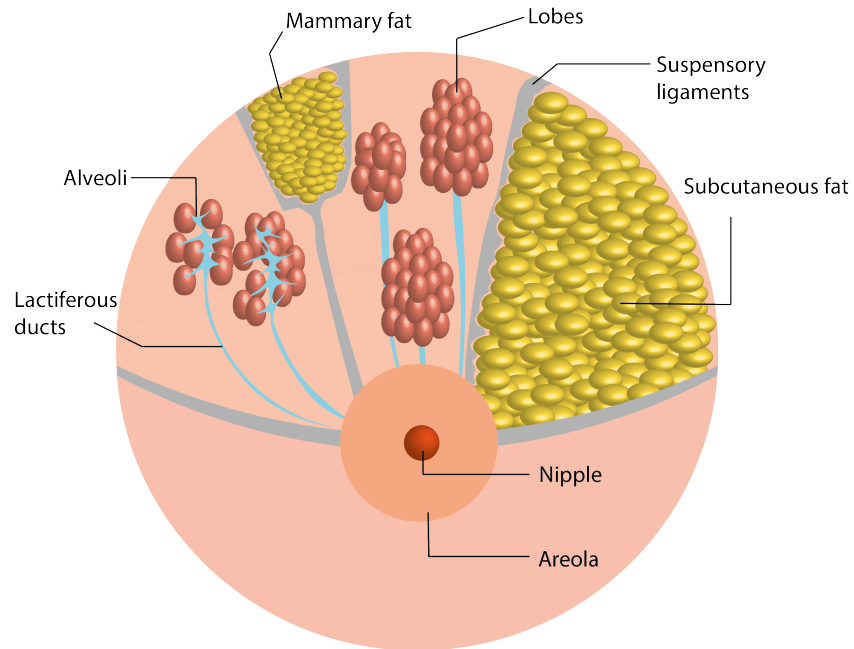


Figure 1.4: **Anatomical structures present in the breast.** Graphical representation of the structures present in the female breast. A layer of subcutaneous fat lies covering the sac like lobe formations, consisting of alveoli (lobules or acini) and lactiferous ducts. Between these lobes exists the mammary fat and supporting the structure of the breast are the suspensory ligaments.

also have an increased risk of thrombosis and an increased platelet count. This last aspect has been associated with low survival rates (Lal et al., 2013).

Research involving the study of exosomes, which can be considered closely related to platelet microparticles due to their characteristics, has found that exosomes released by pancreatic tumour cells help create an optimal environment for migrating metastatic can-

cer cells, via their involvement in pre-metastatic niche formation, a process regulated by TGF β signalling (Costa-Silva et al., 2015). This raises the question of whether breast cancer tumour derived microparticles could present similar characteristics, for which Yuan et al. (2021) has recently provided an answer. Yuan et al. (2021) have found that breast cancer-released exosomes play an important role in the formation of a pre-metastatic niche in bone metastasis conditions, with miR-21 playing a key role in the process.

The androgen receptor (AR) is present in a vast majority of primary tumours and in many metastatic lesions. Although estrogen receptor α (ER α) plays an important role in the growth and development of breast cancer, AR is expressed more commonly *in situ*, in invasive and in metastatic breast cancer. The expression of AR has become a favourable prognostic indicator, as patients with a high expression of it show a good response to chemotherapy and hormonal therapy (Casaburi et al., 2016). Androgens-activated AR inhibits endogenous cyclin D expression and downregulates C-MYC and K-RAS protein expression by upregulating miRNA let-7a. High levels of miR-21 have been associated with breast cancer cell growth. AR contributes to the reduction of breast cancer cell growth by inhibiting miR-21 expression, through the recruitment of HADAC3, part of an AR-mediated transcriptional repression mechanism, on the miR-21 promoter (Casaburi et al., 2016).

Non-coding RNAs have shown a correlation between their circulating levels and cancer stages, but most likely due to the lack of consistency in sample preparation, there continue to be discrepancies across studies ([Abrahamsson and Dabrosin, 2015](#)). In neoplasms, miRNAs target messenger RNA that lead to the synthesis of proteases, adhesion molecules and other components of cellular processes associated with cell integrity. This characteristic suggests that these miRNAs are encouraging as therapeutic targets and should be researched in further detail ([Rana et al., 2013](#)). The altered nature of miRNAs in several malignancies can be attributed to a number of different factors such as chromosomal modifications of miRNA genes, altered epigenetic mechanisms, miRNA synthesis errors or DNA point mutations ([Di Leva and Croce, 2013](#)).

In breast cancer, miR-21 is significantly upregulated, with further increase in the presence of high levels of sex steroids. The anti-estrogen tamoxifen downregulates miR-21. Low levels of miR-21 have also been detected in postmenopausal cohorts. miR-21 affects tumour suppressor protein PTEN, thus having a direct effect on cancer progression. miR-21 could potentially be considered a therapeutic target in breast cancer ([Gao et al., 2015](#)). A possible target for gastric cancer is miR-1, which has been found in upregulated levels in the plasma of patients. miR-10b is downregulated in colon, renal and melanoma neoplasms, but its levels are not affected within breast cancer tumours ([Mo et al., 2012](#)).

The miR-29 family has shown correlations with cycle regulations, cell migration and metastasis formation ([Gebeshuber et al., 2009](#)). An increase of miR-29a levels in murine models has been linked to a high number of metastatic foci in lung cancer. The high tumour cell proliferation was not associated directly with the increased miR-29a levels ([Gebeshuber et al., 2009](#)). The same study found that high levels of miR-29a alter the polarity of cells, thus promoting EMT. Cellular miR-148 has been associated with epithelial to mesenchymal transition and metastasis formation. miR-203 appears to be elevated in patients with metastatic breast cancer and increased numbers of circulating tumour cells. Cellular miR-203 can potentially inhibit bone metastasis in prostate cancer, but appears to increase metastasis in breast cancer, by affecting EMT. In the case of breast cancer, miR-203 levels do not increase significantly compared to healthy controls. However, there are higher levels of extracellular miR-203 in pre-menopausal cohorts, compared to post-menopausal, and even further increased in the luteal phase. With a possible physiological function, miR-146a is present in higher levels in pre-menopausal cohorts, with lower levels in breast cancer and post-menopausal tissue. miR-193b was only found intracellularly, in high levels in pre-menopausal luteal phase compared to the low levels in post-menopausal women, and its levels have not been affected by tamoxifen. In conclusion, levels of extracellular miRNA in breast tissue show a strong correlation with levels of hormone exposure ([Abrahamsson and Dabrosin, 2015](#)).

1.4 Type 2 Diabetes Mellitus

Type 2 Diabetes Mellitus (T2DM) is a noncommunicable disease, also known as "noninsulin dependent diabetes" ([AmericanDiabetesAssociation, 2005](#)), along with cardiovascular disease and hypertension. Over the years, diabetes has significantly raised mortality rates, resulting in rates comparable to those of certain cancers ([Zimmet, 2000](#)). The number of diabetic patients diagnosed has considerably increased over the last 20 years, possibly due to the alert pace of changes in the socio-economic environment ([Amos et al., 1997](#)). T2DM is the most predominant form of diabetes, representing around 90-95% of total cases, across all ages ([Samuel et al., 2018b](#)). Once considered a metabolic disease strictly associated with adulthood, T2DM cases in children and young adults have been increasing significantly in recent years ([SEARCH, 2006](#)). Currently, T2DM has reached epidemic proportions and further studies have shown that an impaired glucose metabolism represents a strong risk factor for the development of gastric and lung cancers and can have a negative impact on future therapies ([Vigneri et al., 2009](#)). [Bowker et al. \(2017\)](#) have found that breast cancer, in particular, has an increased incidence in T2DM patients and underlines the urgency of a better understanding of this link. [Cohut \(2017\)](#) suggests that due to the increase in diabetes and obesity cases, the incidence of cancer will proportionally increase. Two of the key changes in T2DM are a rise in platelet aggrega-

tion and in blood coagulation ([Schafer, 1985](#); [Garcia Frade, 1987](#)) with high levels of PMP markers P-selectin and CD40 present in circulation ([Burnier et al., 2009](#)).

The American Diabetes Association has released, in 2017, a list of classifications of diabetes such as Type 1 Diabetes, Type 2 Diabetes, gestational diabetes mellitus and other specific types of diabetes such as maturity-onset diabetes of the young and neonatal diabetes. Although originally, type 1 diabetes was attributed to children and type 2 diabetes to adults, the barriers are no longer as clear. Due to this, a specific diagnosis is difficult at the time of first diagnosis, however, it can be observed in time by monitoring symptoms. Initial diagnosis is based on fasting plasma glucose measurement, a 2 hour plasma glucose measurement after 75-g oral glucose tolerance test or HbA1c levels measurement, with the latter being the most advantageous. The normal cut point for fasting glucose measurement is 7 mmol/L, which can lead to a third more positive results, and HbA1c has a cut off point of 6.5 % or 48 mmol/mol and is a more convenient test to perform ([AmericanDiabetesAssociation, 2005](#)).

T2DM is characterised by insulin resistance and relative insulin deficiency, noninsulin-dependent diabetes ([Liao et al., 2011](#)). Most T2DM patients are obese, which is itself considered a risk factor for this disease. Other patients present a larger amount of body fat distributed mainly around the abdominal region and diet and

lifestyle are also considered relevant risk factors. This form of diabetes normally goes undiagnosed for long periods of time, due to gradual increase in circulating glucose levels and it often takes years until patients begin to develop or take notice of classic symptoms and further complications. ([AmericanDiabetesAssociation et al., 2014](#); [Samuel et al., 2018b](#); [AmericanDiabetesAssociation, 2005](#)).

[Chen et al. \(2012\)](#) has compiled a list of risk factors for T2DM. They have categorised them in two groups: modifiable and non-modifiable risk factors. Obesity, physical inactivity, smoking, hypertension and previously identified glucose tolerance are considered modifiable risks, whereas age, sex and family history of T2DM are considered unmodifiable risk factors.

The exact mechanisms of T2DM development are unknown, however it has been demonstrated that the β -cells located in the pancreas remain intact and insulin resistance establishes within the organism. Insulin resistance has also been associated with obesity, or an increased amount of visceral fat, but not as pronounced as it is in diabetic patients. Ketoacidosis is also a symptom specific to diabetes, however in the case of T2DM, it is only present in the case of a secondary complication, such as an infection ([American-DiabetesAssociation, 2005](#)).

In patients with breast cancer, there is also an increased risk of thrombosis and high platelet activation. BC patients with a high

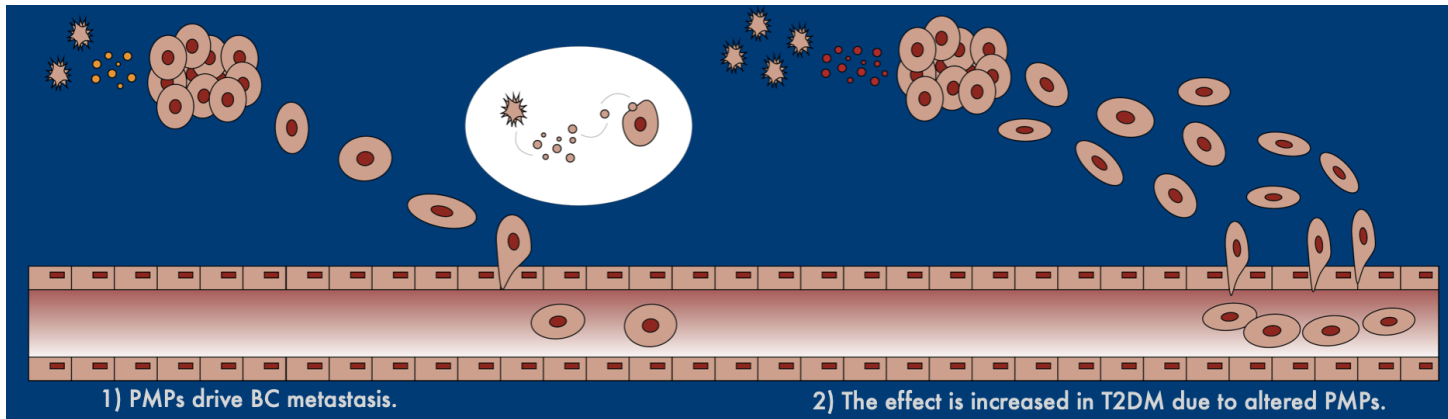
platelet count have a low survival rate, proving a strong link between platelet activity and BC growth and proliferation (Lal et al., 2013). Both BC and T2DM share common risk factors such as age, obesity and reproductive stage (Vona-Davis et al., 2007), although some studies identify diabetes as a risk factor for BC (Madigan et al., 1995; Tavani et al., 1997). High platelet count and platelet hyperactivity have been associated with diabetes and appears to be more severe in diabetic patients presenting vascular instability (Kachekouche et al., 2018) .

1.5 Project Aims

Investigating the implication and activity of the patient's haemostatic system in the development of breast cancer represents a key step in the identification of potential therapeutic targets (Lal et al., 2013). Currently, based on the identification of the miRNA families present in patient samples, it is possible to identify the subtype of breast cancer as well as the cancer development stage, however, this is yet to be implemented in a clinical setting (Di Leva and Croce, 2013). Through these studies, however, the importance of the role miRNA has within the context of gene expression and regulation is highlighted. In the case of breast cancer, as most cancers, the dysregulation of messenger RNA leads to changes in cell function and activity and promotes tumour development (Rana et al., 2013).

The aim of this project is to identify the potential effect PMPs originating from T2DM patients have on BC development by analysing:

- Size and concentration of PMPs in order to ensure quality and appropriate amounts of diabetic and non-diabetic PMP samples used.
- The potential of PMPs to deliver genetic information from origin to target cells.
- miRNA sequencing of ND and T2DM PMPs in order to investigate the presence of altered miRNA expression profiles in T2DM PMPs compared to controls.
- The phenotypic effects elicited by ND and T2DM PMPs on BC cells.



Visual Hypothesis of this study.

Chapter 2

Materials and Methods

2.1 Cell lines

Several breast cancer cell lines were used throughout this study. MDA-MB-231, MDA-MB-468 and BT20 cell lines are representative of basal breast cancer, MCF-7 and T47D representative of luminal breast cancer, MDA-MB-453 and BT474 are representative of HER2 receptor positive breast cancer and HB2 representative of luminal epithelia. As noted on the ATCC website, most cell lines were isolated via pleural effusion. The MDA-MB-453 cells were isolated via pericardial effusion. The BT20 and BT474 cells were isolated from solid tumours. The HB2 cell line was established via the isolation of luminal epithelia from human milk followed by immortalisation with simian virus 40 large T antigen, as explained by [Caradonna and Luparello \(2014\)](#).

Unless otherwise stated, all cell lines were supplied from ECACC, certified mycoplasma free, maintained in DMEM (Gibco), with 10% fetal calf serum (Sigma, UK) and 100U/ml Penicillin and 100 $\mu\text{g}/\text{ml}$ Streptomycin, both obtained from Thermo Fisher Scientific, unless stated otherwise. Cells were cultured at 37°C with 5% CO_2 and passaged at approximately 80% confluency. For a full list of cell lines used and growth media please refer to Table 2.1. All cell lines were cultured in phenol red free DMEM, as phenol red is known to act as a weak oestrogen mimic ([Welshons et al., 1988](#)) with a possible effect on oestrogen sensitive cell lines, such as MCF-7 and T47D.

2.2 Mycoplasma detection and elimination

Mycoplasma detection

Mycoplasma detection was carried out using the VenorGeM Classic detection kit (Minerva Biolabs). Master mix was created using 14.5 μl of water, 2.5 μl of 10x Reaction Buffer, 2.5 μl of Primer/Nucleotide Mix, 2.5 μl internal control DNA and 1 μl Taq (approx. 1 unit). 2 μl of either cell culture supernatant, positive control and negative control (water) were added to the mix and briefly vortexed. The PCR reaction protocol is described in table 2.2.

2% agarose gel was prepared in TBE buffer, with 5% v/v Ethidium Bromide, loaded and ran at 100V for 20 minutes. The PCR results

List of cell lines and conditions		
Cell line	Breast cancer type	Complete growth media
MDA-MB-231	Basal	DMEM/MEM,10% FBS,1%Pen-Strep
MDA-MB-468	Basal	DMEM, 10% FBS, 1%PenStrep
BT20	Basal	DMEM, 10% FBS, 1%PenStrep
MCF-7	Luminal	DMEM, 10 % FBS, 1%PenStrep
T47D	Luminal	DMEM, 10% FBS, 1%PenStrep
MDA-MB-453	HER2 +ve	DMEM, 10 % FBS, 1%PenStrep
BT474	HER2 +ve	DMEM, 10% FBS, 1%PenStrep
HB2	Luminal Epithelia	DMEM, 10 % FBS, 1%PenStrep

Table 2.1: List of cell lines used and their matching growth media and supplements.

Table 2.2: PCR amplification for the VenorGeM Classic detection kit was carried out at:

Cycles	Temperature	Time
1	94°C	2 minutes
39	94°C	30 seconds
	55°C	30 seconds
	72°C	30 seconds
Hold	4-10°C	

were visualised using a ChemiDoc MP Imaging System (Bio-Rad).

Mycoplasma elimination treatment

Cell lines were treated, preventively, using the Mynox Gold (Minerva Biolabs) mycoplasma elimination treatment. The Starter Treat-

ment Mynox Gold (500 μ l) was added to 4.5 ml of cell suspension in 5% FCS and incubated in a T75 flask. When cells reached confluency, at further passages, Mynox Gold Main Treatment (500 μ l) was added two more times to 9.5 ml cell suspension. Cells were then tested using the Venor-GeM Classic detection kit to determine if further treatment was required.

2.3 Platelet microparticle collection

Volunteer recruitment and blood collection

Sample collection was carried out in accordance to the Health Research Authority regulations, IRAS project ID 235632, at the University of Bradford and, following relocation, at the University of Huddersfield for non-diabetic volunteers and at the Bradford Royal Infirmary, Diabetes and Endocrinology Unit for diabetic volunteers. Individuals were asked to fill in a consent form after being given details regarding the project and sample collection. All volunteers were given the opportunity to ask questions regarding collection and the project. All volunteers were informed that samples were to be anonymised, that they would not receive any results back in relation to their sample and that their samples would be destroyed the same day.

For this study, both non-diabetic and Type 2 Diabetic volunteers were recruited for blood donations. Healthy volunteers are defined

as individuals who have no history of chronic illnesses and are not under continuous medication. Diabetic volunteers are defined as individuals who have received a diagnosis of Type 2 Diabetes Mellitus, with confirmed glycated haemoglobin (HbA1c) levels over 6.5% (48 mmol/mol) ([AmericanDiabetesAssociation, 2005](#)).

Platelet microparticle isolation and characterisation was carried out in accordance to the recommendations of the Minimal information for studies of extracellular vesicles 2018 (MISEV2018), released by the International Society for Extracellular Vesicles ([Théry et al., 2018](#)).

Platelet Isolation

24 ml of venous blood was collected using a hypodermic 21g needle connected to a 30 ml syringe containing 6 ml of sterile filtered ACD (29.9 mM sodium citrate, 113.8 mM glucose, 72.6 mM sodium chloride, 2.9 mM citric acid) acting as anticoagulant. The mixture of blood and anticoagulant was transferred to a 50 ml Falcon tube and centrifuged at 191 RCF for 20 minutes at room temperature, within 60 minutes of collection. The platelet rich plasma (PRP) was carefully extracted from the tube using a P1000 pipette and transferred to a 15 ml Falcon tube. Platelet activation was prevented by adding 50ng/ml of Prostaglandin E1 (PGE1) to the PRP and samples were centrifuged again at 762 RCF for 12 minutes. The platelet pellet was resuspended in 500 μ l sterile filtered C/S buffer

(150 mM sodium chloride, 5mM HEPES, 0.55 mM NaH₂PO₄, 7 mM NaHCO₃, 2.7 mM KCl, 0.5 mM MgCl₂, 5.6 mM glucose) and the PRP was transferred to a clean 15 ml tube and centrifuged again at 1470 RCF for 10 minutes. Both resultant pellets were then combined and resuspended in 2.5 ml of C/S buffer and left for one hour at room temperature to allow for PGE1 inactivation before continuing with microparticle isolation. The platelet free plasma was discarded.

Platelet Microparticle Isolation

Platelets were incubated with 0.1 U/ml thrombin at 37°C for one hour in a shaker, to activate the platelets *ex vivo* and induce microparticle release. The reaction was stopped after one hour by adding 20 mM EDTA and 50 ng/ml PGE1. The sample was centrifuged at 1470 RCF for 10 minutes. The supernatant was transferred into two 1.5 ml eppendorf tubes and centrifuged at 20 000 RCF, at 18°C for 90 minutes. The pellets were finally resuspended in 100 µl of sterile C/S buffer and stored at - 80°C until use.

2.4 Platelet microparticle characterisation

The following methods were used to determine the size and origin of the isolated microparticles, in order to ensure they correspond to the available literature.

The Bradford Assay

The Bradford Assay (Bio-Rad) was used to determine protein concentration of PMP samples in order to ensure consistent use of sample concentration across all experiments.

10 μl of sample or standards were pipetted into each well of a clear 96 well plate (StarLab) followed by 200 μl of Bradford Assay reagent. The plate was incubated at room temperature for 10 minutes. Absorbance was then measured at 595 nm. The standards used were 125 $\mu\text{g}/\text{ml}$, 250 $\mu\text{g}/\text{ml}$, 500 $\mu\text{g}/\text{ml}$, 750 $\mu\text{g}/\text{ml}$, 1 mg/ml, 1.5 mg/ml and 2 mg/ml. The concentration used across all experiments has been 100 $\mu\text{g}/\text{ml}$ PMP protein.

Nanosight analysis of PMPs

PMPs size and density was measured via the NanoSight NS300 (Malvern Panalytical). The NanoSight NS300 analyses individual particles and characterises them based on Brownian motion and particle scatter in order to measure size and concentration of platelet microparticle samples. With the help of a 1 ml syringe, a 1 : 20 000 dilution of PMP sample in C/S buffer was loaded onto a syringe pump connected to the NanoSight NS300. The dilution was used to ensure the machine was working at its optimal of 20-100 particles per frame. A laser beam excited the particles and the light scattering was measured by a microscope with the focus

between -98 to -79, camera sensitivity at 75 and shutter at 100. The microparticles were infused at speed 100 first, then slowed to 75 and three 90 second videos were recorded and analysed using the protocol in table 2.3. The detection threshold was 4-7. Concentration and size were measured via the software provided by Malvern Panalytical.

Flow Cytometry Analysis

Flow cytometry is one of the most prevalent methods of PMP analysis, which uses a stream of fluid transferring the cells through an interacting laser beam. Light scattering and fluorescence emission detection measurements help provide information regarding the physical and compositional characteristics of the analysed samples ([Lacroix et al., 2010](#)).

Flow Cytometry analysis was performed at Leeds Beckett University, using the BD Accuri C6 Flow Cytometer (BD Biosciences). The conjugated antibodies used were FITC Annexin V and PE Mouse anti-human CD41a, both acquired from BD Biosciences, see table 2.10.

Table 2.3: 1 ml undiluted PMP samples were loaded onto the NanoSight NS300. The machine protocol for PMP analysis is presented below:

Actions
Syringe load : 100
Delay : 1 second
Repeat Start
Capture : 90 seconds
Delay : 1 second
Repeat 2
Syringe Stop
Process Settings
Export Results

Undiluted non-diabetic PMP samples were incubated in the presence of one or both conjugated antibodies, at the indicated concentrations, as per instructions provided by the supplier, at room temperature for 20 minutes. Samples were then analysed using the BD Accuri C6 Flow Cytometer and analysed using the dedicated BD Accuri C6 software.

PMP purification and labelling

PMP samples were incubated with 1 μ M Cell Tracker Red and/or 1 μ M SytoRNA Select dye for 20 minutes at 37 °C. In the meantime,

Exosome Spin Columns were prepared by allowing the gel to settle for 15 minutes, after adding nuclease free water and any bubbles were eliminated. The columns were placed in collection tubes and centrifuged at 750 RCF for 2 minutes at room temperature to eliminate excess buffer. The orientation of the columns in the centrifuge was noted.

Following incubation, stained PMPs were carefully pipetted on the centre of the gel bed inside the column, without disturbing the gel surface, and the column placed into a 1.5 ml elution tube. Columns were then placed into the centrifuge in the same orientation as before and samples were centrifuged at 750 RCF for 2 minutes at room temperature. The PMP mixture was transferred to the elution tube via centrifugation and the Exosome Spin Columns were discarded.

Fixation and visualisation of labelled PMPs

MCF-7 and MDA-MB-231 cells were seeded the previous day at 20 000 cells per well in serum containing DMEM, in an 8 well chamber slide (Nunc). On the day of the assay, prior to the co-incubation with PMPs, the cells were serum starved for 4 hours. Cells were incubated with fluorescently tagged and untagged PMPs for 30 minutes and 2 hours.

The wells were then washed three times with sterile PBS and fixed in ice cold 95 % methanol for 20 minutes at -20 °C, followed by three more washes in PBS. The well walls were carefully removed using the tools provided in the kit. Once the slide was completely dry, a drop of Vectashield Antifade Mounting Medium with DAPI (Vector Laboratories) was added to each of the wells and a coverslip was applied. Slides were stored at 4 °C until visualised. The conditions prepared were cells incubated without PMPs, cells incubated with untagged PMPs, cells with SytoRNA Select tagged PMPs, cells with Cell Tracker Red tagged PMPs and cells with PMPs tagged with both Cell Tracker red and SytoRNA Select. The concentration of PMPs used was 100 µg/ml.

The slides were visualised using a Nikon Eclipse 80i fluorescence microscope, viewed at x100 objective with oil immersion. They were also visualised using a Zeiss LSM 880 with Airyscan. Images were taken with the x40/1.4 objective with oil immersion and the following three filters were applied: Ch2 : 599 - 734, ChS1: 490 - 606, Ch1 : 410 -508. The lasers used were 594 nm : 4.0% (red), 488 nm : 0.9% (green) and 405 nm : 2.0% (blue).

Scanning Electron Microscopy Analysis of PMPs

PMP samples were purified by ultracentrifugation at 20 000 RCF for 90 minutes at 18 °C and resuspended in nuclease free water. A strong presence of crystals in the samples was observed, which

led to exosome spin columns being used in purifying the PMP samples. Samples were fixed on both glass slides and Polyethylene terephthalate (PET).

SEM was performed using an FEI Instruments Quanta FEG SEM instrument in the back scattering electron mode. Samples were prepared by allowing a small amount of approximately 10 μl to air dry on a suitable mount before gold coating using a Quorum Instruments SC7620 sputter coater to give a coating of approximately 3 angstroms. The back scattered electron images (BSEI) were captured using an accelerating voltage of 20keV. Samples were visualised at magnifications ranging from x500 to x20 000.

2.5 Cell viability measurement of BC cells incubated in the presence of PMPs

Breast cancer cells were seeded at 5000 cells/well in complete growth media in white 96 well plates (Scientific Laboratory Supplies). The cells were serum starved for 4 hours, followed by incubation in 150 μl of SF media with or without 100 $\mu\text{g}/\text{ml}$ diabetic or non-diabetic PMPs throughout the assay. Cell viability was measured at 0, 24, 48 and 72 hours. To measure this, cells were co-incubated with 150 μl of CellTiter Glo Luminescence Cell Viability Assay kit or CellTiter Glo 2.0 (Promega) for 15 minutes at room temperature, in the dark. The basis of this assay is to

quantify the levels of ATP present in the cells, which functions as an indicator for metabolically active cells. Luminescence was measured using the Glomax Explorer Multimode Microplate Reader (Promega). Results were normalised using percentages, where 0 hours was considered as 100%. Statistical analysis was performed using the Prism 6.2 software, by running the Student's t-test.

2.6 Cell Phenotype Characterisation in the presence and absence of PMPs

Cell morphology analysis

The effect of PMP on BC cells has been analysed to determine whether the microparticles influenced cell morphology. BC cell line MDA-MB-231 was incubated with or without 100 $\mu\text{g}/\text{ml}$ NDPMPs to reach 50-60% confluence in a 6 well plate. 10 fields of view per condition were captured at x60 magnification at 0, 2, 4 and 6 hours. Using ImageJ, individual cells were randomly picked and, with the help of the free-hand tool, their cell circularity and surface area were measured. Cell circularity was calculated using the following formula, as presented on the ImageJ website: $\text{circularity} = 4\pi(\text{area}/\text{perimeter}^2)$, where a value of 1 represents a perfect circle and under 1 they represent an elongated polygon. Results of each condition were averaged and compared using the ANOVA test, via GraphPad Prism 6.2.

Scratch Wound Assay

Breast cancer cells were cultured in serum containing media to full confluence in 24 well plates. The next day, the cells were serum starved for 24 hours, allowing for cell cycle phase synchronisation across the monolayer. On the third day, wounds were created manually using 20-200 μl pipette tips to create a straight scratch in the monolayer. The wells were washed with sterile PBS three times and fresh serum free or 10% serum containing media was added with or without 100 $\mu\text{g}/\text{ml}$ PMPs. Wells were photographed at 0, 6, 12 and 24 hours, using the EVOS digital colour fluorescence microscope.

Analysis of the images was performed using the MRI Wound Healing tool for Image J. The surfaces were measured in pixels and the averages were normalised as percentages, where 0 hours was considered as 100%. The means were compared using the ANOVA statistical analysis test, using GraphPad Prism 6.2.

Transwell Migration (Boyden Chamber) Assay

Cells were serum starved for 24 hours in T75 flasks. The following day the cells were resuspended in serum free media in the presence or absence of 100 $\mu\text{g}/\text{ml}$ PMPs. 1 ml of serum free and serum containing media were pipetted at the bottom of the wells of a

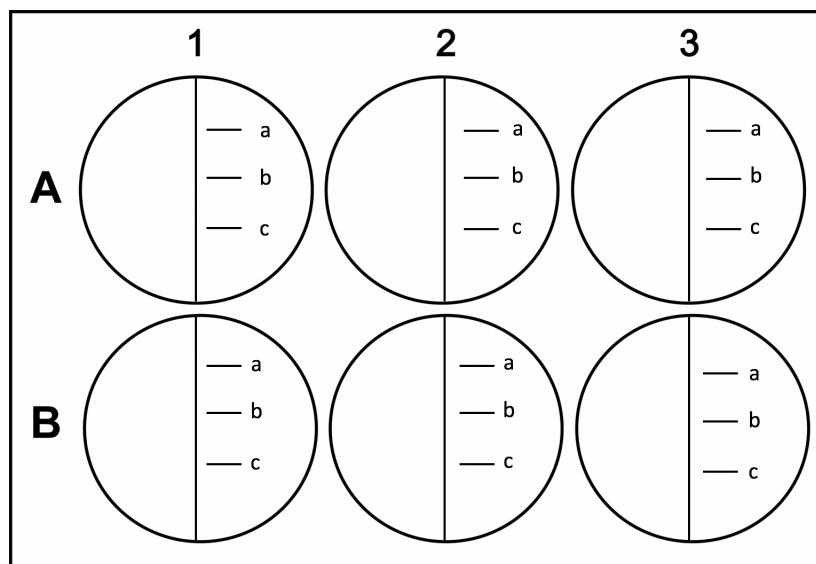


Figure 2.1: **Graphical representation of the wound formation used for the scratch wound assay for 6 well plates.** The central vertical line represents the induced wound. The three lines on the side, labelled *a*, *b*, *c* were used as reference to ensure the pictures were taken in the same place every time.

sterile 24 well plate, to act as chemoattractant. Transwell inserts (24 well plate, 8 μm pore size inserts, Sarstedt) were then carefully lowered on top of the loaded wells and the cells, with or without PMPs, at 10^5 cells/well were seeded on the bottom of the inserts in 500 μl of serum free media. Cells were incubated for 6 hours at 37°C 5 % CO_2 . The inserts were then removed and placed in ice-cold 70% ethanol overnight at -20°C to fix. Fixed cells were stained with Hematoxylin and Eosin and the insert membranes were then carefully removed using fine tools. The membranes were mounted on microscope glass slides using glycerol-gelatin mounting media (Sigma). Pictures of 5 different fields of view were taken

of each membrane and only the number of fully migrated cells were counted from each one. The averages of each condition were compared with each other through the ANOVA test using GraphPad Prism 6.2.

Invasion assay

As with the transwell migration assay, the invasion assay used the same 24 well inserts at 8 μm pore size (Sarstedt). For 24 hours prior to the assay setup, the cells were serum starved in a T75 flask. On the day of the assay, 100 μl of ready to use Geltrex (Gibco) were pipetted to the bottom of each insert and incubated at 37°C for 2 hours. A sterile 24 well plate was prepared by pipetting 1 ml of either serum free or serum containing media on the bottom of each well. The inserts were carefully lowered into the wells, so that no bubbles formed underneath the membranes. Serum starved cells were trypsinised and the cells were resuspended in serum free media. 10^5 cells/well were seeded in each well, with or without 100 $\mu\text{g}/\text{ml}$ PMPs in 500 μl of SF media and the cells were incubated overnight at 37°C 5% CO_2 . Cells were fixed the next day, in ice-cold 95% methanol for 20 minutes at -20 °C, transferred to water and then stained with Hematoxylin and Eosin. The membranes were then removed and mounted onto microscope glass slides using glycerol-gelatin mounting media (Sigma). Pictures of 5 different fields of view were taken of each membrane and only the number of fully migrated cells were counted from each one. The averages

of each condition were compared via the ANOVA statistical test, using the GraphPad Prism 6.2 software.

2.7 RNA extraction

Total RNA was extracted from breast cancer cell lines and platelet microparticles using a series of kits presented below in table 2.4. cDNA libraries were created from the aforementioned total RNA.

Total RNA extraction from BC cell lines

RNA extraction from breast cancer cells was performed using two RNA extraction kits, Aurum Total RNA kit (Biorad) and then Direct-zol RNA MiniPrep (Qiagen). The decision to change the kit was made due to the better performance and ease of use of the Direct-zol RNA MiniPrep, compared to the Aurum Total RNA kit.

Kit	Supplier	Catalogue number
Aurum™ Total RNA Mini Kit	BioRad	7326820
Direct-zol™ RNA MiniPrep Plus w/ Zymo-Spin™ IICG Columns (Capped)	Zymo Research	R2072
Direct-zol™ RNA MicroPrep w/ Zymo-Spin™ IC Columns (Capped)	Zymo Research	R2062

Table 2.4: List of total RNA extraction kits used in this project.

In preparation for both cell extraction methods, cells were seeded to confluence in 6 well plates. The cells were serum starved for 24 hours and PMPs were added at 100 $\mu\text{g}/\text{ml}$ in serum free media, followed by incubation at 37° *C* overnight or for 48 hours. Other conditions used were cells in plain serum free media and serum-containing media.

The initial RNA extraction kit, the Aurum™ Total RNA Mini Kit (BioRad), was used as follows: Confluent cells were washed with PBS and all liquid was removed. Cells were lysed and mixed with 70% ethanol until the viscosity was significantly reduced. Contaminants such as DNA, lipids, proteins were removed by a series of Low Stringency and High Stringency washes, combined with a 15 minute incubation with DNase I. Total RNA was then eluted in a sterile eppendorf via centrifugation. RNA samples were stored at -80° *C* until use.

The Direct-zol RNA MiniPrep is a TRIzol based method for total RNA extraction. Cells were lysed in TRIzol reagent at 100 μl per cm^2 of cell culture surface area. An equal amount of ethanol was further added and the mixture was homogenised and transferred to a Zymo-Spin IIICG Column in a collection tube. DNase I treatment was applied to the base of the column, directly on the membrane and the sample was incubated at room temperature for 15 minutes. Following washes with Direct-zol RNA Pre-Wash and RNA Wash Buffer, the columns were transferred into a

RNase-free 1.5 ml Eppendorf tube and RNA was eluted in 50 μ l of DNase/RNase-Free Water. The resulting total RNA suspension was stored at -80°C .

Total RNA extraction from PMPs

Total RNA from PMPs was extracted using three different kits and techniques, from single and pooled PMP samples. Initially, the AurumTM Total RNA Mini Kit was used to isolate RNA from PMPs as well as breast cancer cells, using the same protocol, however, the results were not satisfactory and new total RNA extraction methods were investigated.

The second method used was based on the TRIzol reagent (Invitrogen), without the use of separating columns using the technique described by [Chomczynski and Mackey \(1995\)](#). PMPs were first pelleted after a 90 minute centrifugation at 20 000 RCF and 18°C , and all buffer was aspirated. PMPs were lysed with the TRIzol reagent and incubated for 5 minutes at room temperature. 80 μ l of chloroform were added and mixed vigorously using a vortex, followed by another 2-3 minute incubation to allow for phase separation. The sample was centrifuged for 15 minutes at 12 000 RCF at 4°C and the aqueous phase on top containing RNA was transferred to a new eppendorf tube. 200 μ l of isopropanol were then added to precipitate the RNA during a 10 minute incubation. The sample was centrifuged again using the same settings. The super-

natant was discarded and the pellet was mixed with 400 μl of 75% ethanol. After a brief vortex, the sample was centrifuged again and the supernatant discarded. The sample was air dried for 5 minutes and the pellet resuspended in 20-50 μl of nuclease free water. Following a 10-15 minute incubation at 55 $^{\circ}\text{C}$ - 60 $^{\circ}\text{C}$, the total RNA was stored at -80 $^{\circ}\text{C}$.

There were a few issues associated with this method, most likely caused by the lack of filter-column use. It was more difficult to ensure the total RNA was cleanly separated from the low phase and the DNA interface. When analysing the quality of the RNA via nanodrop, there appeared to be a high contamination of alcohol.

Total RNA was finally isolated from single sample and pooled sample PMPs, using the Direct-zol RNA MicroPrep kit, from Qiagen. TRIzol reagent was added at 3x volume of suspension. Ethanol was added in equal volume to TRIzol reagent and the solution was mixed thoroughly until it became less viscous and it was transferred to a Zymo-Spin IC Column in a collection tube. Following centrifugation, the sample was treated with DNase I for 15 minutes at room temperature and washed with Direct-zol RNA Pre-wash and RNA Wash Buffer. Columns were then transferred into RNase free 1.5 ml eppendorf tubes and the RNA was eluted in 15 μl of DNase/RNase-Free Water and stored at -80 $^{\circ}\text{C}$.

Turbo-DNA free treatment

Turbo DNA free treatment (Invitrogen) was applied to the eluted RNA in order to remove possible contaminating DNA residue. Turbo DNA free Buffer was added at 0.1 volume of total RNA elution, followed by 1 μl of Turbo DNA free solution. The mixture was incubated at 37°C for 20 to 30 minutes and the reaction was stopped with 0.1 volume of DNase inactivation reagent for 5 minutes at room temperature. The mix was centrifuged at 10 000 RCF for 1.5 minutes and the supernatant containing the RNA was then transferred to a clean tube. The sample was stored at -80°C until use.

Agarose gel electrophoresis

Prior to the electrophoresis of total RNA, the sample was prepared by mixing 1 μg of total RNA with 4 μl of 5 x RNA loading buffer (40 μl of 500 mM EDTA pH 8.0, 360 μl of 37% formaldehyde, 1 ml 100% glycerol, 1542 μl of formamide, 2 μl 10x TAE, 58 μl ddH₂O) with ddH₂O added to top up solution to 20 μl . The RNA sample was heated at 65°C for 5 minutes and incubated on ice for 2 minutes, before it was loaded onto the gel.

1% agarose (Thermo Fisher Scientific) gel was prepared in 100 ml of 1 x Tris Acetate EDTA (TAE) buffer (40mM Tris, 20mM acetic acid, 1mM EDTA pH 8.0) through boiling until completely dis-

solved. Ethidium Bromide at 10 mg/ml (Thermo Fisher Scientific) was added to the gel at 5% v/v and mixed thoroughly. RNA sample was electrophoresed at 120 Volt (V) for 30 minutes and the gel was visualised using ChemiDoc MP Imaging System (Bio-Rad) and analysed via the Image Lab software (Bio-Rad).

2.8 Quantification of RNA

RNA concentrations were measured using the NanoDrop™ 2000 (Thermo Fisher Scientific). Following calibration of the instrument to measure at 0.2 mm path length, 1 μ l of reference sample (elution solution or nuclease-free water) was pipetted onto the centre of the measuring window and the instrument was blanked. Concentration of RNA was measured next and recorded as ng/ μ l. A260/280 absorbance ratio was also read for each sample.

Oligonucleotides

Oligonucleotides were supplied by SIGMA-ALDRICH and designed using the online primer design tools Primer-BLAST (National Center for Biotechnology Information, NCBI) and OligoArchitect (<http://www.oligoarchitect.com/LoginServlet>) and for Stem-loop qPCR the primers were designed using the miRNA Primer Design Tool (<http://genomics.dote.hu:8080/mirnadesigntool/>). For a full list see Table 2.5.

Name	Forward	Reverse
GAPDH	TGTCAGTGGTGGACCTGAC	GTGGTCGTTGAGGGCAATG
TWIST	ACCATCCTCACACCTGTG	GATTGGCACGACCTCTTG
Vimentin	AACCGACACTCCTACAAG	TTATTGAAGCAGAAC- CAAGTT
SNAIL	GTGTCTCCCAGAACTATT	GTTTGAAATATAAAT- ACCAGTGT
MALAT1	CCGCTGCTATTAGAATGC	CTTCAACAATCACTACTCCA
PTEN	TAGAACTAATACCTCAAG	TATTGCTTAGATGGATAA
TP53	TCTGATTGGAGTGGAGTT	TTGTTGGTGTGGTGTTA
LIF-R	GTTGTTCCAGATAACTTGA	TTGTTATACCGTTCTCTTG
FASLG	ATGAGACTGTGAA- GAATAATATCC	TGAGTTGAGACATCCGATT
CDH1	ATTAACCTCACCAATCCTT	TTACACCTTGACCTAACG
KRAS	GCAGACTATCGCTACCTA	CTATTGTCGCACTTGTGT
CDKN1B	GAAGCAAGGAAGATATACAT	CACAGGTAGTACAATGAAG
CCR7	TCACTTGAGATTCTGGTT	GCATCATCAGTATCATAGC

Table 2.5: List of primers and oligonucleotides for RT-qPCR using PCR BioSystems reagents.

When measuring potential EMT marker changes within BC cells, some cultured cells were incubated in the presence of 10 ng/ml TGF β for 48 hours in order to be used as a positive control.

cDNA Synthesis for regular RT-qPCR analysis

cDNA was generated using the qPCRBIO cDNA synthesis kit (PCRBiosystems). Reactions were set up in a nuclease-free 200 μ l PCR tube by mixing 4 μ l of 5x cDNA synthesis mix, the volume equivalent of 500 ng of RNA sample, 1 μ l of 20 x reverse transcriptase (RT) and nuclease free water up to 20 μ l. In reverse

transcriptase negative (NRT) samples the 20 x reverse transcriptase was replaced with 1 μl of water per reaction. The reactions were incubated at 42°C for 30 minutes, followed by a 10 minute incubation at 85°C to denature the reverse transcriptase enzyme. The cDNA samples were diluted 1 in 5 and then stored at -20°C until use.

Quantitative Real Time PCR (RT-qPCR)

RT-qPCR reactions were set up for expression analysis of genes of interest using qPCRBIO SyGreen Mix Hi-ROX (PCR Biosystems). The reaction master mix was prepared by adding 5 μl of 2x qPCRBIO SyGreen Mix, 0.4 μl of 10 μM of sense and antisense primer mix at 400 nM and 3.6 μl of PCR grade dH₂O. 1 μl of cDNA was added to 9 μl of master mix in each well of a Clear Well 96-well PCR plate (BioRad). The plate was briefly centrifuged followed by incubation in a CFX 96 Real-Time PCR Detection System (BioRad), as shown in table 2.6. Data was analysed via the $\Delta\Delta\text{C}_q$ (normalised expression) method.

Table 2.6: Incubation settings for the CFX 96 (BioRad) for RT-qPCR using the PCR Biosystems kit:

Cycles	Temperature	Time
1	95°C	2 minutes
40	95°C	5 seconds
	60 to 65°C	20 to 30 seconds

Stem loop cDNA synthesis

Stem loop cDNA synthesis was performed using iScript Select (BioRad). The 20 μl reaction was prepared using 5x iScript Selection Reaction Mix (4 μl), Let-7a or miR-21 stem loop primer (500nM), Primer Enhancer Solution (2 μl), iScript Reverse Transcriptase (1 μl), PMP RNA (5 μl) and nuclease free water (up to 20 μl). The reaction was incubated at 42 °C for 30 minutes, followed by 85°C for 5 minutes.

Stem Loop RT-qPCR

For the stem loop RT-qPCR reaction, the mix was prepared by combining 10 μl iTaq Universal Probes Supermix, 0.8 μl of specific forward primer, 0.8 μl of Universal Reverse Primer, 0.4 μl Universal Probe 21, 3 μl of nuclease free water and 5 μl of cDNA per individual reaction. Reactions were prepared in a Clear Well 96-well PCR plate (BioRad). The plate was briefly centrifuged and placed into a CFX 96 Real-Time PCR Detection System (BioRad) following the protocol presented in table 2.7. The assay data were viewed and analysed using BIO-RAD CFX Manager software. Gene expression was analysed via the $\Delta\Delta\text{Cq}$ (normalised expression) method. Stem-loop qPCR was used in order to determine the quality of the PMP samples prior to RNA sequencing.

Table 2.7: Incubation settings for the CFX 96 (BioRad) for Stem-Loop qPCR:

Cycles	Temperature	Time
1	95°C	30 seconds
40	95°C	15 seconds
	60°C	30 seconds
Melting curve	65°C - 95°C(+0.5°C increments)	5 second increments with plate read

2.9 RT-qPCR analysis using the miRCURY LNA miRNA Qiagen Kit

The miRCURY LNA miRNA kit from Qiagen was used to measure expression levels of miRNAs found in either total BC cell RNA or total PMP RNA. In order to confirm the potential of PMPs as delivery vehicles for functional miRNAs, actinomycin D was used to inhibit the activity of RNA polymerase II in BC cells. The cells were incubated with either 1 µg/ml actinomycin D or blank vehicle for 24 hours prior to the addition of 100 µg/ml PMPs. After a 48 hour incubation period in the presence of PMPs, total RNA was extracted and further analysed using the kit mentioned above.

Single strand cDNA synthesis

For single strand cDNA synthesis, 20 ng of total RNA extracted from cultured breast cancer cells were used per 20 μl reaction. Each non-PMP RNA sample was diluted to 5 ng / μl in nuclease free water. The reactions were then further prepared on ice. In the case of PMPs, total RNA was isolated from the equivalent of 280 μg of protein for both DPMPs and NDPMPs.

The reaction mix for total RNA derived from cultured BC cells was comprised of 2 μl of 5 x miRCURY RT reaction buffer, 4.5 μl of nuclease free water, 1 μl of 10 x miRCURY Reverse Transcriptase Enzyme Mix, 0.5 μl of UniSp6 RNA spike in and 2 μl of total RNA solution at 5 ng/ μl . In NRT samples, the 10 x Reverse Transcriptase Enzyme Mix was replaced with 1 μl of nuclease free water.

In the case of PMP RNA sample solution the reaction mix was prepared as follows: 2 μl of 5 x miRCURY RT reaction buffer, 1 μl of 10 x miRCURY Reverse Transcriptase Enzyme Mix, 0.5 μl of UniSp6 RNA spike in and 6.5 μl of RNA.

The tubes containing the reactions were placed in a CFX 96 Real-Time PCR Detection System (BioRad) with the following protocol: Incubation for 60 minutes at 42° C then an incubation at 95° C for 5 minutes to heat inactivate the reverse transcriptase. The reaction

was immediately cooled to 4°C and samples were then stored at -20°C until use.

When ready to be used, the cDNA corresponding to the cultured BC cells was diluted 1:60, by adding 590 µl of nuclease free water to the 10 µl of undiluted cDNA. In the case of cDNA originated from PMP RNA, the samples were diluted 1:10, by adding 90 µl of nuclease free water to the original cDNA reaction. Although the original protocol supplied by the kit manufacturer suggests the equivalent of roughly 20 µl of body fluid to be used of the RNA there were no detectable levels of miRNA. The aforementioned modifications were used throughout, as they were found to be more effective.

miRCURY LNA RT-qPCR reactions

miRCURY LNA RT-qPCR reactions all included 5 µl of 2 x miRCURY SYBR Green Master Mix, 1 µl of PCR Primer Mix (list presented in table 2.9), 3 µl of diluted cDNA template and 1 µl of nuclease free water per reaction. The master mix and the cDNA samples were pipetted into a low skirted clear well PCR plate (BioRad) and briefly centrifuged. The protocol on the CFX 96 Real-Time PCR Detection System (BioRad) used is described in table 2.8.

Primer name	Sequence
hsa-miR-21-5p	UAGCUUAUCAGACUGAUGUUGA
hsa-miR-146b-5p	UGAGAACUGAAUUCCAUAGGCUG
hsa-miR-221-3p	AGCUACAUUGUCUGCUGGGUUUC
hsa-miR-125a-5p	UCCCUGAGACCCUUUAACCUGUGA
hsa-miR-93-5p	CAAAGUGCUGUUCGUGCAGGUAG
hsa-miR-30d-5p	UGUAAACAUCCCCGACUGGAAG
hsa-let-7i-5p	UGAGGUAGUAGUUUGUGCUGUU
hsa-let-7e-5p	UGAGGUAGGAGGUUGUAUAGUU
hsa-miR-16-5p	UAGCAGCACGUAAAUAUUGGCG
hsa-miR-1301-3p	UUGCAGCUGCCUGGGAGUGACUUC
hsa-miR-345-5p	GCUGACUCCUAGUCCAGGGCUC

Table 2.9: List of primers used when measuring miRNA expression levels for the LNA miRCURY kit.

Table 2.8: Incubation settings for the CFX 96 (BioRad) for the miRCURY LNA RT-qPCR kit.

Cycles	Temperature	Time
1	95° C	2 minutes
40	95° C	10 seconds
	56° C	60 seconds
Melting curve	60° C - 95° C (+0.5° C increments)	5 second increments with plate read

2.10 Next Generation RNA Sequencing

Next Generation RNA sequencing was used to analyse the miRNA content of DPMP as well as NDPMPs in order to determine whether or not they express different miRNAs or different expression levels. The NDPMP samples were used as control for the DPMP samples. RNA was extracted from twelve PMP samples of each type of microparticles and miRNA-seq compatible cDNA libraries were generated using the NEBNext Multiplex Small RNA Library Prep Set for Illumina (Illumina, Inc.). Libraries were analysed via HiSeq2500 single read 50bp run at the Next Generation Sequencing Facility within the University of Leeds.

Following the initial quality control carried out within the University of Huddersfield, the University of Leeds performed a quality control analysis on the samples using a Bioanalyzer (Agilent).

RNA sequencing bioinformatics analysis was performed as described below by Dr Chinedu A. Anene at the CRUK Barts Centre, Queen Mary University of London.

RNA-Seq alignment and processing

Quality filtered, and adapter trimmed reads (cutadapt v2.5) ([Martin, 2011](#)) were aligned to the GRCh38/hg38 assembly of the human genome using Bowtie2 (v2.3.5.1) ([Langmead and Salzberg,](#)

2012). HTSeq (v0.11.1) (Anders et al., 2015) was used to quantify the miRNA abundance based on the GRCh38 annotation (GENCODE Release 32). The expression levels were normalised by the “counts per million” (CPM). Differential expression (DE) analyses between diabetic and non-diabetic samples were performed using the edgeR R package (Robinson et al., 2010). The DE microRNAs were defined at adjusted p-value < 0.05 .

mRNA targets and gene ontology analysis

To investigate the biological processes associated with the targets of the differentially expressed miRNA, the mRNA targets of the miRNAs were extracted from the miRTarBase database (Hsu et al., 2011). The analysis was restricted to only experimentally validated miRNA – mRNA pairs. The R ClusterProfiler (Yu et al., 2012) and the human Bioconductor annotation database (org.Hs.eg.db) were used to compare the enriched biological processes between the mRNA targets of the differentially expressed miRNAs in diabetes and non-diabetes samples. All enrichment analyses were performed with a strict p-value and q-value < 0.01 cut-off with reduced redundancies by semantic similarity analysis (Wang et al., 2007).

miRNA targets were selected from the generated differential expression table and compared to the miRNA Cancer Association Database (<http://mircancer.ecu.edu/>).

2.11 Protein Expression Analysis

Total protein was isolated from 150 000 cells using 100 μ l Radioimmunoprecipitation assay (RIPA) buffer (SIGMA-ALDRICH) containing protease inhibitor (Protease Inhibitor Cocktail Tablets, Roche) for 30 minutes on ice. Whole cell lysate was sonicated for 30 seconds, followed by the addition of 2 x Laemmli buffer (125 mM Tris HCl, 20% Glycerol, 4% SDS, 0.005 % Bromophenol Blue, pH 6.8) to the sample at 1 x final concentration. The sample was boiled at 100°C for 5 minutes, immediately cooled on ice and stored at -20°C until use.

Antibodies/Proteins	Supplier	Catalogue number
GAPDH Rabbit mAb	Cell Signalling	2118S
Vimentin Rabbit mAB	Cell Signalling	5741S
E-cadherin Mouse mAB	Cell Signalling	14472S
Rabbit anti-Mouse IgG (H+L) Secondary Antibody, HRP	Invitrogen	61-6520
Goat anti-Rabbit IgG (H+L) Cross-Adsorbed Secondary Antibody, HRP	Invitrogen	31462
FITC Annexin V	BD Biosciences	556419
PE Mouse anti-human CD41a Clone HIP8	BD Biosciences	557297

Table 2.10: List of antibodies and proteins used in this project.

12 μ l total protein were loaded on to Any kD Mini-PROTEAN TGX Precast Protein Gel, 15-well (BIO-RAD), and separated at

120 V for one hour, then transferred to a polyvinylidene fluoride (PVDF) membrane (BIO-RAD). The membrane was then blocked with 5% v/v dry low fat milk (Marvel) in TBST (Tris-buffered saline (TBS) and 0.1% Tween 20) for 1 hour at room temperature. The blocked membrane was washed 3 x 5 minutes with TBST and incubated with primary antibody at recommended dilutions (GAPDH 1 : 5000, Vimentin 1 : 1000 and E-cadherin 1 : 1000, table 2.10) in 5% BSA in TBST overnight at 4°C on a shaker. The membrane was washed again three times with TBST before incubation with anti-mouse (1 : 2000) and anti-rabbit (1 : 10 000) secondary antibodies (Bio-Rad) in blocking buffer for 1 hour at room temperature. Finally, the membrane was washed 3 x 5 minutes with TBST and incubated with EZCL blotting substrate (Promega) for one minute at room temperature away from light. The blot was visualised and captured using a ChemiDoc MP Imaging System (Bio-Rad). Images were processed using Image Lab Software (BIO-RAD) and analysed in ImageJ.

2.12 Seahorse Metabolic Analysis

On the day prior to the assay, BC cells were seeded at 20 000 cells per well in the dedicated Seahorse Xfp Analyser (Agilent) miniplates in the following order: BLANK well, 2 x BC cells + ND PMPs, 2 x BC cells + DPMPs, 2 x BC cells, BLANK well. 400 μ l of sterile PBS was added in each moat and the miniplate

was placed for overnight incubation at $37^{\circ}C$ and 5% CO_2 . Also on the same day, a fresh cartridge was prepared by adding 200 μl of sterile water in each well and 400 μl of sterile water in each moat of the cartridge's utility plate. The cartridge was returned onto the utility plate carefully as to avoid the formation of air bubbles and incubated in a non- CO_2 incubator at $37^{\circ}C$ overnight.

On the day of the assay, the cartridge was removed from the incubator and the sterile water was replaced with pre-warmed calibrant. The cartridge was returned to the $37^{\circ}C$ non- CO_2 incubator for a further 45-60 minutes prior to the assay. Dedicated cell culture media was prepared using DMEM (Agilent) with 1 mM sodium pyruvate, 2 mM L-glutamine and 10 mM glucose, at pH 7.4 and kept warm at $37^{\circ}C$ until use. The cultivated BC cells were washed 3 times with dedicated media by removing all but 20 μl and adding 80 μl of freshly prepared media. The final volume was topped to 180 μl /well. The plate was placed in the $37^{\circ}C$ non- CO_2 incubator for 1 hour prior to assay.

Two kits were used, the first was the Agilent Seahorse Xfp Cell Energy Phenotype Test and the second, the Agilent Seahorse Xfp Mito Stress Test. The compounds used for the Cell Energy Phenotype test were Oligomycin (1 μM) and FCCP (1 μM), both added into a stressor mix and loaded into every port A of the cartridge. In the case of the Mito Stress Test, the compounds used were: Oligomycin (1.5 μM), FCCP (1 μM) and Rotenone and Antimycin

A ($0.5 \mu\text{M}$). Each were loaded in ports A,B and C respectively on the cartridge.

After the cartridge containing the utility plate with calibrant was loaded into the machine for calibration, the utility plate was replaced with the miniplate containing treated cells and the assay was continued. Analysis was performed using the Wave software provided by Agilent.

2.13 Inhibition of miRNA-21 activity in BC cells

miRNA-21 activity was inhibited in MDA-MB-231 cells using the transfection complex containing miRCURY LNA miRNA Power Inhibitor for miR-21 or miR-21 mimic (Qiagen) and HiPerfect Transfection Reagent (Qiagen). Both normal and fast forward protocols were tested.

MDA-MB-231 cells were seeded at 10^5 cells/well or 4×10^4 cells/well in complete growth media in 24 well plates (Nunc). Using the fast forward protocol, the transfection complex mix (100 μl SF media, 1 μl of 1.5 μM inhibitor/mimic/vehicle and 3 μl HiPerfect transfection reagent) was added to the cells one hour after seeding. 24 hours after incubation at 37 °C, 5% CO_2 , 100 $\mu\text{g}/\text{ml}$ PMPs, diabetic or non-diabetic, were introduced into the wells and placed

in the incubator again for a further 48 hours. In the case of the normal protocol, the same transfection complex mix was added to the cells 24 hours after seeding and the MDA-MB-231 cells were incubated again for 24 hours until PMPs were added. After this step there were no further differences between the two protocols.

48 hours after PMP incubation, total RNA was extracted from some wells for further analysis and some wells were used for the transwell migration assay. Due to the smaller number of viable cells available, only $3 * 10^4$ cells/well were used in the migration assay.

2.14 Statistical Analysis

All results are expressed as mean \pm standard error of the mean and data were normalised by considering positive controls as 100 %, unless otherwise mentioned. Analysis was performed using the student's t test and ANOVA, depending on the number of samples, verified by Bonferroni's test. Statistical significance was considered at $p < 0.05$.

The analysis was performed using GraphPad Prism 6.2 software and Microsoft Excel. Graphs were generated in GraphPad Prism 6.2 and the P value format used is presented in table 2.11.

Symbol	Meaning
ns	$p > 0.05$
*	$p \leq 0.05$
**	$p \leq 0.01$
***	$p \leq 0.001$
****	$p \leq 0.0001$

Table 2.11: **P** value format used in GraphPad Prism 6.2.

Chapter 3

Platelet Microparticle Isolation and Characterisation

3.1 PMP Isolation

One of the aims of this project is to investigate if PMPs deliver oncogenic miRNAs which affect the phenotype of BC cells. This chapter will demonstrate the origin and purity of extracted PMPs. Platelet microparticles were isolated from blood originating from T2DM diagnosed patients and volunteers with no known chronic illnesses. T2DM PMP samples were isolated by the research team belonging to the Endocrinology and Diabetes Unit within the Bradford Royal Infirmary and the non-diabetic PMP samples were collected and isolated within the University of Bradford, followed by the University of Huddersfield. A person was considered diabetic when their blood HbA1c levels were of minimum 6.5% ([American-](#)

[Diabetes Association, 2010](#)), 47.5 mmol/mol (International Federation of Clinical Chemistry) or 7.8 mmol/L. 24 ml of blood per volunteer were collected in 6 mls of ACD, using a 21 gauge hypodermic needle attached to a 30 ml syringe. This system was chosen over vacutainers in order to avoid platelet activation caused by the vacuum system.

Initially, individual samples of each volunteer would have the protein concentration measured via the Bradford Assay and used in further experiments. Following further use, a significant variation was noticed between results, due to the high variability of the samples, and the decision to pool collected samples before use was made to allow for consistency.

The formation of PMPs *in vivo* is stimulated via two mechanisms, calcium dependent or calmodulin dependent. With the rise of intracellular calcium within platelets, the calcium binds to calpain leading to the denaturation of the platelet cytoskeleton through proteolysis. Activated platelets also release serine proteases, inflammatory cytokines, stress inducers and growth factors promoting neighbouring platelet activation ([Hamzeh-Cognasse et al., 2013](#); [Fong et al., 2011](#)). The release of PMPs is a tightly regulated mechanism, where a multitude of factors contribute to the process, rather than a random event occurring within the organism. Not only is the release itself controlled by the stimuli, but the components of the microparticles are as well ([Bosman et al., 2012](#)).

The distribution of PMP components within the membrane are controlled by three proteins located on and around the membrane, flippase, floppase and scramblase (Nguyen et al., 2011).

PMPs were isolated using the protocol optimised by Anene et al. (2018). Compared to other protocols, as presented by Toth et al. (2008) and Tang et al. (2017), the PMPs were all extracted within 8 hours of the blood being taken from the healthy volunteers. The initial centrifugation of whole blood was carried out at a lower speed of 191 RCF, due to it only requiring a separation between the three layers of red blood cells, white blood cells and platelet rich plasma. Due to the lower speed of the initial centrifugation, a higher volume of platelets remain in the plasma layer, enabling a higher amount of PMPs to be further secreted. Although some protocols in literature have used ACD to inactivate the platelets after the separation of the platelet rich plasma (PRP), the use of PGE1 in the current protocol was considered more effective as PGE1 is known to directly inhibit platelet activation, by binding to the prostacyclin receptor, leading to a decrease in Ca^{2+} levels (Kreutz et al., 2012). The stimulation step using thrombin remained consistent throughout all protocols. The ultracentrifugation step differed across the three protocols mentioned, as the supernatant containing PMPs was centrifuged at 50 000 RCF for 60 minutes, 20 000 RCF for 90 minutes or 17 570 RCF for 30 minutes. Due to equipment availability and previous results, 20 000

RCF over a period of 90 minutes was considered the most appropriate.

An important aspect to take into consideration when extracting PMPs is the fact that they are not included in the category of exosomes ($<0.1 \mu\text{m}$) due to their size, structure and formation mechanisms (Lacroix et al., 2010). While there are ready made kits available for exosome extraction, due to their similarities, some may be appropriate to use, while others would not. Unfortunately these kits were not available for testing during this project.

3.2 PMP characterisation

Initially, to confirm protein content levels of the samples, immediately after isolation, the Bradford assay was performed. Even though the protein concentration suggested the presence of successful extraction of biologic material, it was not enough to demonstrate population purity. Bradford assay example results, as can be seen in table 3.1, were instead used to ensure consistency in the amount of protein used across all experiments. Due to restrictions in the number of PMP samples collected, $100 \mu\text{g}/\text{ml}$ was commonly used in all experiments as this appears to be the most common concentration used across several studies and the closest resembling normal physiological levels.

Examples of PMP samples used	
PMP code	Protein concentration
9897	1.59 mg/ml
10046	1.3 mg/ml
10048	1.14 mg/ml
10050	0.2 mg/ml
10088	0.688 mg/ml
10089	0.55 mg/ml
10090	0.752 mg/ml
10092	1.114 mg/ml
10099	1.733 mg/ml
10245	0.423 mg/ml
10233	0.359 mg/ml
10235	0.557 mg/ml
10232	0.4164 mg/ml
10236	0.715 mg/ml
10238	0.307 mg/ml
10246	0.369 mg/ml
10234	0.554 mg/ml
10248	0.307 mg/ml

Table 3.1: **Examples of PMP sample concentrations used.** Concentrations were measured using the Bradford Assay, as mentioned in the Materials and Methods section.

To confirm the purity and concentration of isolated microparticle fractions, analysis of 1 ml of 50 ng/ml of PMPs was carried out via the Nanosight NS300, which utilises the properties of both light scattering and Brownian motion in order to obtain the size distribution and concentration measurement of particles in liquid suspension. PMPs were identified by measuring their size and were viewed as seen in figure 3.1.

[Ponomareva et al. \(2017\)](#) also found that although all PMPs are within the size range present in literature of 100 nm to 1 μ m, the nature of the platelet stimulant will affect the size of the PMPs. Based on the present Nanosight measurements, the majority of PMPs formed via platelet stimulation using thrombin were around

or below 400 nm in size, see figure 3.2. What can also be observed in figure 3.2 is that NDPMP's size ranges are 90-600 nm, with a peak modal size of 140 nm followed by a slightly smaller one at 217nm, whereas DPMP's size ranges are 80-400 nm with a peak modal size of 102 nm. NDPMPs appear to present a higher size diversity than DPMPs, which present as evenly sized in comparison. This could suggest that DPMPs have a similar composition to each other, however more studies are needed in order to attest this.

In figure 3.3, PMPs have been labelled with both or either anti-CD-41a and anti-Annexin V antibodies tagged with TRITC and FITC respectively and measured using a flow cytometer. In this figure, the granularity and sizes of the microparticles is consistent across the sample. The populations were consistent across all repeats, presenting the same characteristics, strongly suggesting they belonged to the same cell cluster. In figure 3.4, the PMPs were measured using both the PE and FITC filters. Analysis has shown that the extracted PMPs were 84.3 % CD41a positive and 89.8 % Annexin V positive. The sample analysed was also 83.8 % positive for both CD41a and Annexin V when both proteins were fluorescently tagged. This coupled with the visual representation in figures 3.5, 3.6 and 3.7 strongly support the fact that these microparticles measured are indeed of platelet origin.

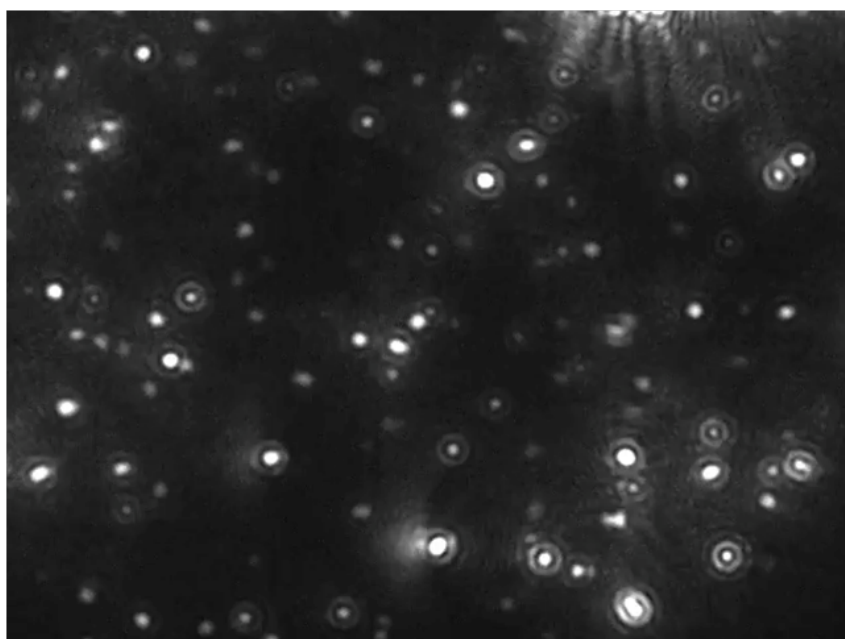
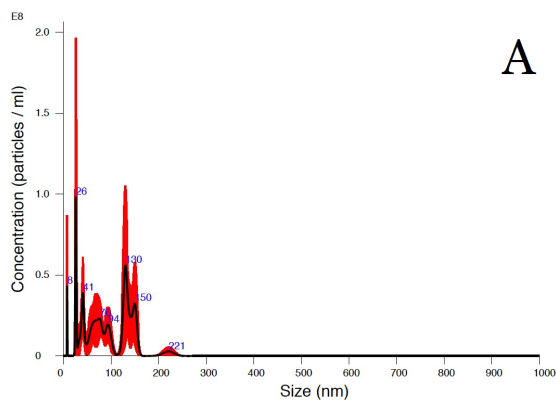


Figure 3.1: **PMP sample visualisation under the Nanosight NS300.**
A representative screenshot of a PMP sample analysis video under the Nanosight NS300, where PMPs are represented by the white dots.

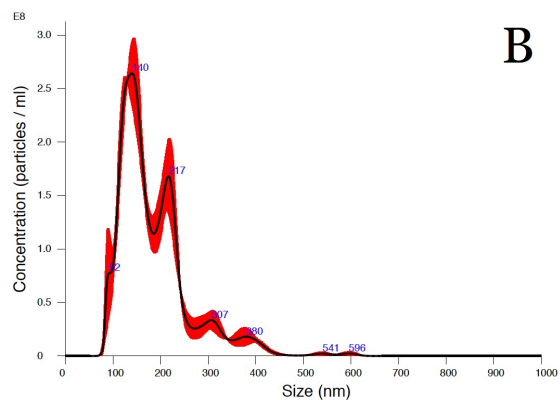
Following confirmation that the microparticles measured are PMPs, SEM analysis was carried out to confirm the physical structure of these microparticles. Analysis was carried out as described in Chapter 2, section Scanning Electron Microscopy. The results, however, were not clear enough to isolate individual PMPs.

3.3 PMPs as transport vectors

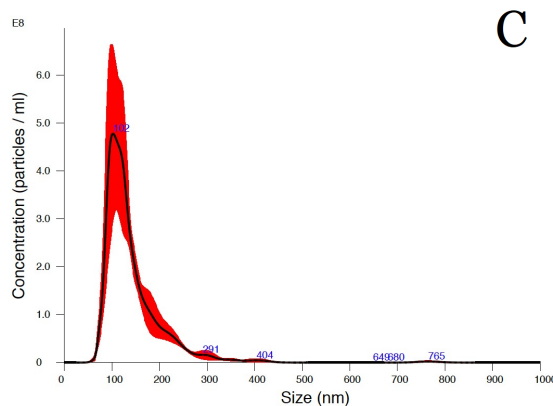
After assessing the quality of the extracted PMP samples from both non-diabetic and diabetic PMPs, the next step in PMP characterisation was to confirm the ability of PMPs to act as delivery vehicles for genetic information (Diehl et al., 2012), with the potential to affect the properties and the behaviour of their target cells. To confirm this, MDA-MB-231 cells and MCF-7 cells were co-incubated with fluorescently tagged PMPs and untagged PMPs. BC cells were tagged with DAPI and PMPs were tagged with Cell Tracker Red in order to confirm their general presence based on the location of their membrane and with SYTO RNASelect which binds to the RNA present in PMPs. Initially, as it can be seen in figure 3.8, MDA-MB-231 cells (DAPI) were incubated overnight with tagged and untagged PMPs and the images were captured using a Nikon Eclipse 80i fluorescence microscope. Due to background fluorescence present, the experiment was repeated and MCF-7 cells, figure 3.9, were incubated with tagged and untagged PMPs for 30 minutes, however, background fluorescence presented itself again, visible in the panel G. In figures 3.10, 3.11 and 3.12 MDA-MB-231 cells were co-incubated with tagged and untagged PMPs for 30 minutes, 2 and 4 hours. As it can be seen in these figures, the longer the incubation time, the more the SYTO RNASelect dye would auto-fluoresce. Despite this, in figure 3.10 it can clearly be observed that PMPs stained with the live membrane



Averaged FTLA Concentration / Size for Experiment:
 CS buffer blank 2019-03-18 12-11-27
 Error bars indicate + / - 1 standard error of the mean



Averaged FTLA Concentration / Size for Experiment:
 bcnh11 2019-03-22 15-07-09
 Error bars indicate + / - 1 standard error of the mean



Averaged FTLA Concentration / Size for Experiment:
 BCN7 2019-03-27 13-59-25
 Error bars indicate + / - 1 standard error of the mean

Figure 3.2: **Results of PMP sample analysis via the Nanosight NS300** are displayed in panels **A-C**, where the x-axis represents size in nm and the y-axis represents the light intensity. The results are presented as line graphs with errors resulted from at least three reading repeats. **A.** Blank C/S buffer, **B.** NDPMPs, **C.** DPMPs.

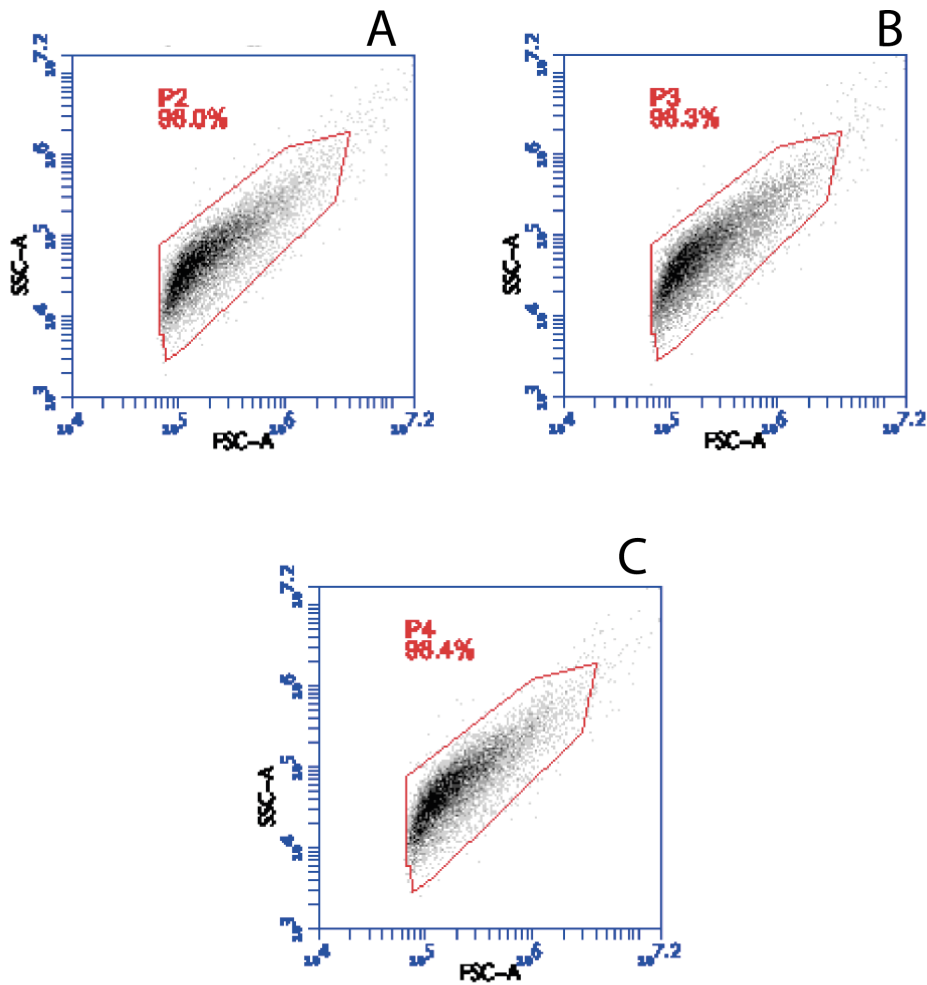


Figure 3.3: **Platelet microparticle characterisation using the BD Biosciences Accuri flow cytometer.** All repeats were measured at 10 000 events, using both filters PE and FITC. The panels above present as scatter plots of forward scatter versus side scatter, presenting both particle size and granularity. **A.** PMPs fluorescently tagged with both anti-CD41a and anti-Annexin V antibodies. **B.** PMPs fluorescently tagged with anti-CD41a antibodies only. **C.** PMPs fluorescently tagged with anti-Annexin V antibodies only.

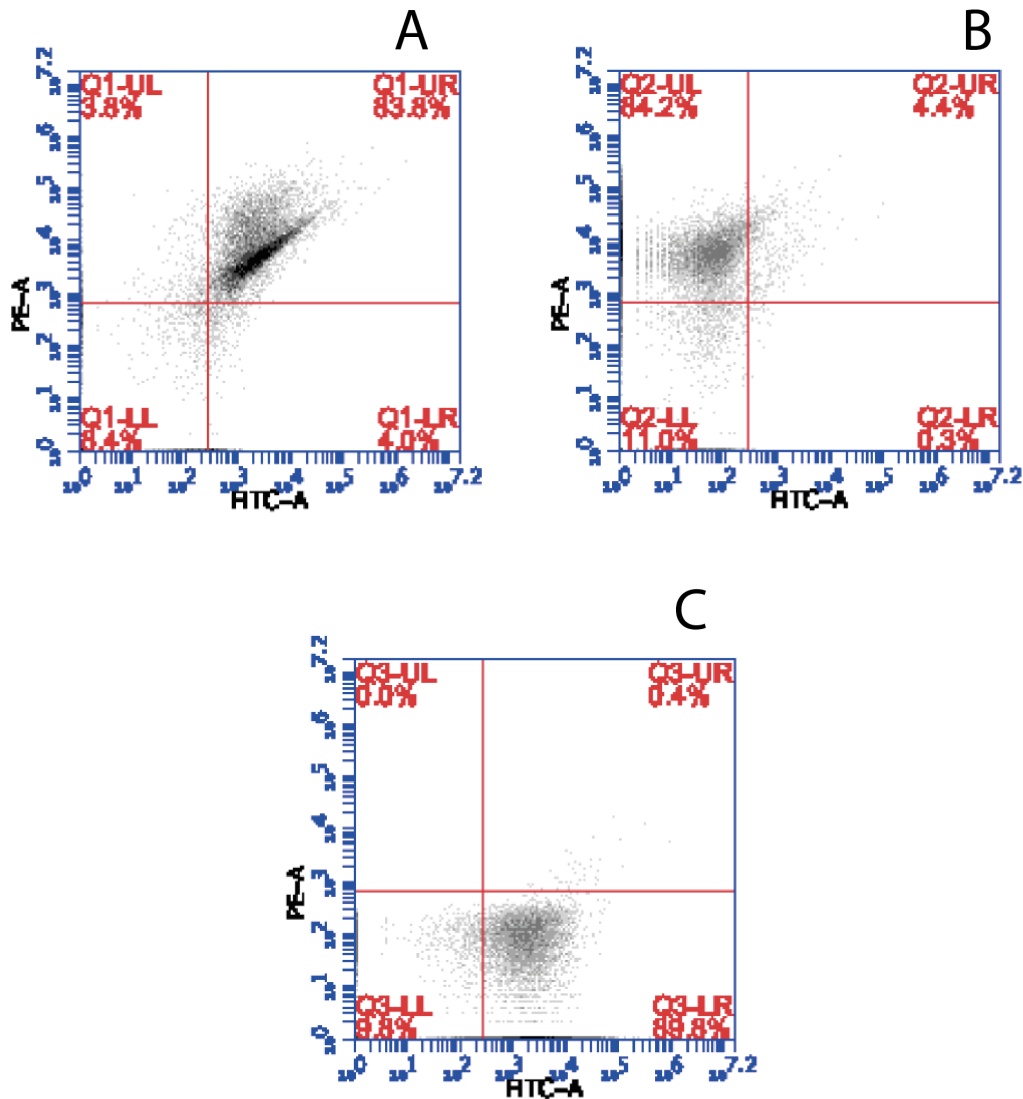


Figure 3.4: **Platelet microparticle characterisation using the BD Biosciences Accuri flow cytometer.** All repeats were measured at 10 000 events, using both filters PE and FITC. The panels above are presented as scatter plots where the x axis represents FITC and the y axis represents PE. **A.** PMPs fluorescently tagged with both anti-CD41a and anti-Annexin V antibodies. **B.** PMPs fluorescently tagged with anti-CD41a antibodies only. **C.** PMPs fluorescently tagged with anti-Annexin V antibodies only.

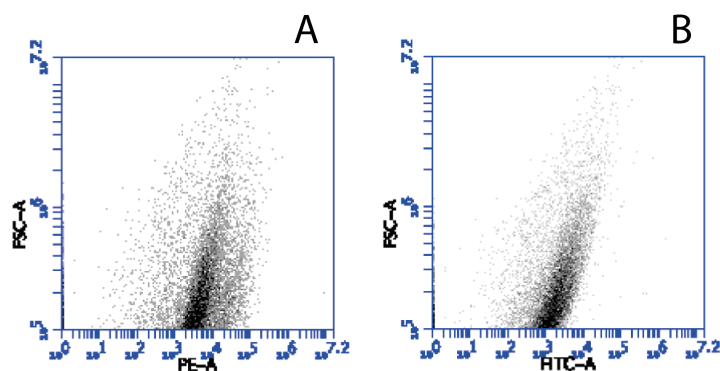


Figure 3.5: **Platelet microparticle characterisation using the BD Biosciences Accuri flow cytometer.** All repeats were measured at 10 000 events, using both filters PE and FITC. The panels above are presented as scatter plots where the x axis represents the fluorescence measurement and the y axis represents the forward scatter. PMPs fluorescently tagged with both anti-CD41a and anti-Annexin V antibodies. **A.** Double tagged PMPs viewed using PE filter vs forward scatter. **B.** Double tagged PMPs viewed using FITC filter vs forward scatter.

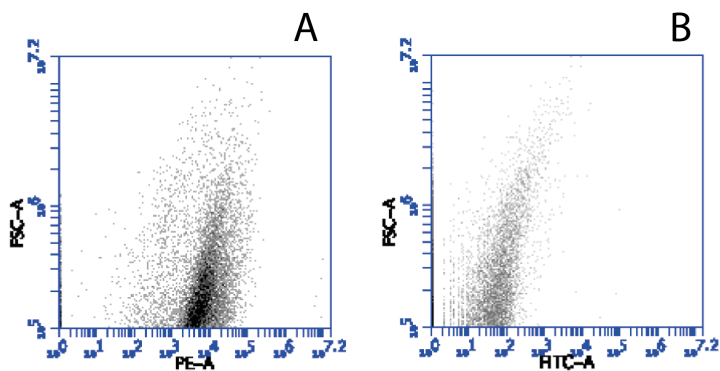


Figure 3.6: **Platelet microparticle characterisation using the BD Biosciences Accuri flow cytometer.** All repeats were measured at 10 000 events, using both filters PE and FITC. The panels above are presented as scatter plots where the x axis represents the fluorescence measurement and the y axis represents the forward scatter. **A.** PMPs fluorescently tagged with anti-CD41a antibodies viewed using PE filter vs forward scatter. **B.** PMP fluorescently tagged with anti-CD41a antibodies viewed using FITC filter vs forward scatter.

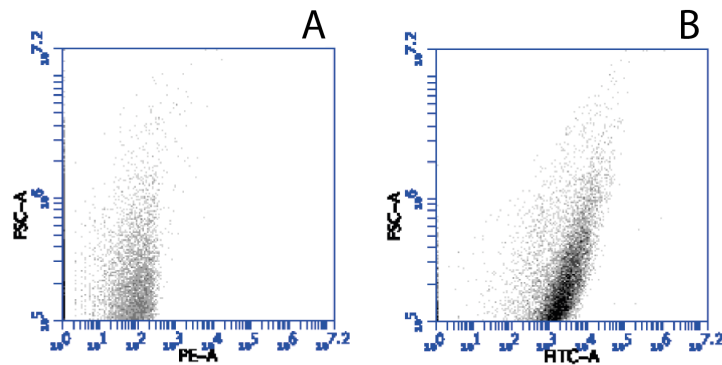


Figure 3.7: **Platelet microparticle characterisation using the BD Biosciences Accuri flow cytometer.** All repeats were measured at 10 000 events, using both filters PE and FITC. The panels above are presented as scatter plots where the x axis represents the fluorescence measurement and the y axis represents the forward scatter. **A.** PMPs fluorescently tagged with anti-Annexin V antibodies viewed using PE filter vs forward scatter. **B.** PMPs fluorescently tagged with anti-Annexin V antibodies viewed using FITC filter vs forward scatter.

dye Cell Tracker Red have been absorbed by the BC cells within the 30 minutes of incubation. The SYTO RNASelect dye has also shown that the RNA within the PMPs was also incorporated by the cells, best visible in panel O in figure 3.10.

3.4 PMPs alter cellular morphology

Following the confirmation that PMPs are delivery vehicles for bioactive molecules, a potential effect of PMPs on the morphology of breast cancer cell lines, particularly MDA-MB-231, has been observed. Apart from MDA-MB-231, no other breast cancer cell line available presented observable morphological alterations following

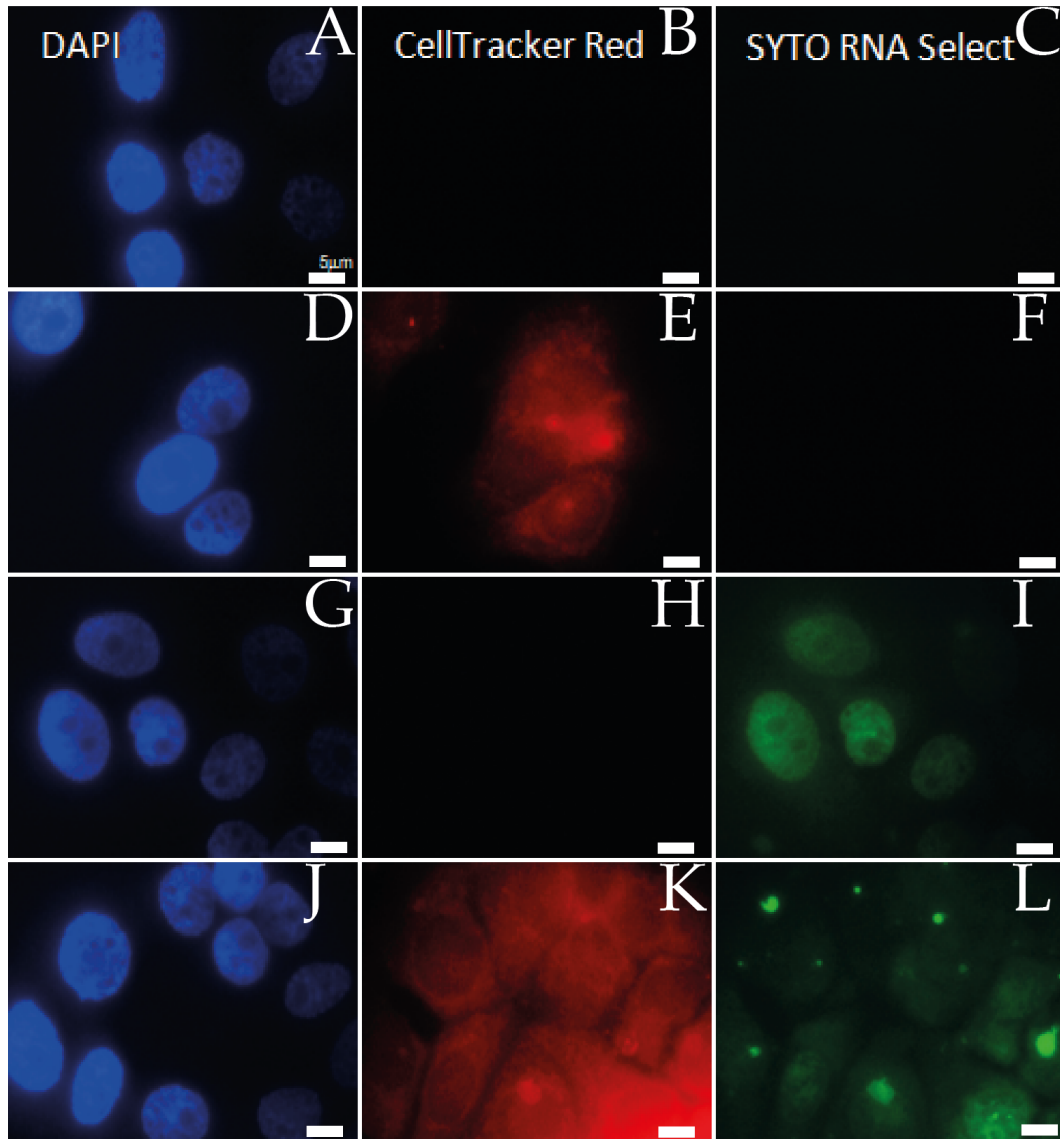


Figure 3.8: **Representative fluorescent microscopy images of MDA-MB-231 cell line** (nuclei stained with DAPI) incubated with unstained PMPs (A-C), PMPs stained with Cell Tracker Red (D-F), PMPs stained with Syto-RNA Select (G-I) and PMPs stained with both Cell Tracker Red and Syto-RNA Select (J-L). Scalebar represents $5\mu m$.

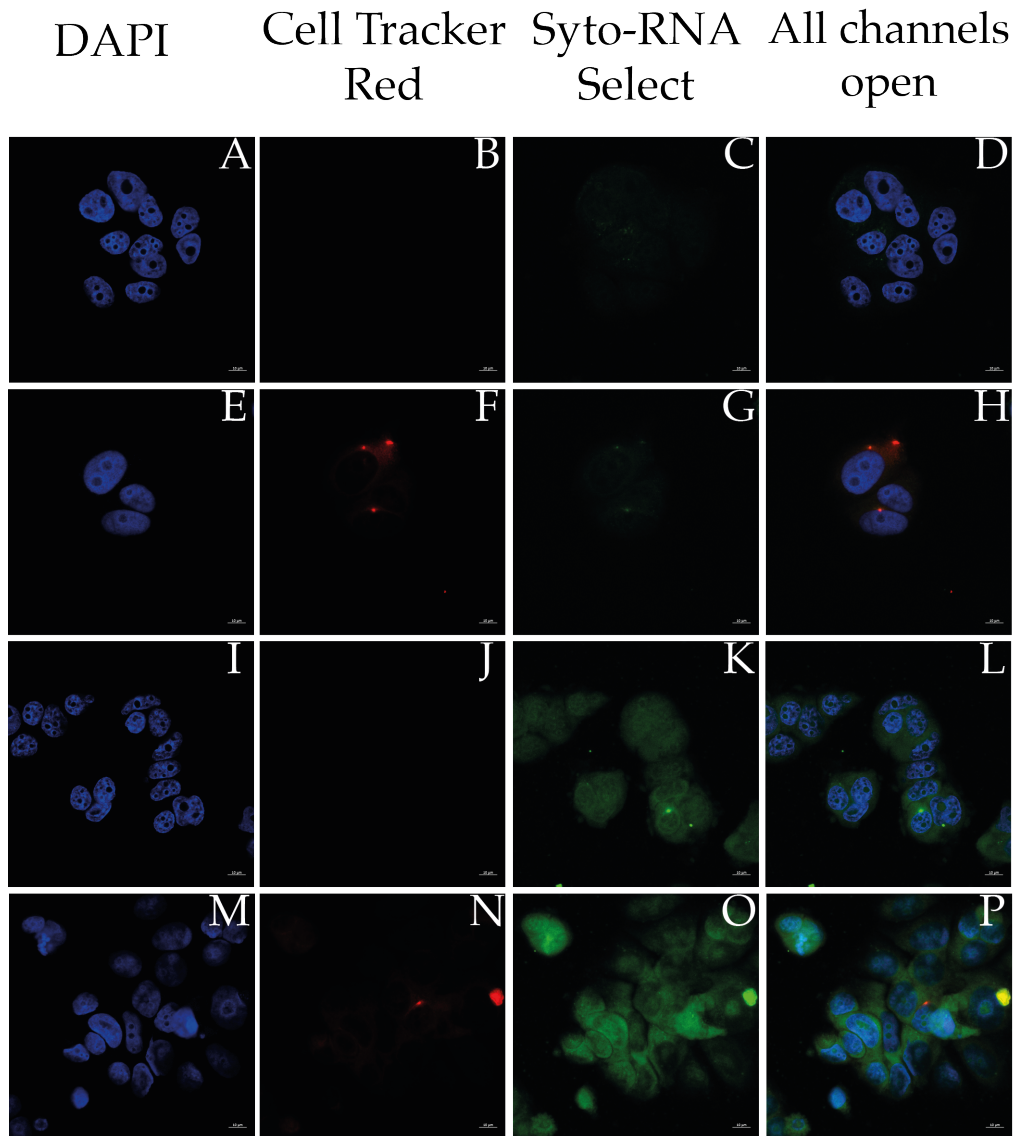


Figure 3.9: **Representative confocal images of MCF-7 cell line** (nuclei stained with DAPI) incubated for 30 minutes with unstained PMPs (A-D), PMPs stained with Cell Tracker Red (E-H), PMPs stained with Syto-RNA Select (I-L) and PMPs stained with both Cell Tracker Red and Syto-RNA Select (M-P). Scalebar represents $10\mu m$.

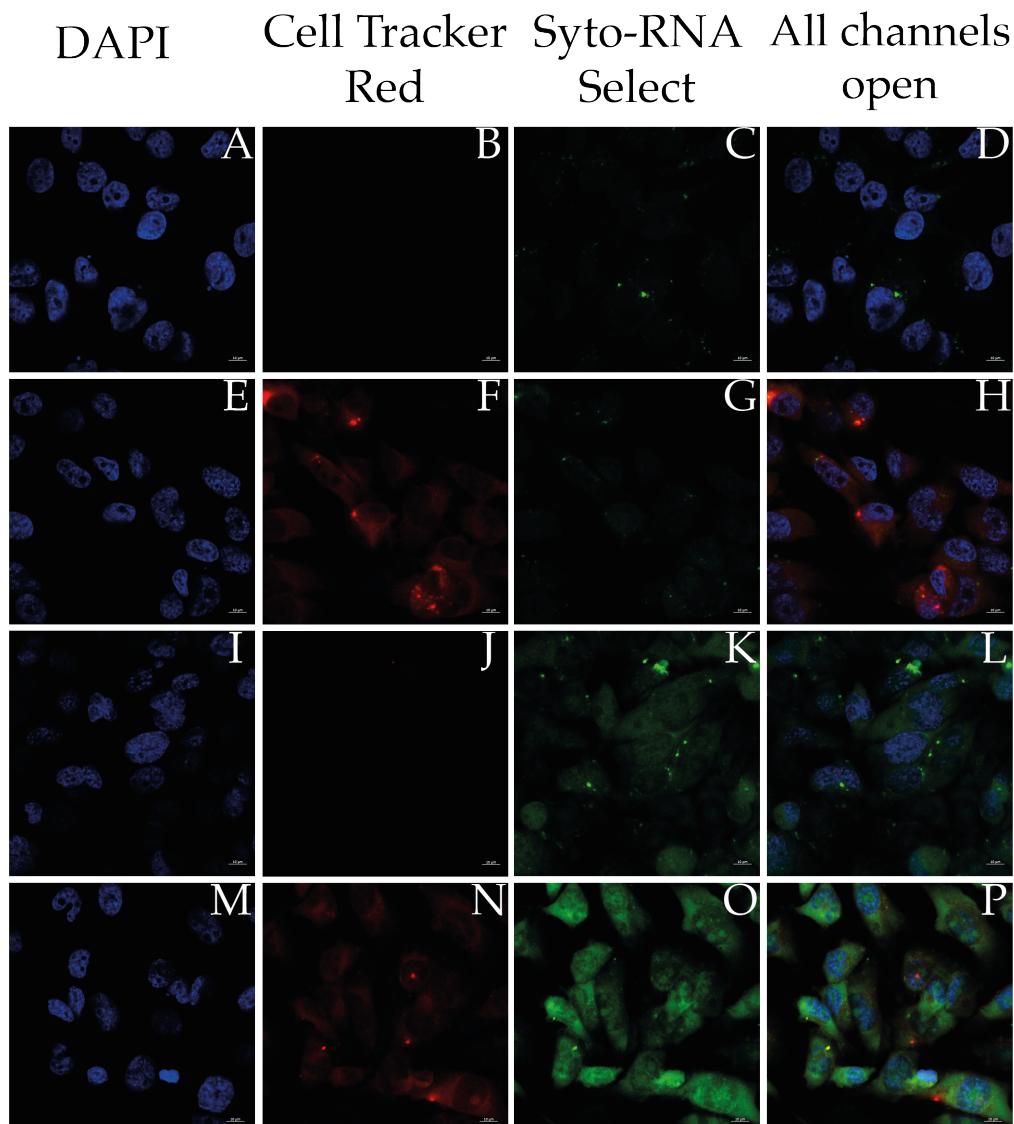


Figure 3.10: **Representative confocal images of MDA-MB-231 cell line** (nuclei stained with DAPI) incubated for 30 minutes with unstained PMPs (A-D), PMPs stained with Cell Tracker Red (E-H), PMPs stained with Syto-RNA Select (I-L) and PMPs stained with both Cell Tracker Red and Syto-RNA Select (M-P). Scalebar represents $10\mu m$.

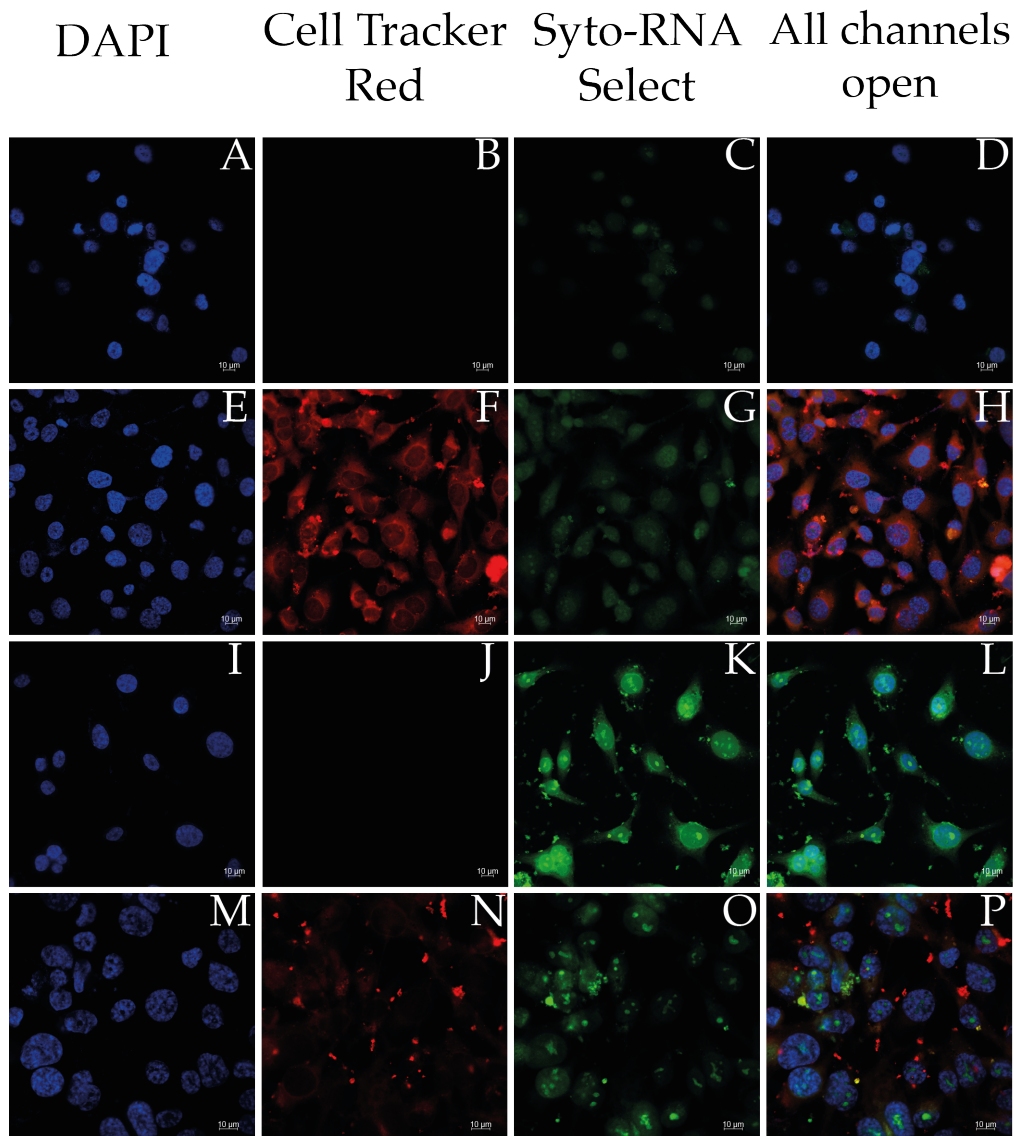


Figure 3.11: **Representative confocal images of MDA-MB-231 cell line** (nuclei stained with DAPI) incubated for 2 hours with unstained PMPs (A-D), PMPs stained with Cell Tracker Red (E-H), PMPs stained with Syto-RNA Select (I-L) and PMPs stained with both Cell Tracker Red and Syto-RNA Select (M-P). Scalebar represents $10\mu m$.

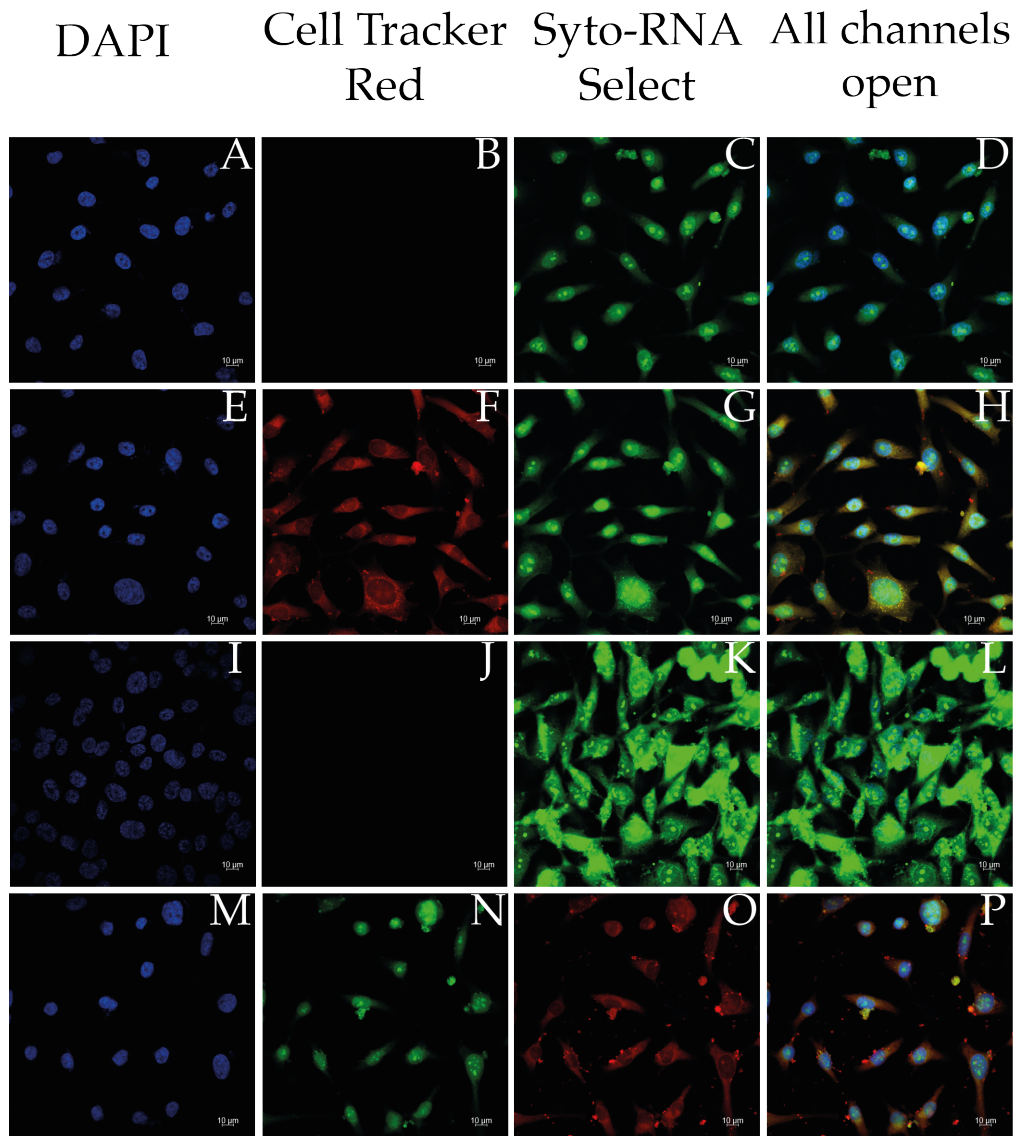


Figure 3.12: **Representative confocal images of MDA-MB-231 cell line** (nuclei stained with DAPI) incubated for 4 hours with unstained PMPs (A-D), PMPs stained with Cell Tracker Red (E-H), PMPs stained with Syto-RNA Select (I-L) and PMPs stained with both Cell Tracker Red and Syto-RNA Select (M-P). Scalebar represents $10\mu m$.

co-incubation with PMPs.

In order to analyse the effects of PMPs on BC cells, MDA-MB-231 cells were incubated in the presence and absence of PMPs at 100 $\mu\text{g}/\text{ml}$, in both serum containing and serum depleted media. Images were taken at 0, 2, 4 and 6 hours and the characteristics of area and circularity of cells were measured using ImageJ.

Before analysing the figures below it is important to mention that all wells containing MDA-MB-231 cells were serum starved overnight before T0 was measured. Taking this into consideration, in figure 3.13 the baseline for cell circularity is different for BC cells transferred to serum containing media and serum starved cells that remained in the same type of media. This shows a fast reaction of the cells in response to changes in their immediate surroundings. From the analysis of PMP internalisation mentioned in the previous section, these microparticles have shown potential to be absorbed by target cells within 30 minutes of co-incubation. This also links to panel B in figure 3.13 where the effects of PMPs on cell circularity peak, following a decrease in their effects in panels C and D at 4 and 6 hours respectively. In panel B of the aforementioned figure, cells incubated in SF media followed by the addition of PMPs at 100 $\mu\text{g}/\text{ml}$ would present similar circularity as the cells incubated in serum containing media with or without the presence of PMPs. In the complete absence of serum and PMPs, cells were significantly different in shape, compared to all other conditions.

Highlights of the effect of PMPs on MDA-MB-231 cells at 0 and 2 hours are presented in figures 3.14, 3.15 and 3.16. In the last two figures, the effect of both serum and PMPs are present at 2 hours. At 0 hours, all cells present a more elongated shape, with processes along most of the edges. Following a 2 hour incubation in both serum and PMPs, the characteristics of the cells have changed. When cells were incubated with only serum containing media, the cells presented a smooth surface, nearly devoid of any appendices, such as filopodia or lamellipodia. The presence of PMPs however, panels C and D, appears to influence the development of such appendices, even if only slightly. Even though SF media appears to influence the development of cellular processes, the added presence of PMPs appears to amplify their formation.

After measuring the effect of PMPs on the average cell shape, the average cell size was also analysed. As seen in figure 3.17, the presence or absence of serum had a more significant impact on cell surface spread rather than the presence or absence of PMPs, with panel D presenting the highest cellular surfaces of cells incubated in SF media.

3.5 PMPs increase BC cell motility

Scratch wound assays were used to compare wound closure rates between cells incubated in serum free DMEM alone and cells incubated in serum free DMEM and 100 $\mu\text{g}/\text{ml}$ NDPMPs. The cell

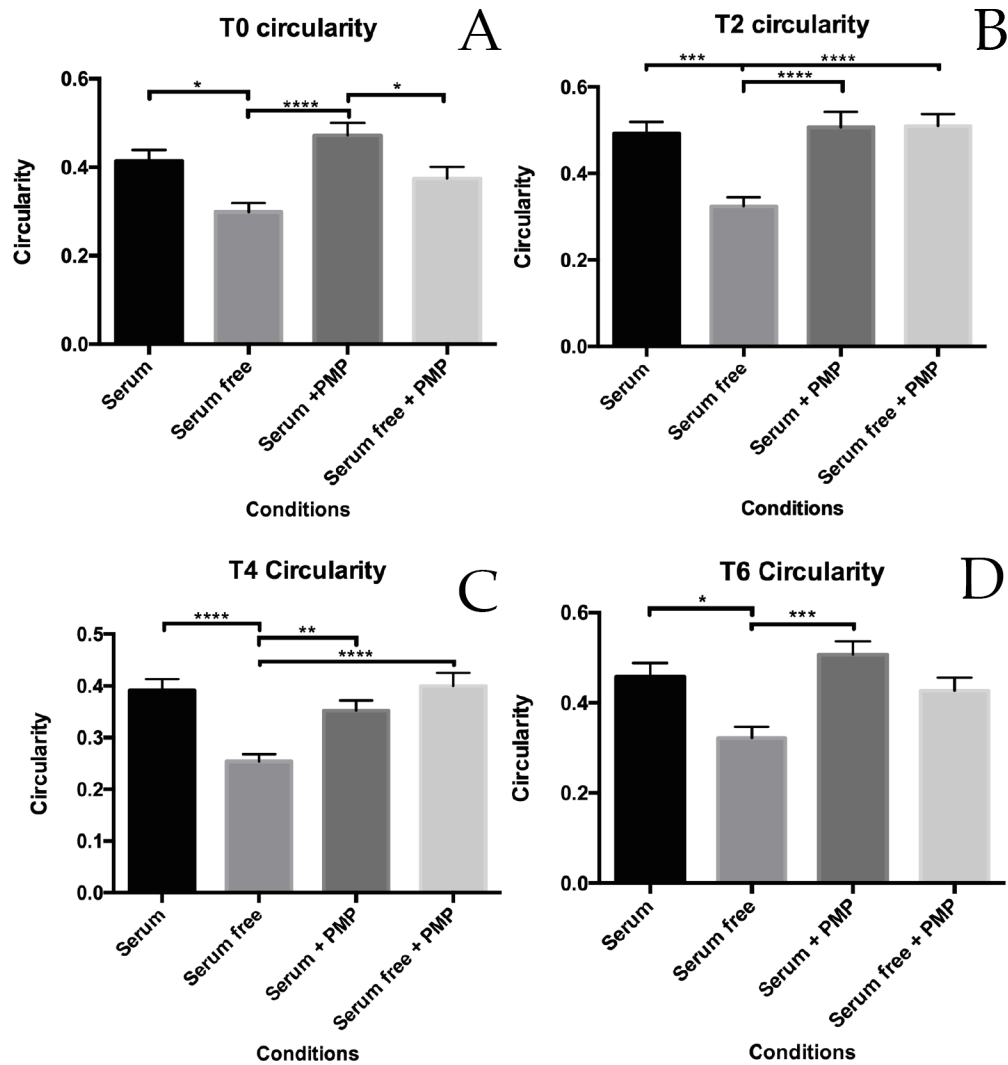


Figure 3.13: Representation of the effect of PMPs on the circularity of the MDA-MB-231 cells they were co-incubated with. The incubation conditions presented were MDA-MB-231 cells in serum containing media only, serum free media only, serum containing media plus 100 μ g/ml ND PMPs and serum free media plus 100 μ g/ml ND PMPs. Each panel represents the incubation time when the images for measuring were captured. A. 0 hours. B. 2 hours. C. 4 hours. D. 6 hours.

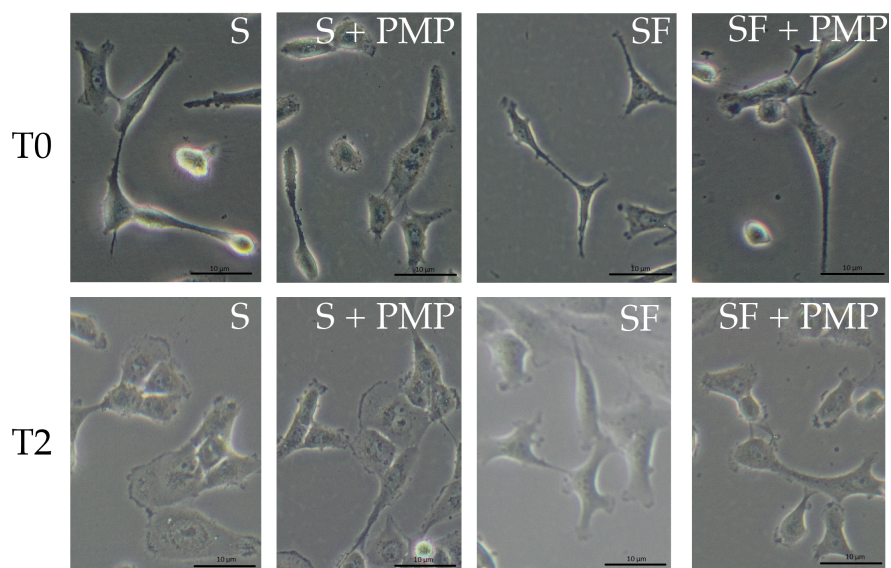


Figure 3.14: **Representative images of MDA-MB-231 under x60 magnification.** The times presented are for baseline (T0) and peak effect of PMPs (T2). Growing conditions are specified in each panel, and the PMPs were added at 100 μ g/ml. Scale bar represents 10 μ m.

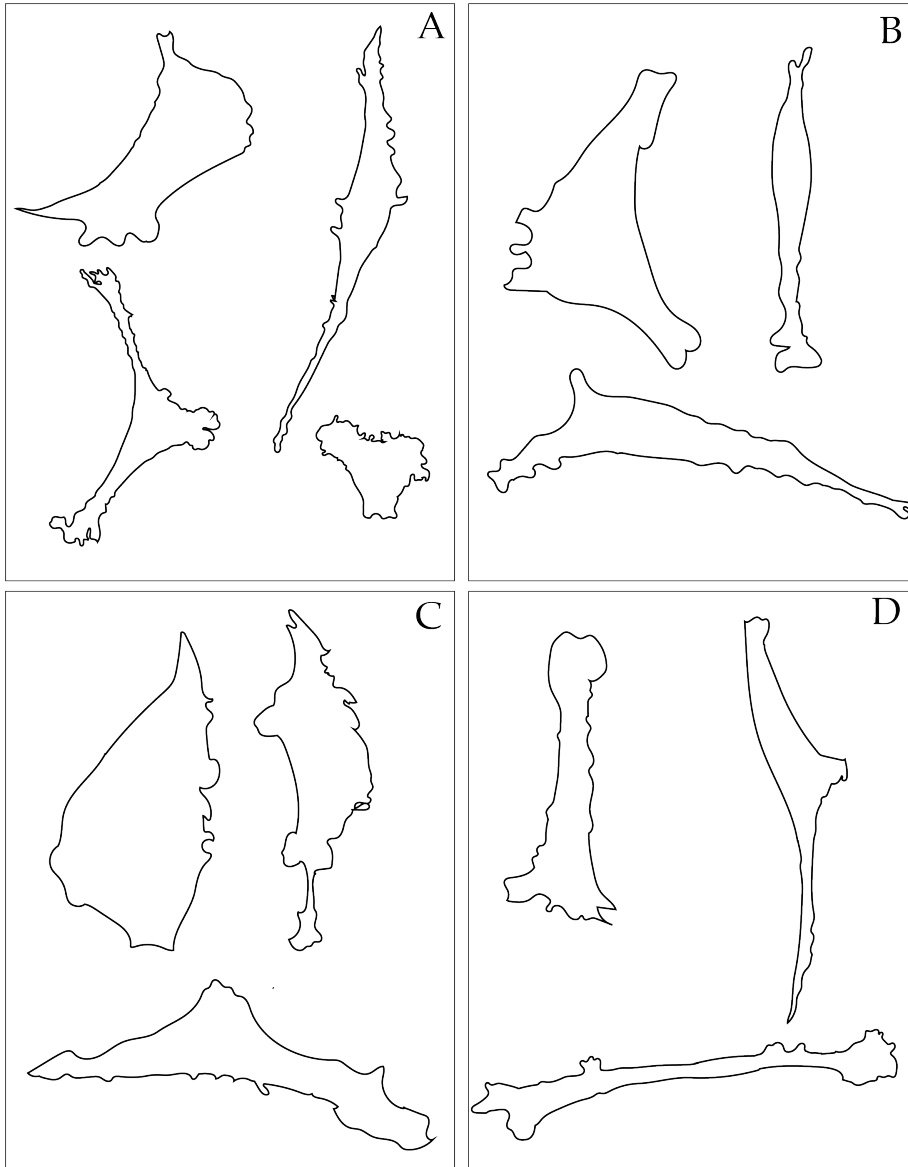


Figure 3.15: **Silhouettes of random MDA-MB-231 cells obtained from images captured at 0 hours.** A. Tracings of MDA-MB-231 cells in serum containing media. B. Tracings of MDA-MB-231 cells in serum free media. C. Tracings of MDA-MB-231 cells in serum containing media and $100 \mu\text{g/ml}$ PMPs. D. Tracings of MDA-MB-231 cells in serum free media and $100 \mu\text{g/ml}$ PMPs. Tracings are not scaled.

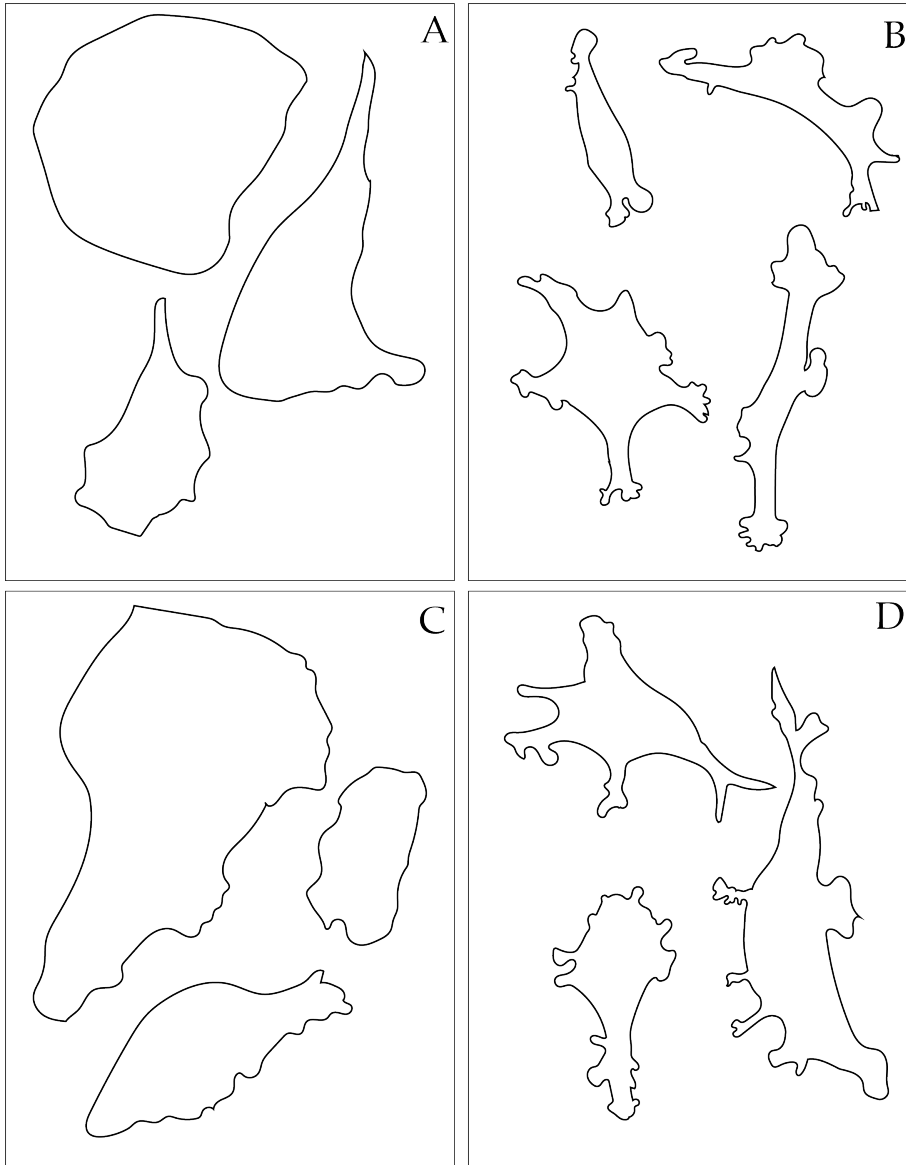


Figure 3.16: **Silhouettes of random MDA-MB-231 cells obtained from images captured at 2 hours.** A. Tracings of MDA-MB-231 cells in serum containing media. B. Tracings of MDA-MB-231 cells in serum free media. C. Tracings of MDA-MB-231 cells in serum containing media and $100 \mu\text{g/ml}$ PMPs. D. Tracings of MDA-MB-231 cells in serum free media and $100 \mu\text{g/ml}$ PMPs. Tracings are not scaled.

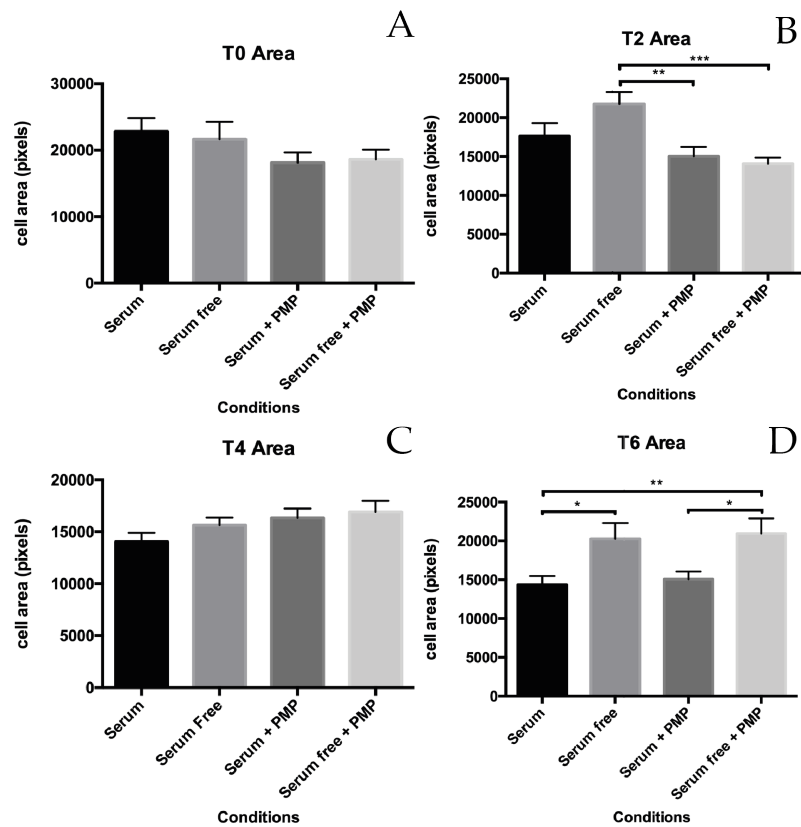


Figure 3.17: Representation of the effect of PMPs on the surface and spread of the MDA-MB-231 cells they were co-incubated with. The incubation conditions presented were MDA-MB-231 cells in serum containing media only, serum free media only, serum containing media plus 100 μ g/ml ND PMPs and serum free media plus 100 μ g/ml ND PMPs. Each panel represents the incubation time when the images for measuring were captured. A. 0 hours. B. 2 hours. C. 4 hours. D. 6 hours.

lines used were MDA-MB-231 (triple negative, basal breast cancer), MDA-MB-453 (HER2 positive breast cancer), MCF-7 (luminal breast cancer) and HB2 (healthy breast representative tissue). The results can be seen in figure 3.18 and figure 3.19, with the wound closure rates represented as both bar charts and trendlines.

In the figures mentioned above, only MDA-MB-231 cells presented a significant difference in wound closure at the 12 hour time point, and only MDA-MB-231 and MCF-7 cells presented a significant difference at the 24 hour time point between the two conditions measured. MDA-MB-453 and HB2 cells presented a similar wound closure pattern in both conditions, with NDPMPs promoting a slightly faster wound closure at the 12 hour time point compared to its non-treated counterpart, in the case of HB2 cells, however, they both reached the same level of wound closure at 24 hours.

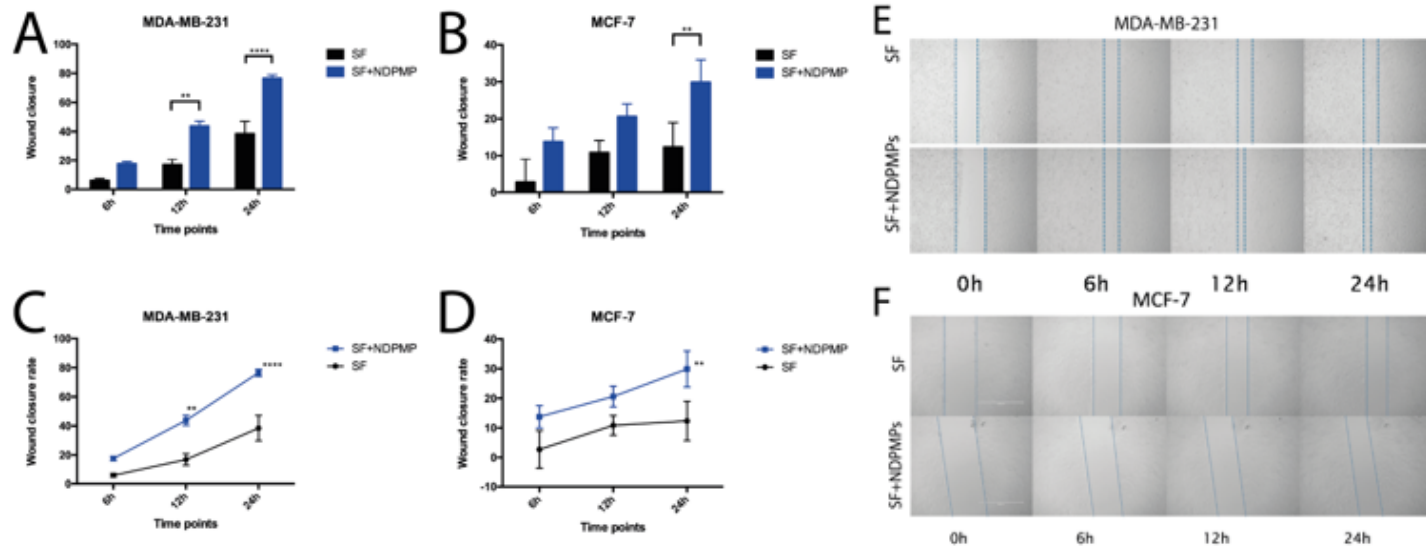


Figure 3.18: **Scratch wound analysis of MDA-MB-231 and MCF-7 cells.** MDA-MB-231 and MCF-7 cells were seeded at a density of 150 000 cells per well in 24 well plates and serum starved overnight. Wounds were created immediately after the addition of the PMPs and wound development was captured at 0, 6, 12 and 24 hours. Wound area was measured using the MRI wound healing tool plugin available for ImageJ and statistical analysis was performed using student's t test via Prism 6.2.

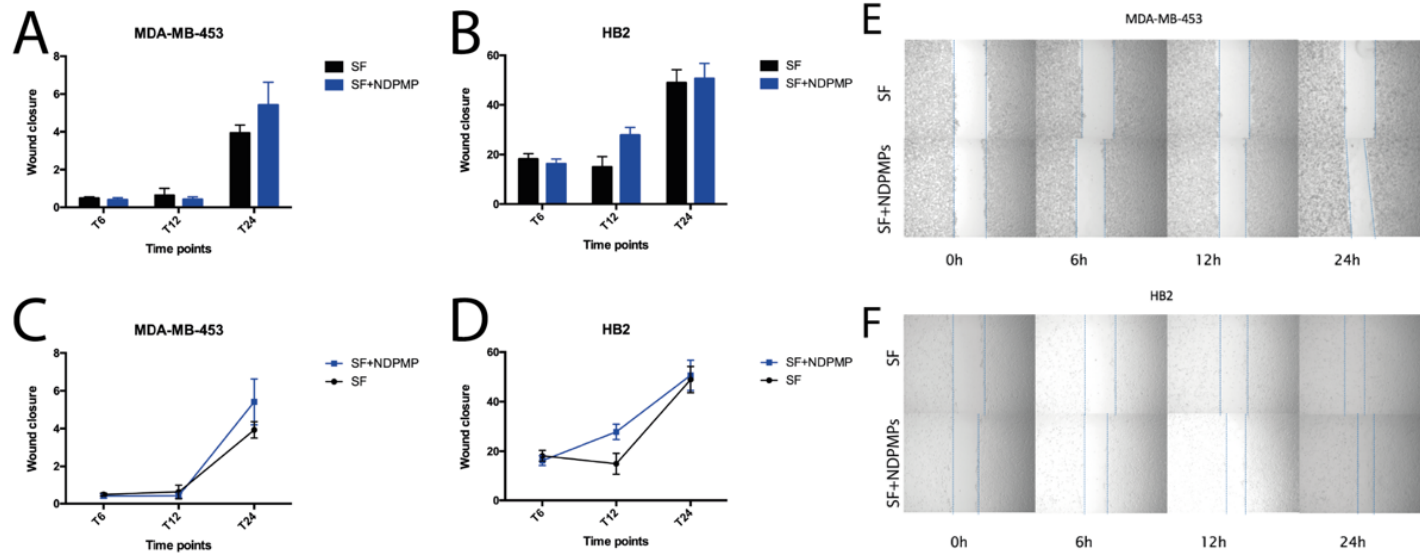


Figure 3.19: **Scratch wound analysis of MDA-MB-453 and HB2 cells.** MDA-MB-453 and HB2 cells were seeded at a density of 150 000 cells per well in 24 well plates and serum starved overnight. Wounds were created immediately after the addition of the PMPs and wound development was captured at 0, 6, 12 and 24 hours. Wound area was measured using the MRI wound healing tool plugin available for ImageJ and statistical analysis was performed using student's t test via Prism 6.2.

3.6 Chapter discussion

This chapter presents the results of PMP isolation optimisation, via confirmation of microparticle origin and purity. During the isolation process, one specific characteristic has been identified upon visual inspection of the samples. DPMPs present possible strong bonds, forming visible clumps, whereas ND PMPs presented as a clear homogeneous mix within the buffer. This could be linked to the more aggressive behaviour associated with T2DM platelets, the origin cells of DPMPs, as observed by (Soma et al., 2016). The main correlation observed was a rise in P-selectin levels, both intracellularly and in plasma as soluble P-selectin. (Tan et al., 2005a) has also observed the possibility of a link between high PMPs release and P-selectin levels, but a direct cause has not been confirmed.

Following Nanosight analysis, the sizes of the isolated microparticles measured were all within the ranges presented in literature (Voloshin et al., 2014), of 0.1 to 1 μm in diameter, as opposed to the size of typical exosomes of 30-100 nm (Zmigrodzka et al., 2016). This also demonstrates the fact that PMPs should not be included in the exosome category, as they present themselves as bigger than the maximum size identified for exosomes in the literature (Wolfers et al., 2001).

PMPs are formed via exocytosis following platelet activation and membrane blebbing or through platelet apoptosis. In both cases,

PMPs contain exposed elements of their platelet origin on their membrane ([Lacroix et al., 2010](#)). Given that flow cytometry analysis of biological samples is one of the most common methods of measuring PMPs, the origin of PMPs was confirmed using a BD Biosciences Accuri flow cytometer. Isolated PMPs suspended in C/S buffer were used instead of plasma, in order to avoid interference from microparticles released by other circulatory cell types. PMPs were fluorescently tagged with antibodies against the proteins CD41a ([Yari et al., 2018](#)) and Annexin V ([Lacroix et al., 2010](#)). CD41a is a molecular part of the GpIIb/IIIa receptor complex typically found on the surface of platelets and megakaryocytes ([Delgado et al., 2003](#)). Annexin V is a protein that binds intracellularly to the PS membrane ([Perreault et al., 2015](#)). Annexin V is normally present as part of the inner membrane of intact platelets. After the activation of platelets and the disregulation of the actin skeleton, followed by the release of the microparticles, this protein may be found on the outer membrane of PMPs, due to the mechanism of membrane folding. The origin of the isolated microparticles was confirmed via flow cytometry analysis as being circulating platelets.

As noted earlier in the text, PMPs are created through different events occurring within and around platelets. Because of this, each PMP expresses a different combination of platelet specific proteins on their membrane surface. [Lacroix et al. \(2010\)](#) suggests the use

of DiOC6 in order to distinguish microparticles surrounded by a closed membrane through the background noise. Another surface marker used by [Perez-Pujol et al. \(2007\)](#) to specifically identify PMP populations was P-selectin (CD62P). Although there were other options available to increase the specificity of this PMP flow cytometric analysis, due to the high variability in membrane contents it was decided that only the presence of annexin V and CD41 were to be identified.

SEM analysis was also used to analyse the structure of PMPs in more detail. Freshly isolated PMPs were not available therefore thawed samples were used. Other studies, such as [Ponomareva et al. \(2017\)](#) have used freshly isolated platelets that were then activated with either arachidonic acid, collagen or ADP. In their case, both platelets and PMPs were measured within the same time frame. Through electron microscopy, [Ponomareva et al. \(2017\)](#) discovered that PMPs were formed in three different structures. There were PMPs in the form of empty vesicles, multivesicular structures and organelle-containing microparticles. This was difficult to confirm, partly because of the limitations of SEM. A Transmission Electron Microscope is better equipped to provide possible cross section images of biological samples, whereas SEM provides quality images of biological surfaces. A TEM was not available for this study. Other methods of visualising small vesicular structures are also available, with one example being presented by ([Brisson et al., 2017](#)) using

cryo-electron microscopy with immuno-gold labelling in order to characterise extracellular vesicles excreted by activated platelets.

According to available literature, PMPs act as vectors for delivering genetic information across from their host cell to their target cell. As it has been measured before, RNA is present in blood through free flowing RNA molecules, which are highly prone to degradation and RNA molecules bound to complexes such as Ago2 or protected by a vesicular membrane as well, in the case of the PMPs ([Wu et al., 2013](#); [Laffont et al., 2013](#)). Through paracrine signalling between cells of identical or different origins, PMPs act as the intermediary, or the package of information to be delivered. During this process, the released microparticles become absorbed by their target cells through endocytosis. In both health and disease, PMPs deliver bioactive molecules which influence the processes of coagulation, inflammation, cellular activation, and in disease environments such as cancer, inflammatory and cardiovascular diseases, infections and autoimmune disorders. This information suggests that PMPs have the potential of becoming clinical biomarkers for these diseases ([Lacroix et al., 2010](#)). [Voloshin et al. \(2014\)](#) also suggests PMPs have the potential to act as important therapeutic targets. Although the emphasis has been on the presence and transport of RNA, it is worth noting that PMPs also deliver growth factors, surface proteins and angiogenic factors ([Zmigrodzka et al., 2016](#)).

Through visualising PMP uptake via confocal microscopy, this study has confirmed that PMPs have a role as transport vectors for functional information transfer, within a short period of time. At the time point of 30 minutes there was no PMP presence observed outside of cellular bodies, suggesting that PMPs are absorbed by their proximal BC cells within less than 30 minutes. This coordinates with other studies that have also found that PMPs become internalised within 30 minutes of co-incubation with other types of cells, such as neutrophils (Duchez et al., 2015). Typically, uptake of microparticles by neighbouring cells has been visualised using confocal microscopy at the 2 hour incubation time point (Terrisse et al., 2010; Faille et al., 2012).

This experiment also highlights the issue of auto-fluorescence, despite attempts to minimise it, particularly following longer exposure time of the samples to the dye. Auto-fluorescence or pseudo-fluorescence can be present if the blue and green filters overlap. This could explain the setbacks of this experiment and also suggest that possibly a different colour dye should be used in the future in order to confirm the presence of RNA in PMPs and their ability to deliver this genetic information to the BC cells that incorporate them.

PMPs have an important role in several diseases, from cardiovascular disease, to cancer and T2DM. Due to their size and stability, PMPs can travel significant distances throughout the organism be-

fore being internalised by their target cells (Barry et al., 1998). In certain cancers, the amounts of PMPs released in circulation are considerably increased, in some cases 4 fold to even 35 fold, depending on cancer type (Lazar and Goldfinger, 2018). Not only are PMP levels altered in disease, but PMP structure and components become altered as well, with especially miRNA composition being affected (Diehl et al., 2012). There has also been a well known clinical association between diabetes and breast cancer, where patients affected by both have significantly decreased chances of survival (Vona-Davis et al., 2007). Although levels of PMPs appear to be significantly increased only after the development of cancer, PMPs in diabetic patients could have a different miRNA signature. This can be used to predict possible development of breast cancer in diabetic patients. This will be addressed further in the following chapter, chapter 4.

Analysing the effects of NDPMPs on BC cell line MDA-MB-231's morphology, there is a clear indicative that PMPs influence cellular modifications such as elongating their shape, more typical of mesenchymal cells equipped for invasion, and increases their cellular surface through the development of processes on the MDA-MB-231 cells. These modifications can lead to an increase in BC severity if the same effects translate on to triple negative breast cancer cells *in vivo*, where the risk of metastasis is increased due to their modified cell shape. The expansion of their cellular surface can also

lead to a possible increased absorption rate of signalling molecules or elimination of signalling molecules through the new processes developed on the cells, in a similar manner to how platelets are formed.

Following the earlier observation, scratch wound migration assays were performed in order to measure the influence PMPs have on BC cell motility. BC cells of three different types and a healthy breast tissue control (HB2) were influenced to some degree by the presence of PMPs. The results were consistent with the findings of [Zarà et al. \(2017\)](#) and [Vismara et al. \(2021\)](#), which show that PMPs increase the migration potential of MDA-MB-231 cells. Due to the limitations of the scratch wound assay and the potential influence cell debris can have on cell migration, this was only used to test the potential effect of PMPs on BC cells, with more detailed analysis being performed using the boyden chamber assay.

As discussed in the first chapter, the perception of platelet microparticles has evolved from being considered platelet debris, with no functional role, to being important vehicles in the transport of bioactive molecules.

Chapter 4

miRNA-seq analysis of non-diabetic and type 2 diabetic-derived PMPs

The general knowledge and understanding of how PMPs work has evolved. Following the demonstration that PMPs deliver functional RNA to their target cells, in some cases with consequence over their target cell morphology, the next questions that arise would be what type of RNAs do these PMPs deliver? And is there a difference between the molecular compositions of NDPMPs and DPMPs? It is hoped that RNA-seq analysis would shed light on these and help guide this project further.

Statistical evidence points to a difference in breast cancer development between patients with or without a diagnosis of Type 2

Diabetes Mellitus, with most of the evidence derived from meta-analysis, as [Samuel et al. \(2018a\)](#) points out. Another aspect of this study was the link between various miRNAs identified within the components of the PMPs and their effect on breast cancer cells. [Iorio et al. \(2005\)](#) shows that breast cancer is linked to a change in expression levels of certain miRNAs, compared to non-cancerous cell miRNA components. In view of this difference between the presence and absence of Type 2 Diabetes within a breast cancer diagnosis context and with the knowledge that PMPs deliver functional molecules to their target cells, the next step of this study was to analyse the difference between ND and D PMPs through Next Generation RNA Sequencing.

4.1 Quality control analysis

Sample quality control was performed using Nanosight and Stem-loop qPCR analyses. A total of 25 samples, 12 NDPMPs and 13 DPMPs were prepared for sequencing. Nanosight measurements were used to determine sample concentration and confirm microparticle sizes are within the accepted range, with an example of results presented in table 4.1. The main focus was to ensure that DPMP samples were of similar quality and concentrations to the NDPMP samples, as they were isolated at different sites.

As was noted in earlier chapters, average microparticle sizes presented in table 4.1 are within the accepted range mentioned in

Sample	Conc.(particles/ml)	Mean size	SD
BCN7	3.70e+010 +/- 1.06e+010	151.8 nm	71.7 nm
BCN9	1.42e+010 +/- 6.20e+008	134.8 nm	63.5 nm
BCN10	1.48e+010 +/- 1.23e+009	148.9 nm	54.9 nm
BCN11	1.96e+010 +/- 1.33e+009	154.5 nm	66.2 nm
BCN12	1.03e+010 +/- 7.20e+008	150.9 nm	62.6 nm
BCN13	1.22e+010 +/- 1.76e+009	148.9 nm	60.6 nm
BCN14	2.50e+010 +/- 4.67e+008	149.6 nm	87.7 nm
BCN15	1.97e+010 +/- 2.32e+008	123.6 nm	52.2 nm
BCN16	5.66e+009 +/- 8.07e+008	146.7 nm	66.1 nm
BCN17	1.10e+010 +/- 1.50e+009	133.0 nm	63.4 nm
BCN18	2.82e+010 +/- 7.63e+008	116.4 nm	52.5 nm
BCN19	8.77e+009 +/- 7.78e+007	140.1 nm	61.8 nm
BCN20	9.58e+009 +/- 7.33e+008	265.5 nm	105.6 nm
BCN21	3.43e+009 +/- 2.61e+008	148.4 nm	86.0 nm
BCNH8	3.60e+010 +/- 5.15e+008	163.1 nm	72.4 nm
BCNH9	2.61e+010 +/- 1.18e+009	190.1 nm	86.6 nm
BCNH11	2.97e+010 +/- 9.68e+008	185.4 nm	77.1 nm
BCNH13	2.18e+010 +/- 8.43e+008	179.3 nm	82.9 nm
BCNH14	2.41e+010 +/- 8.57e+008	165.8 nm	73.5 nm
BCNH15	3.51e+010 +/- 4.08e+008	162.6 nm	70.4 nm

Table 4.1: **Quality control examples of PMP sample concentrations measured via the Nanosight NS300.** Samples labelled BCN were DPMP samples, whereas BCNH were NDPMP samples. The concentrations were calculated as a mean of four separate measurements of the same sample. Mean size represents the mean size/diameter of the PMPs within the samples analysed. SD represents the standard deviation for each sample.

literature, however, towards the lower end of the spectrum, possibly due to the way platelets were stimulated, in this case by the presence of thrombin.

Following Nanosight analysis, stem-loop qPCR was performed to assess the presence of let-7 in the samples, as [Anene et al. \(2018\)](#) has shown that this miRNA is common across all platelet microparticles. Due to the unavailability of a reference gene, the presence of let-7 was considered relevant for Cq values lower than 35, as can be seen in table 4.2.

	Average Cq Value	SEM
100 μ l NDPMPs	31.88	0.33
200 μ l NDPMPs	29.62	1.7

Table 4.2: **Quality control examples of NDPMP sample** via stem-loop RT-qPCR, where the presence of let-7 was measured in the total RNA extracted from the undiluted sample volumes. Due to the unavailability of a housekeeping gene, only the presence of let-7 was measured.

Once the samples were assessed within the University of Huddersfield, they were delivered for Next Generation RNA Sequencing to be performed at the University of Leeds. Further quality control analysis was performed, using an Agilent Bioanalyser. All 25 samples were measured and the results are presented in table 4.3.

Sample	% miRNA	Concentration (pg/ μ l)
C1	24	6.2
C2	29	5.7
C3	N/A	N/A
C4	1	0.6
C5	7	4.9
C6	27	63.8
C7	26	182.2
C8	25	98.7
C9	23	143
C10	14	38.9
C11	23	92
C12	18	18.6
D1	35	23748.5
D2	11	5.5
D3	23	29
D4	19	17.6
D5	29	17
D6	12	10.1
D7	19	22.6
D8	22	84
D9	25	92.6
D10	23	70.9
D11	1	0
D12	14	1.6
D13	43	100

Table 4.3: **Quality control examples of PMP sample concentrations measured via Agilent Bioanalyser.**

4.2 Next Generation RNA Sequencing

Following this second quality control test, the best four DPMP RNA samples (D2, D3, D6 and D9) and the eight best NDPMP RNA samples (C1, C2, C6, C8, C9, C10, C11 and C12) were used for sequencing. The generated results are shown in figures 4.1, 4.2, 4.3, 4.4, 4.5, 4.6, 4.7.

When comparing the expression levels of miRNAs contained by both ND and D PMPs, it has become clear that there is a difference between the contents of PMPs belonging to each category, see figures 4.1, 4.2, 4.3 and 4.7. Even though there is variation between individual PMPs, a series of miRNAs were clearly common across all samples from the same category.

The variation among samples, seen in figures 4.1 and 4.2, was first determined. In figure 4.1, the multidimensional scaling plot shows that the control samples, the NDPMP miRNA populations presented a close similarity in composition, compared to their diabetic counterparts which showed a stronger heterogeneity. The actual miRNA composition of all samples were analysed in figure 4.2, where all dots represent a common miRNA between ND and D PMPs.

Figure 4.3 shows a side by side comparison between the highest expressed miRNAs in both NDPMPs and DPMPs. The results

are presented in the style of a phylogenetic tree, grouping together genetically similar miRNAs. The presence of each miRNA in every sequenced sample is marked on a heatmap, with the colour variance representing the log₂ counts per million (CPM). This heatmap shows the variability of PMP molecular composition, even within the same types of PMPs.

From the data obtained, two sub-ontologies were created, a molecular function one, figure 4.4, and a biological process one, figure 4.5. The purpose of a gene ontology is to offer a comprehensive list of targets associated with the genes identified through the gene mapping of the PMP samples' sequencing. As its name suggests, the molecular function sub-ontology consists of predicted miRNA targets with relation to the functional structures of a cell. The biological product sub-ontology generated represents predicted targets of the expressed miRNAs within the expression of biological products.

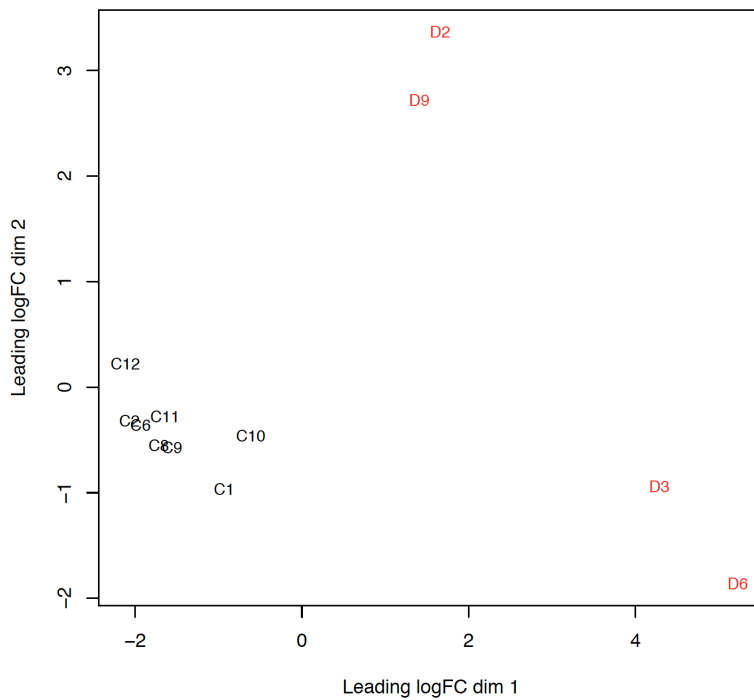


Figure 4.1: **miRNA expression comparison between ND and D PMP RNA.** Multidimensional scaling plot showing relative similarities between the individual samples analysed.

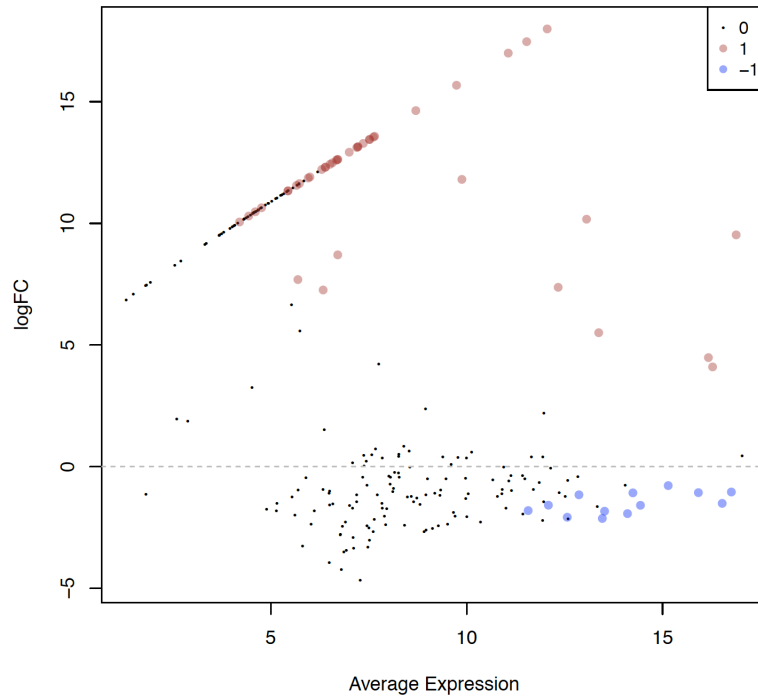


Figure 4.2: **miRNA expression comparison between ND and D PMP RNA.** Visual representation of alignment of miRNAs in both DPMPs and controls via dot plot, where each dot represents an individual sample.

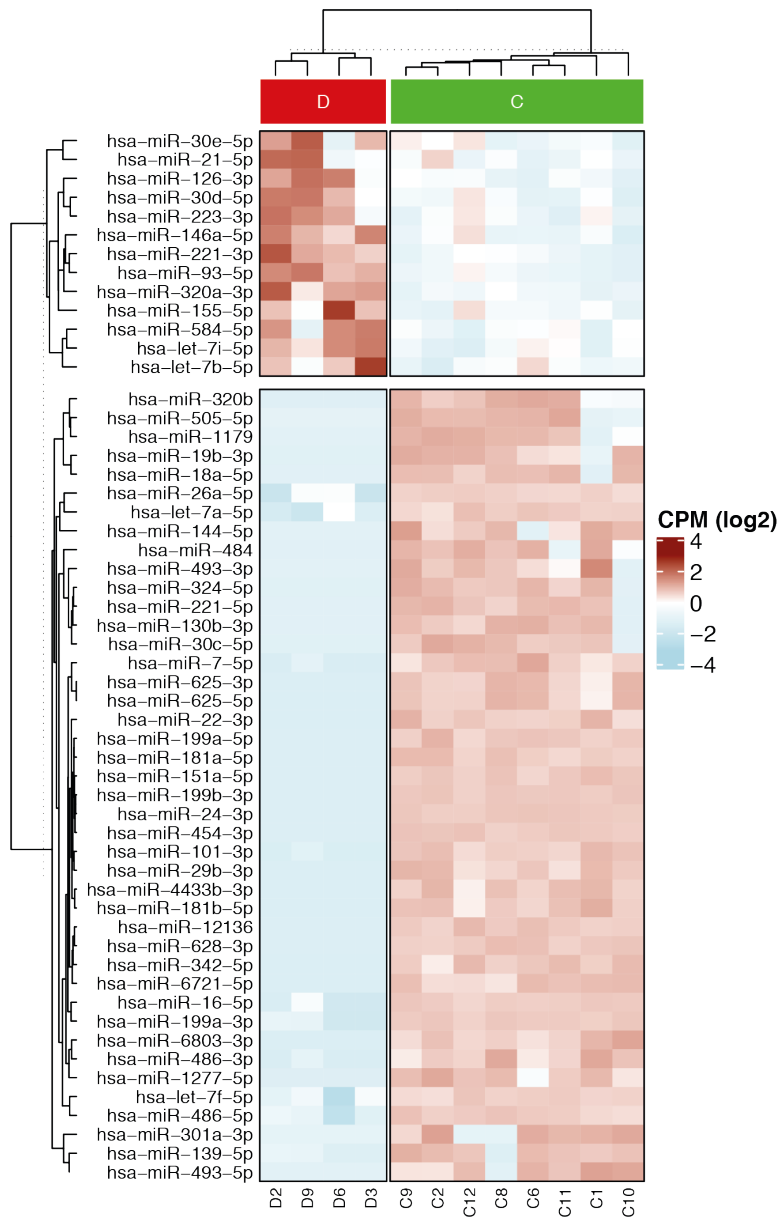


Figure 4.3: **miRNA expression comparison between ND and D PMP RNA.** Phylogenetic tree visualisation of miRNAs present in both types of PMPs, at the highest expression levels in either NDPMPs (C) and Diabetic PMPs (D). CPM represents the **counts per million** reads mapped, presented under log2.

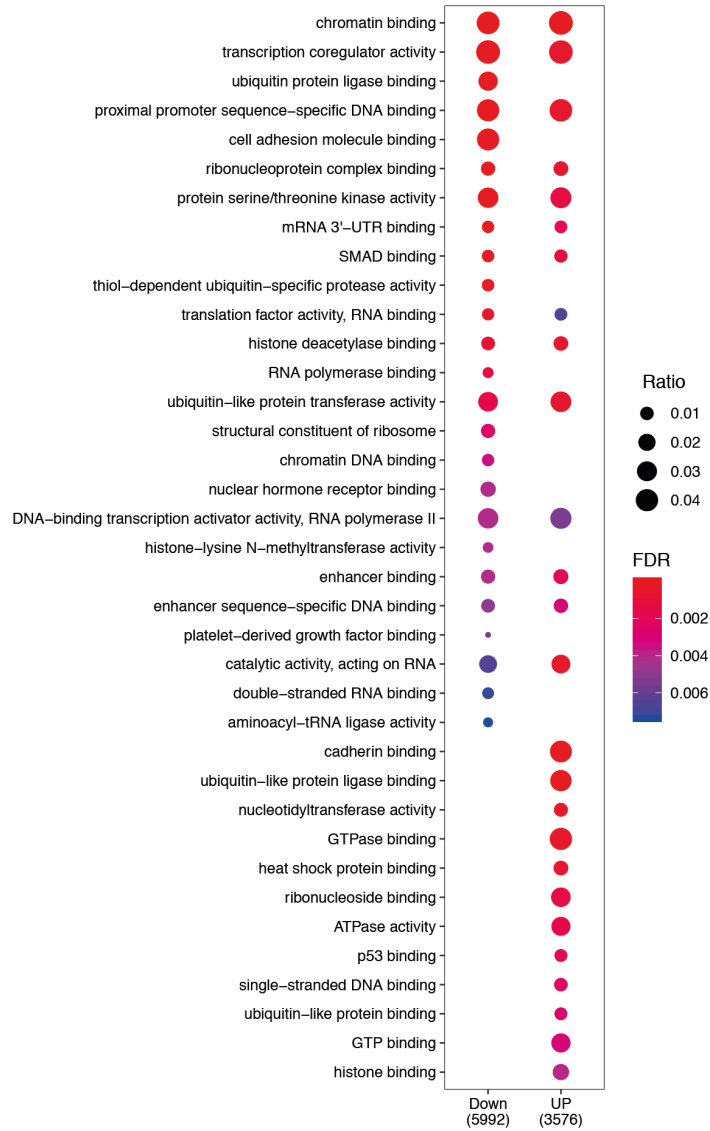


Figure 4.4: **Gene Ontology, sub-ontology molecular function.** Visual representation of the functional targets of the analysed miRNAs mentioned in the figure above.

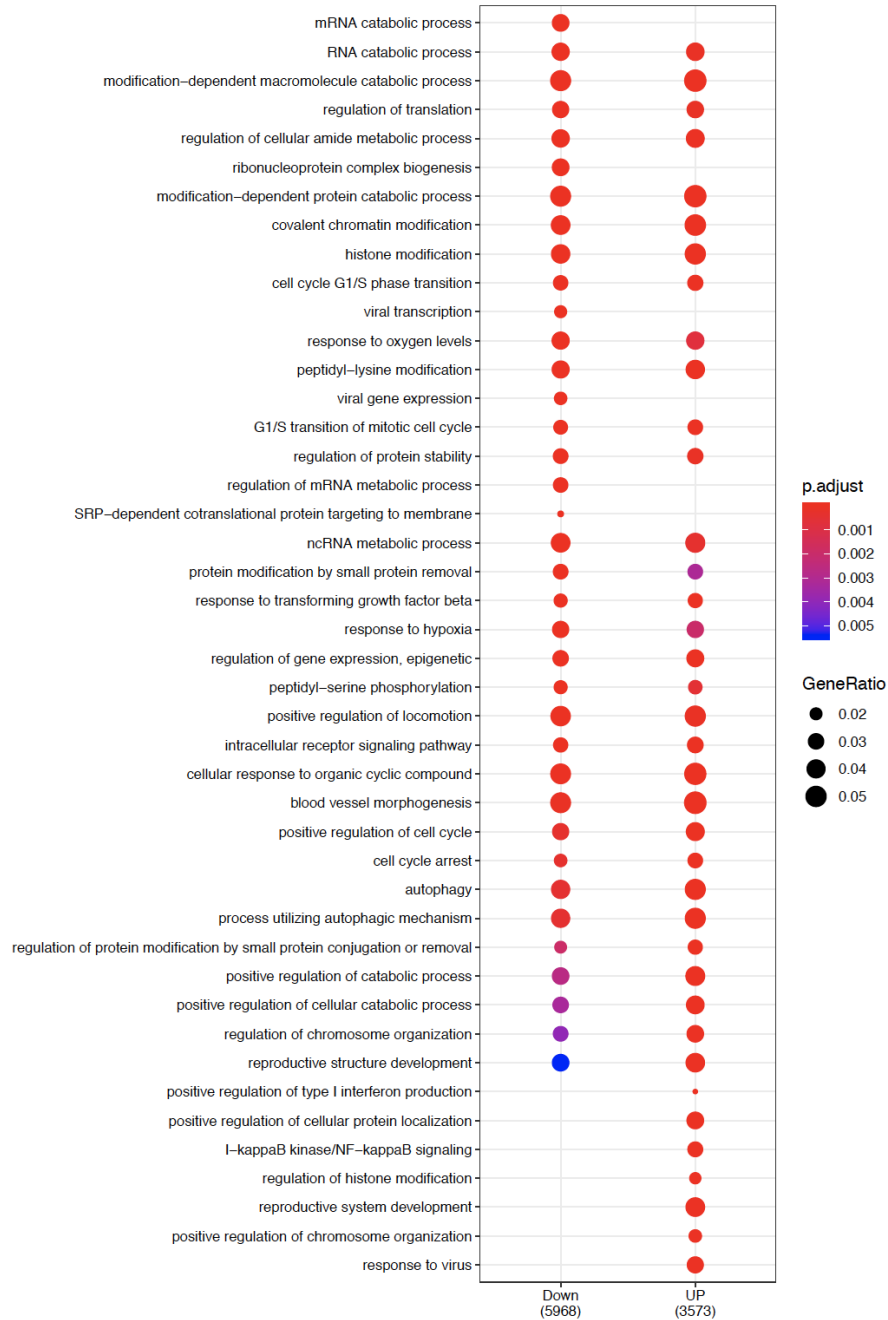


Figure 4.5: **Gene Ontology, sub-ontology biological process.** Visual representation of the functional targets of the analysed miRNAs mentioned in the figure above.

Of the highest expressed miRNAs identified within the DPMP samples, hsa-miR-30e-5p, hsa-miR-21-5p, hsa-miR-126-3p, hsa-miR-30d-5p, hsa-miR-223-3p, hsa-miR-146a-5p, hsa-miR-221-3p, hsa-miR-93-5p, hsa-miR-320a-3p, hsa-miR-155-5p, hsa-let-7i-5p and hsa-let-7b-5p were expressed in higher levels compared to their NDPMP counterparts. Of these miRNAs, hsa-miR-30e-5p (Lin et al., 2016), hsa-miR-126-3p (Wang et al., 2015), hsa-miR-146a-5p, hsa-miR-320a-3p, hsa-let-7i-5p (Lin et al., 2016) and hsa-let-7b-5p (Hu et al., 2013) are typically downregulated in breast cancer. Normally upregulated in breast cancer are hsa-miR-21-5p (Lin et al., 2016), hsa-miR-221-3p (Stinson et al., 2011), hsa-miR-93-5p (Gao et al., 2019) and hsa-miR-155-5p (Jiang et al., 2010). hsa-miR-223-3p is associated in literature with both up and downregulation in breast cancer (Cao et al., 2015; Wei et al., 2017) and hsa-miR-30d-5p (Zhang et al., 2017) is not typically associated with breast cancer.

According to the differential expression table, the miRNAs with the highest logFC (fold change) present in the DPMPs are shown, ranked in order, in figure 4.6. This figure only represents the contents of DPMPs, however, through data normalising, figure 4.7 was produced showing a side by side comparison between the top miRNA found in both or either types of PMPs. In this figure NDPMPs (control) present a higher variety of miRNAs present within the microparticles.

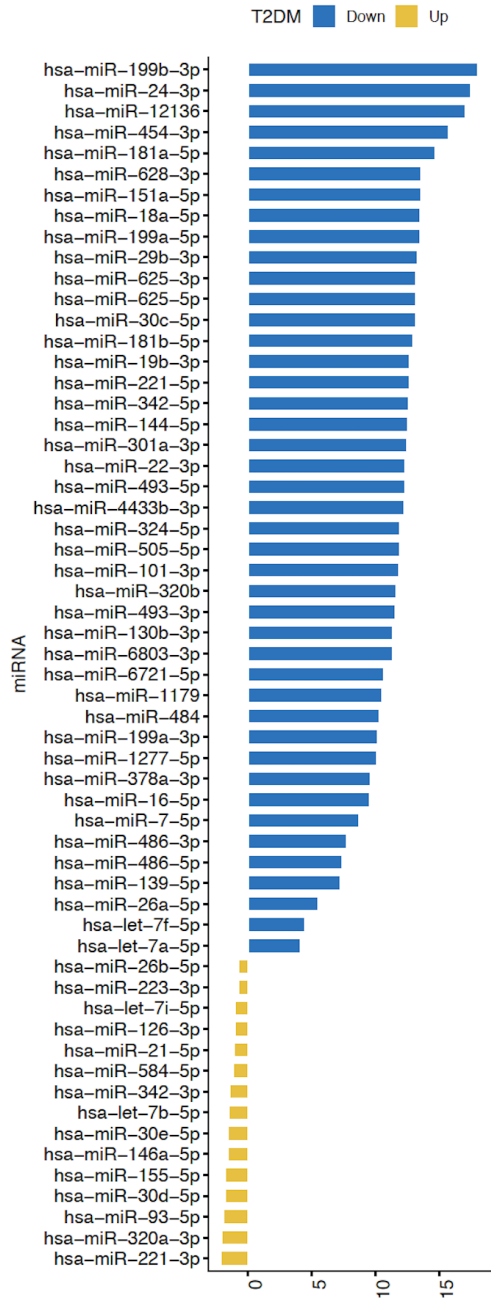


Figure 4.6: List of DPMP miRNAs, ranked by logFC (x axis). This list was used to further determine the target mRNAs.

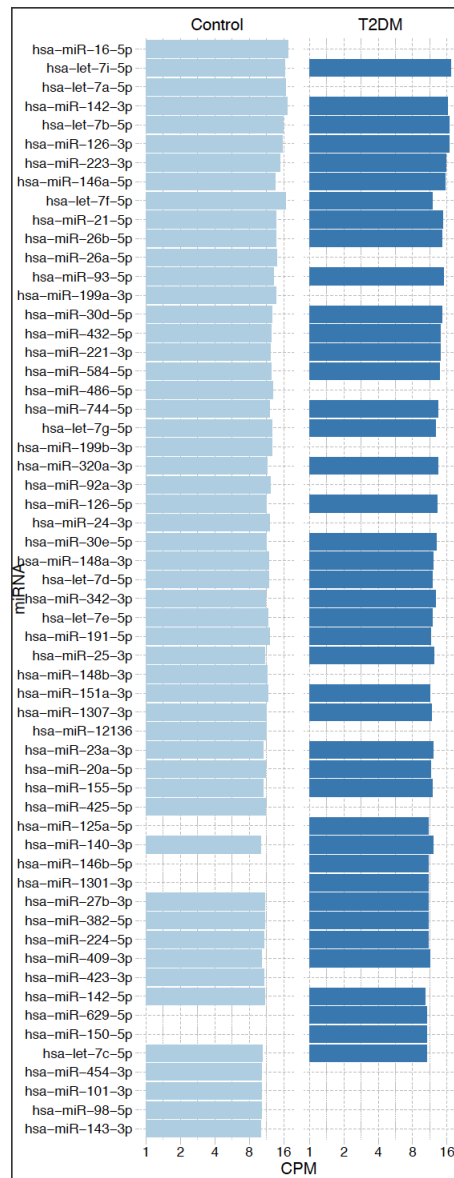


Figure 4.7: Visual representation of top abundance of miRNAs in both NDPMPs and DPMPs. Data was normalised and ranked by counts per million.

Downregulated in BC	Downregulated in BC
hsa-miR-142-3p	hsa-miR-139-3p
hsa-miR-16-5p	hsa-miR-361-5p
hsa-let-7i-5p	hsa-miR-379-5p
hsa-let-7b-5p	hsa-miR-196b-5p
hsa-let-7a-5p	hsa-miR-140-5p
hsa-miR-126-3p	hsa-miR-181a-5p
hsa-miR-146a-5p	hsa-miR-451a
hsa-miR-26b-5p	hsa-miR-130a-3p
hsa-let-7g-5p	hsa-miR-15a-5p
hsa-miR-126-5p	hsa-miR-381-3p
hsa-miR-320a-3p	hsa-miR-335-5p
hsa-miR-148a-3p	hsa-miR-107
hsa-let-7e-5p	hsa-miR-361-3p
hsa-miR-30e-5p	hsa-miR-340-5p
hsa-miR-199b-3p	hsa-miR-425-3p
hsa-let-7d-5p	hsa-miR-10a-5p
hsa-miR-25-3p	hsa-let-7d-3p
hsa-miR-148b-3p	hsa-miR-339-5p
hsa-miR-425-5p	hsa-miR-652-3p
hsa-miR-142-5p	hsa-miR-485-3p
hsa-miR-140-3p	hsa-miR-671-5p
hsa-miR-27b-3p	hsa-miR-30e-3p
hsa-miR-409-3p	hsa-miR-625-3p
hsa-let-7c-5p	hsa-miR-625-5p
hsa-miR-186-5p	hsa-miR-30c-5p
hsa-miR-98-5p	hsa-miR-30a-5p
hsa-miR-185-5p	hsa-miR-485-5p
hsa-miR-143-3p	hsa-miR-92b-5p
hsa-miR-146b-5p	hsa-miR-411-5p
hsa-miR-101-3p	hsa-miR-26b-3p
hsa-miR-17-5p	hsa-miR-127-3p
hsa-miR-1301-3p	hsa-miR-152-3p
hsa-miR-134-5p	hsa-miR-431-5p
hsa-miR-328-3p	

Table 4.4: **List of miRNAs present in DPMPs that are typically downregulated in breast cancer.** This list has been compiled from the top 100 miRNAs (highest logCPM from the differential expression table) cross-referenced with <http://mirccancer.ecu.edu/> .

Upregulated	Both Up and Downregulated
hsa-miR-21-5p	hsa-miR-223-3p
hsa-miR-93-5p	hsa-miR-92a-3p
hsa-miR-221-3p	hsa-miR-223-5p
hsa-miR-191-5p	hsa-miR-29c-3p
hsa-miR-155-5p	hsa-miR-374a-5p
hsa-miR-24-3p	hsa-miR-17-3p
hsa-miR-20a-5p	
hsa-miR-23a-3p	
hsa-miR-423-3p	
hsa-miR-125a-5p	
hsa-miR-224-5p	
hsa-miR-150-5p	
hsa-miR-27a-3p	
hsa-miR-222-3p	
hsa-miR-106b-3p	
hsa-miR-182-5p	
hsa-miR-29a-3p	
hsa-miR-197-3p	
hsa-miR-20b-5p	
hsa-miR-18a-5p	
hsa-miR-370-3p	
hsa-miR-181b-5p	

Table 4.5: **List of miRNAs present in DPMPs that are typically upregulated (right column), or have presented as both upregulated and downregulated (left column) in breast cancer.** This list has been compiled from the top 100 miRNAs (highest logCPM from the differential expression table) cross-referenced with <http://mirancer.ecu.edu/> .

Upregulated but not BC specific	
hsa-let-7f-5p	hsa-miR-1306-5p
hsa-miR-30d-5p	hsa-miR-3615
hsa-miR-432-5p	hsa-miR-190a-5p
hsa-miR-199a-3p	hsa-miR-628-3p
hsa-miR-584-5p	hsa-miR-664b-5p
hsa-miR-744-5p	hsa-miR-151a-5p
hsa-miR-342-3p	hsa-miR-199a-5p
hsa-miR-151a-3p	hsa-miR-491-5p
hsa-miR-1307-3p	hsa-miR-942-5p
hsa-miR-382-5p	hsa-miR-654-3p
hsa-miR-12136	hsa-miR-2110
hsa-miR-454-3p	hsa-miR-5187-5p
hsa-miR-629-5p	hsa-miR-29b-3p
hsa-miR-28-3p	hsa-miR-760
hsa-miR-664a-5p	hsa-miR-3613-5p
hsa-miR-99b-5p	hsa-miR-190b-5p
hsa-miR-15b-5p	hsa-miR-192-5p
hsa-miR-128-3p	hsa-miR-1287-5p
hsa-miR-23b-3p	hsa-miR-363-3p
hsa-miR-1908-5p	hsa-miR-17-3p
hsa-miR-548j-5p	

Table 4.6: **List of miRNAs present in DPMPs that are typically up-regulated but present no specific association with breast cancer.** This list has been compiled from the top 100 miRNAs (highest logCPM from the differential expression table) cross-referenced with <http://mir-cancer.ecu.edu/> .

Using the differential expression table, it was identified that in the 100 highest expressed miRNAs, over half are normally associated with lower expression in breast cancer, table 4.4. There are however, miRNAs present that are typically upregulated in breast cancer and some whose role is not clearly determined, tables 4.5

and 4.6.

4.3 Chapter discussion

Following a detailed analysis of the miRNA composition of platelet microparticles of either diabetic or non-diabetic origin, a comprehensive list has been generated.

Of the miRNAs expressed in DPMPs at a significantly higher level, hsa-miR-30e-5p is one of the highest common expressed associated with breast cancer. Although the typical association is that a T2DM diagnosis could increase the severity of a breast cancer diagnosis, [Liu et al. \(2017\)](#) found that miR-30e, in this study associated with DPMPs, has the potential to inhibit tumour growth and chemoresistance, particularly in breast cancer. [Liu et al. \(2017\)](#) notes there are significantly decreased levels of miR-30e in MCF-7 and MDA-MB-231 cell lines, compared to MCF10A cells representative of normal breast tissue cells.

Another predominantly present miRNA in DPMPs is miR-21. A high presence of this particular miRNA has been associated with breast cancer in patient samples in prior studies and particularly associated with tumour metastasis ([Song et al., 2010](#)). The next miRNA, miR-126, is also highly expressed in DPMPs. High expression of miR-126, however, has been associated with metastatic suppression in breast cancer [Wang et al. \(2015\)](#).

Through an overall comparison of the miRNA composition of the PMPs in question, NDPMPs presented a more consistent and homogeneous composition compared to the DPMPs. The higher variability of these microparticles could be attributed to a potential difference in diabetic platelets or formation mechanism, but given how the samples were collected at different sites, it must not be excluded that a slight difference in the PMP isolation process could have caused this.

Although NDPMPs and DPMPs present a high number of common miRNAs, the significantly different ones were presented, as a direct comparison between the composition of NDPMPs and DPMPs. The phylogenetic tree visualisation offers a better understanding of the similarities between the miRNAs mapped. As seen in figure 4.3, there are certainly visible differences between the two types of PMPs, with DPMPs having a higher amount of miRNAs which are typical of NDPMPs suppressed and vice versa. With this in mind the top two highest expressed miRNAs in DPMPs that are of the same subgroup, miR-30e and miR-21, are known to have opposite effects on breast cancer development.

Through the gene ontologies generated, the molecular function sub-ontology presents a higher variety of modifications, suggesting a strong potential of DPMPs in the development of breast cancer.

Taking all of this into consideration and looking at the top 100 miRNAs with the highest $\log_2 CPM$, a much higher proportion of miRNAs is typically associated with breast cancer reduction through their upregulation (70.5% of top 100 miRNAs associated with BC) than miRNAs which promote the development of breast cancer through upregulation (23% of top 100 miRNAs associated with BC). Although the number of miRNAs positively correlated with BC development is smaller, the individual targets of each of these miRNAs have not been analysed. One of the characteristics of miRNAs aforementioned in the text is that one miRNA can have more than one target. It is important that a comprehensive list and comparison between the miRNAs presented is compiled in the future in order to clearly determine if DPMP composition is the direct cause of BC metastasis, or if there are other mechanisms involved as well.

Chapter 5

The effects of DPMPs versus NDPMPs on breast cancer cell lines

Throughout this project it has been established that NDPMPs influence the characteristics and events within breast cancer cells, from their ability to internalise RNA molecules delivered via PMPs to their influence on morphological modifications. Following the results of the RNA sequencing analysis, there is a clear difference between the compositions of DPMPs and NDPMPs, with DPMPs presenting a potential of influencing the further development of breast cancer through the presence of oncomirs.

In order to determine the extent of the effects of platelet microparticles, whether diabetic or non diabetic on breast cancer cell lines,

phenotypic and gene expression analyses were performed, followed by functional analysis.

5.1 Cell Viability

In order to assess how PMPs impacted on BC cell growth and viability, the CellTiter Glo kit (Promega) was used. MCF-7 and MDA-MB-231 cells were incubated at a density of 5000 cells/well and treated with both 100 $\mu\text{g}/\text{ml}$ ND PMPs and D PMPs, with their effects on cell viability levels measured at 0, 24 and 48 hours. All results were translated into percentages and compared.

As per figure 5.1, MCF-7 cell viability is presented as percentages for the 0, 24 and 48 hour time marks. T0 was considered 100% and the conditions were positive control: MCF-7 cells incubated with 10 % serum containing DMEM, negative control: MCF-7 cells incubated in serum free DMEM and the other two experimental conditions: MCF-7 cells incubated in serum free DMEM with 100 $\mu\text{g}/\text{ml}$ NDPMP and MCF-7 cells incubated in serum free DMEM with 100 $\mu\text{g}/\text{ml}$ DPMP. As it can be seen in figure 5.1, this lumino-metric assay shows that the presence of NDPMPs induce a higher growth rate, however, the presence of DPMPs maintain a better balance between cell growth and cell death.

In figure 5.2 cell viability measurements for MDA-MB-231 using the same luminometric assay, CellTiter-Glo, can be observed. As

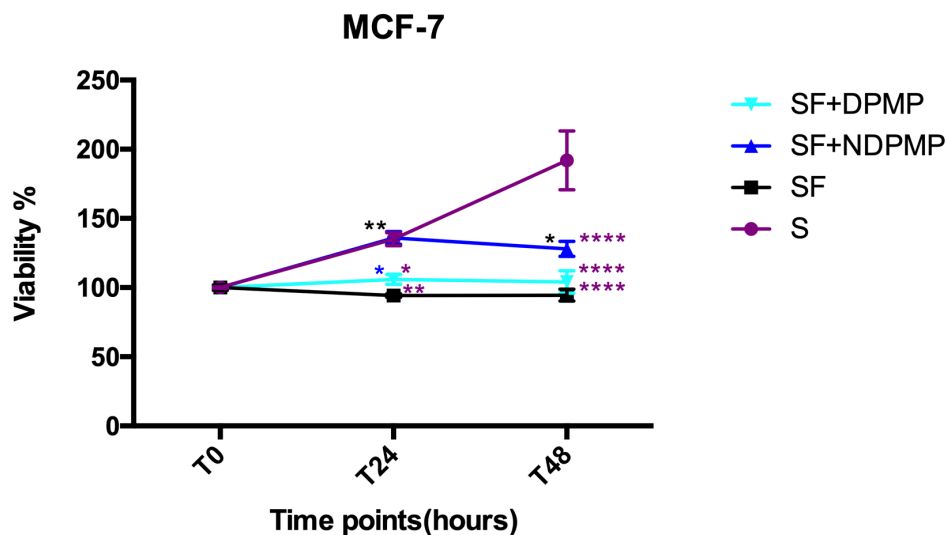


Figure 5.1: **MCF-7 cell viability analysis.** MCF-7 cells were seeded at a density of 5000 cells per well and serum starved for 4 hours before PMPs were added. Cell viability measurements, translated into percentages, of MCF-7 cells incubated in serum free DMEM in the presence of 100 $\mu\text{g}/\text{ml}$ NDPMP (SF+NDPMP) or 100 $\mu\text{g}/\text{ml}$ DPMP (SF+DPMP). Positive control was MCF-7 cells in 10 % serum containing DMEM (S) and negative control was MCF-7 cells in serum free DMEM (SF). Two-way ANOVA test was performed, followed by Tukey's multiple comparisons test, via Prism 6.2. The results of the multiple comparisons were at T24: S vs SF (**, $q=5.625$), S vs SF+NDPMP (ns, $q=0.139$), S vs SF+DPMP (*, $q=4.008$), SF vs SF+NDPMP (**, $q=5.764$), SF vs SF+DPMP (ns, $q=1.162$), SF+NDPMP vs SF + DPMP (*, $q=4.146$). T 48: S vs SF (****, $q=13.48$), S vs SF+NDPMP (****, $q=8.846$), S vs SF+DPMP (****, $q=12.16$), SF vs SF+NDPMP (*, $q=4.630$), SF vs SF+DPMP (ns, $q=1.313$), SF+NDPMP vs SF+DPMP (ns, $q=3.317$). Where q represents the false discovery rate, with a cut off of 5 %.

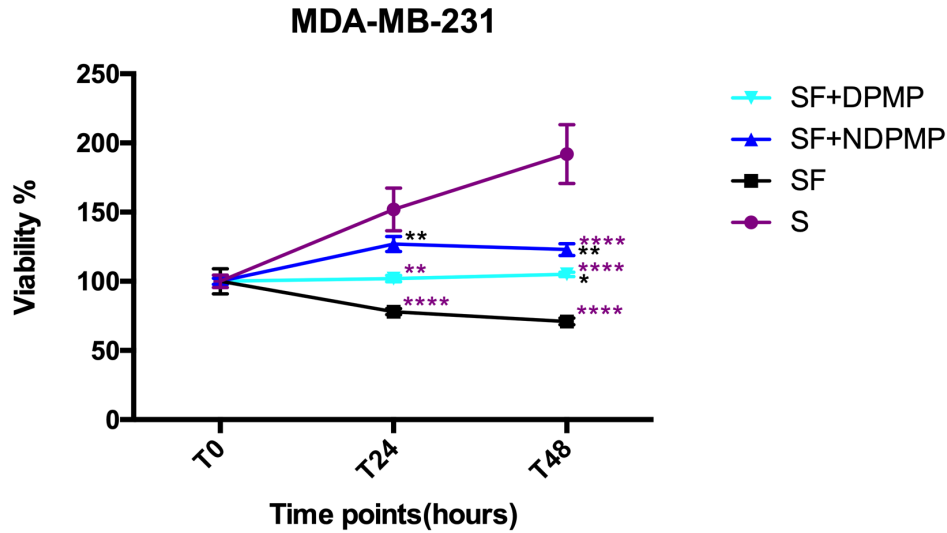


Figure 5.2: **MDA-MB-231 cell viability analysis.** MDA-MB-231 cells were seeded at a density of 5000 cells per well and serum starved for 4 hours before PMPs were added. Cell viability measurements, translated into percentages, of MDA-MB-231 cells incubated in serum free DMEM in the presence of 100 $\mu\text{g}/\text{ml}$ NDPMP (SF+NDPMP) or 100 $\mu\text{g}/\text{ml}$ DPMP (SF+DPMP). Positive control was MDA-MB-231 cells in 10 % serum containing DMEM (S) and negative control was MDA-MB-231 cells in serum free DMEM (SF). Two-way ANOVA test was performed, followed by Tukey's multiple comparisons test, via Prism 6.2. The results of the multiple comparisons were at T24: S vs SF (****, $q=8.713$), S vs SF+NDPMP (ns, $q=2.947$), S vs SF+DPMP (**, $q=5.895$), SF vs SF+NDPMP (**, $q=5.765$), SF vs SF+DPMP (ns, $q=2.818$), SF+NDPMP vs SF + DPMP (ns, $q=2.947$). T 48: S vs SF (****, $q=14.27$), S vs SF+NDPMP (****, $q=8.135$), S vs SF+DPMP (****, $q=10.26$), SF vs SF+NDPMP (**, $q=6.131$), SF vs SF+DPMP (*, $q=4.009$), SF+NDPMP vs SF+DPMP (ns, $q=2.122$). Where q represents the false discovery rate, with a cut off of 5%.

with the MCF-7 cells, the MDA-MB-321 cells were incubated in the same conditions and ATP levels were measured at the same time points. There is a clearer distinction between the trends, but the NDPMPs show the same effect on the MDA-MB-231 cells as they did on the MCF-7 cells, with a spike in viability at 24 hours followed by a decrease at 48 hours. DPMPs appear to influence equal levels of cell viability at the 24 and 48 hour time points. Both types of PMPs influence cell viability in a positive manner, despite the absence of serum in the wells.

5.2 The influence of PMPs on cellular migration

Migration potential of cells under the effects of PMPs were measured using both Scratch Wound assays and Boyden Chamber assays. The scratch wound assay was performed only on cells incubated with NDPMPs, as mentioned in chapter 3, the Boyden Chamber assay was performed on cells incubated with both NDPMPs and DPMPs. While the scratch wound assay focused solely on the migration potential of cells within the same media, the Boyden chamber assay measured, in more depth, the chemotactic and chemokinetic potential of cells. A direct comparison between the effects of NDPMPs versus DPMPs on BC cells has also been analysed.

In this set of experiments, the cell lines used were MDA-MB-231, MCF-7, MDA-MB-453 and T47D. The results can be seen in figures 5.3, 5.4, 5.5 and 5.6. Each figure presents the effects of both NDPMP and DPMPs, in subfigures A and B. Chemokinesis, where the insert containing cells in serum free DMEM was placed over a well containing serum free DMEM, is displayed in the two left bars and chemotaxis, where the insert containing cells in serum free DMEM was placed in a well containing 10% serum DMEM, is displayed in the right two columns. Relative difference between the normalised chemokinetic and chemotactic rates between the two conditions in subfigures E and F.

In figure 5.3, the effect of NDPMPs, subfigure 5.3A, and DPMPs, subfigure 5.3B, on the migration potential of the MDA-MB-231 cell line previously mentioned is presented. Both NDPMPs and DPMPs had a significant effect on the chemokinetic and the chemotactic potential of these cells. As seen in subfigure 5.3A, the effect of NDPMPs on cell migration was significantly greater compared to the controls in both cases of chemokinesis and chemotaxis, whereas in subfigure 5.3B, DPMPs have only had a greater effect in the case of chemokinesis, there was no significant difference between the two conditions under chemotactic conditions. Subfigures 5.3C and D, show representative images of the conditions presented in the top subfigures, where the cells are shown in a purple-like colour and the empty pores are viewed as circles with a dark outline. Subfigures

5.3E and F present the difference between the chemokinetic and chemotactic rates of both NDPMPs and DPMPs. Subfigures E and F were generated by comparison with their respective SF/SF conditions, where SF/SF cell counts were considered 100%. This method only presents a relative comparison, due to the variations between the SF/SF condition counts in the experiments, which could have been caused by a number of factors, such as membrane preparation and area of membrane counting. In the case of this particular cell line, MDA-MB-231, cells incubated in the presence of NDPMPs present a higher rate of migration in both chemokinesis and chemotaxis conditions compared to the same cells incubated in the presence of DPMPs. Despite NDPMPs having a higher effect ratio wise, DPMPs produced a higher cell count overall.

In figure 5.4, MCF-7 cells were incubated with both NDPMPs and DPMPs and their effects on both chemokinesis and chemotaxis were measured. The effect of NDPMPs on MCF-7 cell migration is presented in subfigure 5.4 A and the effect of DPMPs in subfigure 5.4 B. The NDPMPs had a significant increase in chemokinetic migration of the MCF-7 cells, in a similar fashion to their DPMPs co-incubation. When observing the chemotactic migration potential of these cells however, the presence of NDPMPs have decreased cellular migration compared to the control, whereas DPMP co-incubation has led to an increase in the migration of MCF-7 cells. Subfigures 5.4C and D show representative images of fields of view

used in cell counting, and subfigures 5.4E and F show the difference in the migration rates of MCF-7 cells incubated with either NDPMPs or DPMPs. As seen in both subfigures, co-incubation of MCF-7 cells with NDPMPs has led to an increase in cellular migration in both chemokinetic and chemotactic conditions. Even though that appears to be the case after normalisation, it is important to note that in subfigures 5.4 A and B DPMPs have a much higher cell count overall compared to NDPMPs.

For MDA-MB-453 cells incubated with either NDPMPs or DPMPs, NDPMPs had a much higher effect overall, with a significantly raised cell count, figure 5.5. Even so, co-incubation of these cells with DPMPs has led to an increase in migration, under both chemotactic and chemokinetic conditions.

The same cannot be said about the T47D cells incubated under the same conditions. NDPMPs had a clear impact on chemokinesis of the cells, but none on the chemotactic potential, figure 5.6. DPMPs had a higher impact overall on both chemokinesis and chemotaxis and overall much higher than that of NDPMPs.

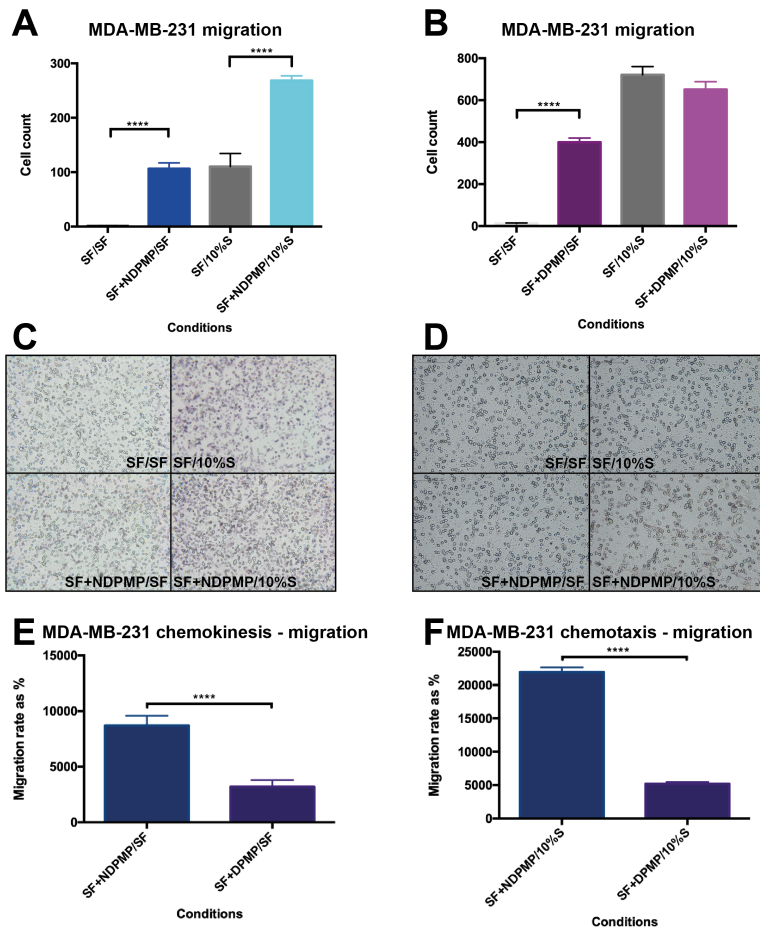


Figure 5.3: **MDA-MB-231 migration measured using transwell chambers.** Cells were seeded at 100 000 cells per well in serum free DMEM and incubated in the presence or absence of 100 $\mu\text{g}/\text{ml}$ non-diabetic or diabetic PMPs. Migrated cells were counted after 6 hours of incubation. **A.** MDA-MB-231 migration measured in the presence and absence of NDPMPs. The two left columns represent the chemokinetic ability of the cells, while the right two columns represent the chemotactic ability of cells. **B.** MDA-MB-231 migration measured in the presence and absence of DPMPs, with chemokinesis and chemotaxis represented the same way. **C.D.** Representative images of the microscopic field of view used to count migration levels of cells. Magnification x40. **E.** The effect of NDPMPs vs. DPMPs on the chemokinesis of these cells. **F.** The effect of NDPMPs vs. DPMPs on the chemotaxis of these cells.

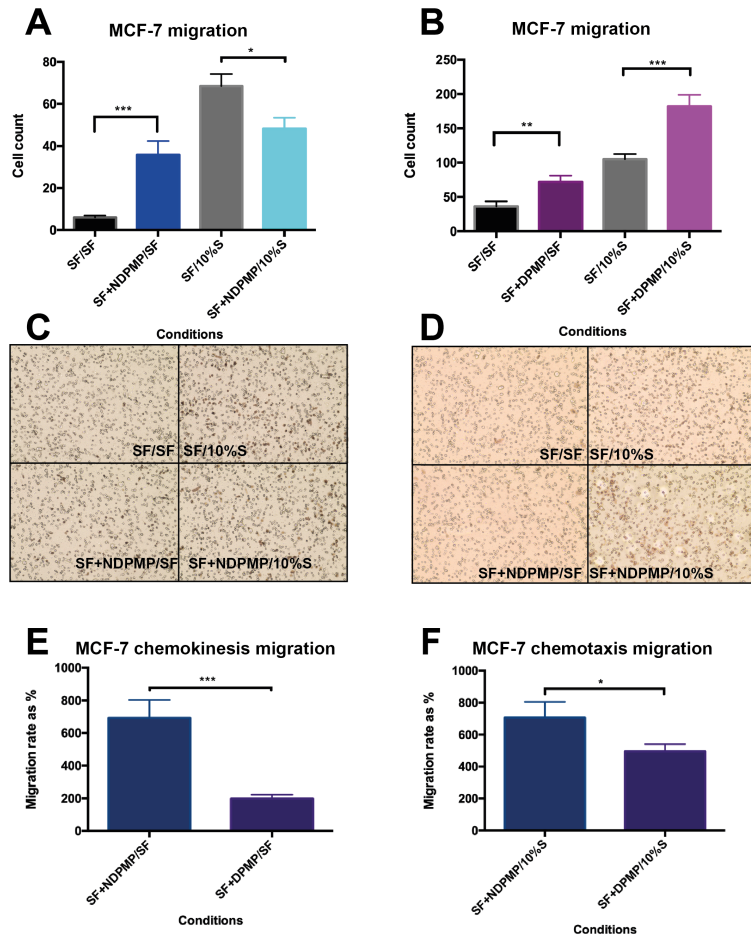


Figure 5.4: **MCF-7 migration measured using transwell chambers.** Cells were seeded at 100 000 cells per well in serum free DMEM and incubated in the presence or absence of 100 $\mu\text{g}/\text{ml}$ non-diabetic or diabetic PMPs. Migrated cells were counted after 6 hours of incubation. **A.** MCF-7 migration measured in the presence and absence of NDPMPs. The two left columns represent the chemokinetic ability of the cells, while the right two columns represent the chemotactic ability of cells. **B.** MCF-7 migration measured in the presence and absence of DPMPs, with chemokinesis and chemotaxis represented the same way. **C. D.** Representative images of the microscopic field of view used to count migration levels of cells. Magnification x40. **E.** The effect of NDPMPs vs. DPMPs on the chemokinesis of these cells. **F.** The effect of NDPMPs vs. DPMPs on the chemotaxis of these cells.

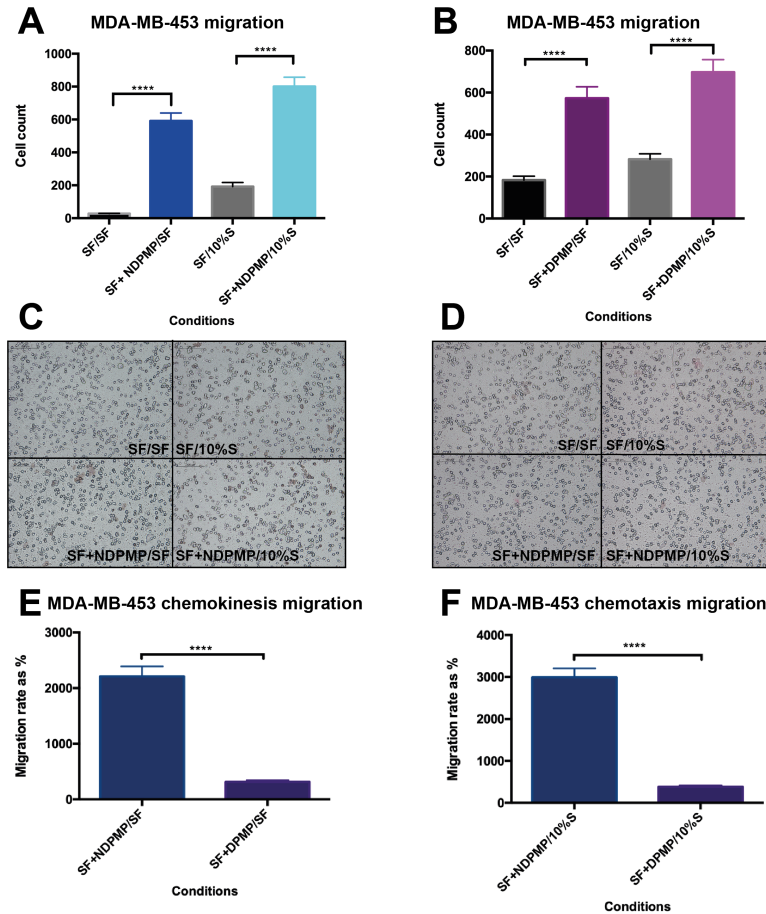


Figure 5.5: **MDA-MB-453 migration measured using transwell chambers.** Cells were seeded at 100 000 cells per well in serum free DMEM and incubated in the presence or absence of 100 $\mu\text{g}/\text{ml}$ non-diabetic or diabetic PMPs. Migrated cells were counted after 6 hours of incubation. **A.** MDA-MB-453 migration measured in the presence and absence of NDPMPs. The two left columns represent the chemokinetic ability of the cells, while the right two columns represent the chemotactic ability of cells. **B.** MDA-MB-453 migration measured in the presence and absence of DPMPs, with chemokinesis and chemotaxis represented the same way. **C.D.** Representative images of the microscopic field of view used to count migration levels of cells. Magnification $\times 40$. **E.** The effect of NDPMPs vs. DPMPs on the chemokinesis of these cells. **F.** The effect of NDPMPs vs. DPMPs on the chemotaxis of these cells.

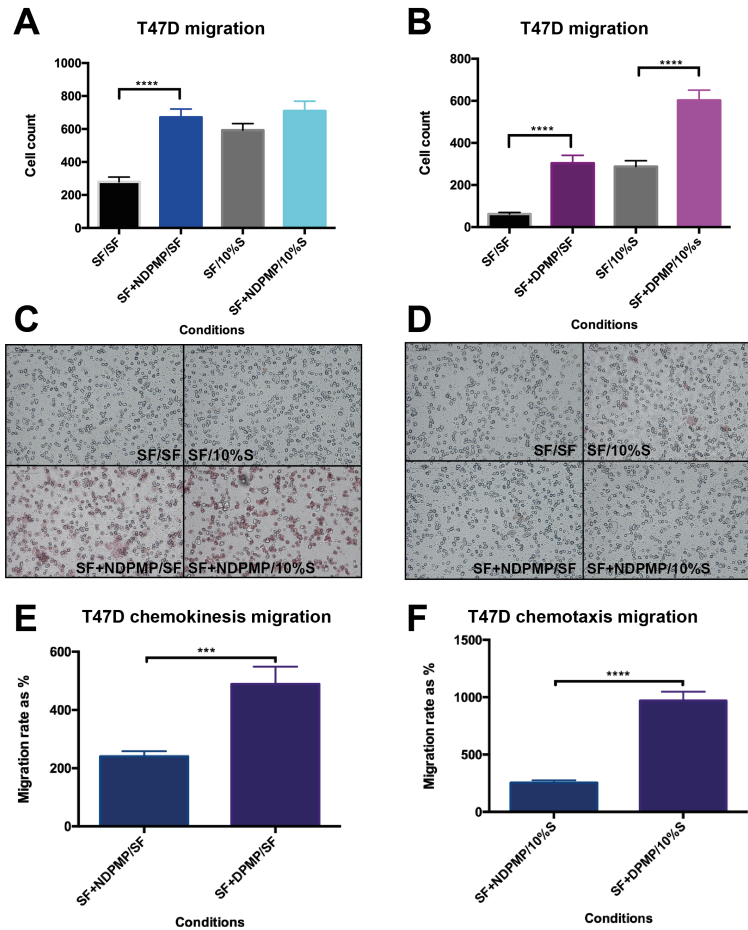


Figure 5.6: **T47D migration measured using transwell chambers.** Cells were seeded at 100 000 cells per well in serum free DMEM and incubated in the presence or absence of 100 $\mu\text{g}/\text{ml}$ non-diabetic or diabetic PMPs. Migrated cells were counted after 6 hours of incubation. **A.** T47D migration measured in the presence and absence of NDPMPs. The two left columns represent the chemokinetic ability of the cells, while the right two columns represent the chemotactic ability of cells. **B.** T47D migration measured in the presence and absence of DPMPs, with chemokinesis and chemotaxis represented the same way. **C. D.** Representative images of the microscopic field of view used to count migration levels of cells. Magnification x40. **E.** The effect of NDPMPs vs. DPMPs on the chemokinesis of these cells. **F.** The effect of NDPMPs vs. DPMPs on the chemotaxis of these cells.

5.3 The influence of PMPs on cellular invasion

The invasion rates of all the four cell lines previously mentioned were measured via co-incubation of these cells with NDPMPs and DPMPs under specific conditions. The results of these experiments can be seen in figures 5.7, 5.8, 5.9 and 5.10, where subfigures A represent the invasion levels of the cell lines incubated in the presence of 100 $\mu\text{g}/\text{ml}$ NDPMPs, whereas the subfigures B show the invasion levels of the cell lines with 100 $\mu\text{g}/\text{ml}$ DPMPs. Subfigures C and D show representative images of each of the conditions studied, in the case of both chemokinesis and chemotaxis, in the presence and absence of either ND and DPMPs. Subfigures E and F present a comparison of the rates of invasion of cells incubated with either NDPMPs and DPMPs.

MDA-MB-231 cells were incubated overnight in the presence and absence of NDPMP, 5.7A, or DPMPs, 5.7B. PMPs of both kinds have shown to increase the invasion levels of the cells compared to their controls, DPMPs however, increased the invasion levels of the MDA-MB-231 cells compared to their ND counterparts in both chemokinetic and chemotactic conditions, 5.7 E and F. MCF-7 cells were incubated in the same conditions, figure 5.8, and only the presence of NDPMPs in conditions of measuring chemokinesis led to an increase in MCF-7 cell invasion, 5.8A. The presence of both

NDPMPs and DPMPs negatively influenced the chemotactic gradient of cells. When comparing the invasion rates of MCF-7 cells incubated in the presence of NDPMPs or DPMPs, the NDPMPs drove to a significantly higher invasion rate compared to the same cells incubated with DPMPs, matching the difference in cell count as well.

MDA-MB-453 and T47D cell lines were also incubated with NDPMPs and DPMPs, figure 5.9 and figure 5.10. In both sets, incubation in the presence of PMPs have not shown a statistically significant difference compared to their controls. However, in chemotactic conditions, NDPMPs have increased invasion in MDA-MB-453 cells, subfigure 5.9F, and DPMPs have increased invasion levels of T47D cells, subfigure 5.10F.

5.4 The effect of DPMPs on BC cell morphology

PMPs, especially DPMPs, have shown to have a dramatic effect on the evolution of different types of breast cancer. Out of all types analysed, the triple negative breast cancer cell line MDA-MB-231 has proven itself to be the most susceptible to the influence of PMPs, therefore the decision was made to focus strictly on this cell line in future experiments to allow for a more detailed observation.

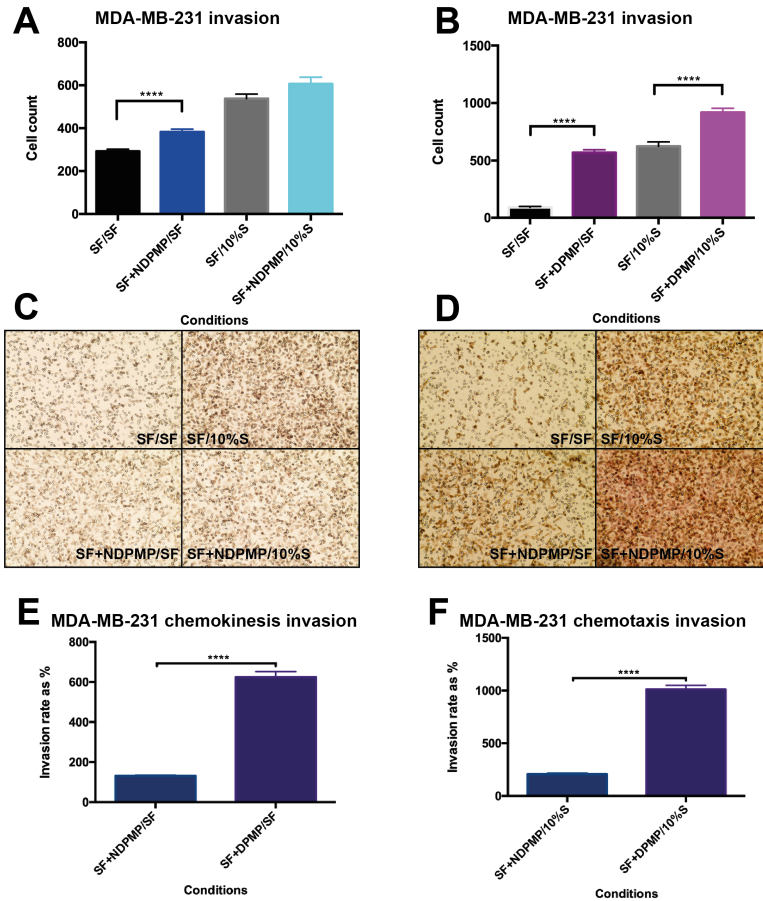


Figure 5.7: MDA-MB-231 invasion levels measured using transwell chambers. Cells were seeded at 100 000 cells per well in serum free DMEM and incubated in the presence or absence of 100 $\mu\text{g}/\text{ml}$ non-diabetic or diabetic PMPs. Invading cells were counted after overnight incubation. **A.** MDA-MB-231 invasion levels measured in the presence and absence of NDPMPs. The two left columns represent the chemokinetic ability of the cells, while the right two columns represent the chemotactic ability of cells. **B.** MDA-MB-231 invasion measured in the presence and absence of DPMPs, with chemokinesis and chemotaxis represented the same way. **C.D.** Representative images of the microscopic field of view used to count invasion levels of cells. Magnification $\times 40$. **E.** The effect of NDPMPs vs. DPMPs on the chemokinesis of these cells. **F.** The effect of NDPMPs vs. DPMPs on the chemotaxis of these cells.

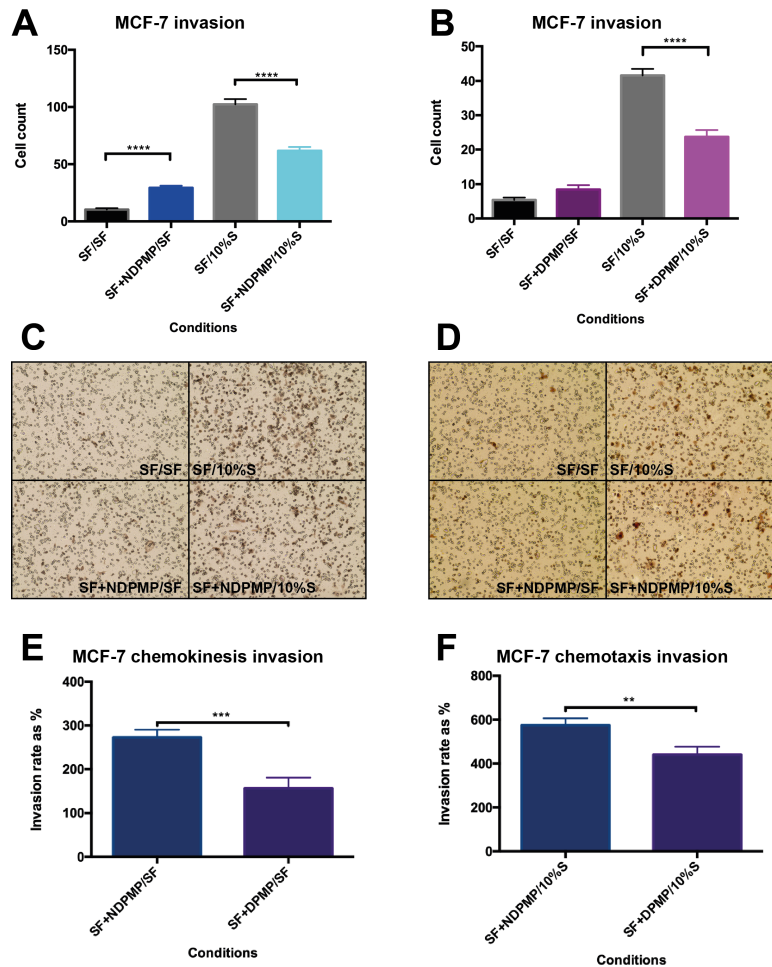


Figure 5.8: MCF-7 invasion levels measured using transwell chambers. Cells were seeded at 100 000 cells per well in serum free DMEM and incubated in the presence or absence of 100 μ g/ml non-diabetic or diabetic PMPs. Invading cells were counted after overnight incubation. **A.** MCF-7 invasion levels measured in the presence and absence of NDPMPs. The two left columns represent the chemokinetic ability of the cells, while the right two columns represent the chemotactic ability of cells. **B.** MCF-7 invasion levels measured in the presence and absence of DPMPs, with chemokinesis and chemotaxis represented the same way. **C.D.** Representative images of the microscopic field of view used to count invasion levels of cells. Magnification x40. **E.** The effect of NDPMPs vs. DPMPs on the chemokinesis of these cells. **F.** The effect of NDPMPs vs. DPMPs on the chemotaxis of these cells.

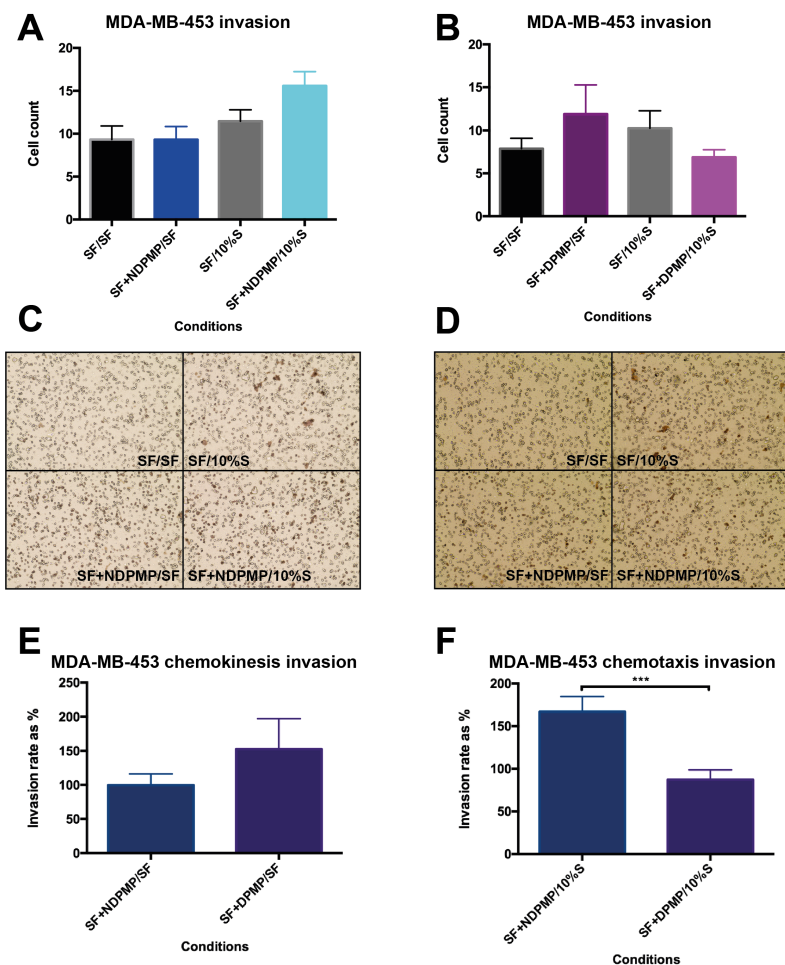


Figure 5.9: **MDA-MB-453 invasion levels measured using transwell chambers.** Cells were seeded at 100 000 cells per well in serum free DMEM and incubated in the presence or absence of 100 $\mu\text{g}/\text{ml}$ non-diabetic or diabetic PMPs. Invading cells were counted after overnight incubation. **A.** MDA-MB-453 invasion levels measured in the presence and absence of NDPMPs. The two left columns represent the chemokinetic ability of the cells, while the right two columns represent the chemotactic ability of cells. **B.** MDA-MB-453 invasion measured in the presence and absence of DPMPs, with chemokinesis and chemotaxis represented the same way. **C.D.** Representative images of the microscopic field of view used to count invasion levels of cells. Magnification x40. **E.** The effect of NDPMPs vs. DPMPs on the chemokinesis of these cells. **F.** The effect of NDPMPs vs. DPMPs on the chemotaxis of these cells.

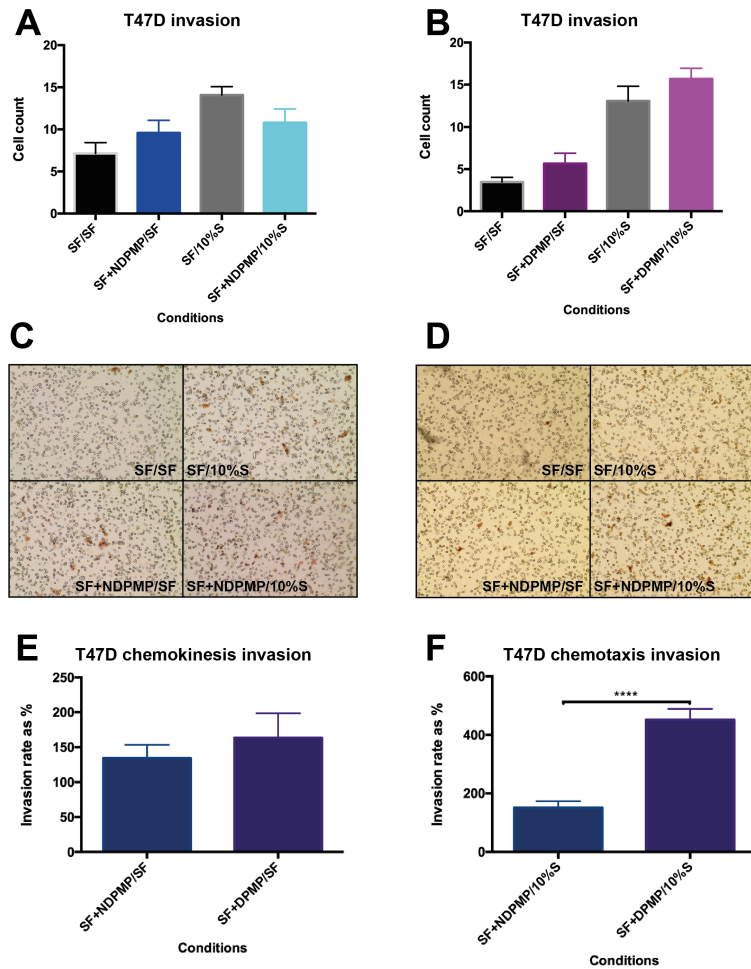


Figure 5.10: **T47D invasion levels measured using transwell chambers.** Cells were seeded at 100 000 cells per well in serum free DMEM and incubated in the presence or absence of 100 $\mu\text{g}/\text{ml}$ non-diabetic or diabetic PMPs. Invading cells were counted after overnight incubation. **A.** T47D invasion levels measured in the presence and absence of NDPMPs. The two left columns represent the chemokinetic ability of the cells, while the right two columns represent the chemotactic ability of cells. **B.** T47D invasion measured in the presence and absence of DPMPs, with chemokinesis and chemotaxis represented the same way. **C.D.** Representative images of the microscopic field of view used to count invasion levels of cells. Magnification x40. **E.** The effect of NDPMPs vs. DPMPs on the chemokinesis of these cells. **F.** The effect of NDPMPs vs. DPMPs on the chemotaxis of these cells.

Following observations that NDPMPs alter the morphology of MDA-MB-231 cells when incubated in each other's presence, the effect of DPMPs on MDA-MB-231 morphology was also measured, using the following conditions: cells incubated in 10% serum containing media, cells incubated in serum free media, cells incubated in 10% serum containing media and 100 $\mu\text{g}/\text{ml}$ DPMPs and cells incubated in serum free media and 100 $\mu\text{g}/\text{ml}$ DPMPs.

The results of the circularity and area measurements are shown in figures 5.11 and 5.12 respectively. Five time points were measured, at one hour prior to the addition of the DPMPs (T-1), at the moment the DPMPs were added (T0), two (T2), four (T4) and six (T6) hours after the addition of DPMPs.

In figure 5.11, the immediate cellular response of the cells to the media change and/or the addition of DPMPs has been almost instant, with the circularity levels raising from roughly 0.3 at T-1 to nearly 0.4 in T0 in all but the cells that remained in serum free media. The peak of the effect of DPMPs is seen in T2, where the presence of DPMPs increases the circularity of the cells in serum free media to levels closer to those in the presence of serum containing media only.

Some noticeable changes are shown in figure 5.12, although not as pronounced. There are no significant differences between the conditions apart from the initial moment of adding the DPMPs

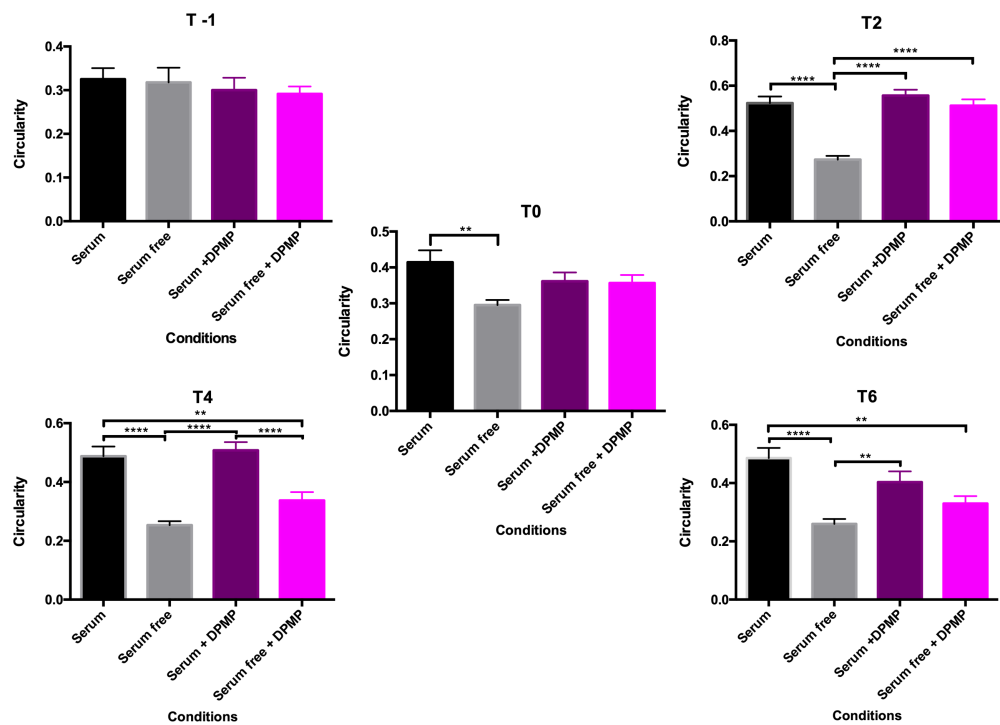


Figure 5.11: Graphical representation of the effect of DPMPs on the circularity of the MDA-MB-231 cells they were co-incubated with. The incubation conditions presented were MDA-MB-231 cells in serum containing media only, serum free media only, serum containing media plus 100 $\mu\text{g}/\text{ml}$ DPMPs and serum free media plus 100 $\mu\text{g}/\text{ml}$ DPMPs. Each panel represents the incubation time when the images for measuring were captured. **A.** -1 hours **B.** 0 hours. **C.** 2 hours. **D.** 4 hours. **E.** 6 hours.

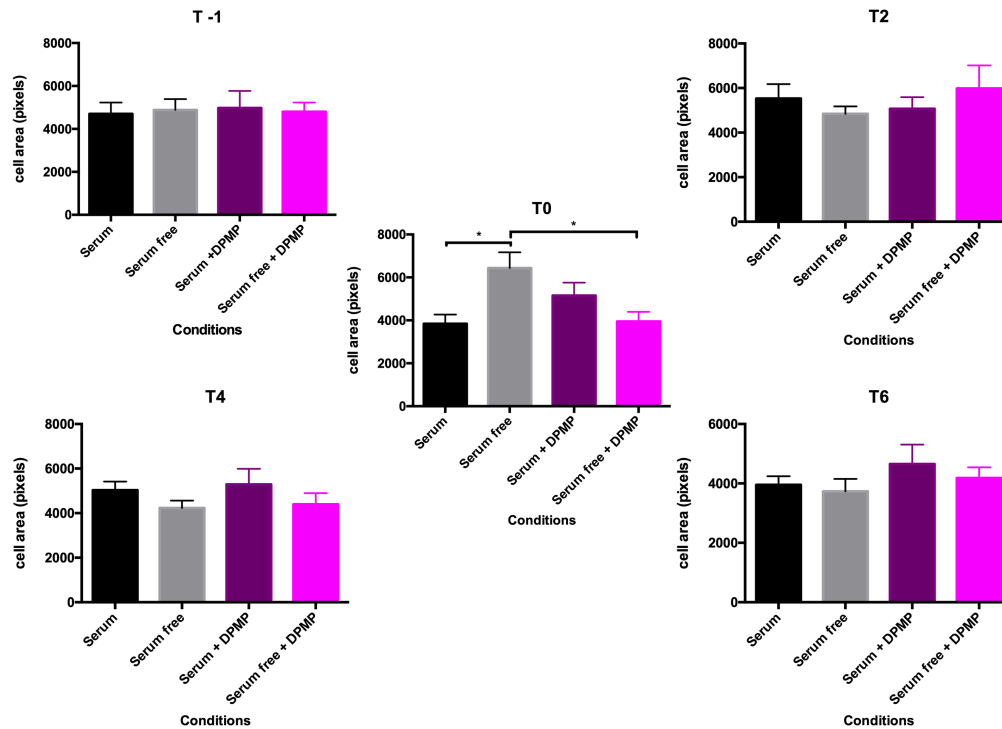


Figure 5.12: Graphical representation of the effect of DPMPs on the area of the MDA-MB-231 cells they were co-incubated with. The incubation conditions presented were MDA-MB-231 cells in serum containing media only, serum free media only, serum containing media plus 100 $\mu\text{g}/\text{ml}$ DPMPs and serum free media plus 100 $\mu\text{g}/\text{ml}$ DPMPs. Each panel represents the incubation time when the images for measuring were captured. **A.** -1 hours. **B.** 0 hours. **C.** 2 hours. **D.** 4 hours. **E.** 6 hours.

(T0), where only cells in serum free DMEM have increased their cellular area.

5.5 The influence of PMPs on EMT.

After investigating the effects of PMPs on phenotypic changes in BC cells, their effect on MDA-MB-231 and MCF-7 cells were verified via known EMT marker levels. These two cell lines were chosen also due to their characteristics situating them at opposite ends of the EMT spectrum, with MCF-7 cells being an epithelial cell line and MDA-MB-231 being a mesenchymal cell line.

MDA-MB-231, figure 5.13, and MCF-7, figure 5.14, cell lines were incubated in the presence of NDPMPs and DPMPs, at a concentration of 100 $\mu\text{g}/\text{ml}$ each. The gene expression levels of the known cancer epithelial to mesenchymal transition (EMT) markers Vimentin, TWIST, SNAIL and possible EMT associate gene, MALAT1, were measured via RT-qPCR.

In order to measure the effect of the PMPs on levels of mRNA associated with each of these EMT markers, a positive control of MDA-MB-231 cells incubated with 10 ng/ml $\text{TGF}\beta$ was used alongside the negative controls of MDA-MB-231 cells incubated in either 10% serum DMEM or serum free DMEM. Similar controls were used to measure EMT markers levels in MCF-7 cells. In both cell lines, Vimentin was expressed at a higher level in cells

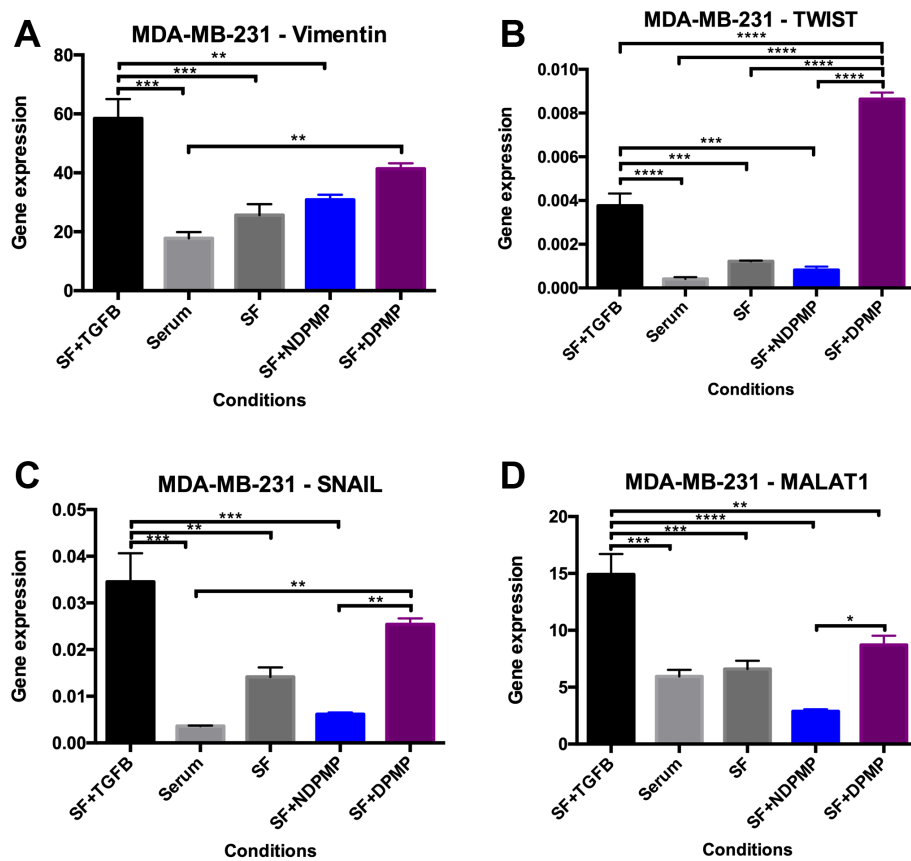


Figure 5.13: mRNA expression levels of EMT markers measured from total RNA of MDA-MB-231 cells. MDA-MB-231 cells were incubated in different conditions. The conditions, from left to right, are serum free+10ng/ml TGF β , 10% serum containing DMEM, serum free, serum free + 100 μ g/ml NDPMP, serum free + 100 μ g/ml DPMPs. The breast cancer specific markers analysed are: **A.**Vimentin, **B.**TWIST, **C.**SNAIL, **D.**MALAT-1

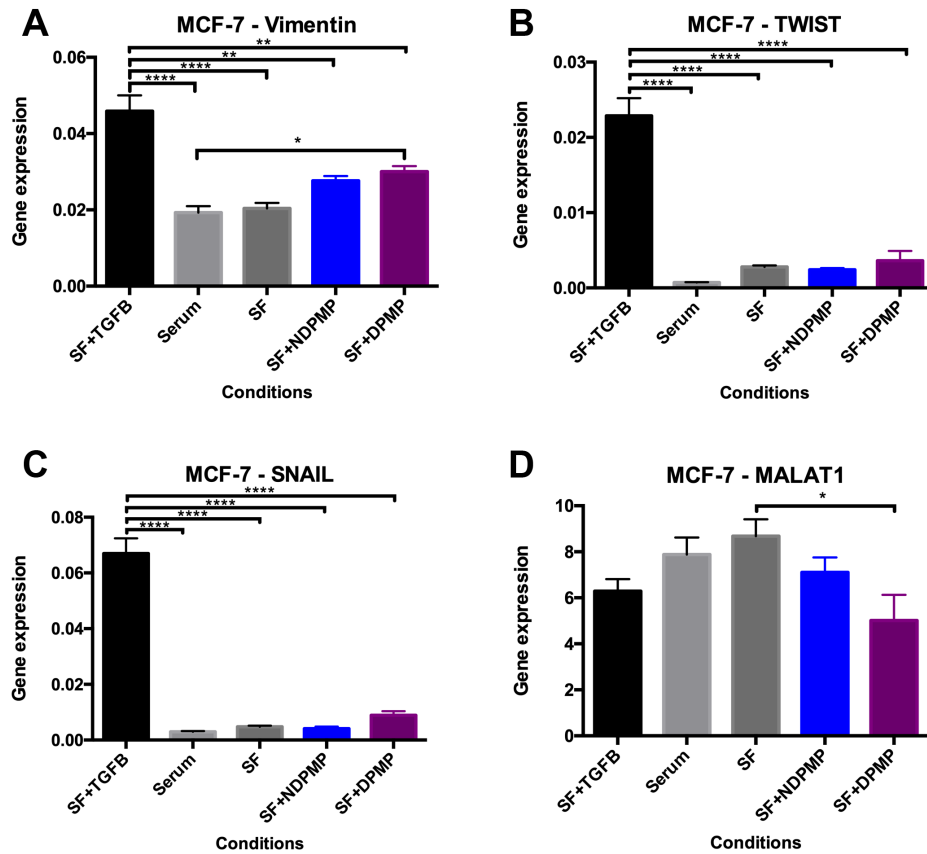


Figure 5.14: mRNA expression levels of EMT markers measured from total RNA of MCF-7 cells. MCF-7 cells were incubated in different conditions. The conditions, from left to right, are serum free+10ng/ml TGF β , 10% serum containing DMEM, serum free, serum free + 100 μ g/ml NDPMP, serum free + 100 μ g/ml DPMPs. The breast cancer specific markers analysed are: **A.**Vimentin, **B.**TWIST, **C.**SNAIL, **D.**MALAT-1

incubated with DPMPs, when compared to their negative control. TWIST was the highest expressed in the case of MDA-MB-231 cells incubated with DPMPs, when compared to the other conditions, whereas in the case of MCF-7, cells incubated in the presence of DPMPs presented no change, same as with NDPMPs. SNAIL and MALAT1 were both higher expressed under the influence of DPMPs, compared to both NDPMPs and their negative controls. In MCF-7 cells, SNAIL was expressed at the same levels in both PMP presence and negative controls, while MALAT1 presented a decrease in expression levels in the presence of DPMPs, compared to their negative control.

5.6 Influence of PMPs on cellular metabolism

Seahorse (Agilent) metabolic analysis was performed, using the Cell Energy Phenotype Test, to investigate the possible effects of PMPs of diabetic or non-diabetic origin on breast cancer cell lines MDA-MB-231, MDA-MB-453, MCF-7 and T47D. As such, oxygen consumption rate (OCR), extracellular acidification rate (ECAR) and proton production rate (PPR) were measured.

As presented in the user guide, this test uses Oligomycin and FCCP to inject into the cells in order to generate a metabolic response. Oligomycin works as an inhibitor of ATP production, driving a rise in the glycolysis rate in order to compensate for the loss of energy. FCCP reactivates the mitochondria through depolarisation

of its membrane, increasing the oxygen consumption rate of the cell overall as it attempts to create a balance between the two mechanisms in the cells again. The overall aim of this test is to provide an insight into the baseline phenotype, stressed phenotype and metabolic potential of the cells analysed.

In figure 5.15, the MBA-MB-231 cell line's metabolic activity in the presence or absence of PMPs was investigated using the cell energy phenotype test kit. As it can be observed in subfigure 5.15A, the oxygen consumption rate is consistent at baseline in the case of all three conditions, whereas, following stress induction, cells incubated with DPMPs present a slight increase in their oxygen consumption rate, and further maintain a higher level compared to the other two conditions. Following the same introduction of stressors, in subfigure 5.15B, both DPMPs and NDPMPs influence a slightly higher acidification rate, compared to controls, with the ECAR increasing further after the addition of FCCP, mirrored by the proton production rate.

In the case of MCF-7 cells, figure 5.16, DPMPs induced a higher acidification rate overall and a bigger stressor response compared to baseline, but no differences in the OCR.

In figure 5.17, both NDPMPs and DPMPs had a similar effect on MDA-MB-453 cells, with both inducing a higher OCR even at baseline, and an increased stressor response, particularly when

observing the alterations in the OCR, subfigure 5.17A. PMPs also induced a higher acidification rate in the cells overall compared to the control, but presented a decrease following the interruption in stressor addition.

The last cell line that was analysed using this kit was T47D, figure 5.18. Interestingly, the strongest impact on both OCR and ECAR was caused by the presence of NDPMPs, presenting higher levels overall.

5.7 miRNA target confirmation

After observing the phenotypic modifications that PMPs induce in BC cells, it was important to identify the possible mechanisms or molecular targets that influence these changes. Given the results presented in Chapter 4, a difference in the molecular composition between NDPMPs and DPMPs was observed, but required further investigation.

Initially, stem-loop qPCR was used to analyse the expression levels of miR-21 and let-7 in cells incubated with PMPs, figure 5.19. Due to the high volume of PMP isolate required to analyse the presence of these miRNAs and the low level of results quality, this technique was not used any further and it was replaced with the miRCURY LNA kit (Qiagen).

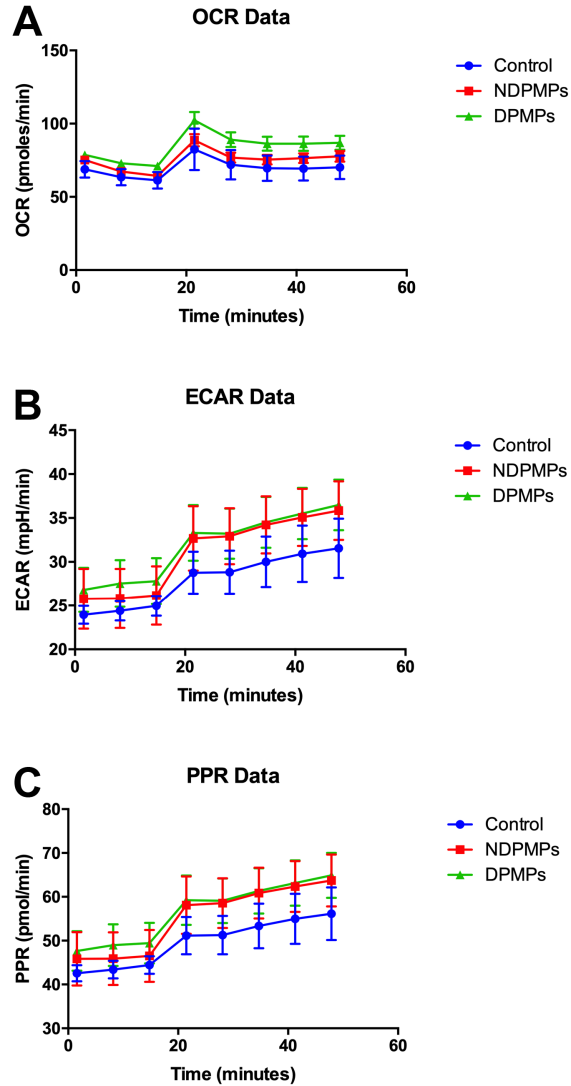


Figure 5.15: Energy phenotype test analysis of the effects of PMPs on MDA-MB-231 cell line. MDA-MB-231 cells were incubated overnight in the presence of 100 $\mu\text{g}/\text{ml}$ PMPs of diabetic or non-diabetic origin and their metabolism was compared against a control (MDA-MB-231 cells incubated in media only) **A.** Oxygen Consumption Rate (OCR). **B.** Extracellular acidification rate (ECAR). **C.** Proton production rate (PPR).

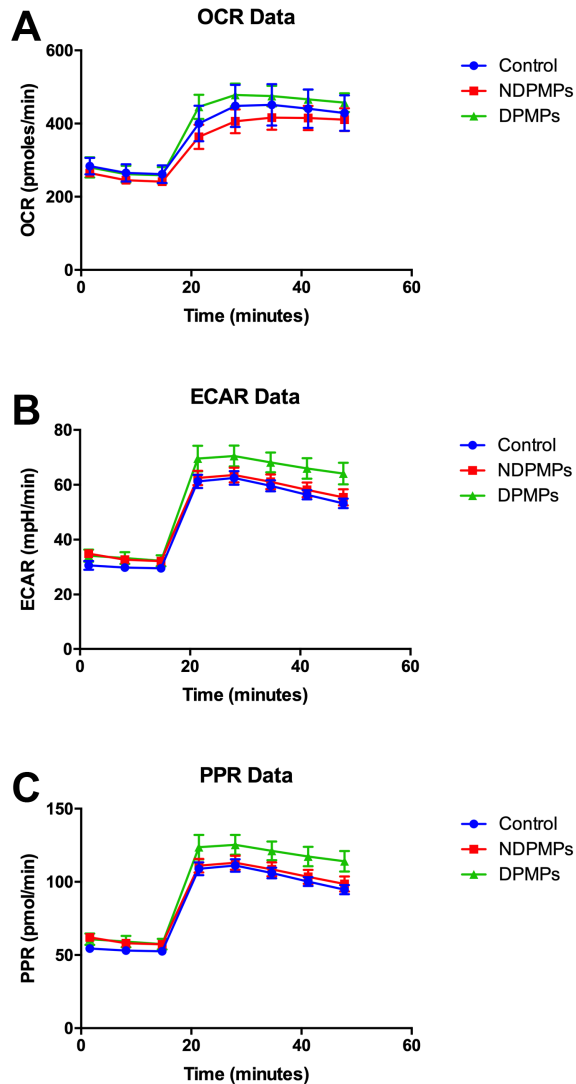


Figure 5.16: **Energy phenotype test analysis of the effects of PMPs on MCF-7 cell line.** MCF-7 cells were incubated overnight in the presence of 100 $\mu\text{g}/\text{ml}$ PMPs of diabetic or non-diabetic origin and their metabolism was compared against a control (MCF-7 cells incubated in media only) **A.** Oxygen Consumption Rate (OCR). **B.** Extracellular acidification rate (ECAR). **C.** Proton production rate (PPR).

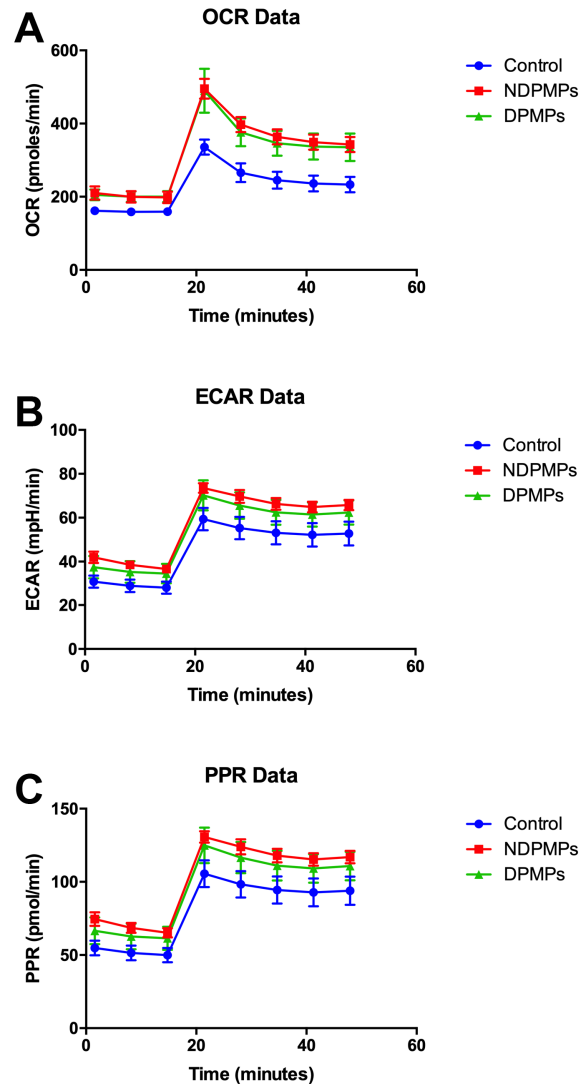


Figure 5.17: Energy phenotype test analysis of the effects of PMPs on MDA-MB-453 cell line. MDA-MB-453 cells were incubated overnight in the presence of 100 $\mu\text{g}/\text{ml}$ PMPs of diabetic or non-diabetic origin and their metabolism was compared against a control (MDA-MB-453 cells incubated in media only) **A.** Oxygen Consumption Rate (OCR). **B.** Extracellular acidification rate (ECAR). **C.** Proton production rate (PPR).

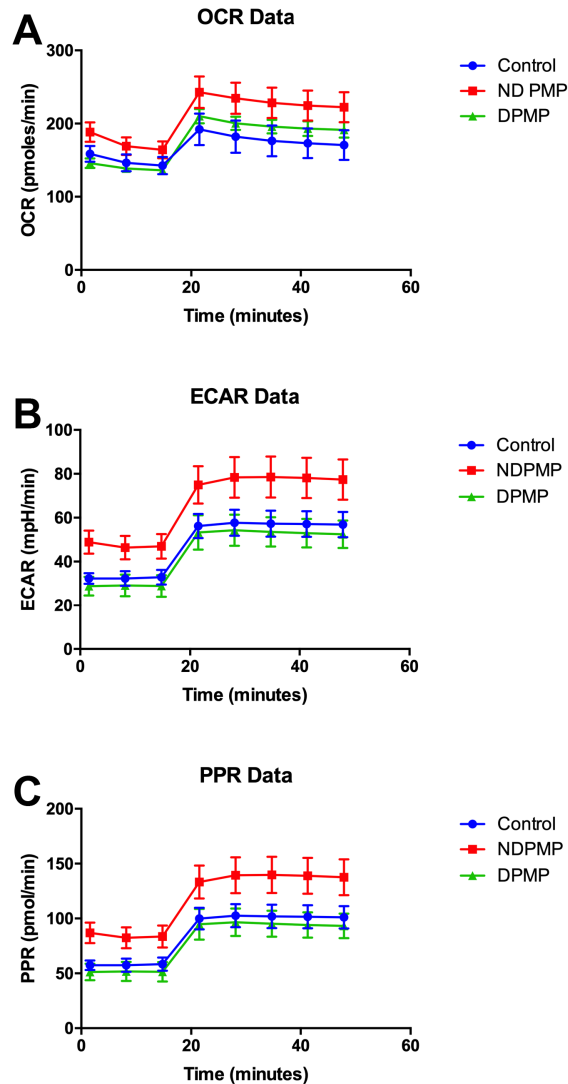


Figure 5.18: **Energy phenotype test analysis of the effects of PMPs on T47D cell line.** T47D cells were incubated overnight in the presence of 100 $\mu\text{g}/\text{ml}$ PMPs of diabetic or non-diabetic origin and their metabolism was compared against a control (T47D cells incubated in media only) **A.** Oxygen Consumption Rate (OCR). **B.** Extracellular acidification rate (ECAR). **C.** Proton production rate (PPR).

Potential miRNAs that can be delivered via PMPs have been identified via RNA seq, see Chapter 4. Their presence was first measured following a 48 hour incubation of MDA-MB-231 cells with or without PMPs, in order to verify if the addition of PMPs induced an alteration in the levels of miRNAs present in cells. Both NDPMPs and DPMPs were added to achieve the concentration of 100 $\mu\text{g}/\text{ml}$ per well. The miRNAs measured were miR-21, miR-221, miR-125a, miR-93, miR-30d, let-7i, miR-16, miR-1301 and miR-345, figure 5.20. These miRNA targets were chosen based on the differential expression table mentioned in the previous chapter, as having the highest expression levels in DPMPs.

In order to confirm PMPs act as delivery vehicles for various miRNAs which appear to further influence BC cell phenotype, MDA-MB-231 cells were pre-treated with actinomycin D, to suppress the activity of RNA Polymerase, therefore preventing the transcription of any new possible cell-generated miRNAs. This would help determine whether or not PMPs induce transcriptional modifications within cells. The treated MDA-MB-231 cells were later incubated with 100 $\mu\text{g}/\text{ml}$ NDPMPs or DPMPs and the results can be seen in figure 5.21. When comparing both figures 5.20 and 5.21, the capacity of the PMPs to deliver biologically active miRNAs is evident in the analysis of the Actinomycin D treated cells, and in the case of almost every miRNA expression level measured, there is an increase compared to the negative control. Comparing

the difference between the miRNA delivery in either NDPMPs or DPMPs, DPMPs deliver a significantly higher amount of miRNAs miR-21-5p, miR-125a-5p, miR-93-5p, miR-30d-5p and miR-16-5p compared to the NDPMPs.

Using the predictive tool TargetScan, biological targets of the miRNAs identified were investigated. For miR-21 PTEN and FASLG were identified as potential targets, TP53 and LIF-R for miR-125a, CDH1 and CDKN1B for miR-221 and KRAS and CCR7 for let-7. Although all of these targets were analysed, only CDH1, CDKN1B and CCR7 were present in detectable amounts in the analysed MDA-MB-231 cells, see figure 5.22. Of these three, only CCR7 was present in higher expression levels in MDA-MB-231 cells incubated with NDPMPs compared to the other two conditions.

5.8 The effect of miR-21 inhibition in MDA-MB-231 cells

With the aim to test the influence of miR-21 delivery via PMPs on target cells, the endogenous activity of miR-21 was inhibited in MDA-MB-231 cells. miR-21 inhibition was achieved using a miR-21 miRCURY LNA miRNA Power Inhibitor and the HiPerfect transfection reagent (both Qiagen). Firstly, both suggested protocols, normal and fast forward, were tested using two different cell seeding densities, 40 000 cells/well and 100 000 cells/well,

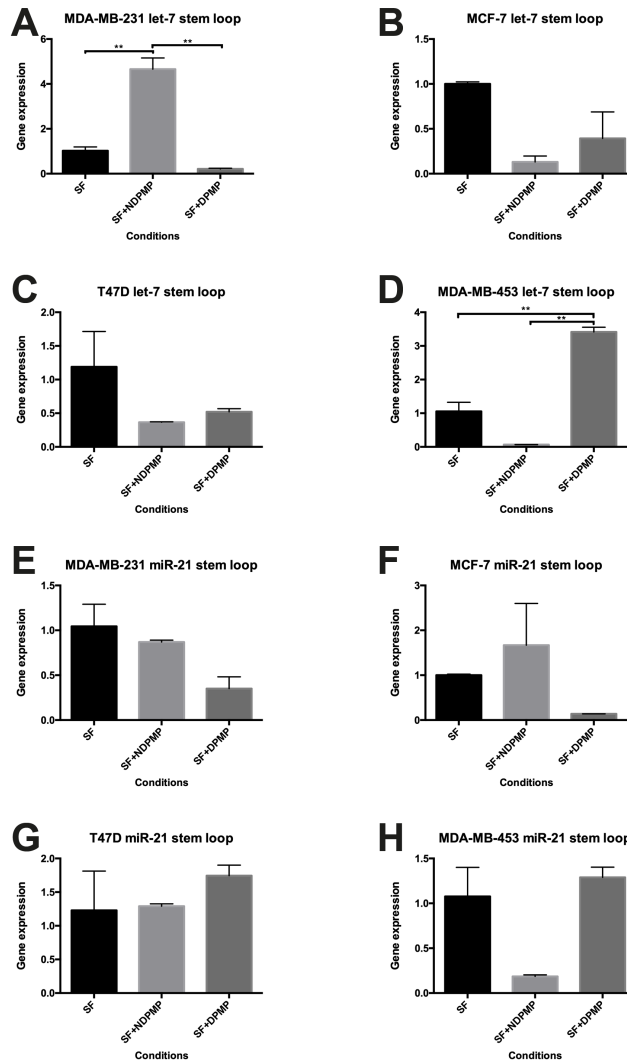


Figure 5.19: Stem-loop qPCR analysis of gene expression levels of miR-21 and let-7 in cells incubated in the presence of either 100 $\mu\text{g/ml}$ NDPMPs or DPMPs for 48 hours. Cells incubated in serum free only were used as control. **A.**Let-7 expression levels in MDA-MB-231 cells. **B.**Let-7 expression levels in MCF-7 cells. **C.**Let-7 expression levels in T47D cells. **D.**Let-7 expression levels in MDA-MB-453 cells. **E.**miR-21 expression levels in MDA-MB-231 cells. **F.**miR-21 expression levels in MCF-7 cells. **G.**miR-21 expression levels in T47D cells. **H.**miR-21 expression levels in MDA-MB-453 cells.

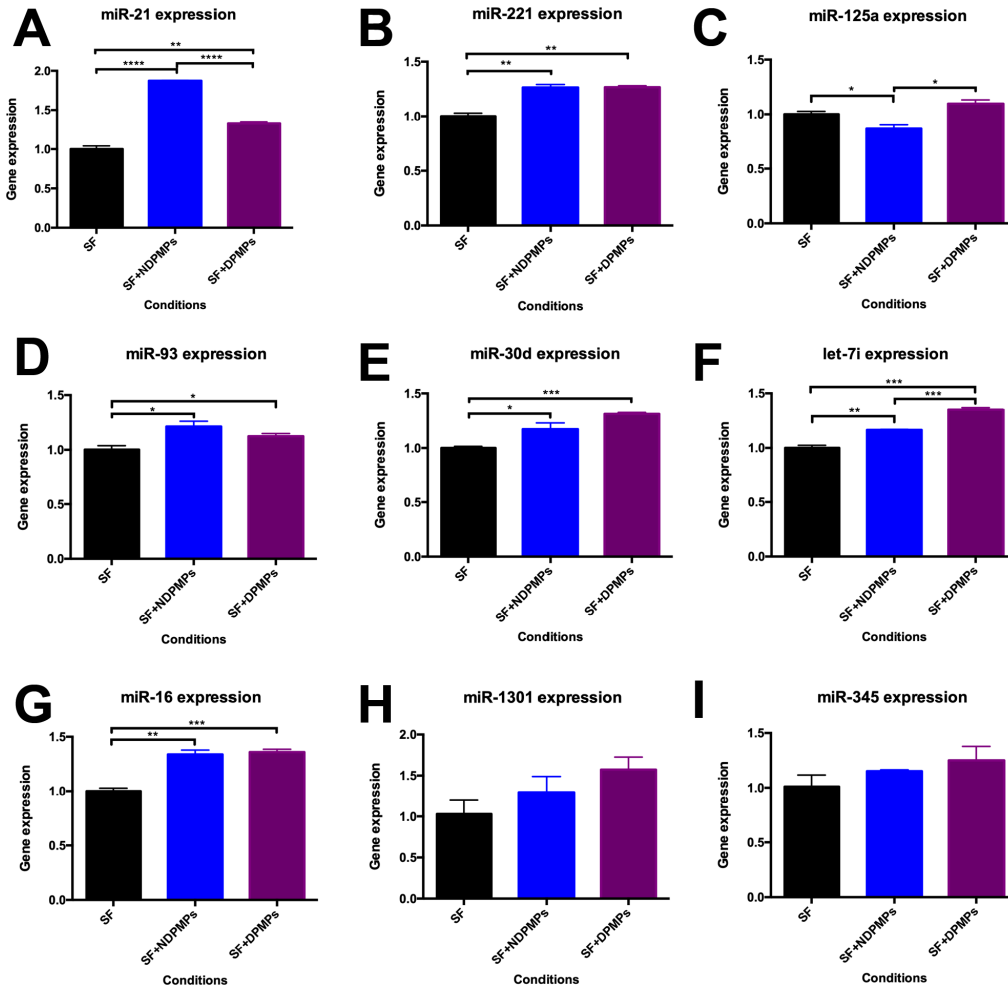


Figure 5.20: miRNA expression levels of targets identified via RNA Seq in MDA-MB-231 cells, untreated with Actinomycin D, treated with 100 $\mu\text{g}/\text{ml}$ NDPMPs or with 100 $\mu\text{g}/\text{ml}$ DPMPs. MDA-MB-231 cells were incubated in 24 well plates and incubated for 48 hours in serum free media and/or either NDPMPs or DPMPs. Results were normalised using the UniSP6 spike in available in the kit. The miRNAs measured were: **A.**miR-21. **B.**miR-221. **C.**miR-125a. **D.**miR-93. **E.**miR-30d. **F.**let-7i. **G.**miR-16. **H.**miR-1301. **I.**miR-345.

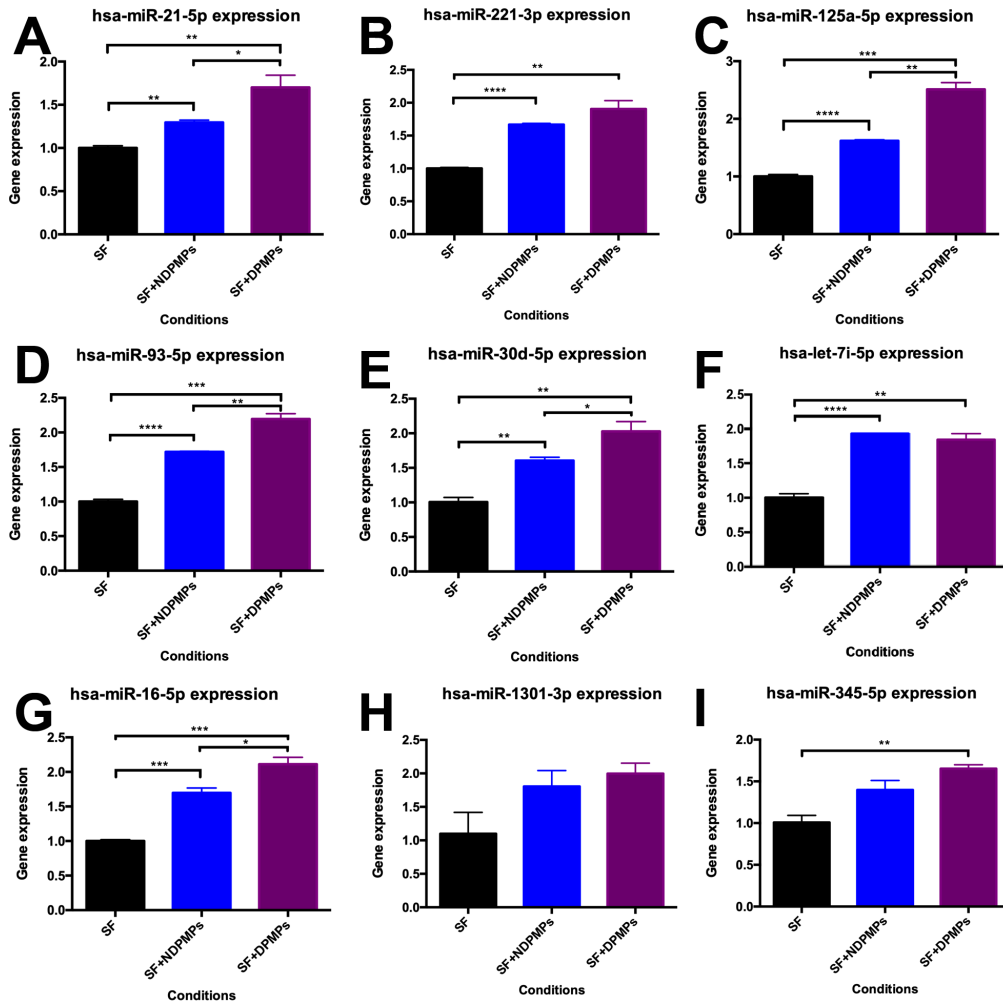


Figure 5.21: miRNA expression levels of targets identified via RNA Seq in incubated MDA-MB-231 cells, treated with 1 $\mu\text{g}/\text{ml}$ Actinomycin D, in the presence of 100 $\mu\text{g}/\text{ml}$ NDPMPs or with 100 $\mu\text{g}/\text{ml}$ DPMPs. MDA-MB-231 cells were incubated in 24 well plates and incubated for 48 hours in serum free media and/or either NDPMPs or DPMPs. Results were normalised using the UniSP6 spike in available in the kit. The miRNAs measured were: A.miR-21. B.miR-221. C.miR-125a. D.miR-93. E.miR-30d. F.let-7i. G.miR-16. H.miR-1301. I.miR-345.

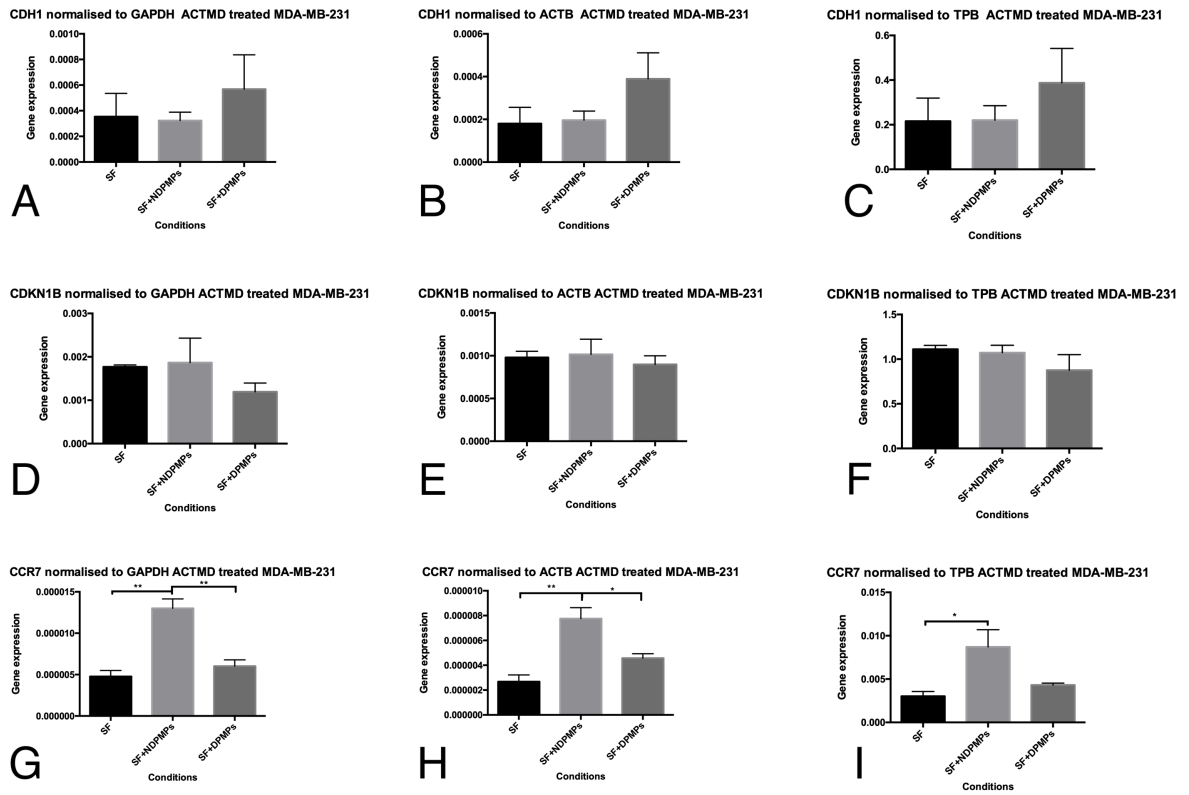


Figure 5.22: RT-qPCR analysis of selected miRNA targets in ACTMD treated MDA-MB-231 cells. MDA-MB-231 cells were treated with 1 $\mu\text{g}/\text{ml}$ Actinomycin D and then incubated in the presence of 100 $\mu\text{g}/\text{ml}$ NDPMPs or DPMPs. Results were normalised using GAPDH, ACTB, or TPB. The targets measured were: **A-C**. CDH1 (a miR-221 target), **D-F**. CDKN1B (a miR-221 target) and **G-I**. CCR7 (a let-7 target).

in 24 well plates, see figure 5.23. The difference between the two protocols was the time of addition of the transfection complexes, at 30 minutes from the time of seeding for the fast forward protocol and at 24 hours from the time of seeding for the normal protocol. The positive control used for comparison were untreated MDA-MB-231 cells. A miR-21 mimic was also used to increase the activity of miR-21. As it can be seen in figure 5.23, the 40 000 cells/well density was the ideal match, with the normal protocol, but the fast forward protocol was used, at the cell density of 40 000 cells/well. The reason this protocol was chosen over the optimal normal one was due to the COVID-19 restrictions set in place by the university, where weekend and after-hours work was not allowed, therefore restricting the choice when advancing with this experiment.

After the confirmation of the transfection protocol to be used, the migration potential of miR-21 inhibited MDA-MB-231 cells was analysed using the Boyden chamber technique mentioned earlier in chapter 5. The results can be seen in both figure 5.24 and figure 5.25, where the results were grouped based on either chemokinetic or chemotactic abilities between the treated cells incubated with either NDPMPs or DPMPs at 100 $\mu\text{g}/\text{ml}$, or grouped based on the chemokinetic or chemotactic differences between MDA-MB-231 cells incubated in the presence of the same type of PMPs. In figure 5.24, the presence of DPMPs significantly increased migra-

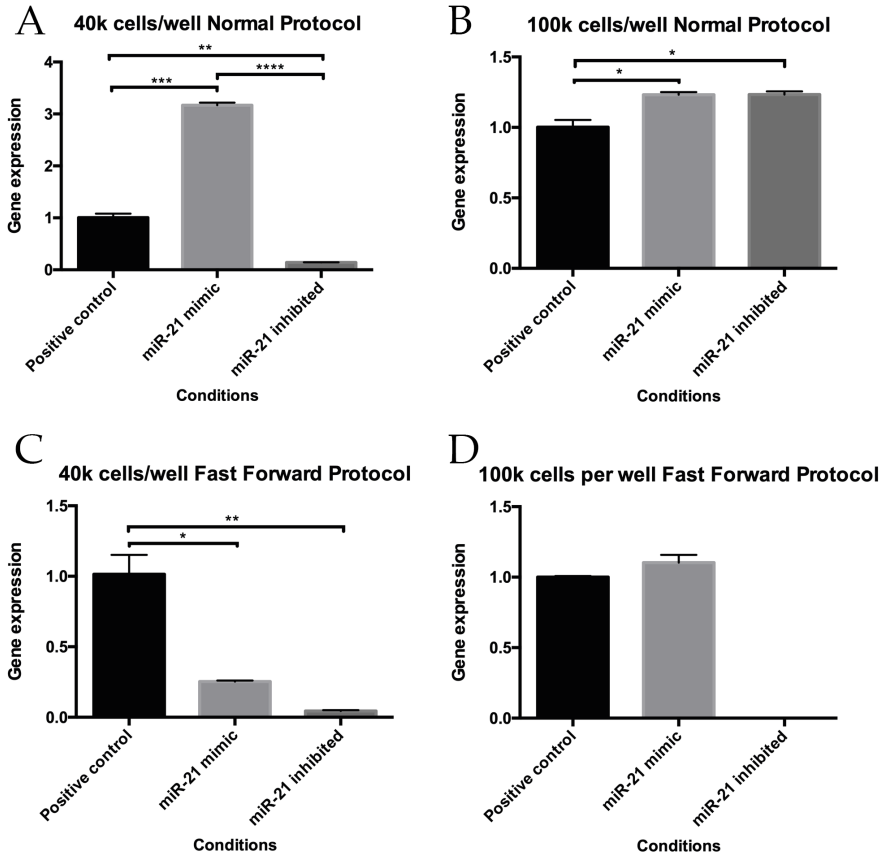


Figure 5.23: miR-21 expression in MDA-MB-231 cells following inhibition treatment using both normal and fast forward transfection protocols, according to the manufacturer. MDA-MB-231 cells were used at two different cellular densities. miR-21 expression was measured in the following conditions: untreated cells, cells treated with a miR-21 mimic and cells where miR-21 was inhibited. **A.** Cells were incubated at 40 000 cells/well and treated using the normal transfection protocol. **B.** Cells were incubated at 100 000 cells/well and treated using the normal transfection protocol. **C.** Cells were incubated at 40 000 cells/well and treated using the fast forward transfection protocol. **D.** Cells were incubated at 100 000 cells/well and treated using the fast forward transfection protocol. miR-21 inhibited value was N/A.

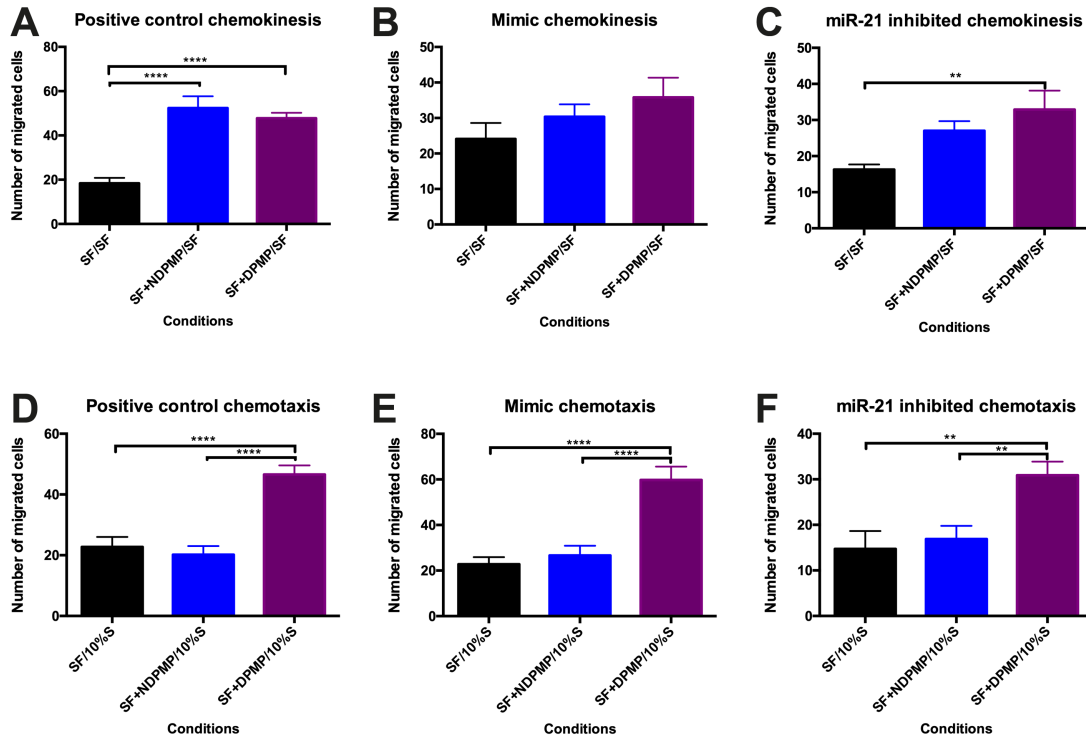


Figure 5.24: Migration levels of MDA-MB-231 cells with inhibited miR-21. MDA-MB-231 cells transfected with a miR-21 inhibitor were co-cubated with PMPs and their migration levels measured via Boyden chamber analysis. Cells incubated in serum free media were used as controls. **A.** Chemokinesis of Positive Control MDA-MB-231 cells, where cells were not transfected with miR-21 inhibitor. **B.** Chemokinesis of MDA-MB-231 cells transfected with a miR-21 mimic. **C.** Chemokinesis of miR-21 inhibited MDA-MB-231 cells. **D.** Chemotaxis of Positive Control MDA-MB-231 cells, where cells were not transfected with miR-21 inhibitor. **E.** Chemotaxis of MDA-MB-231 cells transfected with a miR-21 mimic. **F.** Chemotaxis of miR-21 inhibited MDA-MB-231 cells.

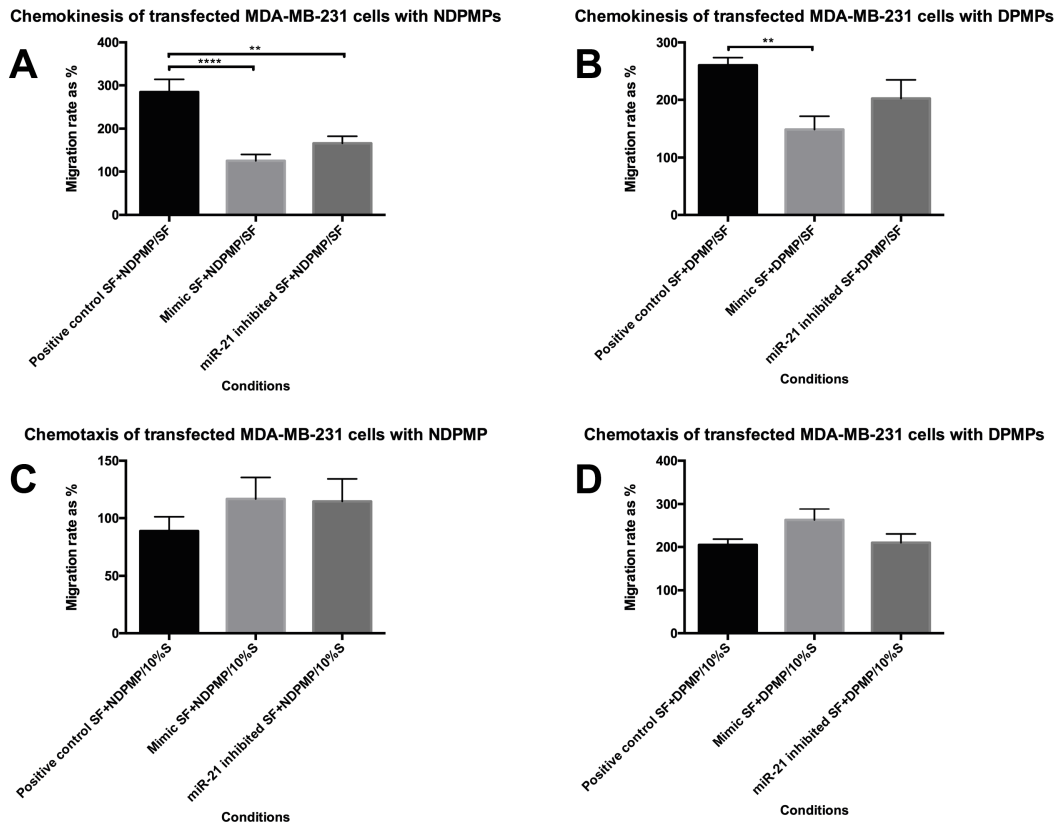


Figure 5.25: **The effect of NDPMPs and DPMPs on migration levels of transfected MDA-MB-231 cells.** **A.** The chemokinetic potential of MDA-MB-231 cells under different treatments incubated with 100 $\mu\text{g}/\text{ml}$ NDPMPs. **B.** The chemokinetic potential of MDA-MB-231 cells under different treatments incubated with 100 $\mu\text{g}/\text{ml}$ DPMPs. **C.** The chemotactic potential of MDA-MB-231 cells under different treatments incubated with 100 $\mu\text{g}/\text{ml}$ NDPMPs. **D.** The chemotactic potential of MDA-MB-231 cells under different treatments incubated with 100 $\mu\text{g}/\text{ml}$ DPMPs.

tion of miR-21 inhibited cells in both cases, under chemokinetic and chemotactic conditions.

5.9 Chapter discussion

There are few studies that have investigated the potential link between DPMPs and cancer progression. [Grande et al. \(2019\)](#) was among the few who reported a link between PMPs extracted from obese patients and tumorigenesis. As obesity is most often directly related to a T2DM diagnosis, this observation could potentially be linked DPMPs as well. Another study investigated another potential link between obesity, T2DM and PMP differences. This study has found that DPMPs are present in higher concentrations in plasma compared to their non-diabetic counterparts, regardless of the donor's BMI. As well as this, DPMPs presented a higher diversity of proteins on their membranes, with one example being fibrinogen, which is associated with high coagulation potential ([Zhang et al., 2014](#)). This current chapter has further investigated the impact DPMPs have on breast cancer progression, compared to its non-diabetic counterparts as well.

It is important to note that, due to the COVID-19 pandemic and the safety restrictions implemented by the university, certain experiments have been affected, either by time frame alterations or by the use of a different protocol in order to fit in the allowed work hours. The most important protocol affected has been the

cell transfection protocol, where the normal one was impossible to be followed.

The effects of both DPMPs and NDPMPs vary depending on the circumstances of their co-incubation with breast cancer cell lines. Some important differences have been noticed between the two PMP types, particularly in the context of cell viability measurements, migrations and invasions. Cell viability analysis was performed on MDA-MB-231 and MCF-7 cells which were incubated with or without PMPs of both types, figures 5.2 and 5.1. The effects of NDPMPs appeared to follow the same trend in both cell lines, where the cells followed a sharp increase in viable cell numbers at the 24 hour time point, near identical or closely comparable with the positive control (cells incubated in 10% serum at 24 hours) followed by a sharp drop at the 48 hour time point. DPMPs maintained a steady level of cellular viability over the 48 hour period tested. This suggests that NDPMPs have a short time frame of influence over cell viability, whereas DPMPs have a steady influence. Although DPMPs were not studied, it has been proven before that NDPMPs positively influence cell viability in the case of neural stem cells, as presented by [Hayon et al. \(2012\)](#).

Initial cell migration analysis was performed using the scratch wound assay. This technique was only used when analysing the effects of NDPMPs and the Boyden chamber assay was used further for a more robust analysis. While the Boyden chamber assay

offers a more clear result, the influence of NDPMPs on wound healing was useful in determining the potential effect of these PMPs on overall cellular migration. After determining that NDPMPs have a strong influence on wound healing, particularly in the case of MDA-MB-231 and MCF-7 cells, figure 3.18, Boyden chamber analysis was carried out.

Migration analysis via Boyden chamber was performed on MDA-MB-231, MCF-7, MDA-MB-453 and T47D cell lines. HB2 cells were no longer used as they did not respond well to the experimental conditions. In comparison, the typical cluster-like proliferation of T47D cells rendered them impossible to use in a scratch wound analysis. In most cell types, NDPMPs influenced a statistically higher migration rate compared to their DPMP counterparts. This could be linked to the burst seen when measuring cell viability that NDPMPs offer at a short time scale, as the assay was measured at the 6 hour time point.

When measuring the invasion rate, via Boyden chamber, DPMPs strongly influenced a higher invasion rate in MDA-MB-231 cells, in both chemokinetic and chemotactic environments, as well as in T47D cells, in the chemotactic environment only. In the case of MCF-7 cells, NDPMPs influenced overall invasion stronger than their diabetic counterparts.

The results overall correlate with other studies on the effects of PMPs on cellular motility ([Janowska-Wieczorek et al., 2006](#)) and in some cases PMPs were shown to promote the migration and invasion of rheumatoid arthritis fibroblast-like synoviocytes ([Wang et al., 2017](#)).

As mentioned earlier in chapter 2, MDA-MB-231 cells are representative of basal breast cancer also known as triple-negative breast cancer, MCF-7 and T47D of luminal breast cancer, MDA-MB-453 of HER2 receptor positive breast cancer and HB2 of normal breast tissue. Taking this into account, DPMPs strongly influence both migration and invasion in the case of basal breast cancer, known to be one of the most aggressive types of breast cancer. In the case of luminal breast cancer, NDPMPs influence migration and invasion more in the case of MCF-7 cells, whereas in the case of T47D cells, DPMPs had a much stronger influence. This change could also be due to the nature of the cell lines, with MCF-7 cells being epithelial cells and T47D being epithelial-like cells, further in the EMT process. When observing the impact of PMPs on the HER2 positive representative cell line, NDPMPs had a more significant influence over MDA-MB-453 migration, however, neither type of PMPs influenced invasion.

When looking at the cell metabolism, DPMPs do not appear to influence OCR or ECAR any more than NDPMPs do, in three of the BC cell lines analysed. In T47D cells though, NDPMPs lead to

a slight increase in the extracellular acidification rate compared to control. This suggests that DPMPs have little influence on BC cell metabolism, thus not interacting with the ATP production/break-down pathways.

Following an observation of the effects of NDPMPs on MDA-MB-231 cell morphology, in Chapter 3, the effect of DPMPs was on the same breast cancer cell line analysed. As the case with the NDPMPs, see figure 3.14, the effect of DPMPs on the cells peaked at T2, two hours after the introduction of the DPMPs, see figure 5.11. Mainly circularity was affected, which could suggest DPMPs induce, in the same manner as the NDPMPs, the formation of cellular processes. A direct comparison between the influence of both PMP types on the detailed structural changes of the cells was not possible due to the unavailability of the initial or a similar microscope. The overall effect of these DPMPs could also be explained by the increase in EMT markers expression in the triple negative breast cancer cells.

To support the migration and invasion data, Vimentin, TWIST, SNAIL and MALAT-1 expression levels were measured in MDA-MB-231 and MCF-7 cells, figure 5.13 and figure 5.14. Vimentin is a common EMT marker and a protein typically found on the membrane of mesenchymal cells associated with cell motility changes ([Gonzales et al., 2001](#)). Although DPMPs appear to influence the invasion of MDA-MB-231 cells more than their migration, this

result still correlates with the high expression levels of vimentin present in MDA-MB-231 cells co-incubated with DPMPs. Vimentin levels in MCF-7 cells were of similar levels in the cells incubated with NDPMPs and DPMPs.

SNAIL, or SNAI1, is another EMT marker measured in MDA-MB-231 and MCF-7 cells. SNAIL is a known suppressor of E-cadherin and a central figure in the EMT process via multiple pathways, especially in the case of distant metastatic sites ([Davidson and Sukumar, 2005](#)). This could suggest why DPMPs, which enhance SNAIL expression levels, figure 5.13, present as a strong influence over MDA-MB-231 cell invasion as opposed to their simple migration. SNAIL levels in MCF-7 cells remained at lower levels, possibly due to the cells sitting at the epithelial end of the EMT spectrum.

TWIST is another pro-metastatic transcription factor analysed in this project, with a significant role in EMT ([Tang et al., 2016](#)). TWIST expression levels were raised significantly in cells incubated with DPMPs compared to the other conditions, in the case of MDA-MB-231, again showing a possible role in mediating cell invasion alongside SNAIL and vimentin.

MALAT1 is a long non-coding RNA associated with cancer development ([Li et al., 2018](#)) which was also studied in this experiment. Although not a specific EMT marker, interestingly, MALAT1 is

present in lower expression levels in MDA-MB-231 cells incubated with NDPMPs, whereas DPMPs appear to have no influence over MALAT1 levels.

After confirming the effects PMPs have on the breast cancer cell lines, the focus was placed on the MDA-MB-231 triple negative cell line in order to confirm delivery and uptake of miRNAs via PMPs. Overall, DPMPs have delivered a significant amount of the measured miRNAs, figure 5.21. However, the simple increased presence of miRNAs in the cells could not confirm whether these miRNAs were bioactive molecules. Following a repeated Boyden chamber migration analysis using miR-21 inhibited MDA-MB-231 cells, figure 5.24, it is clear that DPMPs deliver functional miR-21 which influences cellular migration, when compared to its control.

Following the confirmation of the RNA sequencing analysis and the presence of miRNAs in treated MDA-MB-231 cells, with the help of ACTMD, a few predicted miRNA targets were also investigated. PTEN and FASLG were identified as potential targets for miR-21, TP53 and LIF-R for miR-125a, CDH1 and CDKN1B for miR-221 and KRAS and CCR7 for let-7. Of these only CDH1, CDKN1B and CCR-7 were present within detectable levels. MDA-MB-231 cells were treated with ACTMD and then co-incubated with PMPs for 48 hours. In order to ensure the result was as accurate as possible, given the lower expression levels, three house-keeping genes were selected. The only comparable target was, however, only

CCR7, which presented an increase in expression levels in cells co-incubated with NDPMPs, but similar levels with control when co-incubated with DPMPs. These results could be influenced by the treatment with ACTMD, however, further analysis is required.

Chapter 6

Discussion

A link between breast cancer and circulatory events such as coagulation (Taucher et al., 2003) has been observed in the past. Patients with breast cancer appear to present a higher number of platelets as well as a high VEGF content. When at tumour sites, tumour derived microparticles induce platelet activation and release of their high VEGF content (Taucher et al., 2003), inducing angiogenesis. This is also achieved by autocrine delivery of VEGF by tumour microparticles (Al-Nedawi et al., 2009). Bakewell et al. (2003) investigated the link between platelets and cancer development further and found that platelet integrin β_3 influences tumourigenesis and suggested anti-platelet therapy as a potential treatment in the case of bone cancer.

Following the understanding that platelets and coagulation play a crucial role in cancer development and advancement, the role of

PMPs is brought into question as well, particularly as the assumption of them being simply platelet debris has been disproved. It was important for this project to investigate the impact diabetic and non-diabetic PMPs alike have on breast cancer development and what can be implemented within a clinical context.

There have been many lessons learned when participating in this project, both within the clinical and laboratory setting, that will be explained below.

From the beginning, NDPMPs and DPMPs were isolated at different sites, NDPMPs within the university campus and DPMPs within a hospital setting. The hospital setting was at an advantage, with the blood samples being collected during outpatient clinic appointments and patients eager to donate for breast cancer research once this was brought to their attention as they proved to be suitable candidates. The hospital setting also allowed for patients to talk to each other in the waiting area, some who donated were talking to other potential donors, thus more and more people offered to donate a sample as a means of helping. On the other hand, volunteer recruitment within a university setting proved to be more challenging, with fewer people willing to donate a blood sample. When it came to processing samples, due to the fact that they had to be processed as soon as possible, it had to be done on site in both settings. Due to the nature of the protocol, the research nurses could carry out processing of samples while attending to

their other daily responsibilities. This proves that, in the future, PMP extraction for analysis is accessible in a hospital setting, with minimal equipment use and potential for long term storage, as was the case with the Bradford Royal Infirmary which have their own $-80^{\circ}C$ freezer.

Continuing the narrative of this project, the potential of PMPs to act as delivery vehicles, as suggested by [Laffont et al. \(2013\)](#) as well, has been demonstrated. PMPs have the potential to deliver functional RNA molecules to cells found in their proximity, with a high and relatively fast absorption rate. This is assumed from figures 3.10 and 3.9, where there were no visible PMPs in the extracellular space. This fast absorption rate suggests that PMPs have the potential to be used as therapeutic targets in the future, as per [Azevedo et al. \(2007\)](#)'s review as well.

Both DPMPs and NDPMPs had an effect of some kind on different BC cell lines. Depending on the cell line or migration and invasion analysis, the effects varied, apart from the cell viability, where NDPMPs and DPMPs presented the same effects across the two cell lines analysed, MDA-MB-231 and MCF-7. It can be safely assumed that DPMPs have a stronger effect on cells that already express mesenchymal cell characteristics. This could explain the effect PMPs have on MDA-MB-231 cell morphology, including the formation of cellular appendices in the membrane. Within a clinical setting this could potentially lead to an aggravation of breast

cancer evolution. [Vismara et al. \(2021\)](#) has recently published a study where it analysed the effects of PMPs on four different cancer cell lines, some of which were MDA-MB-231 and MCF-7. The authors of this study have found that the PMPs affect each type of cell line differently, with the highest influence on MDA-MB-231, showing increase in invasiveness and migration. [Vismara et al. \(2021\)](#) pointed out the fact that the influence of PMPs on the BC cell lines studied is so different it shows that PMPs could have both anti-cancer and pro-cancer attributes depending on the nature of their target cells. [Michael et al. \(2017\)](#) also studied the contradictory effect of PMPs on solid tumour cells, belonging to different cancer types. The authors have found that the same applies and that PMPs induce both tumour suppressor and tumour growth effects, depending on either target cell type or stage of development. PMPs appear to have a tumour suppressor effect on early stage tumours.

This project correlates with the findings of the previous studies when the miRNA content of PMPs was investigated. DPMPs in particular presented appropriately 67% of their top 100 miRNAs, based on their CPM, as being tumour suppressors in the case of breast cancer and are typically downregulated in this disease. Interestingly, [Zampetaki et al. \(2010\)](#) has analysed plasma miRNA differences between non-diabetic and diabetic patients and have found that they present a variety of dysregulations, particularly in

the case of miR-126, giving them the potential of becoming useful biomarkers. In contrast with this, however, further analysis of platelet miRNA content conducted by [Stratz et al. \(2014\)](#) presented no differences between T2DM platelets and non-diabetic platelets. In such cases though, [Pordzik et al. \(2019\)](#) points out that differences between studies can occur, depending on the type of T2DM samples available, as poorly controlled T2DM would present a different molecular signature than controlled T2DM. It is thus noted that the study conducted by [Stratz et al. \(2014\)](#) is accurate in the case of controlled T2DM samples. This provides an interesting contrast with the findings of this study which has proven there is a molecular make-up difference between DPMPs and NDPMPs, when looking at poorly controlled T2DM DPMP samples. This could suggest a difference in the PMP formation and release mechanism, where contents might not be randomised as previously thought. This however requires further study.

Returning to the effect of PMPs on BC cells, it is clear that DPMPs influence expression levels of certain EMT markers in MDA-MB-231 cells, as opposed to the epithelial cell line MCF-7, which showed no increases. Given that DPMPs have such a strong effect on MDA-MB-231 cells' phenotype, functional studies were carried on. miR-21 is one of the highest expressed miRNA associated with BC tumour growth present in DPMPs and thus their effect was further investigated. After miR-21 inhibition, MDA-

MB-231 cells incubated with DPMPs have clearly shown an increase in migration compared to their untreated counterparts in both chemokinetic and chemotactic conditions. This highlighted the importance of miR-21 in the context of DPMPs as delivery vehicles. As [Yan et al. \(2008\)](#) has found, miR-21 is associated with advanced breast cancer, metastatic sites and poor patient survival rates. Given the fact that this study has shown an increase in migration in miR-21 inhibited MDA-MB-231 cells incubated with DPMPs compared to controls, it can certainly be correlated with the findings of [Gong et al. \(2011\)](#) and suggest that, in a clinical setting, miR-21 delivered via DPMPs can impact the success of certain BC treatments. [Serebruany et al. \(2015\)](#) and [Shiao et al. \(2017\)](#) suggest that aspirin and other anti-platelet treatments could be taken into consideration, particularly when treating triple negative breast cancer patients. [Chen and Holmes \(2017\)](#) and [Holmes et al. \(2010\)](#) have both concluded that aspirin is a good candidate to supplement breast cancer treatments, following a diagnosis. This long term treatment appears to decrease mortality rates and reduce the risk of remission.

Another study by [Zhang et al. \(2016\)](#) looked at the role of miR-21 in BC evolution, by inhibiting miR-21 in both MCF-7 and MDA-MB-231 cell lines. As expected, miR-21 plays an active role in promoting BC cell motility, complementing the data from this project. While miR-21 is largely associated with breast cancer advance-

ment, [Zhang et al. \(2016\)](#) points out that miR-21 inhibits *STAT3*, a known pro-cancer gene, alongside tumour suppressor genes *bcl-2*, *tpm1*, *pdcd4*, *pten* and *maspin*.

In conclusion, this project has investigated several aspects of the interaction between breast cancer and T2DM PMPs and has found that:

- PMP isolation and storage is accessible for hospitals, with a protocol based primarily on centrifugation, and can be a very important tool in future studies which require patient samples.
- Both DPMPs and NDPMPs affect BC cells differently, depending on the nature of the cells. However, DPMPs have a much stronger effect on mesenchymal BC cell lines, such as the triple negative BC cell line MDA-MB-231.
- While DPMPs increase migration and invasion in MDA-MB-231 cells, they do not appear to have the same effect on other BC cell lines, suggesting the dual character of DPMPs, and PMPs in general based on other studies.
- The mechanisms through which DPMPs influence MDA-MB-231 increase in migration require future analysis, however, miR-21 has been shown to be a key element delivered by DPMPs.
- In terms of translating these findings to clinic level practice, antiplatelet therapy, including aspirin, appears to be a valuable treatment in early

triple negative breast cancer cases. This being said, it is important not to ignore the effects of NDPMPs on other BC cell lines as well.

In terms of future work that could help further the current understanding of how a T2DM influences a BC diagnosis, as well as how to translate this information into a patient-care environment, the following are proposed:

- Formation and structural differences between DPMPs and NDPMPs should be better investigated using a TEM.
- Membrane component differences between DPMPs and NDPMPs should also be investigated, particularly as DPMPs display a clumping effect when isolated.
- The length of the internalisation process of PMPs by cancer cell types should also be assessed, particularly as PMPs prove themselves to be ideal therapeutic targets.
- The effect of DPMPs on solid breast cancer tumour cells (from T2DM or non-T2DM patients), from phenotype changes to functional analysis. As well as this, to analyse miRNA expression associated with DPMPs present within the BC tumours.
- A further investigation into the apparent dual character of PMPs in order to assess their ideal clinical roles.

Presentations and Posters

Poster: *Platelet Microparticles promote metastatic phenotype in breast cancer cells via induction of EMT*. North of England Cell Biology Forum. 29th August 2018.

Presentation: *Platelet Microparticles promote metastatic phenotype in breast cancer cells via induction of EMT*. Yorkshire Breast Cancer Symposium. 13th September 2018.

Poster: *Platelet Microparticles promote metastatic phenotype in breast cancer cells via induction of EMT*. International Association for Breast Cancer Research Conference. 15th - 19th April 2019.

Poster: *Platelet Microparticles promote metastatic phenotype in breast cancer cells via induction of EMT*. Circulating Biomarkers, Exosomes and Liquid Biopsy Europe Conference. 30th October - 1st November 2019.

Appendices

Appendix 1

Consent Form Template

CONSENT FORM

Title of Project: Investigating how platelet-tumour cross talk regulates metastasis

Biological Sciences, School of Applied Sciences

Email: J.R.Boyne@hud.ac.uk

Tel: 0113 812 4596

Researchers: Dr James Boyne, Miss Anca Tutuianu

Please initial or tick each box

1. I understand that I have a free choice about taking part in this project and that I am free to withdraw at any time, without giving any reason.
2. I understand that the research team will take a blood sample for detailed analysis in the University laboratory and I understand the purpose of this.
3. I have read the information provided and have been able to ask any questions.
4. I agree to take part in the above study.

Name of Volunteer

Date

Signature

Researcher

Date

Signature

Version 1
11/01/2019

Appendix 2

Differential Expression Table of DPMP miRNAs resulted from RNA sequencing analysis

GeneID	logFC	logCPM	F	PValue	FDR
hsa-miR-142-3p	0.44651191545908703	17.0298237258841	0.85307493121862799	0.37102275263170098	0.50974104400138098
hsa-miR-16-5p	9.5276316495609699	16.8782136939437	21.366548164801799	5.7068258447431496E-4	4.8711834889057599E-3
hsa-let-7i-5p	-1.04478702132766	16.7557863484835	23.2585734033309	2.5603182057516201E-4	3.3995336176368702E-3
hsa-let-7b-5p	-1.51203693999058	16.522316404954601	15.5834281803811	1.40683491463438E-3	1.12077848199205E-2
hsa-let-7a-5p	4.0979675459039298	16.276592932660002	14.1954466189505	2.0897001032937801E-3	1.42222303495454E-2
hsa-let-7f-5p	4.4801773417412702	16.1701461409586	23.5424389433222	2.4215915021046601E-4	3.3995336176368702E-3
hsa-miR-126-3p	-1.0712996025486301	15.914073260449101	21.856251285245801	3.3939781842148999E-4	3.7252446484777098E-3
hsa-miR-223-3p	-0.78212283955756201	15.143944876786501	10.5571843263509	5.6918440224555797E-3	2.9745126728726999E-2
hsa-miR-146a-5p	-1.5918827589463	14.4351246344585	25.772167686324199	1.58653584529313E-4	2.5278804468337299E-3
hsa-miR-21-5p	-1.0801127224827101	14.242017195061299	8.7285345447856706	1.0270234649856E-2	4.5997903456041302E-2
hsa-miR-93-5p	-1.93297653530187	14.104835967103799	44.886206847736702	9.1241194810864806E-6	2.7258306949745902E-4
hsa-miR-26b-5p	-0.76336664103599805	14.0448442510656	7.9955930845720404	1.32178503686634E-2	5.4466659277768101E-2
hsa-miR-30d-5p	-1.8344304397460001	13.519140363771299	21.498949949190301	3.6534386943077901E-4	3.7252446484777098E-3
hsa-miR-221-3p	-2.1331025114840099	13.461799669809601	32.415768651426397	5.1363345603174703E-5	1.22758395991588E-3
hsa-miR-26a-5p	5.5042146296945198	13.3693424918629	12.2272910390279	3.46279486451925E-3	2.04808490601701E-2
hsa-miR-432-5p	-1.63883025217244	13.3338321966257	5.86198747668442	2.93339063454673E-2	9.8301794654582705E-2
hsa-miR-199a-3p	10.171248104017501	13.059320894551099	101.03684592616899	7.3022586909827005E-8	5.8174660904828802E-6
hsa-miR-584-5p	-1.15969151866819	12.8656276126547	9.3272643304169005	8.4160418675866804E-3	4.1049673599045197E-2
hsa-let-7g-5p	-0.41309854415967601	12.835255921198099	0.62941923085598095	0.44054792069052601	0.57536039915320003
hsa-miR-126-5p	-2.1475742903063901	12.589257569515301	5.6327292680968997	3.2164208311483297E-2	0.10021831123470799
hsa-miR-191-5p	-0.57459541967635297	12.576261519802101	0.34833911575787402	0.56427534906112697	0.69159901756722697
hsa-miR-320a-3p	-2.0820643925789	12.5668078494603	29.7890927769085	7.8536709825805198E-5	1.52408008861801E-3
hsa-miR-744-5p	-1.23357360342001	12.515768560354401	2.0556040938477702	0.17317250532387199	0.29111773894873999

Continued on next page

Continued from previous page

hsa-miR-148a-3p	-1.08176388037674	12.3604977255739	2.9162829484703199	0.10932126206993199	0.20254094290475799
hsa-miR-486-5p	7.3710588331427704	12.3346414881913	72.177322892893798	5.8334674250864205E-7	2.7883974291913098E-5
hsa-let-7e-5p	-5.9972356745226198E-2	12.1432714534716	5.4847175314638704E-3	0.94199061749108204	0.95802450034199405
hsa-miR-30e-5p	-1.5868111925319199	12.0853282035572	9.2063819177073292	8.7570241084293007E-3	4.1858575238292103E-2
hsa-miR-199b-3p	17.9941641584176	12.054564822307499	287.35427784003201	2.2177339469822102E-9	5.3003841332874695E-7
hsa-miR-92a-3p	2.1976200379065101	11.9704725061974	2.8132863369212702	0.11522372894734199	0.21053761769177701
hsa-miR-342-3p	-1.4565321704255101	11.9634978397344	8.19944377759915	1.23098523567138E-2	5.2536691308117903E-2
hsa-let-7d-5p	0.3996568992856	11.9411577359223	0.23856464767160701	0.63265735245392996	0.7375858895848398
hsa-miR-25-3p	-2.2236679494173002	11.9385323881275	4.4820629652607904	5.2261090393714398E-2	0.12583958010618701
hsa-miR-148b-3p	-0.6533205651742298	11.8487430097009	0.26706072026379302	0.61321798179179099	0.72849335829331896
hsa-miR-425-5p	-0.94284924621178101	11.701675014745	0.599419056948165	0.45142427859369	0.58319136531833404
hsa-miR-151a-3p	0.39266338634614301	11.6499257300453	0.21261130917108101	0.65167066003066498	0.748794652631389
hsa-miR-155-5p	-1.8093729004558801	11.568766748883	11.495551159547	4.2858529027733003E-3	2.4388543899114701E-2
hsa-miR-24-3p	17.4698873894847	11.5305010565435	221.10101149734001	9.1759322866688004E-9	1.09652390825692E-6
hsa-miR-20a-5p	-0.49993892723306799	11.482631280166499	1.1003446856141701	0.31161443896626401	0.45518104048750102
hsa-miR-23a-3p	-1.9535975420138201	11.433055786642599	3.29906662585846	9.0359273339767898E-2	0.172766930625636
hsa-miR-1307-3p	-0.37322133873024099	11.4235654944553	0.19235042627967799	0.66752776824070703	0.75953079117184197
hsa-miR-142-5p	-0.99373808949823095	11.144368288631	1.0276199469204601	0.32758149092758798	0.471638411636708
hsa-miR-382-5p	-0.37711549790403498	11.1281394465614	0.14000050415808901	0.71377594732760796	0.79235049879351704
hsa-miR-423-3p	-0.59870862171259398	11.0731671879481	0.22599617167467001	0.64169599598107596	0.74089537700230501
hsa-miR-12136	16.999859725700201	11.0607458728668	119.703199008702	2.3706945561081401E-7	1.4164899972746101E-5
hsa-miR-140-3p	-1.7042891183072	10.9999737433604	3.71625538378508	7.4006895018938298E-2	0.14996901494052201
hsa-miR-27b-3p	-3.1022770719491301E-2	10.9420506192318	1.23797746947527E-3	0.97241924289202497	0.98062531245229501
hsa-miR-409-3p	-0.94760590914042897	10.908024865104901	0.95693568628833403	0.34423718466369302	0.49265082116540598
hsa-let-7c-5p	-1.1306289847873801	10.897882303469499	2.5247840979005498	0.13395209407116401	0.23618288459896
hsa-miR-125a-5p	-1.22792227153636	10.783910520501401	1.63895438118694	0.22086797985787399	0.35427816903377102
hsa-miR-224-5p	-0.54539446427850402	10.6656588745291	0.32489048689468703	0.57753848857629597	0.70069885474780402
hsa-miR-186-5p	-2.29126126700625	10.350886458328601	3.1386489706035401	9.7779833117951701E-2	0.184010867048744
hsa-miR-98-5p	0.58515569947944701	10.1236015036515	0.204992952595484	0.65752080857832695	0.75190178588622103
hsa-miR-185-5p	-1.11939847307028	10.036507236634	0.782092778080545	0.39114409576058701	0.52815502195921005
hsa-miR-150-5p	-2.0572169180150999	10.001041626719701	3.64507138318239	7.6529557835339698E-2	0.15116168861691101
hsa-miR-143-3p	0.34521600007112202	9.9950659640477202	6.85994434491351E-2	0.79712596885916498	0.84297834759885104
hsa-miR-146b-5p	-1.3202944268468	9.9728343144312692	2.0896438519695102	0.169881179008436	0.28795462257458299

Continued on next page

Continued from previous page

hsa-miR-223-5p	-0.479288097912768	9.9716466270866597	0.13762319424973099	0.71609919556234203	0.79235049879351704
hsa-miR-101-3p	11.8074910496059	9.8772724594613894	64.056334284756801	1.1905539400647299E-6	4.2859911110372597E-5
hsa-miR-17-5p	0.36309905501372203	9.7767839226530295	7.8135860447980904E-2	0.78384629149776996	0.840086384161287
hsa-miR-454-3p	15.677880828634899	9.7401945908877199	86.437415122334002	1.25531120406949E-6	4.2859911110372597E-5
hsa-miR-1301-3p	-2.0436568480157402	9.7022934443575508	4.5784596518856802	5.0097891079148298E-2	0.12343707183419
hsa-miR-27a-3p	-1.8865757569316199	9.6635171851046593	2.5185421229621601	0.13439695525296499	0.23618288459896
hsa-miR-134-5p	8.3746716081173803E-2	9.60367704894899	3.41674836043648E-3	0.95419766293265096	0.96632729424111696
hsa-miR-629-5p	-2.3737223016012301	9.5090074378570808	3.2442578775505302	9.2815841007830802E-2	0.17605544445136201
hsa-miR-222-3p	-0.51023040926867302	9.4689262716616192	0.149918564383832	0.70432058219906102	0.78660102404474597
hsa-miR-328-3p	0.38751669720539	9.3894495801994502	8.4189288520278904E-2	0.77586791286385304	0.83528122150658002
hsa-miR-431-5p	-0.96837736776529304	9.3327032585671397	0.54465647812886997	0.47245997968821601	0.60490809666750001
hsa-miR-28-3p	-1.1756796123341799	9.3168283489962	0.54256400504943902	0.473296293208463	0.60490809666750001
hsa-miR-152-3p	-2.4325926135022802	9.2753440960976707	3.6062331948415101	7.7949139579465199E-2	0.15270364229092001
hsa-miR-127-3p	-1.10108846531245	9.1840130305129097	0.88965246427886802	0.36125150349315399	0.50974104400138098
hsa-miR-106b-3p	-2.5556530677501299	9.1273998585683707	3.7008406105734899	7.45446626089908E-2	0.14996901494052201
hsa-miR-139-3p	-0.50108840619003603	8.99888193263358	0.26621428496673399	0.61377589586742498	0.72849335829331896
hsa-miR-361-5p	-2.6066673370863098	8.9617167995775997	2.5699309186555301	0.13078779972510199	0.23502469273909399
hsa-miR-664a-5p	-1.1642367627919801	8.9560680899268093	1.3473409636048701	0.26477450974803501	0.40306438108140402
hsa-miR-379-5p	2.3791792348402199	8.9475871185209197	1.9838660638137	0.18037601698367101	0.29730943489032702
hsa-miR-29c-3p	-2.68644679561028	8.9136512061365103	4.0060309927583901	6.4706964786309704E-2	0.14211242765040299
hsa-miR-196b-5p	-1.56177130420874	8.8059676096022006	2.35276132863306	0.14690748632220199	0.25442673355801698
hsa-miR-140-5p	-1.2898536683987301	8.7275765727721506	0.83724220496276403	0.375374157925703	0.50974104400138098
hsa-miR-181a-5p	14.635903728684999	8.7007100651127498	49.027220187338003	1.9797399206559899E-5	5.2573093448531202E-4
hsa-miR-99b-5p	-1.45881359303188	8.6426486216924605	0.85945863189363503	0.36928947709121301	0.50974104400138098
hsa-miR-15b-5p	-1.22386454241122	8.5841641584672299	0.85963747806618296	0.36924109065850802	0.50974104400138098
hsa-miR-128-3p	-2.50010746044643E-2	8.5474538342770305	2.3043258270269399E-4	0.98809855263717405	0.99225022722808698
hsa-miR-182-5p	0.64214900493952198	8.5301869684279694	0.15016863516714901	0.70408691950324098	0.78660102404474597
hsa-miR-451a	-1.2466007129052099	8.4861191764587804	0.45832268558679001	0.50922436324967901	0.63069644677033199
hsa-miR-29a-3p	-2.4251127424193299	8.4137654204494297	2.6147719272889498	0.12773525384193801	0.23127822475926699
hsa-miR-130a-3p	0.83323145973627	8.3919937770115904	0.26382094564845299	0.61535959162898701	0.72849335829331896
hsa-miR-15a-5p	-0.43890013083013502	8.2744916329369609	5.3839439141398299E-2	0.81980333384831605	0.85935524907784
hsa-miR-23b-3p	0.50151383206111499	8.2648167986223999	0.108167928046559	0.74701175452893998	0.81523200608409396
hsa-miR-197-3p	0.40892085624538899	8.2601659816469297	9.2951931563431997E-2	0.76485424329180696	0.82715006401240598

Continued on next page

Continued from previous page

hsa-miR-1908-5p	-0.25837662995733102	8.2596074568104303	2.73354646180726E-2	0.87099779660960097	0.90116222246621103
hsa-miR-548j-5p	-0.25306883480994702	8.1580893522497906	2.5169785516979199E-2	0.87616580774904995	0.90260184505182295
hsa-miR-381-3p	-0.90392793196765098	8.1284986278903499	0.32484731905006298	0.57756349115195604	0.70069885474780402
hsa-miR-335-5p	-1.0325361157051101	8.1139397228658492	0.40315045465615801	0.53550494283882499	0.65972000689937804
hsa-miR-1306-5p	-0.44332602481635403	8.0550570287706798	7.1063508042145798E-2	0.79360409140594101	0.84297834759885104
hsa-miR-3615	-0.72438684817311305	8.0448661369588095	0.23363533796883601	0.636166097413985	0.73807620039777799
hsa-miR-107	-0.39364580638626701	8.01010050177476	0.117045901605304	0.73724214629433804	0.80876304994022996
hsa-miR-361-3p	-1.74502288718307	7.9581722974940297	1.09691869314565	0.31234180184079602	0.45518104048750102
hsa-miR-340-5p	-2.4030432470787599	7.9300868190787304	1.1341530741593	0.30456177718345401	0.45078438378480001
hsa-miR-425-3p	-2.0527798927770302	7.89876874016245	1.4243295223555901	0.25213660392901999	0.38735058041458598
hsa-miR-10a-5p	-1.7174479376873799	7.8448917881320703	1.2002062299214	0.29140779390034099	0.43529039213863402
hsa-let-7d-3p	0.355669296451537	7.8432874737424996	4.6841990178938898E-2	0.83171279465719805	0.86803213066842999
hsa-miR-374a-5p	-1.5053639765372999	7.8350189850082597	0.84477509236459303	0.37329442347047798	0.50974104400138098
hsa-miR-339-5p	4.2174336777922896	7.7513789675426796	5.82069591692062	2.98215224878585E-2	9.8301794654582705E-2
hsa-miR-652-3p	-1.1591253673289199	7.7177091144415897	0.52135616110644101	0.48191714842475503	0.60940845753183304
hsa-miR-190a-5p	0.71720141667040704	7.6698084990297302	0.18862961806574599	0.67054810433999401	0.75953079117184197
hsa-miR-628-3p	13.579906210672799	7.6497820667376502	36.167232079582597	7.8665418973295395E-5	1.52408008861801E-3
hsa-miR-664b-5p	-2.17275951756706	7.64083485745775	1.31730887895833	0.26993447605211102	0.40831860618009103
hsa-miR-151a-5p	13.549616402808301	7.6196993106126403	35.738099537584702	8.2899753774201199E-5	1.52408008861801E-3
hsa-miR-20b-5p	-2.6795105259118999	7.6126419858258298	2.2179635988815498	0.158157183143319	0.27193932928959103
hsa-miR-485-3p	0.483921806103981	7.5764219311698504	5.9804002607577601E-2	0.81028377416962905	0.85311815870722996
hsa-miR-18a-5p	13.4502827607059	7.5210758213071598	15.649816009448999	2.1422606384252502E-3	1.42222303495454E-2
hsa-miR-199a-5p	13.447839887922401	7.5186726461890601	32.515715783034999	1.2493588907635199E-4	2.13283410637486E-3
hsa-miR-491-5p	-3.04070690971899	7.5150590829939397	2.5521831714819601	0.13202065348153899	0.23546967300065599
hsa-miR-942-5p	-2.52131095764482	7.5014022310283996	2.1307791601152499	0.16600785068494001	0.28339911652643401
hsa-miR-654-3p	-3.31820085681486	7.4746879596836102	2.0272771731138102	0.175972808770363	0.29206598122303301
hsa-miR-2110	-2.4481818936563799	7.4544529434086799	1.2074942934039501	0.29000467841901101	0.43529039213863402
hsa-miR-370-3p	-0.77116619011694298	7.4543596545734099	0.11662088285396	0.73770018781158997	0.80876304994022996
hsa-miR-671-5p	0.21776067169277899	7.4354134183621703	1.2861374894171501E-2	0.91128553107246701	0.93475211127175895
hsa-miR-30e-3p	1.2189200341686199E-2	7.3815821858362796	4.1123699398568397E-5	0.99497207737236903	0.99497207737236903
hsa-miR-5187-5p	0.46146591756287803	7.3721687533290599	0.10178670380612	0.75431345429741403	0.81945870716855496
hsa-miR-29b-3p	13.287698433366099	7.3597040980437001	27.988264743326699	2.3511092231047701E-4	3.3995336176368702E-3
hsa-miR-760	-0.43103731326757599	7.3460156803819601	6.9115083375450095E-2	0.79638341542593205	0.84297834759885104

Continued on next page

Continued from previous page

hsa-miR-3613-5p	-4.6841958722422401	7.2822921331630104	4.4969547694086298	5.1919827293516602E-2	0.12583958010618701
hsa-miR-625-3p	13.150672400957999	7.2238410031492801	25.8260424024967	3.2675903308519201E-4	3.7252446484777098E-3
hsa-miR-625-5p	13.145637855628401	7.2188484232125196	25.5798930610312	3.39663330682738E-4	3.7252446484777098E-3
hsa-miR-30c-5p	13.120642187183	7.1940132272061597	16.2917336567712	1.8634086272752001E-3	1.3102910542451799E-2
hsa-miR-30a-5p	-1.1670196940979101	7.1911535469630499	0.86080261422146798	0.36892609562286199	0.50974104400138098
hsa-miR-485-5p	-1.4571321568478699	7.1903031668606596	0.63396159587985101	0.43893828702471299	0.57536039915320003
hsa-miR-92b-5p	-3.3653078368551501	7.1131308904024397	2.8103217767715498	0.11539927999005301	0.21053761769177701
hsa-miR-190b-5p	-2.9236170856016499	7.1004567219447603	1.5230277297037	0.237080362627104	0.37034122005149001
hsa-miR-192-5p	-1.71475991777382	7.0876388470220499	0.84979999674597395	0.371916641739307	0.50974104400138098
hsa-miR-411-5p	0.150518627617823	7.0850102658982399	7.1869500119250002E-3	0.93361625658102698	0.95356532189258703
hsa-miR-26b-3p	-1.5997197492837201	7.0095048140350098	0.649324921042987	0.433563849165784	0.57249591132940503
hsa-miR-181b-5p	12.925805956687	7.0010877507584599	25.135179965785799	3.6453387434421303E-4	3.7252446484777098E-3
hsa-miR-1287-5p	-3.4565383320466201	6.9241747446366997	2.0453119573043201	0.17418341702790699	0.29111773894873999
hsa-miR-363-3p	-2.2755507165701698	6.9020678296199902	1.4993704195020801	0.24057871447286799	0.37336566726633502
hsa-miR-17-3p	-3.50682291492536	6.8630304175028902	1.8735665146738101	0.19220789015554099	0.31250126358621899
hsa-miR-1843	-2.4520249352705101	6.8280284106644702	1.6143410470925299	0.22418625789951299	0.35720343758655698
hsa-miR-6734-5p	-4.2383000510057496	6.7972026966606904	3.0687791522350101	0.101240273205584	0.189034572626052
hsa-miR-181d-5p	-2.78310698962032	6.7768530164247096	1.88854920968652	0.19054400760550899	0.31191793025833298
hsa-miR-494-3p	-2.80708755038899	6.7740630618609003	1.4199645826126299	0.25283134119111	0.38735058041458598
hsa-miR-19b-3p	12.6305539334484	6.7088810206071798	16.290223580863199	1.8640123784241E-3	1.3102910542451799E-2
hsa-miR-7-5p	8.7045530550517096	6.7078403806103104	19.652911871728101	5.41477124404303E-4	4.8711834889057599E-3
hsa-miR-221-5p	12.622781762196601	6.7013308330360202	13.499547123910499	3.51345109400408E-3	2.04808490601701E-2
hsa-miR-342-5p	12.5945612098248	6.6733607571210403	24.973845483244698	3.7408314461700797E-4	3.7252446484777098E-3
hsa-miR-185-3p	-1.5417272073900601	6.5821159736434396	0.69557112812280797	0.41800450456656901	0.55811774632072697
hsa-miR-144-5p	12.4897535303677	6.5698194074667402	11.709589522957	5.5047739521141698E-3	2.9745126728726999E-2
hsa-miR-301a-3p	12.429415087216601	6.5106538862593304	9.1201534772198691	1.13517704366351E-2	4.93286024428327E-2
hsa-miR-3138	-1.00664103531549	6.5008030341432503	0.26328311746463101	0.61571673968185803	0.72849335829331896
hsa-miR-25-5p	-1.5905311710638801	6.4974948176703498	0.51332419311383803	0.48525276915907301	0.610396904363255
hsa-miR-1270	-3.95008490387294	6.4911021753449702	2.48645591141667	0.136712610674254	0.238498641979173
hsa-miR-6852-5p	-1.10283550115963	6.4851700515795496	0.25872543346534899	0.61876214114453398	0.72849335829331896
hsa-miR-22-3p	12.314274198360099	6.3967526695227397	23.660954411760699	4.6381450172932698E-4	4.4340666365323602E-3
hsa-miR-493-5p	12.302229030641501	6.3850260323958201	11.709796124539199	5.5044765413533496E-3	2.9745126728726999E-2
hsa-miR-4446-3p	1.5106238846060001	6.3630063014688201	0.45814067230688998	0.509307172496545	0.63069644677033199

Continued on next page

Continued from previous page

hsa-miR-139-5p	7.2602091878353701	6.3352395466649396	10.5383833657287	5.7250034708010104E-3	2.9745126728726999E-2
hsa-miR-339-3p	-0.93583393900212897	6.33148350535064	0.25247075777052	0.62299748568303703	0.72988430920708702
hsa-miR-4433b-3p	12.2160908248394	6.3003090902014298	22.5063815310059	5.6434576939109798E-4	4.8711834889057599E-3
hsa-miR-1-3p	12.108902213039199	6.1944252510732802	6.4908210438172196	2.66383842571692E-2	9.2269186050194699E-2
hsa-miR-320c	-1.81307015106226	6.1103503701900701	1.0691113033298401	0.31833452018555702	0.46110272923847301
hsa-miR-326	-2.3673965923055502	6.02575133325933	0.91254529023278497	0.35532750232354998	0.50549567294838404
hsa-miR-324-5p	11.907138194260501	5.9962627554856098	14.4434693449228	2.8120252605452001E-3	1.7686158875534298E-2
hsa-miR-505-5p	11.865377976903201	5.9552846520398903	9.5472544465957494	1.00046059561892E-2	4.5982708144792599E-2
hsa-miR-532-5p	-0.45693550803586203	5.89362155641561	4.1749959891606001E-2	0.84097967878270996	0.87388757925681504
hsa-miR-183-5p	11.7472640273421	5.8388018437185796	4.68641797442955	5.2652543977484201E-2	0.12583958010618701
hsa-miR-1292-5p	-3.2752290094601499	5.8101630840354197	1.8130043745655899	0.19912538124793899	0.32156058188011799
hsa-miR-19a-3p	5.5820975991320001	5.7386861954792199	6.5405530823000504	2.2511151944959801E-2	8.4065083044459199E-2
hsa-miR-320b	11.6343055207582	5.7288343027065496	14.8026678786772	2.5895493346513002E-3	1.6727088945450299E-2
hsa-miR-122-5p	11.624694552587201	5.7196287572834397	7.9829607595696999	1.6139339132196999E-2	6.3056419719205406E-2
hsa-miR-32-5p	11.6185147579004	5.7131296988653002	8.3532423499401602	1.43546528327455E-2	5.8148508932646802E-2
hsa-miR-374a-3p	-0.96619589724298205	5.69426686665593	0.16649761990072401	0.68929361912626996	0.77708101401499297
hsa-miR-486-3p	7.6885749633681497	5.69050631712879	15.0915607363345	1.59390694961932E-3	1.2288508418032799E-2
hsa-miR-369-3p	11.5745059220065	5.6704679789065597	6.6027966487973799	2.5610413484362601E-2	9.1356549593472502E-2
hsa-miR-493-3p	11.560709852420899	5.6566199371622599	9.6567496585650492	9.6904114688890208E-3	4.5411928256166197E-2
hsa-miR-34a-5p	-2.0077506693882001	5.6130443004022101	0.71985039766776104	0.41018537681723899	0.55075452280516901
hsa-miR-144-3p	11.4638696080219	5.5618330414860804	5.0048424508283302	4.6355485604844898E-2	0.118791093131608
hsa-miR-33a-5p	-1.24320278470838	5.5401646778119904	0.31562263244787703	0.58295813603125102	0.70367168945186398
hsa-miR-671-3p	6.6581170682296804	5.5277331482872896	6.0072827788356502	2.7690426523553399E-2	9.4543027701846499E-2
hsa-miR-200c-3p	11.3412218964022	5.4419712725619203	6.0256613832859696	3.1475385333558897E-2	0.10021831123470799
hsa-miR-130b-3p	11.3392234515763	5.4405700689203398	11.3103515179503	6.1168272662436903E-3	3.1104717375154099E-2
hsa-miR-6803-3p	11.332754267343701	5.4343322809194703	18.311061434583699	1.22798414350973E-3	1.01202831137526E-2
hsa-miR-181a-2-3p	11.3022138339013	5.4043323311025899	6.1422996361945597	3.0169872802392101E-2	9.8301794654582705E-2
hsa-miR-125b-5p	11.2212800191464	5.3253096078378004	8.0933249185585492	1.55810648766393E-2	6.2064575091946697E-2
hsa-miR-628-5p	11.1752280348594	5.2806761632882004	7.9410186611896396	1.63577323120951E-2	6.3056419719205406E-2
hsa-miR-574-3p	11.1459153435276	5.2515260143285296	5.9074906296032204	3.2867826824799898E-2	0.100710392450348
hsa-miR-1229-3p	11.044603262857001	5.15354035593134	5.9559616193893303	3.2287907803650602E-2	0.10021831123470799
hsa-miR-4433a-5p	-1.51891751818787	5.1530361228678698	0.492377409178334	0.49414315102453599	0.61832572300975996
hsa-miR-3679-5p	-1.82766470438845	5.1393159039947003	0.61492058556773499	0.44575027199254702	0.57899084242510201

Continued on next page

Continued from previous page

hsa-miR-28-5p	11.0124503486026	5.12207668206206	5.7618116853546004	3.4687649357337098E-2	0.10494111641017199
hsa-miR-3173-5p	10.9104335216499	5.0234291686265502	5.24130463881355	4.2262262372076101E-2	0.116099778240531
hsa-miR-106b-5p	10.824237658394599	4.9403917109039801	5.0942652516927902	4.4753562441205097E-2	0.117799717133434
hsa-miR-195-5p	10.8103150206184	4.9268349331574202	7.5955617387820604	1.8297214879347701E-2	6.9413243748636694E-2
hsa-miR-345-5p	-1.76718201380532	4.8928141062268002	0.53398659961988104	0.47675095808162699	0.606082335008026
hsa-miR-590-3p	10.7420484092492	4.8602011836048602	6.4962057575141401	2.65878329024949E-2	9.2269186050194699E-2
hsa-miR-6721-5p	10.6410366747778	4.7627689134217102	16.759981221375	1.68684967232541E-3	1.25986584901804E-2
hsa-miR-191-3p	10.6377222100033	4.7582308209828099	6.7032845871011597	2.4728103833568899E-2	8.9545709336711493E-2
hsa-miR-132-3p	10.6156991181269	4.7387634129666898	5.6362251782799104	3.6354436699509801E-2	0.105887457467765
hsa-miR-941	10.559039155877	4.68274435691088	5.5468507663810502	3.7599488021383201E-2	0.105887457467765
hsa-miR-146b-3p	10.5572632931916	4.6819001772937998	5.5426879768875796	3.7658719183096302E-2	0.105887457467765
hsa-miR-766-5p	10.5411391735727	4.6666877208583797	5.6257899470561297	3.6497221648229203E-2	0.105887457467765
hsa-miR-96-5p	10.493344579776901	4.6209024229505697	4.5929071010986204	5.4695415346151702E-2	0.12942776502703199
hsa-miR-1179	10.475679216864201	4.6028795709603703	9.4174703729376095	1.0392831743206E-2	4.5997903456041302E-2
hsa-miR-6842-3p	10.4731025221046	4.6019330364139899	5.06929419279275	4.5194072072644899E-2	0.117799717133434
hsa-miR-369-5p	10.4703036074949	4.5975254967367203	4.9849512504421396	4.6721183072682797E-2	0.118791093131608
hsa-miR-130b-5p	10.4668984301153	4.5944009606971896	5.4537533836441803	3.89513992059232E-2	0.10824865593274
hsa-miR-589-5p	10.4356785122032	4.56466483395943	5.1321717669784199	4.4094726041252502E-2	0.117799717133434
hsa-miR-1307-5p	10.4308767954694	4.56056727179479	5.5450733632859999	3.7624764462247003E-2	0.105887457467765
hsa-miR-335-3p	10.4008941384706	4.53171154175591	4.5019619980630798	5.6775165755609501E-2	0.13303200603520299
hsa-miR-92b-3p	3.25011752354856	4.5204223627467499	1.5858641564265099	0.228106861100069	0.36104330995308898
hsa-miR-331-3p	10.3439502649675	4.47639843118026	5.0607781702576302	4.5345497808685797E-2	0.117799717133434
hsa-miR-484	10.301213955382	4.4349201482584597	11.224897318634399	6.2581177218345397E-3	3.1160211156634501E-2
hsa-miR-1277-3p	10.276000973286701	4.4122784825248598	5.0618716256279903	4.5326020525754199E-2	0.117799717133434
hsa-miR-1226-3p	10.236692478437201	4.3741686000549498	4.8556359347345497	4.9185591546761102E-2	0.12339007238965299
hsa-miR-1249-3p	10.181787701848799	4.3214391748414096	4.0531274894132903	6.85667660576674E-2	0.14502174413966801
hsa-miR-5189-5p	10.1776286431671	4.3168029389596798	4.3362454711206802	6.0817496781731303E-2	0.13830000759199601
hsa-miR-454-5p	10.1647588985642	4.3051112524931296	4.3753245915692602	5.9833532242285797E-2	0.13750205967217599
hsa-miR-1277-5p	10.055941654203901	4.2006182314268496	13.553363242053599	3.4682688739299502E-3	2.04808490601701E-2
hsa-miR-769-5p	10.0081066979314	4.15375072739364	4.23009546320284	6.3591292790994194E-2	0.14204036427147301
hsa-miR-29c-5p	9.9267716551256893	4.0760599419249299	4.1851233846621199	6.4812780811271897E-2	0.14211242765040299
hsa-miR-5698	9.9025477628075809	4.05512636272588	4.8365480591697301	4.9562539537266297E-2	0.12339007238965299
hsa-miR-543	9.8602092732856796	4.0151461297962703	3.8539845403485602	7.4746563437538702E-2	0.14996901494052201

Continued on next page

Continued from previous page

hsa-miR-1306-3p	9.7949515915336907	3.95349561641126	4.4450037739004902	5.8126651568329697E-2	0.13487640509544499
hsa-miR-3605-3p	9.6336054293569298	3.7985502482339402	3.7164719077708299	7.9414326407322294E-2	0.15384255268247199
hsa-miR-378a-3p	9.57153466190457	3.74089068686036	8.62581907602946	1.3189932461492099E-2	5.4466659277768101E-2
hsa-miR-320d	9.5205176506204001	3.69276923503516	6.8447865120411997	2.3546538025066201E-2	8.6578809046012506E-2
hsa-miR-23a-5p	9.5104198353353002	3.6828330541484999	4.31587975989114	6.1338078680969098E-2	0.13830000759199601
hsa-miR-10399-3p	9.5077999999497607	3.6795996887352702	4.1155286134267399	6.6759924392576497E-2	0.143744341710142
hsa-miR-487b-3p	9.1627276502237205	3.35199030472184	3.85255332315834	7.4793387076670395E-2	0.14996901494052201
hsa-miR-576-5p	9.1226829193826493	3.3155267858678799	3.8371909347662601	7.5298250179341705E-2	0.14996901494052201
hsa-miR-106a-5p	1.85952901176014	2.8770909226324402	1.5624282242016201	0.231400818048424	0.36384733890508802
hsa-miR-6741-5p	8.4552632055857604	2.7009019978941602	4.0235661088136503	6.9443536547980897E-2	0.14558776521901301
hsa-miR-4485-3p	1.94304151350929	2.5990203424934699	0.67202918419003999	0.42581224966259701	0.56538404260756003
hsa-miR-1273h-3p	8.2824132340329601	2.54582045806767	4.0927421551900602	6.7412901806905706E-2	0.14385431724866499
hsa-miR-877-3p	7.5806692418553903	1.9245451200164101	5.5444520065549696	3.76336055979129E-2	0.105887457467765
hsa-miR-1299	7.4673272456317203	1.8231103727852001	3.7050499521477298	7.9817893441951906E-2	0.15384255268247199
hsa-let-7b-3p	-1.13320266774698	1.8110678050764	1.1293378792248101	0.30555259486668501	0.45078438378480001
hsa-miR-3168	7.4396237062990096	1.80240684876028	6.1179886425098902	3.04365389307076E-2	9.8301794654582705E-2
hsa-miR-3135b	7.0915873356350403	1.4889381619241999	3.86658556296545	7.4335853435682206E-2	0.14996901494052201
hsa-miR-3182	6.8538826734248497	1.3091245445036399	4.1155819208153597	6.6758405862401199E-2	0.143744341710142

Bibliography

- Abrahamsson, A. and Dabrosin, C. (2015). Tissue specific expression of extracellular microRNA in human breast cancers and normal human breast tissue in vivo. *Oncotarget* *6*, 22959.
- Al-Nedawi, K., Meehan, B., Kerbel, R. S., Allison, A. C. and Rak, J. (2009). Endothelial expression of autocrine VEGF upon the uptake of tumor-derived microvesicles containing oncogenic EGFR. *Proceedings of the National Academy of Sciences* *106*, 3794–3799.
- AmericanDiabetesAssociation (2005). Diagnosis and classification of diabetes mellitus. *Diabetes care* *28*, S5–S10.
- AmericanDiabetesAssociation (2010). Diagnosis and Classification of Diabetes Mellitus. *Diabetes Care* *34*.
- AmericanDiabetesAssociation et al. (2014). Diagnosis and classification of diabetes mellitus. *Diabetes care* *37*, 81–90.
- Amos, A. F., McCarty, D. J. and Zimmet, P. (1997). The rising global burden of diabetes and its complications: estimates and projections to the year 2010. *Diabetic medicine* *14*, 7–85.

- Anders, S., Pyl, P. T. and Huber, W. (2015). HTSeq—a Python framework to work with high-throughput sequencing data. *Bioinformatics* 31, 166–169.
- Andrews, R. K. and Berndt, M. C. (2004). Platelet physiology and thrombosis. *Thrombosis research* 114, 447–453.
- Anene, C., Graham, A. M., Boyne, J. and Roberts, W. (2018). Platelet microparticle delivered microRNA-Let-7a promotes the angiogenic switch. *Biochimica et Biophysica Acta (BBA) - Molecular Basis of Disease* 1864, 2633–2643.
- A.S.o.C.O. (2011). Major Milestones Against Cancer. American Society of Clinical Oncology.
- Azevedo, L. C., Pedro, M. A. and Laurindo, F. R. (2007). Circulating microparticles as therapeutic targets in cardiovascular diseases. *Recent Patents on Cardiovascular Drug Discovery (Discontinued)* 2, 41–51.
- Azzam, H. and Zagloul, M. (2009). Elevated platelet microparticle levels in valvular atrial fibrillation. *Hematology* 14, 357–360.
- Baaten, C. C., Ten Cate, H., van der Meijden, P. E. and Heemskerk, J. W. (2017). Platelet populations and priming in hematological diseases. *Blood reviews* 31, 389–399.
- Bain, A. R., Ainslie, P. N., Bammert, T. D., Hijmans, J. G., Sekhon, M., Hoiland, R. L., Flück, D., Donnelly, J. and DeSouza, C. A. (2017). Passive heat stress reduces circulating endothelial and platelet microparticles. *Experimental physiology* 102, 663–669.

- Bakewell, S. J., Nestor, P., Prasad, S., Tomasson, M. H., Dowland, N., Mehrotra, M., Scarborough, R., Kanter, J., Abe, K., Phillips, D. et al. (2003). Platelet and osteoclast $\beta 3$ integrins are critical for bone metastasis. *Proceedings of the National Academy of Sciences* *100*, 14205–14210.
- Bal, L., Ederhy, S., Di Angelantonio, E., Toti, F., Zobairi, F., Dufaitre, G., Meuleman, C., Mallat, Z., Boccara, F., Tedgui, A. et al. (2010). Circulating procoagulant microparticles in acute pulmonary embolism: A case–control study. *International journal of cardiology* *145*, 321–322.
- Barry, O. P., Praticò, D., Lawson, J. A. and FitzGerald, G. A. (1997). Transcellular activation of platelets and endothelial cells by bioactive lipids in platelet microparticles. *The Journal of clinical investigation* *99*, 2118–2127.
- Barry, O. P., Pratico, D., Savani, R. C., FitzGerald and GA (1998). Modulation of monocyte-endothelial cell interactions by platelet microparticles. *The Journal of clinical investigation* *102*, 136–144.
- Bender, M., Thon, J. N., Ehrlicher, A. J., Wu, S., Mazutis, L., Deschmann, E., Sola-Visner, M., Italiano, J. E. and Hartwig, J. H. (2015). Microtubule sliding drives proplatelet elongation and is dependent on cytoplasmic dynein. *Blood, The Journal of the American Society of Hematology* *125*, 860–868.
- Bernimoulin, M., Waters, E., Foy, M., Steele, B., Sullivan, M., Falet, H., Walsh, M., Barteneva, N., GENG, J.-G., Hartwig, J. et al. (2009). Dif-

- ferential stimulation of monocytic cells results in distinct populations of microparticles. *Journal of Thrombosis and Haemostasis* 7, 1019–1028.
- Boilard, E., Nigrovic, P. A., Larabee, K., Watts, G. F., Coblyn, J. S., Weinblatt, M. E., Massarotti, E. M., Remold-O'Donnell, E., Farndale, R. W., Ware, J. et al. (2010). Platelets amplify inflammation in arthritis via collagen-dependent microparticle production. *Science* 327, 580–583.
- Bosman, G. J., Lasonder, E., Groenen-Dopp, Y. A., Willekens, F. L. and Werre, J. M. (2012). The proteome of erythrocyte-derived microparticles from plasma: new clues for erythrocyte aging and vesiculation. *Journal of proteomics* 76, 203–210.
- Boudreau, L. H., Duchez, A.-C., Cloutier, N., Soulet, D., Martin, N., Bollinger, J., Paré, A., Rousseau, M., Naika, G. S., Lévesque, T. et al. (2014). Platelets release mitochondria serving as substrate for bactericidal group IIA-secreted phospholipase A2 to promote inflammation. *Blood, The Journal of the American Society of Hematology* 124, 2173–2183.
- Bowker, S. L., Lin, M., Eurich, D. T. and Johnson, J. A. (2017). Time-Varying Risk for Breast Cancer Following Initiation of Glucose-Lowering Therapy in Women with Type 2 Diabetes: Exploring Detection Bias. *Canadian Journal of Diabetes* 41, 204–210.
- Breasted, J. H. (1930). *The Edwin Smith surgical papyrus* Chicago IL University.
- Brisson, A. R., Tan, S., Linares, R., Gounou, C. and Arraud, N. (2017). Extracellular vesicles from activated platelets: a semiquantitative cryo-

- electron microscopy and immuno-gold labeling study. *Platelets* 28, 263–271.
- Burnier, L., Fontana, P., Kwak, B. R. and Angelillo-Scherrer, A. (2009). Cell-derived microparticles in haemostasis and vascular medicine. *Thrombosis and haemostasis* 101, 439–451.
- Caine, G., Lip, G. and Blann, A. (2004). Platelet-derived VEGF, Flt-1, Angiopoietin-1 and P-selectin in breast and prostate cancer: further evidence for a role of platelets in tumour angiogenesis. *Annals of medicine* 36, 273–277.
- Cao, L., Zhang, X., Cao, F., Wang, Y., Shen, Y., Yang, C., Uzan, G., Peng, B. and Zhang, D. (2015). Inhibiting inducible miR-223 further reduces viable cells in human cancer cell lines MCF-7 and PC3 treated by celastrol. *BMC cancer* 15, 1–11.
- Caradonna, F. and Luparello, C. (2014). Cytogenetic characterization of HB2 epithelial cells from the human breast. *In Vitro Cellular & Developmental Biology-Animal* 50, 48–55.
- Casaburi, I., Cesario, M. G., Dona, A., Rizza, P., Aquila, S., Avena, P., Lanzino, M., Pellegrino, M., Vivacqua, A., Tucci, P. et al. (2016). Androgens downregulate miR-21 expression in breast cancer cells underlining the protective role of androgen receptor. *Oncotarget* 7, 12651.
- Chen, L., Magliano, D. J. and Zimmet, P. Z. (2012). The worldwide epidemiology of type 2 diabetes mellitus—present and future perspectives. *Nature reviews endocrinology* 8, 228.

- Chen, W. Y. and Holmes, M. D. (2017). Role of aspirin in breast cancer survival. *Current oncology reports* 19, 1–8.
- Chen, X., Ba, Y., Ma, L., Cai, X., Yin, Y., Wang, K., Guo, J., Zhang, Y., Chen, J., Guo, X. et al. (2008). Characterization of microRNAs in serum: a novel class of biomarkers for diagnosis of cancer and other diseases. *Cell research* 18, 997–1006.
- Chomczynski, P. and Mackey, K. (1995). Short technical reports. Modification of the TRI reagent procedure for isolation of RNA from polysaccharide-and proteoglycan-rich sources. *Biotechniques* 19, 942–945.
- Clavel-Chapelon, F. and Gerber, M. (2002). Reproductive factors and breast cancer risk. Do they differ according to age at diagnosis? *Breast cancer research and treatment* 72, 107–115.
- Cohut, M. (2017). 'Alarming' rise in cancer rates driven by diabetes, obesity.
- Coleman, M. P., Quaresma, M., Berrino, F., Lutz, J.-M., De Angelis, R., Capocaccia, R., Baili, P., Rachet, B., Gatta, G., Hakulinen, T. et al. (2008). Cancer survival in five continents: a worldwide population-based study (CONCORD). *The lancet oncology* 9, 730–756.
- Collino, F., Deregibus, M. C., Bruno, S., Sterpone, L., Aghemo, G., Viltono, L., Tetta, C. and Camussi, G. (2010). Microvesicles derived from adult human bone marrow and tissue specific mesenchymal stem cells shuttle selected pattern of miRNAs. *PloS one* 5, e11803.
- Cooper, W. A. (1941). The history of radical mastectomy. *Ann Med Hist* 3, 36–54.

- Costa-Silva, B., Aiello, N. M., Ocean, A. J., Singh, S., Zhang, H., Thakur, B. K., Becker, A., Hoshino, A., Mark, M. T., Molina, H. et al. (2015). Pancreatic cancer exosomes initiate pre-metastatic niche formation in the liver. *Nature cell biology* 17, 816–826.
- Dahiya, N., Sarachana, T., Vu, L., Becker, K. G., Wood III, W. H., Zhang, Y., Atreya, C. D., Danaee, A., Inusa, B., Howard, J. et al. (2015). Platelet MicroRNAs: An Overview.
- Dangwal, S. and Thum, T. (2013). MicroRNAs in platelet physiology and pathology. *Haemostaseologie* 33, 17–20.
- Davidson, N. E. and Sukumar, S. (2005). Of Snail, mice, and women. *Cancer cell* 8, 173–174.
- De Moulin, D. (2012). A short history of breast cancer. Springer Science & Business Media.
- Delgado, A. V., Alexander, S. L., Mcmanus, A. T. and Pusateri, A. E. (2003). Antibodies against human cell receptors, CD36, CD41a, and CD62P cross-react with porcine platelets. *Cytometry* 56B, 62–67.
- den Dekker, E., van Abel, M., van der Vuurst, H., van Eys, G. J., Akkerman, J.-W. N. and Heemskerk, J. W. (2003). Cell-to-cell variability in the differentiation program of human megakaryocytes. *Biochimica et Biophysica Acta (BBA)-Molecular Cell Research* 1643, 85–94.
- Di Leva, G. and Croce, C. M. (2013). miRNA profiling of cancer. *Current opinion in genetics & development* 23, 3–11.

- Di Lullo, G. A., Sweeney, S. M., Körkkö, J., Ala-Kokko, L. and San Antonio, J. D. (2002). Mapping the ligand-binding sites and disease-associated mutations on the most abundant protein in the human, type I collagen. *Journal of Biological Chemistry* 277, 4223–4231.
- Diehl, P., Fricke, A., Sander, L., Stamm, J., Bassler, N., Htun, N., Ziemann, M., Helbing, T., El-Osta, A., Jowett, J. B. et al. (2012). Microparticles: major transport vehicles for distinct microRNAs in circulation. *Cardiovascular research* 93, 633–644.
- Duchez, A.-C., Boudreau, L. H., Naika, G. S., Bollinger, J., Belleannée, C., Cloutier, N., Laffont, B., Mendoza-Villarreal, R. E., Lévesque, T., Rollet-Labelle, E. et al. (2015). Platelet microparticles are internalized in neutrophils via the concerted activity of 12-lipoxygenase and secreted phospholipase A2-IIA. *Proceedings of the National Academy of Sciences* 112, E3564–E3573.
- Faille, D., El-Assaad, F., Mitchell, A. J., Alessi, M.-C., Chimini, G., Fusai, T., Grau, G. E. and Combes, V. (2012). Endocytosis and intracellular processing of platelet microparticles by brain endothelial cells. *Journal of cellular and molecular medicine* 16, 1731–1738.
- Falanga, A., Tartari, C. J. and Marchetti, M. (2012). Microparticles in tumor progression. *Thrombosis research* 129, 132–136.
- Ferlay, J., Shin, H.-R., Bray, F., Forman, D., Mathers, C. and Parkin, D. M. (2010). GLOBOCAN 2008, cancer incidence and mortality worldwide:

- IARC CancerBase No. 10 [Internet]. Lyon, France: International Agency for Research on Cancer 2.
- Ferlay, J., Soerjomataram, I., Dikshit, R., Eser, S., Mathers, C., Rebelo, M., Parkin, D. M., Forman, D. and Bray, F. (2015). Cancer incidence and mortality worldwide: sources, methods and major patterns in GLOBOCAN 2012. *International journal of cancer* 136, E359–E386.
- Flaumenhaft, R., Dilks, J. R., Richardson, J., Alden, E., Patel-Hett, S. R., Battinelli, E., Klement, G. L., Sola-Visner, M. and Italiano Jr, J. E. (2009). Megakaryocyte-derived microparticles: direct visualization and distinction from platelet-derived microparticles. *Blood, The Journal of the American Society of Hematology* 113, 1112–1121.
- Fong, K. P., Barry, C., Tran, A. N., Traxler, E. A., Wannemacher, K. M., Tang, H.-Y., Speicher, K. D., Blair, I. A., Speicher, D. W., Grosser, T. et al. (2011). Deciphering the human platelet sheddome. *Blood* 117, e15–e26.
- Fox, J., Austin, C., Reynolds, C. and Steffen, P. (1991). Evidence that agonist-induced activation of calpain causes the shedding of procoagulant-containing microvesicles from the membrane of aggregating platelets. *Journal of Biological Chemistry* 266, 13289–13295.
- Gao, S., Tian, H., Guo, Y., Li, Y., Guo, Z., Zhu, X. and Chen, X. (2015). miRNA oligonucleotide and sponge for miRNA-21 inhibition mediated by PEI-PLL in breast cancer therapy. *Acta biomaterialia* 25, 184–193.

- Gao, Y., Deng, K., Liu, X., Dai, M., Chen, X., Chen, J., Chen, J., Huang, Y., Dai, S. and Chen, J. (2019). Molecular mechanism and role of microRNA-93 in human cancers: A study based on bioinformatics analysis, meta-analysis, and quantitative polymerase chain reaction validation. *Journal of cellular biochemistry* 120, 6370–6383.
- Garcia Frade, L. (1987). dela Calle H, Alava l, Navarro JL, Creighton LJ, Gaffney PJ. Diabetes as a hypercoagulable state: its relationship with fibrin fragments and vascular damage. *Thromb Res* 47, 533–540.
- Gebeshuber, C. A., Zatloukal, K. and Martinez, J. (2009). miR-29a suppresses tristetraprolin, which is a regulator of epithelial polarity and metastasis. *EMBO reports* 10, 400–405.
- George, J. N., Pickett, E. B., Saucerman, S., McEver, R. P., Kunicki, T. J., Kieffer, N., Newman, P. et al. (1986). Platelet surface glycoproteins. Studies on resting and activated platelets and platelet membrane microparticles in normal subjects, and observations in patients during adult respiratory distress syndrome and cardiac surgery. *The Journal of clinical investigation* 78, 340–348.
- Gidlof, O., Brug, M. V. D., Ohman, J., Gilje, P., Olde, B., Wahlestedt, C. and Erlinge, D. (2013). Platelets activated during myocardial infarction release functional miRNA, which can be taken up by endothelial cells and regulate ICAM1 expression. *Blood* 121, 3908–3917.
- Gilbert, G. E., Sims, P., Wiedmer, T., Furie, B., Furie, B. and Shattil, S.

- (1991). Platelet-derived microparticles express high affinity receptors for factor VIII. *Journal of Biological Chemistry* *266*, 17261–17268.
- Gitz, E., Pollitt, A. Y., Gitz-Francois, J. J., Alshehri, O., Mori, J., Montague, S., Nash, G. B., Douglas, M. R., Gardiner, E. E., Andrews, R. K. et al. (2014). CLEC-2 expression is maintained on activated platelets and on platelet microparticles. *Blood, The Journal of the American Society of Hematology* *124*, 2262–2270.
- Gong, C., Yao, Y., Wang, Y., Liu, B., Wu, W., Chen, J., Su, F., Yao, H. and Song, E. (2011). Up-regulation of miR-21 mediates resistance to trastuzumab therapy for breast cancer. *Journal of Biological Chemistry* *286*, 19127–19137.
- Gonzales, M., Weksler, B., Tsuruta, D., Goldman, R. D., Yoon, K. J., Hopkinson, S. B., Flitney, F. W. and Jones, J. C. (2001). Structure and function of a vimentin-associated matrix adhesion in endothelial cells. *Molecular Biology of the Cell* *12*, 85–100.
- Grande, R., Dovizio, M., Marcone, S., Szklanna, P. B., Bruno, A., Ebhardt, H. A., Cassidy, H., Ní Áinle, F., Caprodossi, A., Lanuti, P. et al. (2019). Platelet-derived microparticles from obese individuals: characterization of number, size, proteomics, and crosstalk with cancer and endothelial cells. *Frontiers in pharmacology* *10*, 7.
- Grozovsky, R., Giannini, S., Falet, H. and Hoffmeister, K. M. (2015). Regulating billions of blood platelets: glycans and beyond. *Blood* *126*, 1877–1884.

- Hamzeh-Cognasse, H., Damien, P., Nguyen, K. A., Zeni, F., Pozzetto, B., Cognasse, F. and Garraud, O. (2013). Contribution of activated platelets to plasma IL-27 levels. *Critical Care* 17, 1–2.
- Hanahan, D. and Weinberg, R. A. (2011). Hallmarks of cancer: the next generation. *cell* 144, 646–674.
- Harris, J., Lippman, M. and Veronesi, U. (1992). Leading cause of death in American women aged between 40 and 55. *N Engl J Med* 1, 319–479.
- Hayon, Y., Dashevsky, O., Shai, E., Varon, D. and Leker, R. R. (2012). Platelet microparticles promote neural stem cell proliferation, survival and differentiation. *Journal of Molecular Neuroscience* 47, 659–665.
- Holmes, M. D., Chen, W. Y., Li, L., Hertzmark, E., Spiegelman, D. and Hankinson, S. E. (2010). Aspirin intake and survival after breast cancer. *Journal of Clinical Oncology* 28, 1467.
- Horigome, H., Hiramatsu, Y., Shigeta, O., Nagasawa, T. and Matsui, A. (2002). Overproduction of platelet microparticles in cyanotic congenital heart disease with polycythemia. *Journal of the American college of cardiology* 39, 1072–1077.
- Howlader, N., Noone, A., Krapcho, M., Garshell, J., Miller, D., Altekruse, S., Kosary, C., Yu, M., Ruhl, J., Tatalovich, Z. et al. (2013). SEER cancer statistics review, 1975–2010, National Cancer Institute. Bethesda, MD, USA.
- Hsu, S.-D., Lin, F.-M., Wu, W.-Y., Liang, C., Huang, W.-C., Chan, W.-L.,

- Tsai, W.-T., Chen, G.-Z., Lee, C.-J., Chiu, C.-M. et al. (2011). miR-TarBase: a database curates experimentally validated microRNA–target interactions. *Nucleic acids research* *39*, D163–D169.
- Hu, X., Guo, J., Zheng, L., Li, C., Zheng, T. M., Tanyi, J. L., Liang, S., Benedetto, C., Mitidieri, M., Katsaros, D. et al. (2013). The heterochronic microRNA let-7 inhibits cell motility by regulating the genes in the actin cytoskeleton pathway in breast cancer. *Molecular cancer research* *11*, 240–250.
- Iorio, M. V., Ferracin, M., Liu, C.-G., Veronese, A., Spizzo, R., Sabbioni, S., Magri, E., Pedriali, M., Fabbri, M., Campiglio, M. et al. (2005). MicroRNA gene expression deregulation in human breast cancer. *Cancer research* *65*, 7065–7070.
- Iqbal, J., Ginsburg, O., Rochon, P. A., Sun, P. and Narod, S. A. (2015). Differences in breast cancer stage at diagnosis and cancer-specific survival by race and ethnicity in the United States. *Jama* *313*, 165–173.
- Janowska-Wieczorek, A., Marquez-Curtis, L. A., Wysoczynski, M. and Ratajczak, M. Z. (2006). Enhancing effect of platelet-derived microvesicles on the invasive potential of breast cancer cells. *Transfusion* *46*, 1199–1209.
- Jatoi, I., Anderson, W. F., Rao, S. R. and Devesa, S. S. (2005). Breast cancer trends among black and white women in the United States. *Journal of Clinical Oncology* *23*, 7836–7841.
- Jiang, S., Zhang, H.-W., Lu, M.-H., He, X.-H., Li, Y., Gu, H., Liu, M.-F. and Wang, E.-D. (2010). MicroRNA-155 functions as an OncomiR in breast

- cancer by targeting the suppressor of cytokine signaling 1 gene. *Cancer research* *70*, 3119–3127.
- Josefsson, E. C., Burnett, D. L., Lebois, M., Debrincat, M. A., White, M. J., Henley, K. J., Lane, R. M., Moujalled, D., Preston, S. P., O’Reilly, L. A. et al. (2014). Platelet production proceeds independently of the intrinsic and extrinsic apoptosis pathways. *Nature communications* *5*, 1–14.
- Kachekouche, Y., Dali-Sahi, M., Benmansour, D. and Dennouni-Medjati, N. (2018). Hematological profile associated with type 2 diabetes mellitus. *Diabetes & Metabolic Syndrome: Clinical Research & Reviews* *12*, 309–312.
- Knijff-Dutmer, E., Koerts, J., Nieuwland, R., Kalsbeek-Batenburg, E. v. and Van De Laar, M. (2002). Elevated levels of platelet microparticles are associated with disease activity in rheumatoid arthritis. *Arthritis & Rheumatism: Official Journal of the American College of Rheumatology* *46*, 1498–1503.
- Koga, H., Sugiyama, S., Kugiyama, K., Fukushima, H., Watanabe, K., Sakamoto, T., Yoshimura, M., Jinnouchi, H. and Ogawa, H. (2006). Elevated levels of remnant lipoproteins are associated with plasma platelet microparticles in patients with type-2 diabetes mellitus without obstructive coronary artery disease. *European heart journal* *27*, 817–823.
- Kreutz, R. P., Nystrom, P., Kreutz, Y., Miao, J., Kovacs, R., Desta, Z., Flockhart, D. A. and Jin, Y. (2012). Inhibition of platelet aggregation by prostaglandin E1 (PGE1) in diabetic patients during therapy with clopidogrel and aspirin. *Platelets* *24*, 145–150.

- Krueger, L. A., Barnard, M. R., Frelinger Iii, A., Furman, M. I. and Michelson, A. D. (2002). Immunophenotypic analysis of platelets. *Current protocols in cytometry* 19, 6–10.
- Kumar, V., Abbas, A. K., Fausto, N., Aster, J. C. et al. (2005). Pathologic basis of disease.
- Lacroix, R., Robert, S., Poncelet, P. and Dignat-George, F. (2010). Overcoming limitations of microparticle measurement by flow cytometry. In *Seminars in thrombosis and hemostasis* vol. 36, pp. 807–818, © Thieme Medical Publishers Thieme Medical Publishers.
- Laffont, B., Corduan, A., Plé, H., Duchez, A.-C., Cloutier, N., Boilard, E. and Provost, P. (2013). Activated platelets can deliver mRNA regulatory Ago2.microRNA complexes to endothelial cells via microparticles. *Blood* 122.
- Lal, I., Dittus, K. and Holmes, C. E. (2013). Platelets, coagulation and fibrinolysis in breast cancer progression. *Breast Cancer Research* 15, 207.
- Landry, P., Plante, I., Ouellet, D. L., Perron, M. P., Rousseau, G. and Provost, P. (2009). Existence of a microRNA pathway in anucleate platelets. *Nature structural & molecular biology* 16, 961.
- Langmead, B. and Salzberg, S. L. (2012). Fast gapped-read alignment with Bowtie 2. *Nature methods* 9, 357.
- Lazar, S. and Goldfinger, L. E. (2018). Platelet microparticles and miRNA transfer in cancer progression: Many targets, modes of action, and effects across cancer stages. *Frontiers in cardiovascular medicine* 5, 13.

- Lefrançois, E., Ortiz-Muñoz, G., Caudrillier, A., Mallavia, B., Liu, F., Sayah, D. M., Thornton, E. E., Headley, M. B., David, T., Coughlin, S. R. et al. (2017). The lung is a site of platelet biogenesis and a reservoir for haematopoietic progenitors. *Nature* 544, 105–109.
- Lewison, E. F. (1953). The surgical treatment of breast cancer: an historical and collective review. *Surgery* 34, 904–953.
- Li, C. I., Beaber, E. F., Tang, M.-T. C., Porter, P. L., Daling, J. R. and Malone, K. E. (2013). Reproductive factors and risk of estrogen receptor positive, triple-negative, and HER2-neu overexpressing breast cancer among women 20–44 years of age. *Breast cancer research and treatment* 137, 579–587.
- Li, Z.-X., Zhu, Q.-N., Zhang, H.-B., Hu, Y., Wang, G. and Zhu, Y.-S. (2018). MALAT1: a potential biomarker in cancer. *Cancer management and research* 10, 6757.
- Liang, H., Yan, X., Pan, Y., Wang, Y., Wang, N., Li, L., Liu, Y., Chen, X., Zhang, C.-Y., Gu, H. et al. (2015). MicroRNA-223 delivered by platelet-derived microvesicles promotes lung cancer cell invasion via targeting tumor suppressor EPB41L3. *Molecular cancer* 14, 58.
- Liao, S., Li, J., Wei, W., Wang, L., Zhang, Y., Li, J., Wang, C. and Sun, S. (2011). Association between diabetes mellitus and breast cancer risk: a meta-analysis of the literature. *Asian Pac J Cancer Prev* 12, 1061–1065.
- Lin, Z., Li, J.-W., Wang, Y., Chen, T., Ren, N., Yang, L., Xu, W., He, H.,

- Jiang, Y., Chen, X. et al. (2016). Abnormal miRNA-30e Expression is Associated with Breast Cancer Progression. *Clinical laboratory* 62, 121.
- Liu, M.-m., Li, Z., Han, X.-d., Shi, J.-h., Tu, D.-y., Song, W., Zhang, J., Qiu, X.-l., Ren, Y. and Zhen, L.-l. (2017). MiR-30e inhibits tumor growth and chemoresistance via targeting IRS1 in Breast Cancer. *Scientific reports* 7, 1–10.
- Lyons, A. S. and Petrucelli, R. J. (1988). Medicine: An Illustrated History. *Annals of Internal Medicine* 108, 509.
- Madigan, M. P., Ziegler, R. G., Benichou, J., Byrne, C. and Hoover, R. N. (1995). Proportion of breast cancer cases in the United States explained by well-established risk factors. *JNCI: Journal of the National Cancer Institute* 87, 1681–1685.
- Martin, M. (2011). Cutadapt removes adapter sequences from high-throughput sequencing reads. *EMBnet. journal* 17, 10–12.
- McPherson, K., Steel, C. and Dixon, J. (2000). ABC of breast diseases: breast cancer—epidemiology, risk factors, and genetics. *BMJ: British Medical Journal* 321, 624.
- Merten, M., Pakala, R., Thiagarajan, P. and Benedict, C. R. (1999). Platelet microparticles promote platelet interaction with subendothelial matrix in a glycoprotein IIb/IIIa-dependent mechanism. *Circulation* 99, 2577–2582.
- Mezouar, S., Mege, D., Darbousset, R., Farge, D., Debourdeau, P., Dignat-George, F., Panicot-Dubois, L. and Dubois, C. (2014). Involvement of

- platelet-derived microparticles in tumor progression and thrombosis. In *Seminars in oncology* vol. 41, pp. 346–358, Elsevier.
- Michael, J. V., Wurtzel, J. G., Mao, G. F., Rao, A. K., Kolpakov, M. A., Sabri, A., Hoffman, N. E., Rajan, S., Tomar, D., Madesh, M. et al. (2017). Platelet microparticles infiltrating solid tumors transfer miRNAs that suppress tumor growth. *Blood, The Journal of the American Society of Hematology* 130, 567–580.
- Mo, M.-H., Chen, L., Fu, Y., Wang, W. and Fu, S. W. (2012). Cell-free circulating miRNA biomarkers in cancer. *Journal of Cancer* 3, 432.
- Mohamed, A., Krajewski, K., Cakar, B. and Ma, C. X. (2013). Targeted therapy for breast cancer. *The American journal of pathology* 183, 1096–1112.
- NationalCancerInstitute (2018). *Breast Cancer During Pregnancy*.
- Neve, R. M., Chin, K., Fridlyand, J., Yeh, J., Baehner, F. L., Fevr, T., Clark, L., Bayani, N., Coppe, J.-P., Tong, F. et al. (2006). A collection of breast cancer cell lines for the study of functionally distinct cancer subtypes. *Cancer cell* 10, 515–527.
- Nguyen, D. B., Wagner-Britz, L., Maia, S., Steffen, P., Wagner, C., Kaestner, L. and Bernhardt, I. (2011). Regulation of phosphatidylserine exposure in red blood cells. *Cellular physiology and biochemistry* 28, 847–856.
- Nieswandt, B., Pleines, I. and Bender, M. (2011). Platelet adhesion and activation mechanisms in arterial thrombosis and ischaemic stroke. *Journal of Thrombosis and Haemostasis* 9, 92–104.

- Perez-Pujol, S., Marker, P. H. and Key, N. S. (2007). Platelet microparticles are heterogeneous and highly dependent on the activation mechanism: studies using a new digital flow cytometer. *Cytometry Part A: The Journal of the International Society for Analytical Cytology* *71*, 38–45.
- Perreault, A., Knight, J. C., Wang, M., Way, J. and Wuest, F. (2015). 18F-Labeled wild-type annexin V: comparison of random and site-selective radiolabeling methods. *Amino Acids* *48*, 65–74.
- Peto, J. (2001). Cancer epidemiology in the last century and the next decade. *Nature* *411*, 390–395.
- Ponomareva, A., Nevzorova, T., Mordakhanova, E., Andrianova, I., Rauova, L., Litvinov, R. and Weisel, J. (2017). Intracellular origin and ultrastructure of platelet-derived microparticles. *Journal of Thrombosis and Haemostasis* *15*, 1655–1667.
- Pordzik, J., Jakubik, D., Jarosz-Popek, J., Wicik, Z., Eyileten, C., De Rosa, S., Indolfi, C., Siller-Matula, J. M., Czajka, P. and Postula, M. (2019). Significance of circulating microRNAs in diabetes mellitus type 2 and platelet reactivity: bioinformatic analysis and review. *Cardiovascular diabetology* *18*, 1–19.
- Potentia, S., Zeisberg, E. and Kalluri, R. (2008). The role of endothelial-to-mesenchymal transition in cancer progression. *British journal of cancer* *99*, 1375.
- Rana, S., Malinowska, K. and Zöller, M. (2013). Exosomal tumor microRNA modulates premetastatic organ cells. *Neoplasia* *15*, IN14–IN31.

- Rasche, H. (2001). Haemostasis and thrombosis: an overview. *European Heart Journal Supplements* 3, Q3–Q7.
- Robinson, M. D., McCarthy, D. J. and Smyth, G. K. (2010). edgeR: a Bioconductor package for differential expression analysis of digital gene expression data. *Bioinformatics* 26, 139–140.
- Rojas, K. and Stuckey, A. (2016). Breast cancer epidemiology and risk factors. *Clinical obstetrics and gynecology* 59, 651–672.
- Saito, R., Shoda, K., Maruyama, S., Yamamoto, A., Takiguchi, K., Furuya, S., Hosomura, N., Akaike, H., Kawaguchi, Y., Amemiya, H. et al. (2021). Platelets enhance malignant behaviours of gastric cancer cells via direct contacts. *British Journal of Cancer* 124, 570–573.
- Sambrano, G. R., Weiss, E. J., Zheng, Y.-W., Huang, W. and Coughlin, S. R. (2001). Role of thrombin signalling in platelets in haemostasis and thrombosis. *Nature* 413, 74–78.
- Samuel, S. M., Varghese, E., Varghese, S. and Büsselberg, D. (2018a). Challenges and perspectives in the treatment of diabetes associated breast cancer. *Cancer treatment reviews* 70, 98–111.
- Samuel, S. M., Varghese, E., Varghese, S. and Büsselberg, D. (2018b). Challenges and perspectives in the treatment of diabetes associated breast cancer. *Cancer Treatment Reviews* 70, 98–111.
- Schafer, A. I. (1985). The hypercoagulable states. *Annals of Internal Medicine* 102, 814–828.

- SEARCH (2006). The burden of diabetes mellitus among US youth: prevalence estimates from the SEARCH for Diabetes in Youth Study. *Pediatrics* *118*, 1510–1518.
- Seltzer, V. (1994). The breast: embryology, development, and anatomy. *Clinical obstetrics and gynecology* *37*, 879–880.
- Semple, J. W. (2013). Platelets deliver small packages of genetic function. *Blood* *122*, 155–156.
- Serebruany, V. L., Cherepanov, V., Cabrera-Fuentes, H. A. and Kim, M. H. (2015). Solid cancers after antiplatelet therapy: confirmations, controversies, and challenges. *Thrombosis and haemostasis* *114*, 1104–1112.
- Shiao, J., Thomas, K., Rahimi, A., Rao, R., Yan, J., Xie, X.-J., DaSilva, M., Spangler, A., Leitch, M., Wooldridge, R. et al. (2017). Aspirin/antiplatelet agent use improves disease-free survival and reduces the risk of distant metastases in Stage II and III triple-negative breast cancer patients. *Breast cancer research and treatment* *161*, 463–471.
- Sims, P. J., Faioni, E., Wiedmer, T. and Shattil, S. (1988). Complement proteins C5b-9 cause release of membrane vesicles from the platelet surface that are enriched in the membrane receptor for coagulation factor Va and express prothrombinase activity. *Journal of Biological Chemistry* *263*, 18205–18212.
- Singh, R., Pochampally, R., Watabe, K., Lu, Z. and Mo, Y.-Y. (2014). Exosome-mediated transfer of miR-10b promotes cell invasion in breast cancer. *Molecular cancer* *13*, 256.

- Soma, P., Swanepoel, A. C., Du Plooy, J. N., Mqoco, T. and Pretorius, E. (2016). Flow cytometric analysis of platelets type 2 diabetes mellitus reveals ‘angry’platelets. *Cardiovascular diabetology* 15, 1–7.
- Song, B., Wang, C., Liu, J., Wang, X., Lv, L., Wei, L., Xie, L., Zheng, Y. and Song, X. (2010). MicroRNA-21 regulates breast cancer invasion partly by targeting tissue inhibitor of metalloproteinase 3 expression. *Journal of experimental & clinical cancer research* 29, 1–8.
- Stegner, D., Judith, M., Angay, O., Gorelashvili, M. G., Semeniak, D., Pinnecker, J., Schmithausen, P., Meyer, I., Friedrich, M., Dütting, S. et al. (2017). Thrombopoiesis is spatially regulated by the bone marrow vasculature. *Nature communications* 8, 1–11.
- Stinson, S., Lackner, M. R., Adai, A. T., Yu, N., Kim, H.-J., O’Brien, C., Spoerke, J., Jhunjhunwala, S., Boyd, Z., Januario, T. et al. (2011). TRPS1 targeting by miR-221/222 promotes the epithelial-to-mesenchymal transition in breast cancer. *Science signaling* 4, ra41–ra41.
- Stratz, C., Nührenberg, T., Fiebich, B. L., Amann, M., Kumar, A., Binder, H., Hoffmann, I., Valina, C., Hochholzer, W., Trenk, D. et al. (2014). Controlled type II diabetes mellitus has no major influence on platelet micro-RNA expression. *Thrombosis and haemostasis* 112, 902–911.
- Tan, K. T., Tayebjee, M. H., Lynd, C., Blann, A. D. and Lip, G. Y. (2005a). Platelet microparticles and soluble P selectin in peripheral artery disease: relationship to extent of disease and platelet activation markers. *Annals of medicine* 37, 61–66.

- Tan, K. T., Tayebjee, M. H., Macfadyen, R. J., Lip, G. Y. and Blann, A. D. (2005b). Elevated platelet microparticles in stable coronary artery disease are unrelated to disease severity or to indices of inflammation. *Platelets* *16*, 368–371.
- Tang, H., Massi, D., Hemmings, B. A., Mandalà, M., Hu, Z., Wicki, A. and Xue, G. (2016). AKT-ions with a TWIST between EMT and MET. *Oncotarget* *7*, 62767.
- Tang, M., Jiang, L., Lin, Y., Wu, X., Wang, K., He, Q., Wang, X. and Li, W. (2017). Platelet microparticle-mediated transfer of miR-939 to epithelial ovarian cancer cells promotes epithelial to mesenchymal transition. *Oncotarget* *8*.
- Taucher, S., Salat, A., Gnant, M., Kwasny, W., Mlineritsch, B., Menzel, R.-C., Schmid, M., Smola, M. G., Stierer, M., Tausch, C. et al. (2003). Impact of pretreatment thrombocytosis on survival in primary breast cancer. *Thrombosis and haemostasis* *89*, 1098–1106.
- Tavani, A., Braga, C., La Vecchia, C., Negri, E., Russo, A. and Franceschi, S. (1997). Attributable risks for breast cancer in Italy: education, family history and reproductive and hormonal factors. *International journal of cancer* *70*, 159–163.
- Terrisse, A., Puech, N., Allart, S., Gourdy, P., Xuereb, J., Payrastre, B. and Sie, P. (2010). Internalization of microparticles by endothelial cells promotes platelet/endothelial cell interaction under flow. *Journal of Thrombosis and Haemostasis* *8*, 2810–2819.

- Théry, C., Witwer, K. W., Aikawa, E., Alcaraz, M. J., Anderson, J. D., Andriantsitohaina, R., Antoniou, A., Arab, T., Archer, F., Atkin-Smith, G. K. et al. (2018). Minimal information for studies of extracellular vesicles 2018 (MISEV2018): a position statement of the International Society for Extracellular Vesicles and update of the MISEV2014 guidelines. *Journal of extracellular vesicles* 7, 1535750.
- Toss, A., Venturelli, M., Peterle, C., Piacentini, F., Cascinu, S. and Cortesi, L. (2017). Molecular biomarkers for prediction of targeted therapy response in metastatic breast cancer: trick or treat? *International journal of molecular sciences* 18, 85.
- Toth, B., Liebhardt, S., Steinig, K., Ditsch, N., Rank, A., Bauerfeind, I., Spannagl, M., Friese, K. and Reininger, A. J. (2008). Platelet-derived microparticles and coagulation activation in breast cancer patients. *Thrombosis and haemostasis* 100.
- van der Meijden, P. E. and Heemskerk, J. W. (2019). Platelet biology and functions: new concepts and clinical perspectives. *Nature Reviews Cardiology* 16, 166–179.
- van der Zee, P. M., Biró, É., Ko, Y., de Winter, R. J., Hack, C. E., Sturk, A. and Nieuwland, R. (2006). P-selectin-and CD63-exposing platelet microparticles reflect platelet activation in peripheral arterial disease and myocardial infarction. *Clinical chemistry* 52, 657–664.
- Varon, D., Hayon, Y., Dashevsky, O. and Shai, E. (2012). Involvement of

- platelet derived microparticles in tumor metastasis and tissue regeneration. *Thrombosis research* 130, 98–99.
- Versteeg, H. H., Heemskerk, J. W., Levi, M. and Reitsma, P. H. (2013). New fundamentals in hemostasis. *Physiological reviews* 93, 327–358.
- Vigneri, P., Frasca, F., Sciacca, L., Pandini, G. and Vigneri, R. (2009). Diabetes and cancer. *Endocrine-related cancer* 16, 1103–1123.
- Vismara, M., Zarà, M., Negri, S., Canino, J., Canobbio, I., Barbieri, S. S., Moccia, F., Torti, M. and Guidetti, G. F. (2021). Platelet-derived extracellular vesicles regulate cell cycle progression and cell migration in breast cancer cells. *Biochimica et Biophysica Acta (BBA)-Molecular Cell Research* 1868, 118886.
- Voloshin, T., Fremder, E. and Shaked, Y. (2014). Small but mighty: microparticles as mediators of tumor progression. *Cancer Microenvironment* 7, 11–21.
- Vona-Davis, L., Howard-McNatt, M. and Rose, D. (2007). Adiposity, type 2 diabetes and the metabolic syndrome in breast cancer. *Obesity Reviews* 8, 395–408.
- Wang, C.-Z., Yuan, P. and Li, Y. (2015). MiR-126 regulated breast cancer cell invasion by targeting ADAM9. *International journal of clinical and experimental pathology* 8, 6547.
- Wang, J. Z., Du, Z., Payattakool, R., Yu, P. S. and Chen, C.-F. (2007). A new method to measure the semantic similarity of GO terms. *Bioinformatics* 23, 1274–1281.

- Wang, W., Liu, J., Yang, B., Ma, Z., Liu, G., Shen, W. and Zhang, Y. (2017). Modulation of platelet-derived microparticles to adhesion and motility of human rheumatoid arthritis fibroblast-like synoviocytes. *PloS one* *12*, e0181003.
- Wei, Y., Guo, D., Hou, X. and Jiang, D. (2017). miRNA-223 suppresses FOXO1 and functions as a potential tumor marker in breast cancer. *Cellular and Molecular Biology (Noisy-le-Grand, France)* *63*, 113–118.
- Welshons, W. V., Wolf, M. F., Murphy, C. S. and Jordan, V. C. (1988). Estrogenic activity of phenol red. *Molecular and cellular endocrinology* *57*, 169–178.
- Willeit, P., Zampetaki, A., Dudek, K., Kaudewitz, D., King, A., Kirkby, N. S., Crosby-Nwaobi, R., Prokopi, M., Drozdov, I., Langley, S. R. et al. (2013). Circulating microRNAs as novel biomarkers for platelet activation. *Circulation research* *112*, 595–600.
- Wolfers, J., Lozier, A., Raposo, G., Regnault, A., Théry, C., Masurier, C., Flament, C., Pouzieux, S., Faure, F., Tursz, T. et al. (2001). Tumor-derived exosomes are a source of shared tumor rejection antigens for CTL cross-priming. *Nature medicine* *7*, 297–303.
- Wu, Z., Ji, C., Li, H., Qiu, G., Gao, C. and Weng, X. (2013). Membrane microparticles and diseases. *Eur Rev Med Pharmacol Sci* *17*, 2420–2427.
- Yan, L.-X., Huang, X.-F., Shao, Q., Huang, M.-Y., Deng, L., Wu, Q.-L., Zeng, Y.-X. and Shao, J.-Y. (2008). MicroRNA miR-21 overexpression

- in human breast cancer is associated with advanced clinical stage, lymph node metastasis and patient poor prognosis. *Rna* 14, 2348–2360.
- Yari, F., Motefaker, M., Nikougofar, M. and Khayati, Z. (2018). Interaction of platelet-derived microparticles with a human B-lymphoblast cell line: A clue for the immunologic function of the microparticles. *Transfusion Medicine and Hemotherapy* 45, 55–61.
- Yu, G., Wang, L.-G., Han, Y. and He, Q.-Y. (2012). clusterProfiler: an R package for comparing biological themes among gene clusters. *Omics: a journal of integrative biology* 16, 284–287.
- Yuan, X., Qian, N., Ling, S., Li, Y., Sun, W., Li, J., Du, R., Zhong, G., Liu, C., Yu, G. et al. (2021). Breast cancer exosomes contribute to pre-metastatic niche formation and promote bone metastasis of tumor cells. *Theranostics* 11, 1429.
- Zampetaki, A., Kiechl, S., Drozdov, I., Willeit, P., Mayr, U., Prokopi, M., Mayr, A., Weger, S., Oberhollenzer, F., Bonora, E. et al. (2010). Plasma microRNA profiling reveals loss of endothelial miR-126 and other microRNAs in type 2 diabetes. *Circulation research* 107, 810–817.
- Zarà, M., Guidetti, G. F., Boselli, D., Villa, C., Canobbio, I., Seppi, C., Visconte, C., Canino, J. and Torti, M. (2017). Release of prometastatic platelet-derived microparticles induced by breast cancer cells: a novel positive feedback mechanism for metastasis. *TH Open* 1, e155–e163.
- Zhang, C., Liu, K., Li, T., Fang, J., Ding, Y., Sun, L., Tu, T., Jiang, X.,

- Du, S., Hu, J. et al. (2016). miR-21: A gene of dual regulation in breast cancer. *International journal of oncology* 48, 161–172.
- Zhang, R., Xu, J., Zhao, J. and Bai, J. (2017). Mir-30d suppresses cell proliferation of colon cancer cells by inhibiting cell autophagy and promoting cell apoptosis. *Tumor Biology* 39, 1010428317703984.
- Zhang, X., McGeoch, S. C., Johnstone, A. M., Holtrop, G., Sneddon, A. A., MacRury, S. M., Megson, I. L., Pearson, D. W., Abraham, P., De Roos, B. et al. (2014). Platelet-derived microparticle count and surface molecule expression differ between subjects with and without type 2 diabetes, independently of obesity status. *Journal of thrombosis and thrombolysis* 37, 455–463.
- Zhu, W., Qin, W., Atasoy, U. and Sauter, E. R. (2009). Circulating microRNAs in breast cancer and healthy subjects. *BMC research notes* 2, 1–5.
- Zimmet, P. (2000). Globalization, coca-colonization and the chronic disease epidemic: can the Doomsday scenario be averted. *Journal of internal medicine* 247, 301–310.
- Zmigrodzka, M., Guzera, M., Miskiewicz, A., Jagielski, D. and Winnicka, A. (2016). The biology of extracellular vesicles with focus on platelet microparticles and their role in cancer development and progression. *Tumor Biology* 37, 14391–14401.